EIGHTH EUROPEAN CONFERENCE ON CONTROLLED FUSION AND PLASMA PHYSICS

Volume II

Invited Papers

VIII FUSION
PRAGUE 1977

EIGHTH EUROPEAN CONFERENCE ON CONTROLLED FUSION AND PLASMA PHYSICS

VOLUME II

INVITED PAPERS

SUPPLEMENTARY PAPERS

POST-DEADLINE PAPERS

Prague, Czechoslovakia, 19-23 September 1977

The Conference Proceedings (Vol. I: Contributed Papers, Vol. II: Invited and Supplementary Papers) will be distributed free of charge to all registered participants. They will also be sold at the price 50 Swiss Francs after the Conference. The price of a single volume will be 30 Swiss Francs. Orders should be placed with the Conference Secretariat, during the meeting, or sent to the Institute of Plasma Physics, Czechoslovak Academy of Sciences, Pod vodárenskou věží 4, 180 69 Prague 8, Czechoslovakia, after the meeting.

C O N T E N T S

I N V I T E D P A P E R S

P R E F A C E

This volume contains the texts of the invited lectures, post-deadline contributions that were read at the Conference and the supplementary pages to papers already published in the first volume of the Proceedings.

The invited lectures were selected by the Paper Selection and Programme Committee from suggestions recommended to the Organizing Committee by heads of leading plasma research groups through the world. The texts of these lectures are included in this volume. They are printed in a logical order, regrouping those pertaining to the same subject, rather than in their order of presentation. We deeply regret that the deceased academician G.I. Budker, doyen of all invited lecturers, can nevermore be our teacher and senior colleague.

Please note that in addition to the page numbers the supplementary papers have the same numbers as the contributed papers and the post-deadline papers have been given numbers as if published at the end of the first volume.

Except for retyping of manuscripts not suitable for reproduction and some minor editorial corrections, the texts are photographic reproductions of the original papers. It means that the authors must bear responsibility for the content of their papers.

The Organizing Committee

ORGANIZING COMMITTEE

V. Kopecký, chairman
academician B. Kvasil, honorary vice-chairman
J. Váňa, vice-chairman
J. Kracík, vice-chairman
R. Klíma, scientific secretary

K. Jakubka
Mrs P. Jarošová
K. Jungwirth
Š. Körbel
J. Maloch
Mrs V. Nováková
P. Pasternak
K. Šobra
P. Šunka

PAPER SELECTION AND PROGRAMME COMMITTEE

C. Bobeldijk, Rijnhuizen, Jutphaas, the Netherlands
O.N. Krokhin, Moscow, U.S.S.R.
A.M. Messiaen, Brussels, Belgium
K.A. Razumova, Moscow, U.S.S.R.
P. Šunka, Prague, Czechoslovakia
D.R. Sweetman, Culham, England

FINANCIAL SUPPORT

The Organizations listed below have contributed financially to the Conference. Their support is gratefully acknowledged:

CZECHOSLOVAK ATOMIC ENERGY COMMISSION

CZECH TECHNICAL UNIVERSITY

INVITED PAPERS

ON THE ION ENERGY BALANCE IN TFR WITH AND WITHOUT NEUTRAL INJECTION HEATING

TFR Group
(presented by J.P. GIRARD)

ASSOCIATION EURATOM-CEA SUR LA FUSION
Département de Physique du Plasma et de la Fusion Contrôlée
Centre d'Etudes Nucléaires
Boîte Postale n° 6. 92260 FONTENAY-AUX-ROSES (FRANCE)

If at first sight a correct ion energy balance seems much easier to establish and understand than the electron one, however the precise knowledge of many plasma quantities, which are not always well measured or estimated, is also acquired.

At stationary state, a rough energy balance can be written as follows [1, 2]

$$P_{ei}(r)+P_{bi}(r) = P_{ex}(r)+P_{x}(r)+P_{D}(r) \qquad (1)$$

- P_{ei} (n_e, T_e, T_i [Z]) is the classical energy exchange term between electrons and ions which can be written

$$P_{ei} = 1.26\ 10^{-26}\ \frac{n_e^2}{A_i}\ \frac{T_e-T_i}{T_e^{3/2}}\ [Z]\ (w, ev, cm^{-3})$$

- $P_{bi}(n_e, T_e, E_i)$ is the energy exchange term between fast captured ions and plasma ions. This term will be entirely calculated numerically and explained later in the text.

- P_{ex} (n_i, n_o, T_i) is the charge exchange loss term which can be written approximatively : $P_{ex} = \frac{3}{2}\ n_i\ n_o < \sigma_{ex} v> \left\{ T_i - T_o \right\}$. This expression is approximated because it does not take into account the interaction of 2 maxwellien distributions n_i and n_o and supposes that there is no reabsorption of neutrals inside the plasma.

P_x (n_e, n_i, Z_{eff} T_i) is the conduction loss term which has to be written :

$$P_x = -\frac{1}{r}\frac{\partial}{\partial r}\left(r n_i \chi_i \frac{\partial T_i}{\partial r}\right) \text{ with } \chi_i = \frac{\rho_i^2 q^2}{\tau_i} \frac{0.665\,(1+0.43\nu)}{\varepsilon^{3/2}+1.03\varepsilon^{3/4}\nu^{1/2}+0.185\nu} \text{ [3]}$$

- P_D (n_i, n_o, T_e, T_i) is the convection loss term which has been written with the help of the continuity equation :

$$P_D = \frac{5}{2}\frac{1}{r}\frac{\partial}{\partial r} T_i \int_o^r n_e n_o \langle \sigma_i v_e \rangle r\, dr$$

In this expression we have not taken into account recombination.

All the symbols are usual except : T_o is the energy of the recycled neutrals, E_i is the energy of fast injected neutrals,

$$\nu = \frac{Rq}{v_i \tau_i} \qquad \tau_i = \frac{2 10^7 \sqrt{A_i}\, T_i^{3/2}}{n_e Z_{ion} \operatorname{Ln} \Lambda} \left\{ s,\ cm^{-3},\ ev \right\}$$

$$Z_{ion} = \frac{1}{n_e}\left\{ n_i + \sum_{j+i} n_j Z_j^2 \sqrt{\frac{2\,mj}{m_i+m_j}} \right\} \text{ [Z]} = \frac{1}{n_e}\sum \frac{n_j Z_j^2}{A_j}$$

ρ_i and v_i are the larmor radius and the velocity of the ions respectively. We will use also in the text the integral inside a Magnetic Surface

$$\mathcal{P} = 4\pi^2 R \int_o^r p\, r\, dr$$

what do we know about all these quantities in T.F.R. ?

n_e (r) . The electron density is measured by a 9 channel HCN interferometer, so it is usually very well-known up to the boundary of the plasma. This measurement is also confirmed by Thomson Scattering.

T_e (r) . The electron temperature is systematically measured by Thomson Scattering but up to r = 12,13 cm only (the plasma radius a is 20 cm). Only in a few cases do we have measurements up to 20 cm. This has large consequences, because we must extrapolate T_e (r) up to 20 cm,

for terms as important as $\mathcal{P}_{ei}$ sensitive to the contribution of large volumes at the plasma periphery or Z_{eff} which depends on the temperature profile, from which we can have an idea about the purity of the plasma.

n_i (r) . The ion density has been determined by a special experiment. We have measured the attenuation of an H° beam passing through the T.F.R plasma [4]. This attenuation is proportional to the total cross-sections :

$$\sigma_t = \sigma_{D,H} \frac{n_{o,H}}{n_e} + \frac{<\sigma e\ v_e>}{v_{bi}} + \sum_{i,z} \frac{n_{i,z}}{n_e} \sigma_{i,z} \quad (2)$$

Knowing the cross-sections $\sigma_{D,H}$, $\sigma_{i,z}$ which have been now measured [5] we can deduce σ_c from attenuation of the beam versus energy [Fig. 1]. The best fit gives $n_D/n_e \simeq 0.75$. The n_i profile has been measured up to 10 cm and we find n_i proportionnal to n_e which has been extrapolated up to 20 cm. The given value is typical of plasma with $Z_{eff} = 3$ and oxygen dominant impurity density : 2.5 % n_e
The present determination is also important for fast neutral injection because it enables us to calculate the initial capture profile of fast injected neutrals. The ion temperature profile has been mainly measured by recording the energy distribution of fast escaping

$T_i(r)$ atoms using an electrostatic analyzer which has been moved up and down (from + 13 to - 13 cm in the plasma) in the median plane between 2 main toroidal coils and also in a plane making an angle of 8° in the toroidal direction . By this experiment we have confirmed that one part of the profile is close to the real temperature profile except for the correction due to the different attenuation of fast neutrals during their flight inside the plasma..This correction depends on n_i (r), but mainly on n_o(r) the density of neutrals. Up to now we have not completely explored the possibility of determining T_i(r) by measurements of the Doppler broadening of impurity lines which could confirm the charge exchange measurements. We measure some ion temperature by this method with the help of CIV emission which seems to show that T_i is higher than T_e at the plasma boundary, but in the high

magnetic field of T.F.R we must take into account Lorentz effect which could overestimate the broadening. It has been reported [6] how difficult it was on TFR to compare the ion temperature deduced by measurement of neutron flux and charge exchange neutrals, so only in few cases we get a good comparison. During fast neutrals injection the comparison has not been possible, the reason why is explained in [7].

n_o (r) . The density of neutrals is known by measurements of absolute emission of H_β light from the plasma. But this involves an Abel inversion which is always controversial, specially if the non inverted data presents a hollow at the center. In that case the error on the central value can be very very large. n_o (r) can also be measured by absolute determination of the flux of the charge exchange neutrals if n_i (r) is well known. When the comparison of these two measurements is possible and made they differ from a factor of about 2. Nevertheless these measurements have not been made in all cases or are not physically plausible, so we have used for the correction some of our measurements and some of the ATC measurements [1]. The neutral density has been written : $n_o(r) = n_o(o) + n_o(a)e^{-\frac{a-r}{\lambda}}$ where λ is a sort of penetration length. We have found for example :

$$\lambda \sim \frac{9.6\ 10^{13}}{n_e(o)}\ (cm^{-3}, cm),\ \text{Log}\ n_o(o) = 58.5 - 1.23\ \text{Log}\ n_e(o)$$

The knowledge of $n_o(r)$ is also important in 2 terms of the energy balance. First in the charge exchange loss term - Roughly speaking the charge exchange loss terms is of order of 20-30 kW for central neutral density of about 10^8 cm^{-3}. But mainly $n_o(r)$ is important in the diffusion term P_D term which is the most important at the plasma periphery.

P_{bi} . Some words are still to be said about P_{bi}. We have already mentioned that P_{bi} depends critically on σ_t which can be measured or calculated if the impurity composition of the plasma is known - In the case of T.F.R the injection is done pratically perpendicular to the magnetic field (80°) so the confinement diagram is particular [Fig. 2] 4 different zones can be seen on the diagram : zone I where

the particles are passing, zone II where the particles describe "banana" trajectories , zone III where the particles are lost on the limiter, zone IV where the particles are blocked in the magnetic ripples and are fastly lost, the latter having been verified experimentally. With the help of a Monte Carlo type code [8], taking into account the real particles trajectories we calculate numerically the energy deposition inside the plasma. Fig. 3 shows for 2 typical plasmas the energy transferred to the plasma $P_{bi} + P_{be}$, the energy transferred to the ions P_{bi}, and the energy lost by charge exchange P_{ex}. Having defined all the needed quantities, we can now come to the experimental results, first to the ohmic heating case.

If we look upon the central ion temperature, it is enlightening to consider the old fashion representation of Artsimovitch [9] for D^+ and H^+ plasma [Fig. 4]. It immediately shows a difference of behavior between H^+ and D^+ plasma, roughly speaking it seems that the same curve can be obtained if we don't take into account the mass of the ion (A_i) in the Artsimovitch formula, which is really a non classical effect that we will find out all through the text. We have not found a satisfactory explanation to this phenomenon.

Now we will mainly consider the shots whose characteristics are given in tables 1 - 2. Fig. 5 shows the complete energy balance inside a magnetic surface for a well-documented shot. We observe that the energy balance is not exactly equilibrate. The plasma seems to diffuse a little bit faster than neoclassically. At the plasma center, the principal loss is heat conduction, at the outer part of the plasma it is the diffusion term which is dominant and more important than the neoclassical diffusion coefficient. The classical ions energy confinement time is 37 ms at the center and decreases with radius down to 12 ms at the boundary. Up to now we have only introduced neoclassical heat conduction. But due to the ripple in the magnetic field of T.F.R the ion heat conduction is increased [10, 11]. The new balance has been calculated with this supplementary conduction and it has been found that in all ohmic heating cases, the added term is small.

(In the less collisional plasma the ion conduction coefficient due to ripple is at maximum 250 cm^2/s at 16.5 cm where $X_{i\ neoclassical} = 1500\ cm^2/s$). This will not be the case during fast neutrals injection where the ion temperature is much higher and the collisionality smaller. Fig. 5 presents a good case in which $\mathcal{P}_{ei}$ is always positive. But in some cases simple extrapolations of $T_e(r)$ and $T_i(r)$ bring us to find $T_i(r) > T_e(r)$ for $r > 13$-14 cm and $\mathcal{P}_{ei}$ becomes negative and very large. The fact that $T_i(r)$ is larger than $T_e(r)$ at the plasma boundary is classically possible, the outer zone being heated by conduction from the inside and by hot neutrals coming from the plasma center. But finding $\mathcal{P}_{ei}(a) < 0$ is classically impossible in ohmic heated plasma. We believe that $\mathcal{P}_{ei}(a)$ can always be found positive, by changing only the extrapolation of $T_i(r)$ a little bit, as shown on Fig. 6, where in one case we find $\mathcal{P}_{ei}(a) = -4.3\ 10^5$ W and in the other case $P_{ei} = 2.8\ 10^5$ W. Nevertheless this phenomenon will be emphasised by fast neutrals injection and will be harder to explain.

In conclusion for ohmic heated plasma we have found that the conduction anomaly

$$\frac{X_{i\ experimental}}{X_{i\ neoclassical}} = \alpha \quad \text{is} \quad 0.8 < \alpha < 2 \text{ for } D^+ \text{ plasma}$$
$$2 < \alpha < 5 \text{ for } H^+ \text{ plasma}$$

without any obvious dependence of α with ν^* ($\nu^* = \frac{Rq\varepsilon^{-3/2}}{\nu_i \tau_i}$) for $0<r<12$ cm

The classical overall energy confinement time is of order of 10-15 ms for H^+ plasma, 20-30 ms for D^+ plasma. Again we find the plasma diffuses faster in H^+ than in D^+.

Let's consider now the case of the fast neutrals injection heated plasma. The main results obtained during fast neutral injection are the following :

1) The central ion temperature increases proportionally to $P_{bi}/\bar{n}_e$ (Fig. 7). This gives us $\Delta T_{i\ (ev)} = (20\text{-}24) P_{bi}/\bar{n}_e$ (kw, 10^{13} cm^{-3})

with a non significant difference between H^+ and D^+ plasma which at first sight is non neoclassical. But most important of all we have not observed any saturation of ΔT_i up to a 560 kW captured power which confirms the results of Ormak [12] and ATC [13].

2) At low injection level, we can easily calculate ΔT_i by a perturbation method [14] which gives :

$$\frac{\Delta T_i}{T_i} = \frac{\frac{P_{bi}}{P_{ei}} + \frac{\Delta n_e}{n_e}\left(1 + n_e \frac{\partial L_n \tau_{Ei}}{\partial n_e}\right)}{\frac{3}{2} - T_i \frac{\partial L_n \tau_{Ei}}{\partial T_i}} \qquad (3)$$

in the considered case $\Delta n_e/n_e < 5\%$ So (3) can be written

$$\frac{\Delta T_i}{T_i} = \frac{P_{bi}/P_{ei}}{\frac{3}{2} - T_i \frac{\partial L_n \tau_{Ei}}{\partial T_i}}$$

Fig. 8 shows the results for a 200 kA plasma. We see that $\frac{\Delta T_i}{T_i} = \frac{2}{3} P_{bi}/P_{ei}$ which can be a neoclassical dependence for a plasma which is not yet in a pure banana regime and no more in the plateau regime. This relation means that the ion energy confinement time is independent from the ion temperature.

3) After beam cut-off the e-folding time of the ion temperature can give an idea of the ion energy confinement time. In fact for the plasma center, the energy equation can be written :

$$\frac{3}{2} \frac{d}{dt} n_i T_i = P_{ei}(t) + P_{bi} \exp - \frac{t}{\tau s} - \frac{3}{2} \frac{n_i T_i}{\tau_{Ei}} \qquad (4)$$

τ_s being the slowing-down time of the fast injected neutrals. During the injection in many cases we have found $n_i(t)$ = constant, $T_e(t)$ = constant and supposing that τ_{Ei} varies as T_i^{α} equation (4) gives :

$$(5)\quad \Delta T_i(t) = \Delta T_{i_{Max}} \left(1 - \frac{\frac{T_e}{T_e - T_{io}} - \alpha}{\frac{T_e}{T_e - T_{io}} - \alpha - \tau_{Ei}/\tau_s} \right) \exp - \left(\frac{T_e}{T_e - T_{io}} - \alpha \right) \frac{t}{\tau_{Eio}} + \left(\frac{T_e}{T_o - T_{io}} - \alpha \right) \frac{\exp^{-t/\tau_s}}{\frac{T_e}{T_e - T_{io}} - \alpha - \frac{\tau_{Eio}}{\tau_s}}$$

In the case where $\tau_{Eio} >> \tau_s$ (let us recall that $\tau_s \simeq 5$ ms) we obtain the approximate solution :

$$\Delta T_i = \Delta T_{i_{Max}} \exp - \left(\frac{T_e}{T_e - T_{io}} - \alpha \right) \frac{t}{\tau_{Eio}} \qquad (6)$$

this shows immediately that the observed e folding time is not equal to τ_{Ei} but to

$$\tau_{obs} = \tau_{Eio} \left(\frac{T_e - T_{io}}{T_e + \alpha (T_{io} - T_e)} \right)$$ the last term being smaller than 1.

The observed e folding time can range from 10 to 20 ms [Fig. 9] which will give $\tau_{Eio} \simeq 15 - 30$ ms. But in some cases this time can be very short $\tau_{obs} \leq 5$ ms and in that case the energy balance could not be explained classically. Furthermore, if we consider the decrease of the 5 kev neutral flux, we generally find a non-corrected e- folding time of 8-10 ms which can give 12-15 ms, which is quite short. In the case when the energy balance can be calculated [Fig. 10], the conduction anomaly α isn't found to be increased compared to the ohmic heating case even if ν_i^* decreases now to 0.45.

Nevertheless in some cases it seems very difficult to explain our results up to 20 cm. because the ion temperature is always larger than T_e at large radia [Fig. 11] and $\mathcal{P}_{ei}$ negative. This first point is difficult to explain by the deformation of the fast energy tail of the ion distribution [15] due to fast neutrals injection and some increased energy transfer between the fast ions and the plasma ions cannot be excluded. This can be supported by the observed increase of the plasma emission during injection, around the electron diamagnetic frequency [Fig. 12] but also and mainly around the ion cyclotron

harmonics which can be the evidence of an interaction between the fast ions and the plasma [Fig. 13]. Nevertheless the slowing down spectrum [Fig. 14] compares quite well to Fokker-Planck calculations [15]. Furthermore the decrease after beam cut-off of a given energy (22.5 Kev for example) is reasonably long (5-6 ms), much longer in any case than the calculated time predicted by beam-plasma instability calculations [16]. So we have not a really convincing explanation to this imperfect energy balance, except perhaps one which is given by simulation calculations. In fact simulation calculations give results very similar to experimental results [Fig. 15] if we suppose that the ion temperature has the most peaked profile which can be deduced from the experimental points and that the electron temperature is a little bit higher than the extrapolated one at the periphery.

On the other hand, the fast neutral injection in T.F.R has shown that : the perpendicular injection is as efficient as parallel injection. Non collisional plasma can be obtained but no spectacular results happen. The electron temperature does not change in general, which implies a decrease of the overall electron temperature confinement time, which can be linked with the observed impurity contamination of the plasma (mainly in our case by Molybdenum and oxygen. This last point has already been observed on ATC [17]).

In conclusion the study of the ion energy balance of the T.F.R plasma during the ohmic heated phase and the fast neutral injection phase shows that the ion heat conduction is closed to the neoclassical one for D^+ plasma, but a factor 2-5 larger in H^+, we also find that the diffusion of particles is much higher than the neoclassical one which is already known. The fast neutral injection shows that it is very difficult to establish in some cases a likely, classical energy balance up to the plasma boundary and an anomalous energy transfer between fast ions and the plasma cannot be completely excluded, more careful measurements of $T_e(r)$ and $T_i(r)$ up to the plasma boundary are needed to establish whether such an anomalous energy transfer does occur.

REFERENCES

[1] P.E. STOTT - Plasma physics vol. 18 p. 251, 1976.

[2] M. BERNARD - Rapport EURCEA FC 891, Avril 1977.

[3] F.L. HINTON et al. - Review of modern physics vol. 48 n° 2, p.239, 1976.

[4] T.F.R. Group - Submitted to nuclear Fusion.

[5] A. SALOP et al. - Phy. Rev. A13, B1312, 1976.

[6] T.F.R. Group - 7th European Conference on controlled fusion and plasmaphysics vol. II, Lausanne 1975.

[7] T.F.R. Group - Submitted to nuclear fusion.

[8] R. DEICAS et al. - Rapport EUR-CEA FC 726.

[9] L. ARTSIMOVITCH - Nuclear Fusion 2, 215, 1972.

[10] DNESTROVSKI et al. - Nuclear Fusion 15 - 6, p.1185, Dec. 1975.

[11] UCKAN et al. - ORNL TM/5603, Sept. 1976.

[12] R.A. ELLIS et al. - Nuclear Fusion, Letters, vol. 16, 3, p. 524, 1976.

[13] L.A. BERRY et al. - IAEA, CN 35/A4.1, Berchstesgaden Oct. 1976.

[14] L.A. BERRY et al. - IAEA, CN 35/A4.1, Tokyo, 1974.

[15] J.G. CORDEY, IAE, CN 33/A16.1, Tokyo, 1974.

[16] V.M. KULYGIN et al. - JETP, vol 43, n° 6, June 1976.

[17] S. COHEN - Journal of Nuclear Materials, 63, p. 65-73, 1976.

TABLE 1

PLASMA (D) AND INJECTION (D)

run	I_p KA	B_t KGs	$\bar{n}_e$ 10^{13}	nl 10^{15} cm^{-2}	P_E (KW)	P_N (KW)	P_{Ni} (KW)	P_{Ne} (KW)	$T_{i(o)}$ before	$T_{i(o)}$ during	$\Delta T_{i(o)}$
1	400	60	4.4	2.2	450	160	40	60	950	1150	120-200
2	380	60	5.	2.5	1100	385	96	140	1000	1300	300-350
3	200	50	2.8	1.4	680	240	67	50	800	1200	400
4	200	50	3.	1.5	950	330	90	115	800	1350	500-600
5	200	50	2.8	1.4	1300	455	110	110	800	1600-1700	800-900
6	300	55	5.	2.5	1340	480	116	170	920	1400	420
7	300	50	5.	2.5	1620	560	141	200	900	1400	500

TABLE 2

PLASMA (H) AND INJECTION (H)

run	I_p KA	$\bar{n}_e$ $10^{13} cm^{-3}$	nl 10^{15} cm^{-2}	P_E KW	P_{Ni} KW	P_{NE} KW	$T_{i(o)}$ before	$T_i(o)$ During	$\Delta T_i(o)$
1	300	4.6	2.3	988	46	60	850	1150	300
2	300	6.	3.	1130	85	109	900	1300	350-400
3	375	7.5	3.75	1140	101	130	950	1370	400-420
4	360	7.2	3.6	1140	100	130	950	1300	300-350
5	360	6.8	3.4	1170	118	122	950	1300	300-350
6	375	7.5	3.75	1220	123	138	950	1350	400
7	300	4.4	2.2	192	18	34	830	930	90-100
8	300	4.4	2.2	369	23	34	850	1030	180

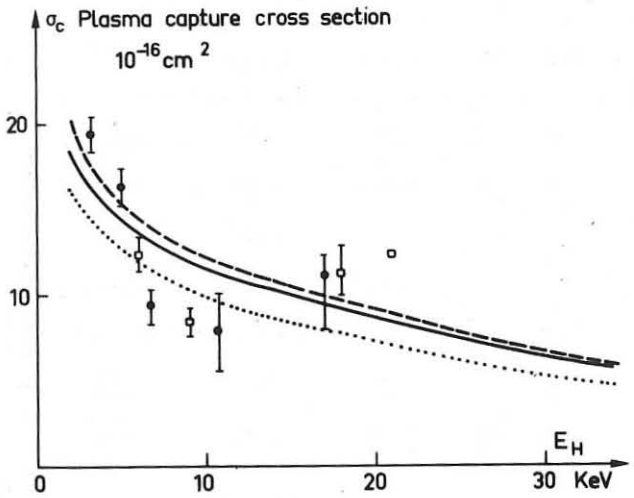

Fig.1

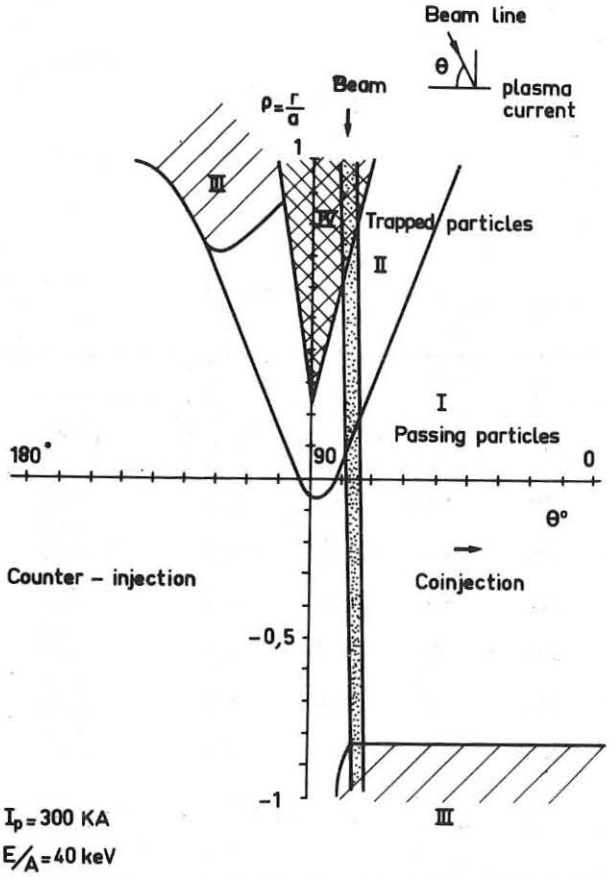

FIG.2

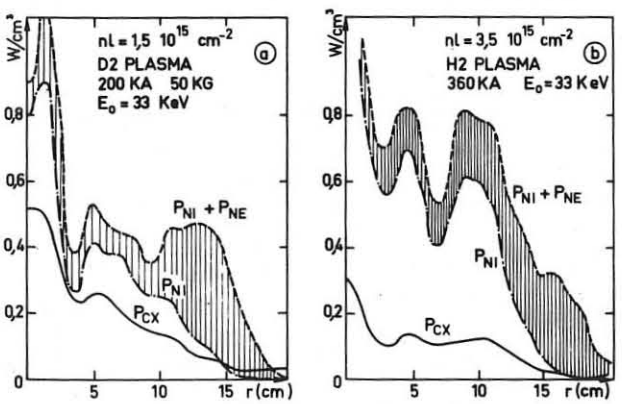

Fig. 3

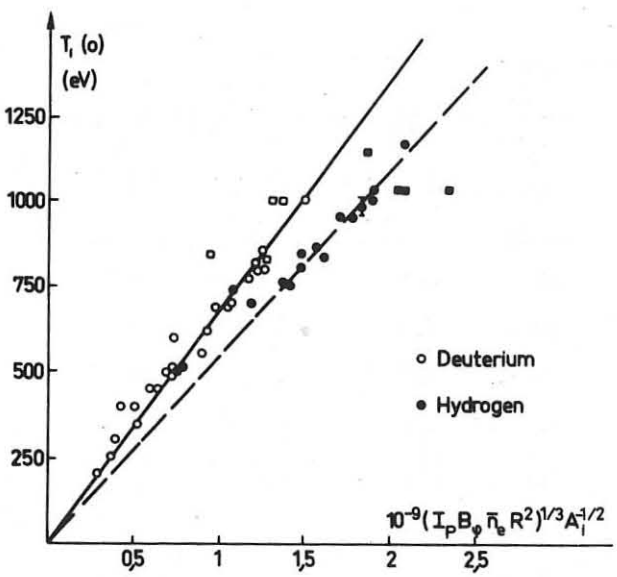

Fig 4

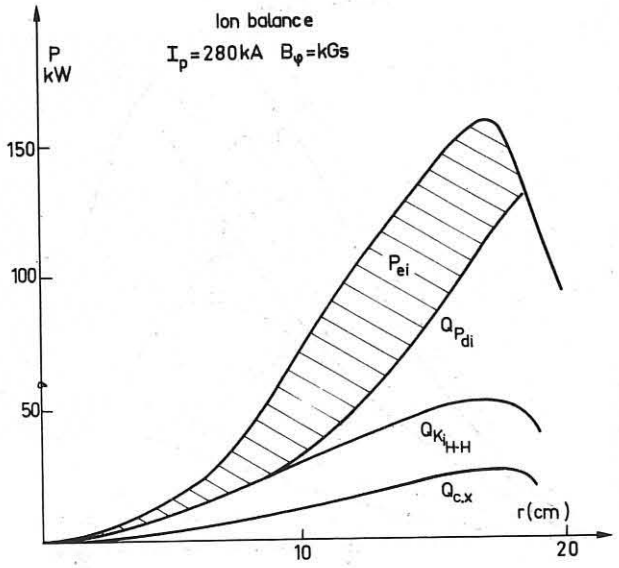

Fig. 5

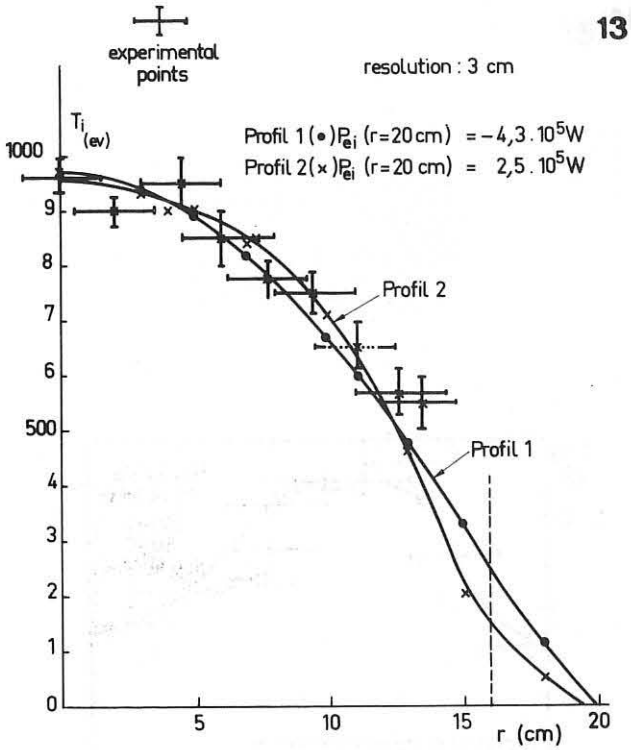

Fig. 6

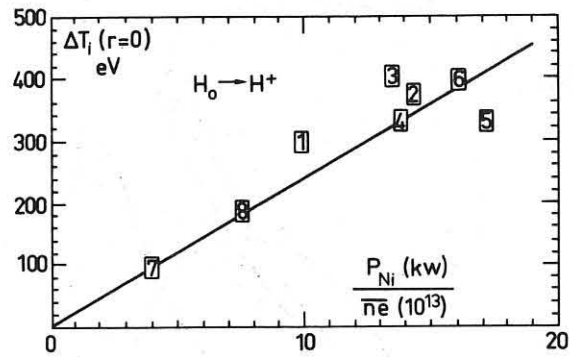

Fig 7a

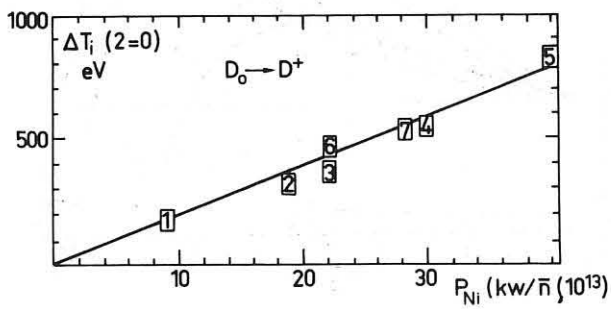

Fig 7b

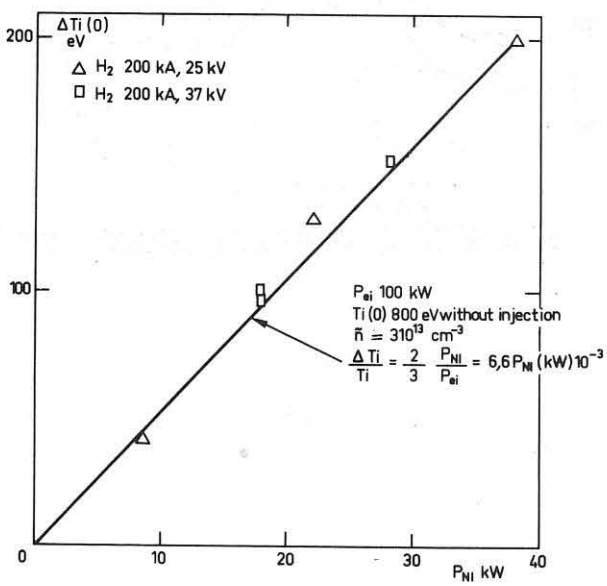

FIG.8

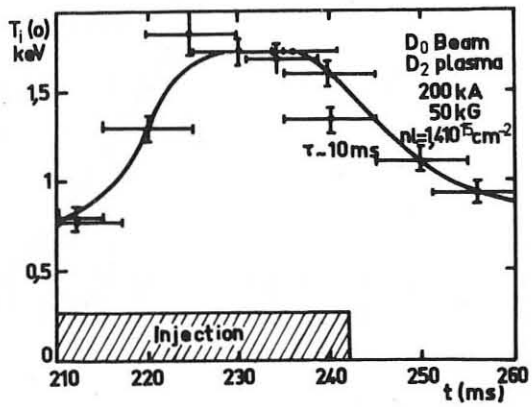

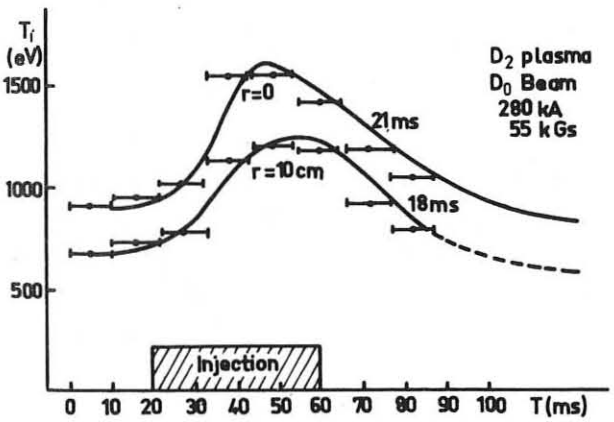

Fig 9

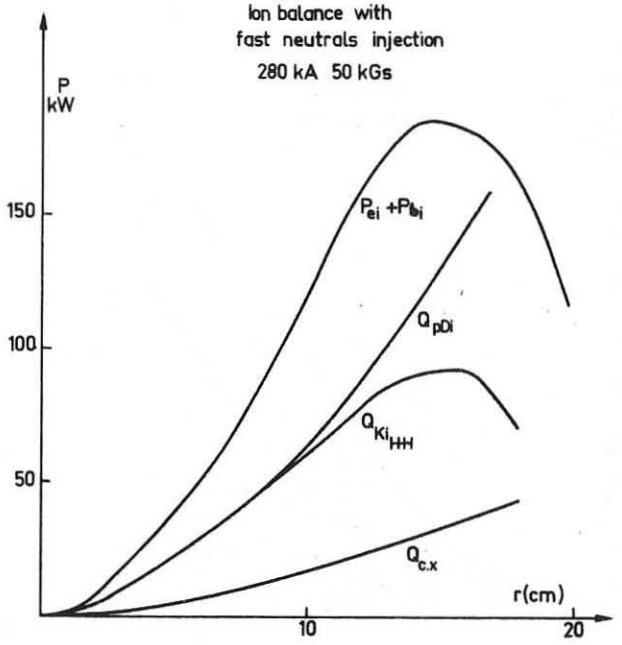

Fig. 10

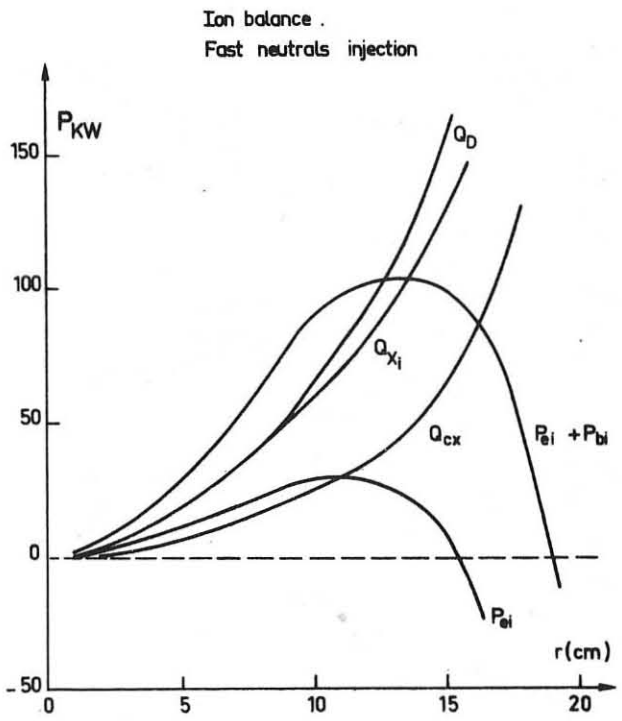

Fig. 11

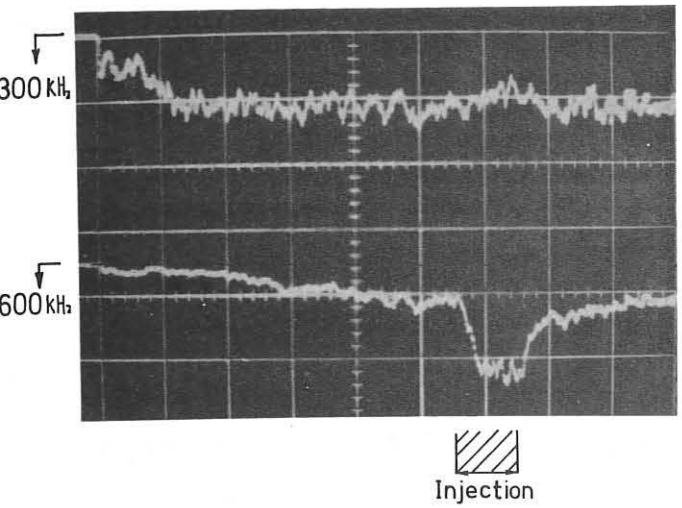

FIG. 12

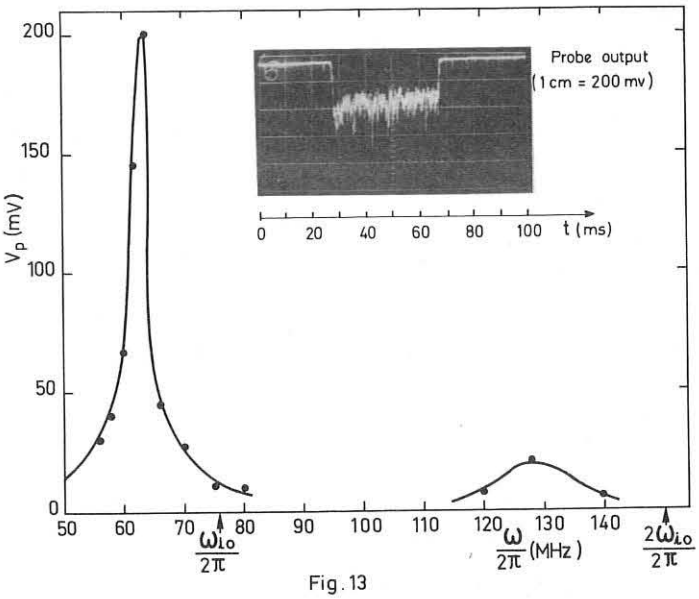

Fig. 13

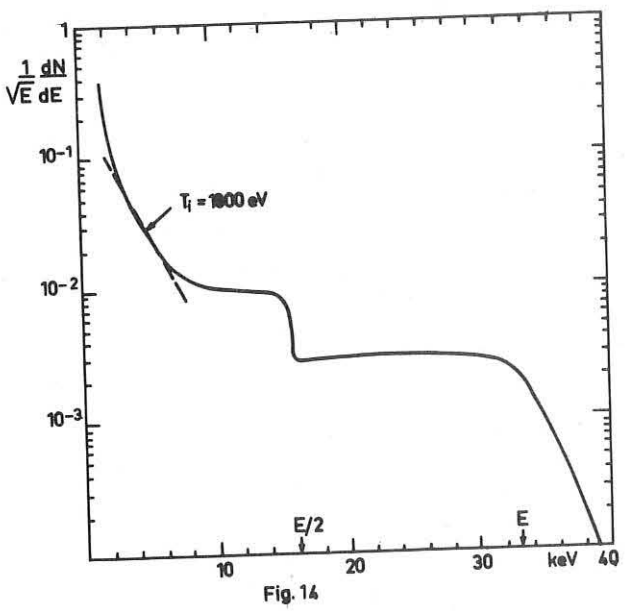

Fig. 14

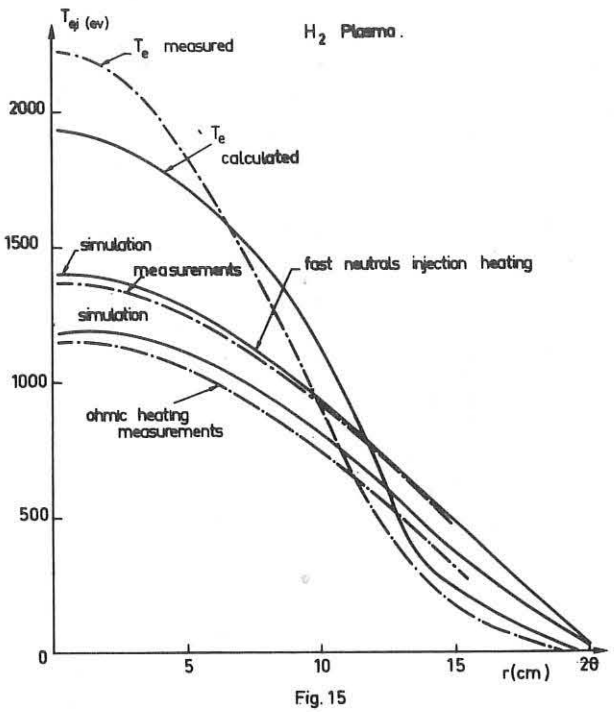

Fig. 15

RECENT RESULTS FROM THE PLT TOKAMAK

V. Arunasalam, C. Barnes, K. Bol, D. Boyd, K. Brau, N. Bretz, M. Brusati, S. Cohen, S. Davis, D. Dimock, F. Dylla, D. Eames, P. Efthimion, H. Eubank, H. Furth, R. Goldston, R. Hawryluk, K. Hill, E. Hinnov, R. Horton, J. Hosea, H. Hsuan, D. Ignat, F. Jobes, D. Johnson, M. Mattioli*, E. Mazzucato, E. Meservey, P. Moriette*, N. Sauthoff, J. Schivell, G. Schmidt, R. Smith, F. Stauffer, W. Stodiek, J. Strachan, S. Suckewer, S. von Goeler

Plasma Physics Laboratory, Princeton University,
Princeton, New Jersey 08540, USA

As reported at the Berchtesgaden meeting[1], the optimum plasma parameters during the initial phase of PLT operation were obtained by an empirical approach either in helium gas or in hydrogen gas with appreciable oxygen content. The second operating period has mainly been devoted to an investigation of this observation, and to an effort to vary, and especially to lower, the effective ion charge, Z, with a goal of obtaining stable discharges at high plasma densities. The third phase, supplementary heating with neutral beams, is beginning. This paper reports some of the results of the second phase.

The main result has been the recognition of the importance of radiation in the power balance. In smaller tokamaks, the energy confinement was mostly determined by plasma transport. In PLT, although transport is important, even in the central core of the plasma, power loss by radiation is often equally important. This reflects the fact that as devices are made larger, the ohmic power input density decreases and the confinement due to plasma transport improves, and so volume effects like radiation will gain importance.

In Section I, we discuss impurity behavior, specifically the control of oxygen by discharge cleaning and the identification and quantitative measurement of tungsten radiation. In Section II, we compare the main types of PLT discharges, classified by tungsten content and MHD instability properties. In Section III, we discuss plasma confinement.

I. Impurity Behavior

(A) Low Z Impurities - The second phase of PLT operation begain with an effort to remove oxygen (the dominant low-Z impurity) from the discharge by low temperature discharge cleaning in hydrogen (TDC). It has been shown by Taylor[2] that TDC removes oxygen better than higher temperature discharges (Figure 1). The method is to raise the hydrogen pressure until the

---

* On leave from Fontenay aux Roses

ohmic heating current is throttled from ~50 kA, to ~5 kA, the exact level being adjusted so as to maximize the pressure of water vapor at the pumps. Carbon is removed efficiently by either method, chiefly as methane. Table I illustrates the reduction of the relative oxygen and carbon concentration effected by the TDC method.

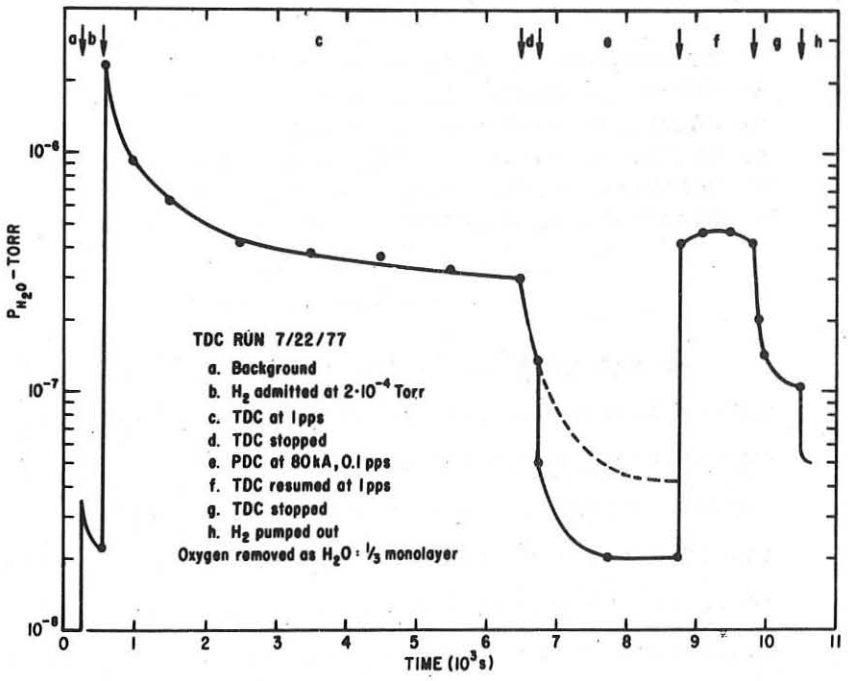

Fig. 1 Discharge cleaning in PLT. The partial pressure of water vapor is measured with the mass analyser during discharge cleaning and plotted against time. During the time invervals a, b, c..., indicated by arrows at the top of the graph, conditions were changed. The water vapor pressure is very high when TDC (time interval c and f) is applied and very low when PDC is used (time interval e).

(B) High Z Impurities: Tungsten - The primary effect of diminished light impurity concentration was an increase in radiation from the plasma core, sufficient to cause collapse of the electron temperature (Figure 2). Careful investigation[3] of iron, chromium and nickel (wall material) shows that their contribution to the power loss is not important; no evidence of an accumulation of iron in the center of the discharge was detected. Most of this radiation is attributable to tungsten, the limiter material and much effort has been devoted to a quantitative evaluation of the effect of tungsten.

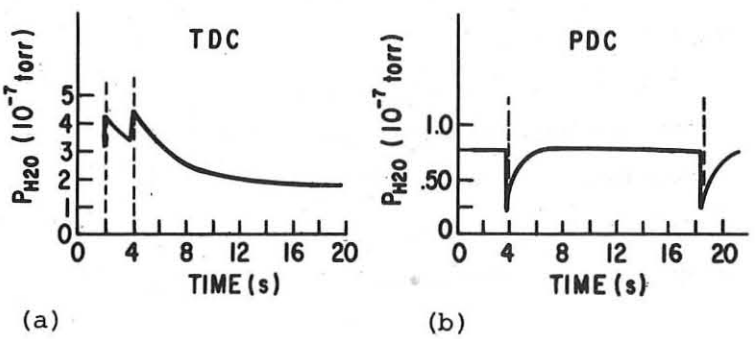

Subfigure (a) and (b) show the water vapor reading between shots for TDC and PDC respectively. The TDC shot produces water, a PDC shot decreases water.

In experiments at NRL[4] and Oak Ridge[5], strong bands of tungsten lines around 50 Å have been discovered which are believed to be $\Delta n=0$ transitions (4d-4f) (4p-4d)(4s-4p) from the ionization states W XVIII (ionization potential ~420 eV) to W XLVI (ionization potential ~2400 eV).[6] Also, computer calculations of radiative power have been performed with the average ion model[7] which predict unexpectedly high emissivities.

Experimentally, the radiation has been investigated with a grazing incidence VUV spectrometer and with unshielded surface barrier diodes (USX-detectors). A VUV spectrum is shown in Figure 3. There are three bands of radiation, centered around 33, 50, and 59 Å, with the intensity in the ratio 3:5:2, each consisting of many overlapping lines. The broader band ($0.1<h\nu<1$ keV) USX-detector data are in close agreement with the VUV results. These diagnostics make possible relatively exact measurements of the total intensity of the tungsten radiation.

Table I

Gas Discharge Cleaning	Helium PDC	Deuterium PDC	Hydrogen TDC	Helium TDC	Deuterium TDC
Date	9/28-29/76	10/5/76	2/10-11/77	3/2/77	5/4/77
$\frac{n_{oxygen}}{n_e}$*	1.5%	7.5%	0.5%	0.5%	1.0%
$\frac{n_{carbon}}{n_e}$*	1.8%	1.2%	0.4%	0.4%	0.7%
Z_{eff}*	3.2	5.6	1.4	2.3	1.6

*Spectroscopic measurements during the initial stages of discharge. Later in the discharge, the Z_{eff} from the influx was usually somewhat higher.

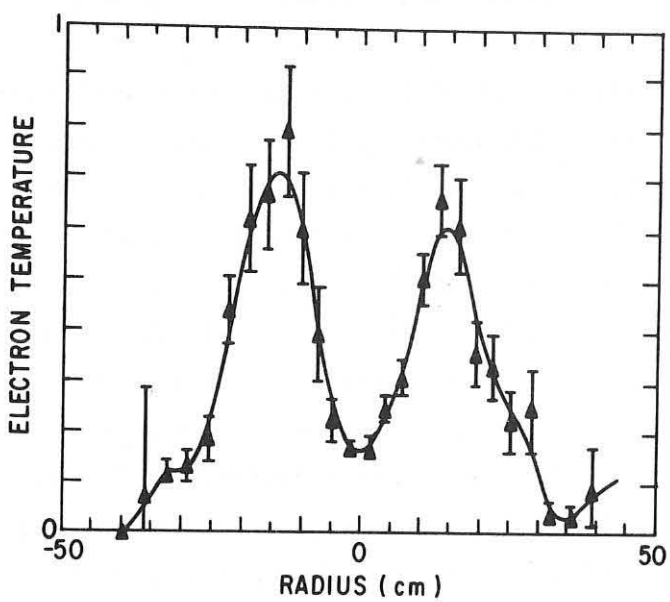

Fig. 2 Hollow radial profile of the electron temperature measured by Thomson scattering in a low density deuterium discharge. In the hollow region, power loss due to tungsten radiation exceeds ohmic heating power input. The Z_{eff} is relatively low, however. Discharge conditions: B_{TF} = 32 kG, I_{OH} = 360 kA, V_{OH} = 2.1 V, D_2, a = 40 cm, $\langle n \rangle = 2.6\ 10^{13} cm^{-3}$, $\tau_{E_e}^{-1}$ = 8.65 ms, Z_{eff} = 2.3.

II. Discharge Types

During the first PLT phase, discharges were classified by certain MHD instability patterns: m=1 "sawtooth" discharges, "large m=2," "small m=2," etc. During the second phase, the concentration of tungsten became a classifying parameter of equal importance. The control of tungsten concentration is thus a major consideration in selecting operation conditions. In this regard, measurements of both ion and electron temperatures at the plasma edge have confirmed the view that there is positive correlation between edge temperature and tungsten concentration. However, it is clear that edge temperatures and MHD instabilities are coupled through changes in current profile, and the relative importance of each has not yet been sorted out. The mechanism for tungsten injection also remains unclear: Sufficient amounts could be released either by sputtering from the limiter by highly stripped oxygen ions accelerated in the sheath, or by unipolar arcs on the limiter.[8] Arc Tracks, in fact, can be seen on the limiter.

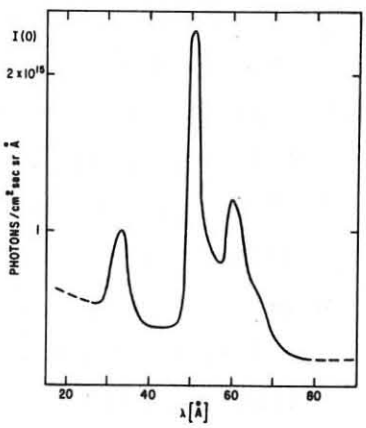

Fig. 3 VUV-spectrum in the 50 Å region, showing the tungsten bands centered around 33, 50, and 59 Å.

Table 2 compares five different discharge regimes which differ in the way the plasma edge was cooled, but with similar currents and toroidal fields (I_p = 400-500 kA, B_T = 30-35 kG). These are discussed in more detail below.

(A) Discharges with Hollow Temperature Profiles - (Type I) - Hollow temperature profiles develop reproducibly at low filling pressures after thorough discharge cleaning with TDC. (They were sometimes observed before TDC was applied.) The time development of the electron temperature is shown in Figure 4. The transition from a peaked to a hollow profile at time t=150 ms is typical although it is sometimes observed that the profile can stay hollow throughout the discharge, or that a minor disruption can fill in the hole. Due to the small current ($\propto T_e^{3/2}$) in the central region, the central ohmic heating power input is smaller not only than the total radiated power, seen by the bolometer, but also smaller than the tungsten radiation alone (Table 2). The radiation is therefore sufficient to maintain the hollow profile. Actually, heat must be transported into the hollow region to make up the difference between radiation loss and

Table 2

	I	II	III	IV	V
	Hollow Discharge	Peaked m=2 Discharge	Sawtooth Discharge With Gas Programming	High Density Helium	Discharge with Low Z Contamination
1. Working Gas	H_2,D_2,He	H_2,D_2,He	H_2,D_2	He	H_2+O H_2+Ne
2. Discharge Cleaning	TDC	TDC PDC	TDC	TDC	PDC
3. $T_e(0)$ (keV)	$\lesssim$.3 ($T_{e\ max} \approx$ 0.5-0.8)	0.7-1.5	1.0-2.0	0.8-1.4	1.4-2.5
4. $T_e(r)$	Hollow	Peaked Intermittent	Peaked	Peaked	Peaked
5. $n(0)$ (10^{13} cm^{-3})	3-4	3-5	4-8	10-15	3-6
6. Z_{eff} (From Laser)	2.5-5.0	3.0-5.0	2.0-5.0	$\approx$2	5.0-15.0
7. τ_{E_e} (ms)	$\lesssim$5	$\lesssim$15	$\lesssim$30	$\lesssim$50	$\lesssim$30
8. Tungsten Radiation (USX) W(0) (mW cm^{-3})	~500	~700	~400	~150	~200
9. Bolometer Radiation W(0) (mW cm^{-3})	~800	~800	$\approx$400	~400	~400
10. Central Ohmic Power Input $W_{OH}(0)$ (mW cm^{-3})	~200 W_{max} ~1000	~1100	~1200	~1000	~1000
11. $T_i(0)$ (Charge Exchange) (keV)	0.5	$\lesssim$0.9	$\lesssim$1.2	Not Measured	?
12. T_{Ei} (ms)		$\lesssim$70	$\lesssim$100	Not Measured	?
13. Fusion Neutrons (sec^{-1})	$\lesssim 10^7$	$\lesssim 10^9$	$\lesssim 10^{10}$	---	10^{10}
14. MHD Instabilities From X-Rays	m=3 (m=2)	m=2	m=1 Sawteeth	m=1 Small Sawteeth	m=1 Large Sawteeth

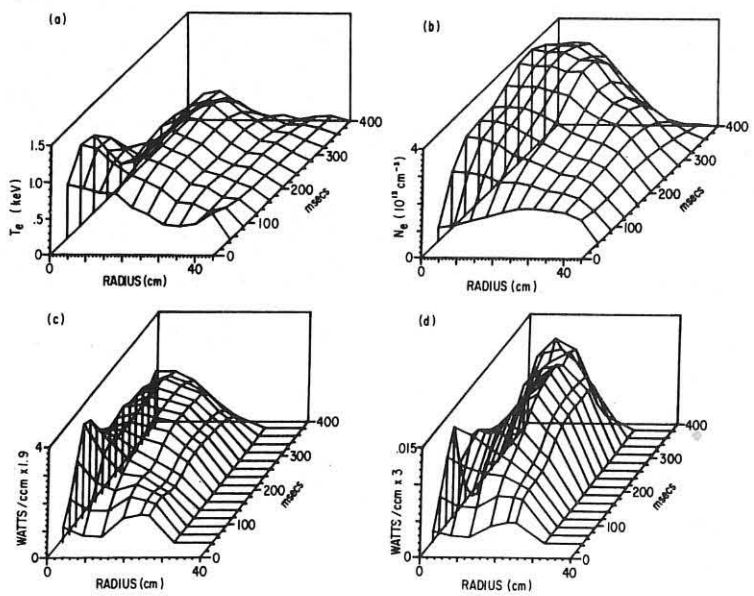

Fig. 4 Time development of a hollow deuterium discharge. (a) and (b) plasma electron temperature T_e and density n_e from Thomson scattering, (c) radiation in the 50 Å region from Abel inverted USX-data, (d) radiation in the 14 Å region from the USX detector. (The factors 1.9 and 3 on the ordinate are corrections for detector efficiency.)

power input. The transition from the peaked to the hollow profile is being analysed in terms of the thermal instability[9], with only partially satisfactory results. From the data during the peaked and the hollow phases, an empirical value for the heat conductivity is derived which is about the same for both phases. The calculated heat conductivity is so large that it inhibits the formation of the hole. Either a lowering of the heat conductivity, possibly locally during the transition period or an enhanced tungsten concentration in the center has to be assumed to allow the mechanism of Reference 8 to work. These results are, however, preliminary.

Hollow discharges tend to turn into peaked m=2 discharges (Type II) after some time of operation, often going through a period when discharges are intermittently hollow or peaked. In the Type II discharges (Figure 5) the central tungsten radiation is often stronger than in hollow discharges. The initial level, however, is low and rises later. Also, the oxygen content is usually somewhat higher. The main discharges in PLT apparently allow oxygen to build back up on the walls instead of removing it as the low-temperature discharges do; this gradually leads to transition from hollow to peaked discharges.

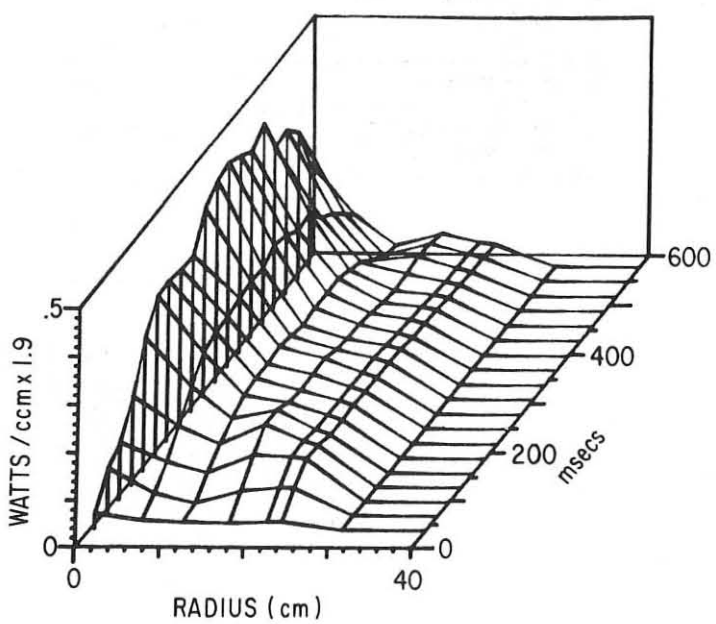

Fig. 5 Time development of the tungsten radiation in a peaked deuterium discharge.

(B) Programming of the Flow of Neutral Gas - With careful programming of the flow of neutral gas, the tungsten influx can be minimized. In practice, this means a high enough initial pressure to prevent too broad a current channel, and as much gas fed in during the discharge as possible while avoiding disruptions. The resulting discharges (Type III) have higher density, less tungsten radiation (Figure 6), higher electron and ion temperatures, and may exhibit sawteeth oscillations associated with the m=1 tearing mode.

In helium, gas programming is especially successful, and the central plasma density can be increased to 1.5 X 10^{14} cm^{-3}. We have therefore grouped these discharges in a separate column in Table 2 (Type IV). These discharges have the best confinement. The tungsten radiation level is very much reduced. In hydrogen, the initial tungsten level is about the same as in helium, but it has not been possible to keep it low during the later stages (Figure 6). This is probably a primary reason why the results in helium are better than in hydrogen or deuterium.

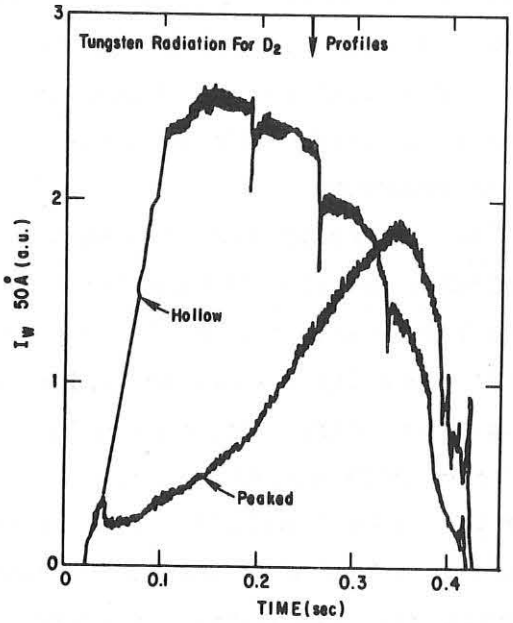

Fig. 6 Comparison of the 50 Å radiation in a hollow deuterium discharge (Type I) and a sawtooth discharge with gas programming (Type III). The late rise of the tungsten radiation in the deuterium discharge was avoided in high density helium discharges.

(C) Neon Injection - Increasing the low Z impurity content, of course, reverses the effects of discharge cleaning and reduces the tungsten radiation. This occurs either naturally, when the machine is dirty or when a leak opens up in the vacuum vessel, or artifically by pulsing neon injection, as shown in Figure 7. Initially, the deuterium discharge has a very high level of tungsten radiation. Around the time t≈200 ms, neon is injected, the tungsten radiation drops by a factor 5, and the central electron temperature increases from 900 eV to 2000 eV.

Discharges with low-Z contamination have the highest electron temperature (up to at least 2.5 keV). However, the density is limited by disruptions to relatively low values.

III. Energy Confinement

Measurement of the increase in temperature of the limiter after a plasma shot shows that only a small fraction (5-10%) of the total ohmic heating input is deposited on the limiter. Bolometer measurements indicate that 70-90% of the power input goes to the wall as radiation (including a small contribution by charge exchange neutrals). The difference, 5-30%, may

represent charged particle transport to the vacuum vessel wall but is within the probable error of the measurements. The predominance of radiation losses distinguishes PLT from our earlier tokamaks.

For the energy balance within the plasma, we encounter two situations. In the first case, the local ohmic heating heating power input is almost balanced by radiation loss. This occurs in discharges with strong tungsten radiation (Type I and II). The energy balance in a hollow discharge is shown in Figure 8a. The curves for power input and radiation track each other closely (lower left). Plasma transport plays a minor role in the overall energy balance.

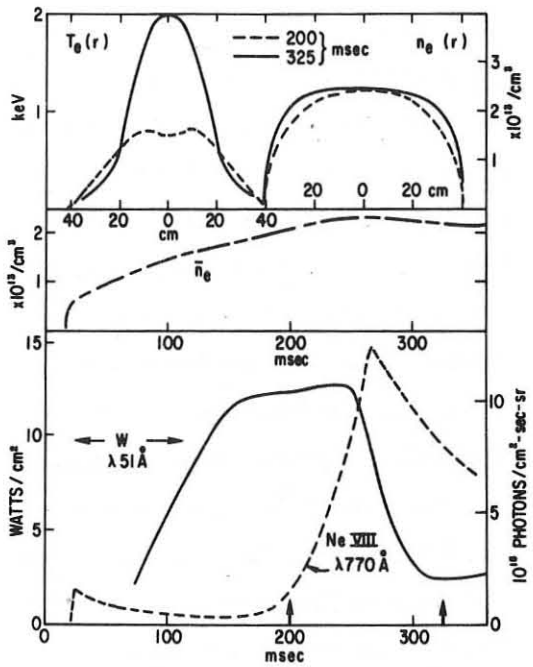

Fig. 7 Effect of injecting neon into a deuterium discharge at ~200 ms. The 50 Å tungsten radiation decreases strongly as neon enters the discharge (bottom). The electron temperature rises rapidly in the center and cools somewhat on the outside of the plasma column (top).

When tungsten radiation is small relative to power input (Type III, IV, V), plasma heat transport plays a larger role, particularly in the central region (Figure 8b). At larger radii near the limiter, radiation loss catches up with the power input. This outer radiation zone represents a virtual limiter[10], a highly desirable feature for protecting the physical limiter.

"Gross" confinement times, τ_E, that is total energy content (ion plus electron) divided by total ohmic heating power, are shown in Figures 9 and 10. Figure 9 refers to discharges before TDC, and Figure 10 to recent TDC-cleaned helium discharges. The best confinement times are around 70 ms, and we tentatively conclude that they follow the familiar $n_e a^2$ scaling.

In order to obtain a true measure of energy transport through the plasma, some account must be taken of radiation. All the discharges of Figures 9 and 10 were optimized for confinement time (i.e., those of Types III, IV, V), and the radiation from the central core in those cases is typically 20-50% of the input power. The range is due partly to

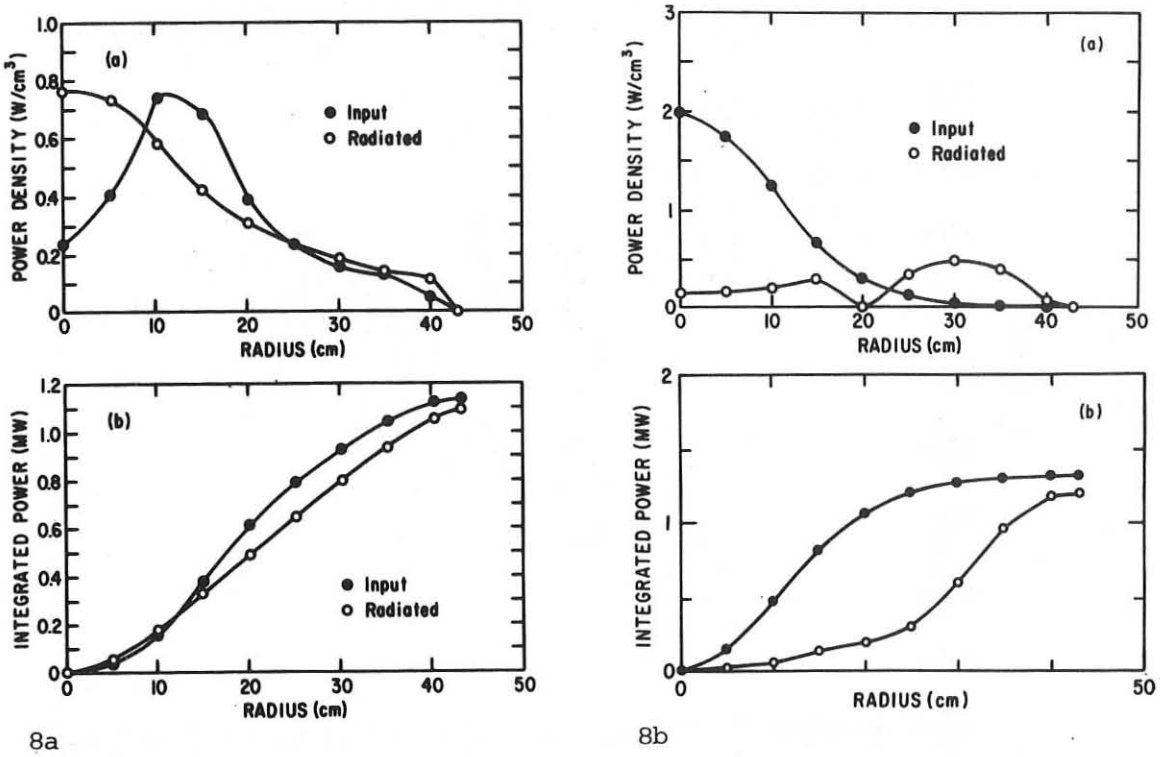

Fig. 8 Internal energy balance for a hollow deuterium discharge (a), and neon discharge (b). Plotted are (top) power input and radiation loss per cm^3 vs radius, and (bottom) the volume integrals over these quantities up to radius r.

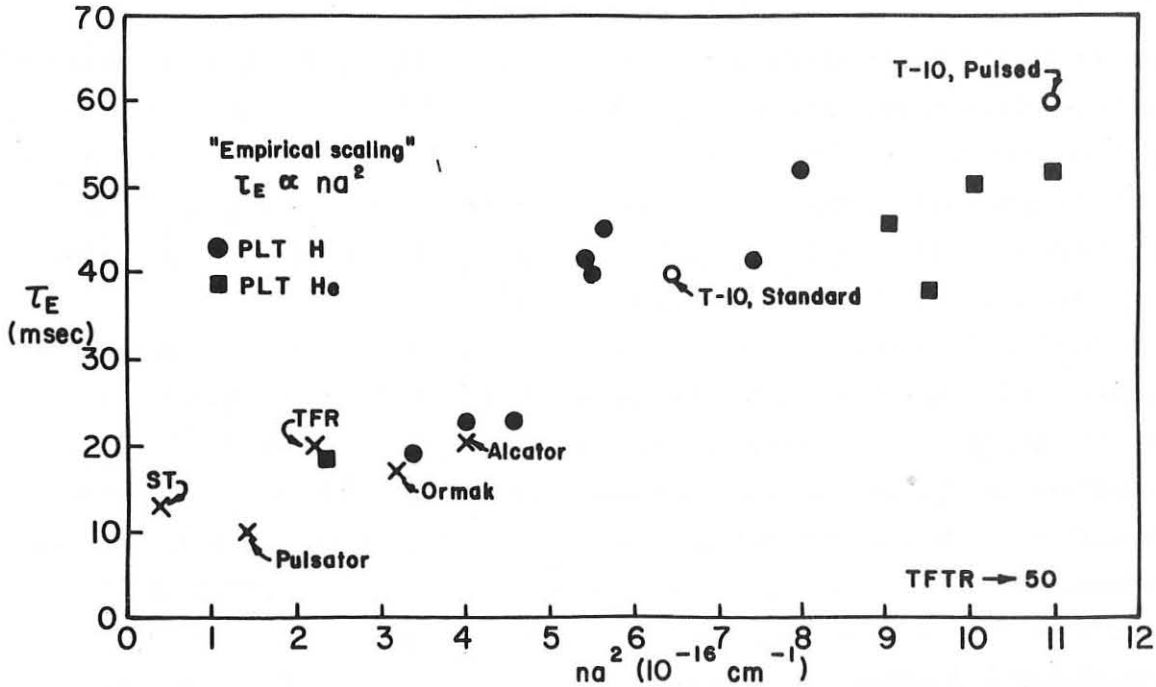

Fig. 9 Energy confinement time vs $n_e a^2$ where n_e is the average density and a is the limiter radius.

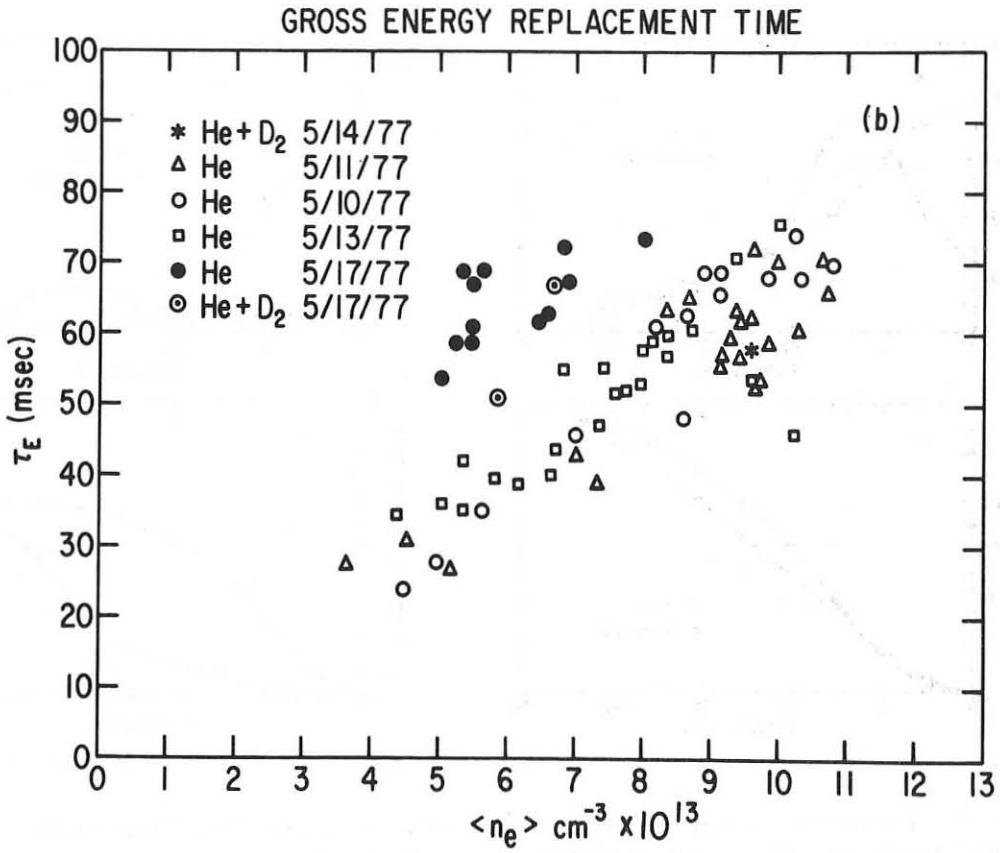

Fig. 10 Energy confinement time vs density for high density helium discharges.

changes in discharge conditions, but also reflects a systematic tendency of the bolometric measurements to give higher loss rates than VUV spectroscopy. In these cases, then, the "transport confinement time," $W_{tot}/P_{in}-P_{rad}$), is at least 20% higher than the "gross" confinement time, or $\gtrsim$85 ms in the best cases. A systematic analysis of local energy transport in a variety of discharges is still in a preliminary stage.

For the investigation of the ion heat transport, the ion temperature was measured with charge exchange (using a neutral beam to enhance the neutral density in the center), with neutrons, and from the Doppler broadening of impurity lines. A typical radial profile of the ion temperature in a peaked sawtooth discharge (Type III) is shown in Figure 11. A detailed investigation of the ion energy balance, following Stott[11], shows that neoclassical heat conduction is the dominant process in determining the radial ion temperature profile. Charge exchange losses must be low because of the low neutral density in PLT. Some details are given in Figure 11 (lower right). In hollow discharges, the central ion temperature actually exceeds the electron temperature, because of the ion heat transport into the hollow region.

Summary

Low-temperature discharge cleaning has been used successfully on PLT to reduce the amount of oxygen (the primary low Z impurity in the discharge). With this reduction of low Z impurity concentration, the highest electron density is $\langle n_e \rangle \simeq 10^{14}$ cm^{-3}, and longest "gross" energy confinement time is $\tau_E \simeq 70$ msec yielding a "transport" confinement time $\gtrsim 85$ ms. The effective ion charge, Z, has been reduced, but larger values of density and confinement time have not yet been achieved in D_2 discharges, and to only a slight extent in helium discharges. Gas injection programming must be used to obtain these good values; otherwise large amounts of tungsten radiation can overwhelm the discharge, causing it to develop a hole in the radial electron temperature profile; the associated confinement time can then be very low (~5 msec). It appears likely that edge cooling of the plasma is the mechanism that inhibits the influx of tungsten and makes possible the development of discharges with 70 msec confinement.

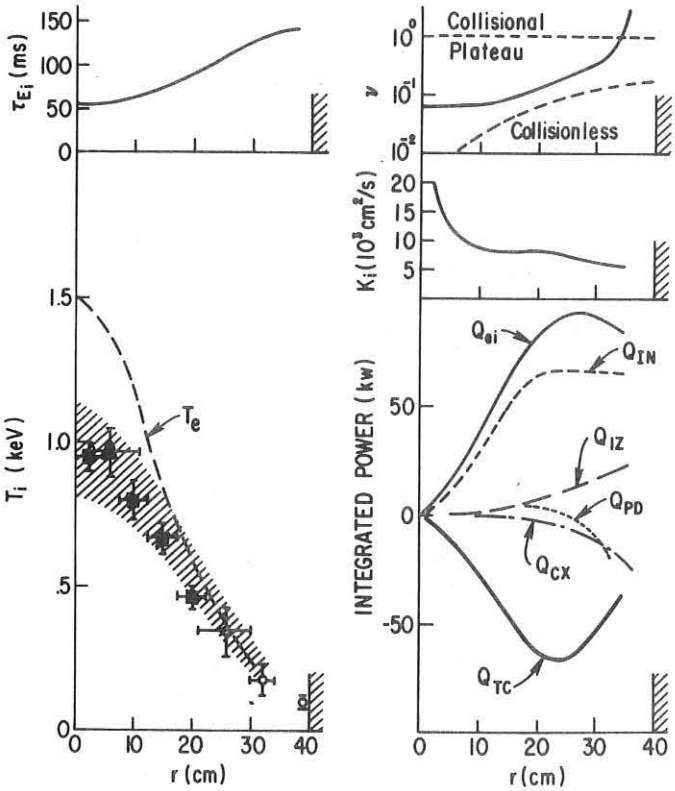

Fig. 11 Ion energy balance. The ion temperature profile was measured with charge exchange ■ neutrons ▲, and Doppler broadening o (lower left). The ion temperature calculated with a computer code (shaded area), using Thomson scattering electron temperatures and a neutral gas diffusion code which incorporates electron ion coupling (Q_{ei}), neoclassical thermal conduction (Q_{TC}), particle diffusion (Q_{pd}), charge exchange (Q_{CX}) and electron ionization (Q_{IZ}) (lower right). Plotted also are the ion energy confinement time, τ_{Ei} (top left), the neoclassical heat conductivity K_i (top right), and the collisionality parameter $\nu^*/\varepsilon^{3/2}$ (top right).

Acknowledgements

The continuing support of Drs. M.B. Gottlieb and H.P. Furth is gratefully acknowledged. These experiments were carried out with the excellent technical assistance of M. Perron and his crew and the fine support of the computer group under F. Seibel.

REFERENCES

[1] D. Grove, et al.: Plasma Physics and Controlled Nuclear Research, Berchtesgaden, 1976 (Vienna, International Atomic Energy Agency, 1977), Vol. 1, p. 21.

[2] R.J. Taylor and L. Oren: UCLA Report, PPG-294 UCLA (1977).

[3] E. Hinnov, et al.: Bull. American Physical Society, 21, 1159 (1976).

[4] R.G. Burkhalter, et al.: Naval Research Laboratory Report, NRL-3444 (1977).

[5] R.C. Isler, et al.: Phys Lett. (to be published).

[6] R.D. Cowan: Los Alamos Sci. Lab. Report, LA-6679-MS (1977).

[7] R.V. Jenson, et al.: Princeton Plasma Physics Laboratory, PPPL-1334 (March, 1977).

[8] G.M. McCracken: Private communication.

[9] H.P. Furth et al.: Phys. Fluids 13, 3020 (1970).

[10] W. Stodiek: 5th European Conference on Controlled Fusion and Plasma Physics, (Grenoble, Centre d'Etudes Nucleaires, 1972) Vol. 2, p. 1.

[11] P.E. Stott: Plasma Physics 18, 251 (April, 1976).

REVIEW OF TOKAMAK THEORY RESULTS

V.D.Shafranov
I.V.Kurchatov Institute of Atomic Energy

One of the remarkable achievments in controlled nuclear fusion research was a creation of a new physical object - the high-temperature toroidal plasma column. It lives for about 1 s in large installations. One can manipulate with it: to form different shapes of its cross-section, to compress and to move the column. All this confirms the macroscopical stability of a tokamak plasma under appropriate conditions. It is natural that the major part of theoretical works on controlled fusion is devoted currently to studies of processes in such a plasma in accordance with experimental needs.

The change in stability conditions leads, sometimes unexpectedly, to disruption of the column, plasma contamination and cooling. Investigation of these processes remains to be the main theoretical problem.

A disruptive instability impedes but does not prevent us from achieving the goal - the heating of the plasma up to temperatures necessary for a fusion reactor. One of the objects of the present-day theory is analysis of difficulties arising in a reactor plasma due to the presence of the fusion reaction products - high-energy α-particles - and due to the interaction of a high-temperature plasma with chamber walls as well.

In accordance with the said above one can distinguish three main lines in the tokamak theory: I. Macroscopically stable plasmas; II. Macroinstabilities; III. Reactor plasmas.

I. Macroscopically Stable Plasmas.

There are following problems here: a) Transport; b) Impurities; c) Run-away electrons; d) HF heating; e) Neutral atom injection; f) High problem and evolution of a two-dimensional equilibrium. We shall consider briefly their status.

a) Transport. As was known for a few years a classical transport theory in a toroidal geometry (so-called neoclassics) explains satisfactorily only the energy balance of the plasma ion component. In order to achieve full agreement of calculat-

ed density and temperature profiles with empirical ones correction factors or items are introduced phenomenologically into one-dimensional transport codes.

Dnestrovsky and Kostomarov /1/, for example, introduce a factor of anomality depending on the ratio γ of the drift current velocity to the sound velocity into resistance $\zeta = \gamma \zeta_{cl}$ and that with additional factors γ_1, γ_2 into heat conductivity and diffusion coefficients: $\chi_e = \gamma_1 \gamma \chi_{neocl}$, $\gamma_1 \approx 7$, $\mathcal{D} = \gamma_2 \gamma \mathcal{D}_{neocl}$ Mercier et al. /2/,/3/ use an enhanced Pfirsch-Schluter transport coefficient, the factor of anomality being $\sim 10^3$. A multi-regime code by Duchs et al./4/ depending on a collision frequency uses seven different expressions for transport coefficients - turbulent ones connected with drift instabilities in the range of rare collisions, pseudoclassical, and Bohm's ones. One can find description of other codes in reviews by Hogan /5/ and Watkins /6/. Available codes satisfy immediate needs of physicists. But the risk always remains to fail when extrapolating the results to reactor parameters. For this reason attempts are currently being made to find a more reliable base for extrapolation in the form of tokamak scaling laws. After the Kadomtsev's paper /7/ devoted to the tokamak scaling laws an appreciable progress has been made by Connor and Taylor /8/. In their paper relations between the scaling laws for energy confinement time τ and the model adopted for plasma description have been established. In particular, in the ohmically heated plasma assuming quasineutral conditions, $B\tau = F(na^2, a^5 B^4)$, $T = a^{-1/2} F(na^2, a^5 B^4)$. Comparison with empirical scaling laws helps to choose the most suitable plasma model and thus to proceed with clearing up the transport mechanism.

As to microscopical mechanisms of anomalous losses, at least three slightly different ones based on the drift-type instabilities could be proposed: a turbulent one (particle-wave-particle collisions), a classical one enhanced due to large excursion of particles in fluctuating fields, and the most interesting one - destruction of toroidal topology and accordingly, of closed drift toroidal surfaces for electrons. In the recent paper /9/ Callen has shown that a longitudinal

current density $j_{\parallel} = \frac{i}{k_{\parallel}} \nabla \cdot ne(v_{i\perp} - v_{e\perp})$ induced by observed drift oscillations appears to be sufficient to generate a transverse magnetic field responsible for destruction of nested toroidal surfaces.

b) Impurities. During the last 2 or 3 years a number of calculations of hot plasma energy losses due to impurities has been carried out. Gervids and Kogan /10/ have calculated such losses and corresponding lethal concentrations for impurities of an arbitrary atomic number Z at thermonuclear temperatures in the range 10 to 40 keV. Further calculations of radiation losses /11/,/12/,/13/, and especially /14/ for a number of mid- and high-Z impurities have covered the range of lower temperatures T_e=(0.1-10) keV where radiation losses can exceed losses at thermonuclear temperatures by one or more orders of magnitude. Jensen, Post et al./14/ have shown, in particular, that a lethal concentration for tungsten is 10^{-2}% at T_e=10keV

Such a high sensitivity of energy balance to impurities makes them one of the key problems of quasistationary toroidal systems. A lot of recent papers are devoted to the transport theory for both single-species impurities and multi-component plasmas. Nevertheless, an impurity diffusion process has not yet been cleared up completely. Recently an impurity effect on neutral atom injection has also aroused interest. High-Z impurities prevent neutrals from penetration into central regions of the plasma column.

c) Run-away electrons. Rather a clear picture of the relaxation process of run-away electrons generated in a tokamak plasma in some operational regimes is developed. Pogutse and Parail /15/ and others /16/, /17/ have not only explained relaxation oscillations of a diamagnetic signal observed in the presence of a run-away electron beam but also estimated a fraction of high energy, low parallel velocity electrons which caused TFR liner damage /18/. The beam relaxation occurs in two stages: 1) parallel velocity losses due to excitation of anomalous cyclotron Doppler oscillations. This leads to a peak in the tail of the electron distribution function responsible for the following stage: 2) the further parallel velocity losses due to development of beam instability by the

Cherenkov's mechanism.

The problem remains concerning details of run-away kinetics and beam intensity. This problem becoms rather burning with respect to large T-10-type devices where an electron beam interacting with a limiter generates appreciable doses of hard radiation.

d) HF Heating. Here I would like to mention only two methods attracting most attention in the case of a tokamak.

Experiments of Alikayev et al. and calculations /18/,/19/ have shown that the mechanism of electron-cyclotron heating is linear, heating does not deteriorate plasma confinement, it is very convinient in terms of an experiment (the power is introduced along waveguides of miniature cross-section which does not disturb the usual system geometry. The problem is connected mainly with high power, millimetre wavelength generators.

Heating at the lower hybrid frequency $\omega_{LH} = [\omega_{He}\omega_{Hi}\omega_{pe}^2/(\omega_{pe}^2+\omega_{He}^2)]^{1/2}$ corresponding to a decimetre wavelength range is as yet low effective. The theory shows /20/,/21/,/22/ that there exist effective linear mechanisms of lower hybrid wave energy transmission to short wavelength oscillations with a frequency of $\omega = \omega_{pe} K_z/K$. In the result the plasma periphery is heated and the energy is readily dissipated to the walls. For this reason a tendency has appeared to use higher non-resonant frequencies for heating /23/. This should permit to transmit the HF field energy to the plasma column center. In this case only electrons absorb the HF field energy. In large devices with a high discharge duration collisional heating of ions by electrons is no problem.

e) Neutral atom injection seems at present to be the most effective plasma heating method. The following problems connected with injection are being solved theoretically:

Calculation of the distribution function of fast ions originated from injected atom ionisation /24/ including the case when impurities are present /25/.

A number of calculations on instabilities in the presence of fast ions has been done but they do not change essentially the results of Berk et al. /26/: instabilities can be avoided

or they cause turbulence with diffusion time much longer than the slowing down of the beam.

The problem of maintaining the toroidal current by injection (Ohkawa current) has been reconsidered /27/. This current has been proved to flow not only in the case when the plasma and injected ion charges are different but also in the most interesting case when they are the same.

Calculations of a fraction of neutral atoms scattered due to charge exchange and falling on the chamber walls have shown /28/ that under reactor conditions the injection power should be of the order of or higher than 200 keV for a neutral atom load on the wall to be not higher than 100 W/cm^2.

The problem of transport in a non-equilibrium plasma with a fast ion beam remains to be solved.

f) High β problem and evolution of two-dimensional equilibrium. The possibility to introduce already in the nearest future high powers into the plasma by neutral injection has aroused an important theoretical problem: how the plasma equilibrium will develop when one increases continuously the β parameter. To answer the question one should use transport equations which are essentially unknown. It seems, therefore, there is no reliable basis to solve the problem of two-dimensional evolution. But the situation is considerably facilitated when the time of the pressure increase is much lower than the characteristic dissipative time (skin time, energy confinement time). In this case the plasma pressure dependence on the poloidal flux $P(\psi)$ could be calculated using adiabatic laws, the poloidal current $f(\psi)$ is being found from flux-conserving conditions leading to conservation of the safety factor functional dependence $q(\psi)$. Corresponding calculations of equilibrium with high β values of up to 15 to 20% at $q(\psi)$ changing in accordance with stability requirements from 1 on the axis to 4 on the periphery have been carried out /29/. These calculations became the base of the flux-conserving tokamak concept. A somewhat unexpected and favorable result of these calculations is that only the current density is strongly peaked while the pressure gradient remains comparatively moderate. In the paper /30/ a progress has been

achieved in the theory of two-dimensional non-flux-conserving evolution.

II. Macroinstabilities.

Until recently hydromagnetic instabilities in tokamaks were subdivided into 1) surface-type kink instabilities with modes m=1,2,3,... having the largest growth rates, 2) internal kink instabilities, m=1, and 3) local internal instabilities.

The theory of kink instabilities which are well observed in the initial stage of the discharge and in disruptions was developed at first for two limiting cases: 1) free-boundary plasmawhen outside the current channel there exist a vacuum region of zero conductivity, 2) fixed-boundary plasma - a tearing mode. Pogutse and Yurchenko /31/ have recently traced the transition between these cases assuming that outside the current channel there is a low-density plasma of an arbitrary temperature. The increase in both the temperature and density of an external plasma causes the widening of stability zones.

Arsenin /32/ has explained in a very simple way the fact that observed growth rates of a kink instability are always lower than maximum theoretical values. He has taken into account that the going into the instability zone occurs at a slow change of the parameter $q \sim a^2/J$ (according to the change of the current J). If T is the characteristic time of this change than the growth rate apperes to be of the order of $\gamma \sim (\Omega^2 T)^{1/3}$ which agrees well with an experiment. The theory explains also the oscillations preceding the instabilities.

An internal kink mode with m=1 as well as a kink mode are observed well in experiments by relaxational splashes of soft X-ray radiation. These relaxations are explained well by plasma heating, increase in conductivity and current density, and reduction of q(0) up to the critical value each time following the development of the instability and its stopping due to flattening and increase of q(r) in the column center in accordance with the Kadomtsev theory and non-linear calculations. The calculation of the critical value of q(0) for a kink instability in a torus has appeared to be rather

subtle because of curvature effects.

A comprehensive criterion of stability of an internal kink mode m=1 has been derived by Bussac et al. /33/. In contrast to the case of a linear column the stability condition of the mode m=1, n=1 in the torus depends on the plasma pressure. The poloidal β critical value varies from 0.3 to 0.1 when q(0) varies from 1 to the minimum admissible value q(0)=0.5 (for lower ones n=2,3,... kink modes unaffected by curvature develop).

As for an internal local instability of a Sydam type, it has not yet been identified in tokamak plasmas. Probably this is due to the fact that the Mercier criterion for a local plasma stability is easily satisfied under usual conditions (a round column cross-sections, moderate β values), provided $q^2(r) > 1$. Application of this criterion to the plasma with a rather high pressure value $\beta \sim (a/R)^{4/3}/q^2$ has shown that an increase of the pressure makes the plasma even more stable /34/. The paradox arisen - the emprovement of stability with the increase of the thermodynamical nonequilibrium of the plasma - no longer arises after numerical investigations of high β toroidal plasma stability.

Impressive calculations performed recently in Princeton /35/,/36/ (see also /37/) in connection with the flux-conserving tokamak concept have found out the balooning instability which was expected on the base of simple physical arguments. This instability sets a limit on the plasma pressure. Analysis of the Mercier criterion of stability undertaken in connection with this instability by Zakharov has shown that in contrast to the basic perturbation mode which is resonant with respect to the given magnetic surface m/n=q coupled modes m+1 and m-1 are not local. For this reason the Mercier criterion is not a sufficient one for internal modes and in fact the pressure gradient for these modes appeares to be a destabilizing factor.

Pogutse and Yurchenko have found another reason for restrictions on the β value: the effect of curvature on a kink instability. This effect is linear in $\varepsilon = a/R$ and causes the closing of the gaps of instability. The critical β value

is found to depend on the current distribution and is of the order of a/Rq^2.

More adequate to numerical results are investigations of a balooning mode in a tokamak by Glasser et al.in Princeton. Modes localised in the azimuthal direction which are strongly changed along the magnetic field lines and unaffected by the shear are found analitically in full agreement with numerical results.

As to a numerical value of critical β it is found to be of the order of a/Rq^2 and amounts to 3 to 5 % (calculations of the Princeton and Oak Ridge groups). It can achieve the value of 12% for specially chosen equilibria according to Wesson (Culham).

No much progress has been achieved in theoretical explanations of disruptive instabilities. However, a picture of the process development derived from experimental data has permitted Arsenin /40/ to propose a method of its suppression by feed-back stabilization of a tearing instability which is thought to provide conditions for a disruption.

III. Reactor Plasmas.

Programs in a number of countries of realization during the nearest 5 or 10 years of a demonstrational fusion experiment have resulted in development of a theory of the thermonuclear, or reactor plasma, i.e. the plasma with a temperature of about ten kilovolts in which rather an intensive fusion reaction proceeds.

Here the new problems are those connected with particles (the products of the reaction) and interaction of thermonuclear plasmas with chamber walls.

In paper /38/ the losses of α particles from toroidal plasmas due to a toroidal drift are calculated. The angular distribution and energy spectrum of α particles incident on the reactor first wall has been considered./39/. So-called thermonuclear microinstabilities - excitation of Alfven and magnetosonic waves and corresponding transport have been also studied./40/,/41/.

The problem of protection of the tokamak reactor first

wall from sputtering by hot plasmas has been studied /42/,/43/. Studies have shown that in the near-wall region a layer of rather a dense and cold plasma protecting effectively the wall and the limiter from erosion can form.

A high value of heat conductivity necessary to cool a near-wall region can be achieved by artificial destruction of magnetic surfaces by resonant perturbations as is proposed in the paper by Feneberg /44/.

Another possibility of the wall protection is connected with localization in the near-wall region of a cold dense plasma with high-Z impurities - a so-called "virtual limiter" /45/ which can be formed during the first contact of the plasma with a material limiter covered by a readily evaporating high-Z material. Having entered the high-Z dense plasma the hot particles loose their energy due to excitation and ionisation processes. Then this energy is released as X-ray radiation which does not affect the wall.

The conclusion based on these calculations is as follows: there is no principle obstacles in the way of realization of a tokamak fusion reactor.

References.

1. Ю.Н.Днестровский,Д.П.Костомаров. В сборнике "Вычислительные методы в физике плазмы", т.9 Дополнение.МИР,М.1974.
2. C.Mercier et al. Proc.5th Europ.Conf.,Grenoble,2,157(1972)
3. C.Mercier,F.Werkoff, Plasma Phys.and Control.Nucl.Fus.Res., 1976,Sixth Conf.Proc.,IAEA 2,29(1977).
4. D.F.Duchs et al.,Nucl.Fusion, 17,565(1977).
5. J.T.Hogan, in "Methods in Computational Physics", Academic Press, Vol.16(1976),131-164.
6. M.L.Watkins et al., ibid. p.165-209.
7. Б.Б.Кадомцев, Физика плазмы, 1, 531 (1975)
8. J.W.Connor,J.B.Taylor, Proc.8th Europ.Conf.,Praha,1977.
9. J.D.Callen, Preprint ORNL/TM-5974(1977).
10. В.И.Гервидс, В.И.Коган, Письма ЖЭТФ, 21,329 (1975). Препринт ИАЭ-2722, Москва (1976)
11. A.L.Merts,R.D.Cowan,N.H.Magee, LA-6220-MS(1976).
12. C.B.Tarter, UCRL-78119(1976).

13.C.Breton et al.Nucl.Fusion 16,891(1976),EUR-CEA-FC-853(1976).
14.R.V.Jensen et al., PPPL-1334 (1977).
15.V.V.Parail,O.P.Pogutse, Fizika plazmy 2,228 (1976).
16.C.S.Liu,Y.Mok, Phys.Rev.Lett., 38,162(1977).
17.K.Molvig et al., Phys.Rev.Lett.,38,1404(1977).
18.V.V.Alikaev et al., Fizika plazmy 3,230(1977).
19.A.G.Litvak et al.,Nucl.Fusion,17,659(1977).
20.M.Porkolab, Phys.Fluids, 17, 1432(1975).
21.R.L.Berger et al., PPPl-1308(1976).
22.V.V.Parail, Preprint IAE-2608(1976).
23.A.M.Rubentchik, Zh.tekh.Fiz.(Letters),2,521(1976).
24.J.W.Connor,J.G.Cordey, Nucl.Fusion, 14,185(1974).
25.Yu.N.Dnestrovsky et al., Nucl.Fusion,17,3(1977).
26.H.L.Bert et al.,Nucl.Fusion,15,819(1975).
27.V.V.Fomenko, Nucl.Fusion 15,1091(1975).
28.A.S.Kukushkin et al.Plasma Phys.and Contr.Nucl.Fus.Res.,1976, Sixth Conf.Proc.Berchtesgaden,1976,IAEA,1,615(1977).
29.R.A.Dory,Y.K.M.Peng, Nucl.Fusion 17,21(1977).
30.L.E.Zakharov et al., Third International Conference on Plasma Theory,Trieste, April 1977.
31.O.P.Pogutse,E.I.Yurtchenko,Fizika plazmy,3,504(1977).
32.V.V.Arsenin,Proc.8th Europ.Conf., Prague(1977).
33.M.N.Bussac et al., Phys.Rev.Lett., 35,1638(1975).
34.A.B.Mikhailovsky,Nucl.Fusion,14,483(1977).
35.A.M.M.Todd et al.,Phys.Rev.Lett.,38,826 (1977).
36.J.M.Green et al.8th Europ.Conf.on Contr.Nucl.Fus.and Plasma Phys.,Prague,1977.
37.G.Bateman and Y.K.M.Peng, Phys.Rev.Lett.,38,829(1977).
38.Ya.I.Kolesnitchenko et al., Fizika plazmy,2,911(1976).
39.V.S.Belikov et al., Fizika plazmy,3,178,487(1977)
40.V.A.Mazur,A.B.Mikhailovsky,Nucl.Fusion,17,193(1977).
41.V.S.Belikov et al., Fizika plazmy,3,263(1977).
42.T.F.Volkov et al., Plasma Physics and Contr.Nucl.Fus.Res., 1976,Sixth Conf.Proc.Berchtesgaden,3,359(1977).
43.E.Engelmann et al., ibid.,2,19(1977).
44.W.Feneberg,Proc.8th Europ.Conf., Prague (1977).
45.A.Sestero,Nucl.Fusion 17,115(1977).

PROGRESS IN TOKAMAK EXPERIMENTAL RESEARCH IN THE SOVIET UNION.

Tokamak Group. Presented by G.A. Bobrovskii.
I.V. Kurchatov Institute of Atomic Energy, Moscow, USSR.

The Soviet tokamak experimental research program has been concerned mainly with: impurities, disruptive instability, electron runaway and additional heating, during the year after the Berchtesgaden Conference.

Three approaches were taken in studies of impurities:

1. Determination of the plasma impurity level and mechanism of impurity influx.
2. Use of a carbon limiter in a tokamak.
3. Construction of a divertor in a finger-ring tokamak.

In the disruptive instability we were interested in the succession of phenomena resulting in a precursor and its development into a large disruption and in the role of low-m helical perturbations in the disruption process. Attention was also paid to the stabilization of helical perturbations.

Studies of the electron energy distribution function were continued in order to determine to what extent the electron acceleration mechanism obeys the classical law.

Additional heating studies include investigations of HF-heating at frequencies near the lower hybrid resonance and at considerably higher frequencies, and also investigations of neutral beam injection at a safety factor $q \sim 2$.

The experiments, described in the paper,were performed on Tokamaks T-4, TM-3, T-12, TO-1 (Kurchatov Institute, Moscow), FT-1 (Ioffe Institute, Leningrad) and R-O (Sukhumi PhTI).

In addition, new information was obtained from processing of T-10 and T-6 experimental results.

The T-10 Tokamak was put in operation in September again after almost an one-year break. The toroidal field coils have been tested to the maximum design value of 5 T.

I.

The main task in the impurity problem is to study physical mechanisms resulting in impurity transport. The absence of the high impurity level in the center of plasma column, observed in

all world tokamaks operating at electron densities over $5...8.10^{13}$ cm^{-3}, seems to give an evidence that the impurities do not accumulate in plasma for the time of discharge. It was shown on T-10 that the effective ionic charge in the center $Z_{eff}(0)$ is near 1 for 0.8 s /1,2/. Moreover, there is indirect evidence that Z_{eff} grows towards the periphery /1/. It is natural to assume that the impurity influx to the center , if any , has a very small rate.

A study of impurity diffusion was performed on T-4 /3/. The problem has been formulated as follows: by measurement of the line intensities of ions of successive stages of ionization the direction and the rate of impurity diffusion in the plasma column cross-section are determined. Oxygen already existing as an impurity in hydrogen plasma and pulsed injected argon were chosen for investigation.

The radial profiles of hydrogen- and helium-like oxygen ions are given in Fig. 1 together with the diffusive flux of the O^{+7} ions. One can see that in most parts of the cross-section an outward diffusion exists. The measurements of the ionization fluxes of oxygen ions of lower stages of ionization show that the outward diffusion of the O^{+5} and/or O^{+6} ions also exists.

It is known that impurity accumulationmust occur in the central region if transport processes are classical or neoclassical (see, for example, /4/). However, there is experimental evidence of anomalously large electron transport. Taking into account enhanced electron diffusion and assuming neoclassical transport for ions in the banana and plateau regimes Strizhov has shown that in model, used by him, the calculated fluxeswere of the same character as the experimental one. The diffusive fluxes of the O^{+7} ions calculated for the T-4 Tokamak are given in Fig. 1. However, only qualitative description can be offered by this model because both the influx value and the intensity profile of O^{+7} and O^{+6} radiation differ essentially from the experimental ones.

The experiments, performed on T-4 and T-10,make it possible

to hope that impurities are not accumulated in the center of the plasma column at least for the discharge, which is in contradiction with theoretical waitings. If this suggestion is proved in further experiments it will mean that a mechanism exists in tokamaks which decreases effectively the impurity influx to the center.

The level of plasma contamination in T-10, although comparatively low, cause, nevertheless, substantial radiative losses. The spectra of Fe and Cr measured in T-10 /2/ are presented in Fig. 2 and give evidence that chromium is ionized to the helium like stage while iron is ionized only to the lithium-like one. The material of the limiter seems to be in plasma together with those impurities going from the walls. The use of low-Z materials seems to be profitable for reducing the losses connected with impurities. The first attempt in this field was the use of a carbon limiter. Such a limiter was placed in T-4 following the Petula and TFR examples. In the T-4 experiment the carbon limiter hole radius was 1.5 cm smaller than that of the tungsten-rhenium one, previously used. The use of the carbon limiter leads to the following results in the I=100 kA, H_z=3 T, $\bar{n}_e$= 2.10^{13} cm^{-3} regime. The oxygen flux was not practically changed as determined from O^{+4} ion radiation. The carbon influx was increased as determined from C^{+4} ion radiation and became 3 times larger than that of oxygen. Loop voltage was decreased more than twice reaching 1.5 to 1.8 V. The intensity of hard X-ray radiation from the limiter was sharply decreased. Z_{eff} in the center taken from the sawtooth analysis was decreased 1.5 to 2 times reaching $Z_{eff}(0)$= 2 or 3. Intensity of the tungsten M-series was decreased by an order of magnitude. Wall losses, measured by a bolometer, reached 20 % of the input power. Their absolute value was decreased by a factor of 2 or 3. There was no dangerous destruction of the limiter after a series of 1000 runs; however, its surface became covered by a film of sputtered material from the chamber walls and from the previous limiter left in the chamber. This result, which is not surprising, shows that changing the limiter only is not an effective way to

remove heavy impurities. Consequently, the whole discharge chamber should be made of a light material of a low sputtering yield.

A divertor is another way for impurity removal. The first divertor in the Soviet Union was made in T-12 finger-ring tokamak /5/. It is an axisimmetric poloidal divertor. The first experiments showed that the divertor made it possible to increase the discharge duration and to decrease radiative losses in the vicinity of the material limiter.

II.

The disruptive instability still prevents reaching a low value of safety factor in tokamak. Considerable progress in investigation of this phenomenon has been achieved by using good time-resolution methods of measurement of X-radiation, MHD-activity, loop voltage and of some other characteristics of the plasma column. In our opinion, to understand this phenomenon the accurate classification of disruptions is necessary. The classification may be offered as follows /6-8/:

1. Internal mode caused by m=0 and m=1 modes. It is manifested as sawtooth oscillations of soft X-ray intensity. External activity of this mode is low.

2. Small disruption (SD). The negative voltage spike is of a small amplitude. Modes of m=3 and m=4 are registered which do not touch central region. SD begins with development of helical harmonic with an m/n ratio near the safety factor value at limiter: $m/n \simeq q(a_L)$. The perturbation is somewhat distorted during the disruption. This means the appearance of harmonics with higher m/n. However, the initial harmonic remains dominant. SD is accompanied by energy losses which can be substantial.

3. Precursor. It looks like SD initiated by m=2 mode at the periphery. This mode seems to cause the m=1 mode at smaller radii and the latter, in its turn, seems to cause m=0 mode in the center. The m=0 mode is the flattening of temperature and current profiles, and therefore of the safety factor, in the center. This flattening obviously reduces plasma stability against helical perturbations with higher m. Poloidal field

oscillations during precursor are of a few per cent.

4. Large disruption (LD) goes through two stages. The first stage is practically a repetition of precursor, usually differing in having a larger intensity. As in precursor, the m=1 mode is coupled with the m=2 mode. As LD develops, this coupling seems to be broken. Frequency and amplitude of the m=1 mode are increased, and the safety factor profile is flattened (the m=0 mode). This flattening is accompanied by the m=2 perturbation increase. The loop voltage is slightly lowered. A sharp drop of the loop voltage happens in the second stage of LD. The m=2 mode, which is moderated, serves as a background for a harmonic of higher m with rapidly increasing intensity. Amplitude of the latter becomes 2 to 4 times larger than the maximum amplitude of the perturbation in the first stage of LD. Energy losses during LD are 2 to 3 times larger than those in SD. They are a great part of the plasma thermal energy before the disruption.

The fact that precursor does not always develop into destructive LD allows hope that the LD can be avoided by stabilizing the m=2 perturbation during the precursor. Encouraging results for such stabilization by feedback control were obtained in R-O (Sukhumi) /9/ and in TO-1. In both cases, the additional m=2 helical winding was used.

III.

Helical perturbations play an essential role not only in the disruptive instability, but at the initial stage of a discharge, when the plasma column is formed, and in providing an impurity flux from the chamber walls.

In /10/ the phenomena were observed, when an initial stage of the T-4 discharge was studied, which could be interpreted as the contraction of the current channel due to development of the peripheral MHD-perturbations of higher modes ($m=q(a_L)$, $n=1$). These perturbations seem to be responsible for a skin-effect attenuation at low densities: $\bar{n}_e < 3.10^{13} cm^{-3}$. The absence of current skinning at higher densities can be explained by periphery cooling due to ionization and radiation. When the plasma column was formed under such conditions, the m=3

perturbation and the disruptive instability were observed at $q(a_L) = 10$. The MHD-perturbations of lower modes seem to set a limit to the maximum plasma density /11/.

The surface perturbations lead to outflux of hot particles to walls and to increase of impurity fluxes. A notable increase of the electron density was registered by a Langmuir double probe in the vicinity of the wall in the TM-3 Tokamak /12/ when the resonant magnetic surfaces with $q>4$ were placed there.

IV.

The runaway electron beam becomes more and more dangerous as tokamak sizes are increased. The investigations of the electron energy distribution function could help in looking for a way to guard the bulk of electrons against the acceleration.

The distribution function f_ε in the vicinity of the thermal energy ($\varepsilon \sim (5 \text{ to } 10).T_e$) follows the formula /13/:

$$\ln f_\varepsilon \sim -\varepsilon/T_e + \tfrac{1}{2}E/E_D(\varepsilon/T_e)^2 \qquad (1)$$

(E_D is the Dreicer field), according to the present conception. In Fig. 3 the curves described by (1) are compared with the X-ray spectra registered in T-10 along three chords of the column cross-section /1/. One can see appearance of discrepancy between theory and experiment at larger distances from the center in spite of the fact that conditions for acceleration are worse at the periphery (E/E_D is smaller, Z_{eff} is larger). A similar result was obtained in TM-3 /14/. Gurevitch et al. tried to explain this phenomenon by diffusing of electrons from the hot central region of the plasma column. The number density of fast electrons is larger in exponential manner in that region (see (1)) and a noticeable part of them is trapped in local mirrors. They drift vertically to the periphery and then become untrapped through Coulomb collisions. Thus, the distribution function is enriched in fast electrons at the periphery.

The existance of hotter electrons at the periphery can cause a variation of plasma column conductivity and must be taken into account when calculating the radial profile of the current density /2/.

V.

A large number of different factors should be taken into consideration when interpreting charge-exchange spectra. So, ion temperature T_i in T-10 was increased from $\sim$ 600 eV to $\sim$800 eV when plasma selfabsorption of neutral atoms and drift of locally trapped ions have been considered. At densities achieved in some of present tokamaks the radiative recombination of protons must be taken into account, too (Fig. 4) /15/. The recombination will lead to an increase of the neutral density n_a in the center by some orders of magnitude in future tokamaks. On one hand, this will deteriorate the energy balance of the ion component; on the other hand, this improves the perspective of T_i-measurement by neutral spectra. That is why the direct measurements of n_a in the plasma column cross-section are important. The first attempt in the Soviet Union was undertaken by Burakov et al. on FT-1. The local measurements of n_a were performed there by the resonant fluorescence method using a dye laser (Fig. 5). The lower limit of sensitivity was estimated to be 10^9 cm^{-3}.

VI.

The additional heating methods are being investigated in the Soviet Union tokamaks.

We were interested in frequencies near the lower hybrid resonance and considerably higher frequencies when studying the HF-heating. The higher frequncies allow to avoid HF-power absorption at a plasma periphery: according to the theoretical predictions /16/ , the length to absorption due to decays is proportional to ω^3 and it becomes of the order of plasma transverse dimentions at high frequencies. Absorption of HF-power by suprathermal electrons should be expected in this heating method. The method is promising for the heating the bulk of electrons in large tokamaks where the energy confinement time is longer than the time of maxwellization. To test the theoretical predictions Alikaev and Il'in investigated HF-power absorption at $\omega \simeq 4\,\omega_{LH}$ in the TM-3 Tokamak. An electromagnetic wave was shown to be absorbed by electrons with longitudinal energy $\varepsilon_{\parallel} \sim 10$ to 100 T_e. The loop voltage decrease and the plasma column displacement increase, observed

during the HF-pulse, can be interpreted as an increase of $\mathcal{E}_{\parallel}$ of those electrons. Then the absorbed power is 20 to 40 % of the input power. One could explain the results in terms of the linear Landau damping, too.

The heating was confirmed when processing the results of the experiments on heating of plasma by Alfven waves /17/. The rise of temperature (mainly of T_e) was 100 eV under HF-power not more than 100 kW.

Neutral injection is developed on T-11. After a year break the Tokamak was put in operation. Ä source without magnetic field was installed in an injector. The injector can provide the $I \leqslant 35$ A, $P \leqslant 400$kW hydrogen beam or the $I \leqslant 25$ A, $P \leqslant 300$ kW deuterium atom beam. The energy of atoms E= 15 to 25 keV. The heating studies are performed at $q \simeq 2$.

VII.

The results of the Soviet tokamak research can be briefly summarized in the following way.

1. It has been shown that in spite of the continous impurity influx to the column periphery there is no evidence of appreciable impurity accumulation in the central hot regions,at least in the course of the process. Impurity accumulation is prevented by an outward diffusion of ions of higher stages of ionization.

2. The consequence of events is traced during the disruptive instability. The m=2 helical perturbation and the m=1 mode induced by it are shown to be the most dangerous. They result in a precursor which goes as a rule to a destroying large disruption. At present the hope for suppression of the disruptive instability is connected with stabilization of m=2 mode.

3. Helical perturbations (together with ionization and radiation at a high initial pressure) prevent from skin formation at the initial stage of the discharge. Their negative role consists in an increase of the impurity flux from the walls.

4. Continous acceleration of an appreciable part of the electrons does not occur as a rule. However, the electron distribution function is markedly deformed by an electric field. One should take into account the existance of suprathermal electrons while measuring T_e by X-ray spectroscopy and while calcu

lating conductivity over the plasma column cross-section.

5. The frequencies considerably higher than ω_{LH} seem promising for heating plasmas in large tokamaks.

R E F E R E N C E S.

1. Berlizov et al. Plasma Phys. and Contr. Nucl. Fusion Res. 1976, IAEA, Vienna, 1977, v.1, p.3 .
2. Berlizov A.B. et al. In Proc. of this Conference.
3. Abramov V.A. et al. Ibid.
4. Dnestrovskii Yu. N. et al. Nucl. Fusion, 16, 513 (1976).
5. Bortnikov A.V. et al. In Proc. of this Conference.
6. Mirnov S.V., Semenov I.B. See /1/, p.291 .
7. Merezhkin V.G. Preprint IAE- 2790, M., 1977.
8. Mirnov S.V., Semenov I.B. In Proc. of this Conference.
9. Demirchanov R.A., Kirov A.G., Astapenko G.I. et al. Ibid.
10. Mirnov S.V., Semenov I.B. The paper, presented to the Work. Group on Initial Stage and Runaway Electr., USA, April 1977.
11. Murakami M. et al. Nucl. Fusion, 16, 347 (1976).
12. Bobrovskii G.A., Kondrat'ev A.A. Fiz. Plasmy, 3, 209(1977)
13. Lebedev A.N. Sov. Phys. - JETP, 21, 931 (1965).
14. Bobrovskii G.A. et al. Fiz. Plasmy, 2, 898 (1976).
15. Gordeev Yu.S. et al. ZhETF, Pis'ma, 25, 223 (1977).
16. Rubentchik A.M. ZhTF, Pis'ma, 2, 521 (1976).
17. Vdovin V.L. et al. In Proc. of this Conference.

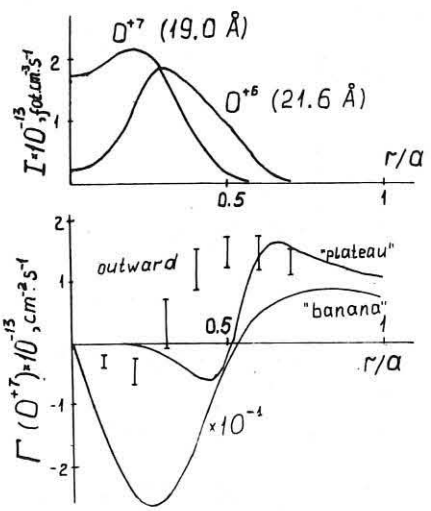

Fig. 1

a) Profiles of line radiation of the oxygen ions.

b) Diffusive fluxes of the O^{+7} iones (I - experiment). T-4 data.

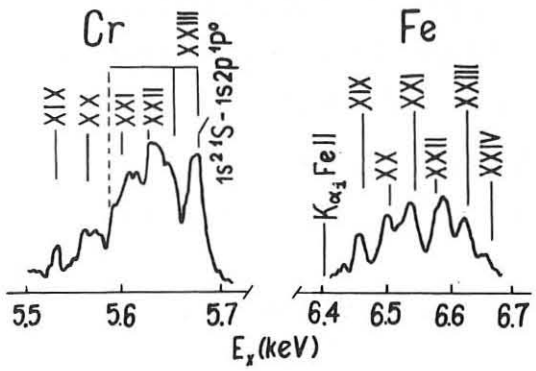

Fig. 2. Chromium and iron spectra obtained on T-10.

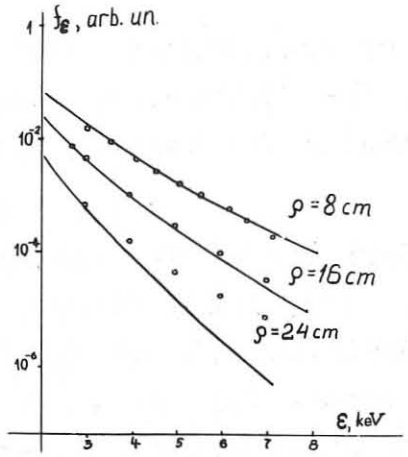

Fig. 3. Comparison of calculated electron distribution functions with experimental spectra obtained on T-10.(o o o).

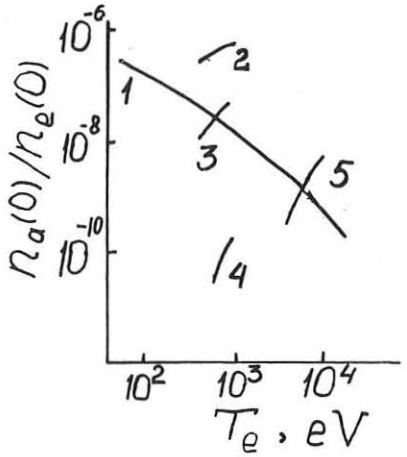

Fig. 4.

Relative density of neutrals appeared in center of plasma column due to recombination (1) and due to charge-exchange in T-4 (2), T-10 (3), Alcator (4) and in reactor (5). Data of/15/.

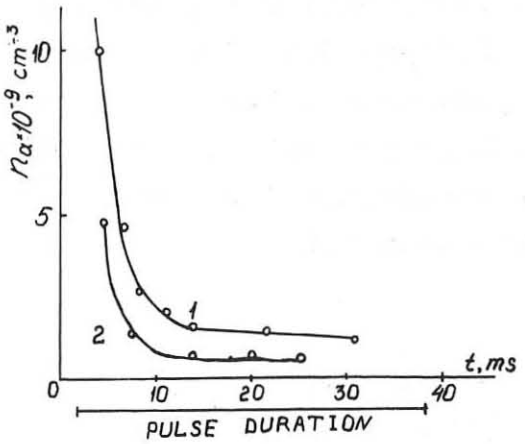

Fig. 5.

Density of hydrogen atoms in FT-1 registered 10 cm away from the center under poor (1) and good (2) vacuum conditions in the chamber.

REVIEW OF RESULTS FROM DITE TOKAMAK

J.W.M. Paul

A.E. Costley, S.J. Fielding, M.J. Forrest, R.D. Gill, J. Hugill,

G.M. McCracken, N.J. Peacock, P.E. Stott

Culham Laboratory, Abingdon, Oxon, OX14 3DB, UK
(Euratom/UKAEA Fusion Association)

Abstract: The behaviour of DITE tokamak is discussed in relation to the origin, effect and control of impurities. The beneficial effects of gettering the walls, a cold plasma blanket and the bundle divertor are discussed and plasmas with $Z_{eff} \sim 1$, $\zeta \sim 4$ and $\tau_E \sim 30$ ms are described. Power balance and transport are considered for three types of discharges; low Z (oxygen) dominated, high Z (metal) dominated and high density "pure" plasmas. Neutral injection into the latter produces electron heating and changes the current distribution.

1. INTRODUCTION: This paper provides an overall picture of the behaviour of the DITE tokamak and thereby places the six more detailed contributed papers [1 - 6] in context. This approach allows more emphasis to be placed on the significance of the work for tokamak research.

The main theme is that the plasma behaviour is dominated by impurities, unless special measures are taken to obtain "pure" plasmas. The radiative power loss and the enhanced Z_{eff} produced by impurities, affect the power balance, hence the profiles $T_e(r)$ and thereby the basic transport and stability of the tokamak.

The main achievements of the DITE programme are as follows: (1) Control of low and high Z impurities by the divertor, (2) Control of low Z impurities by gettering which allows, (3) High density operation with "pure" plasma ($Z_{eff} \sim 1$, $\zeta \sim 4$) and helps elucidate the nature of the density limit, (4) Identification of arcing as the main source of metallic impurities and demonstration of methods of controlling it, (5) Electron heating and modification of the current profile by neutral injection, (6) First measurement of profile q(r) by the scattering technique.

2. EXPERIMENT

The machine parameters are: R = 1.17 m, a = 0.26 m, $B_T \leq 2.8$ T, $I \leq 250$ kA from capacitor banks and the torus is modular with two ceramic gaps (Fig. 1).

The two neutral injectors (30 kV) deliver a total of 0.2 MW to the

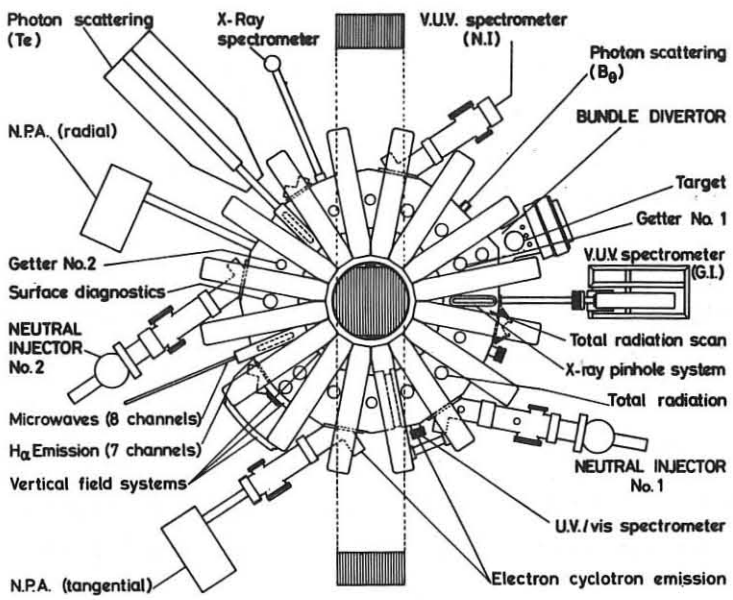

Fig.1 Schematic layout.

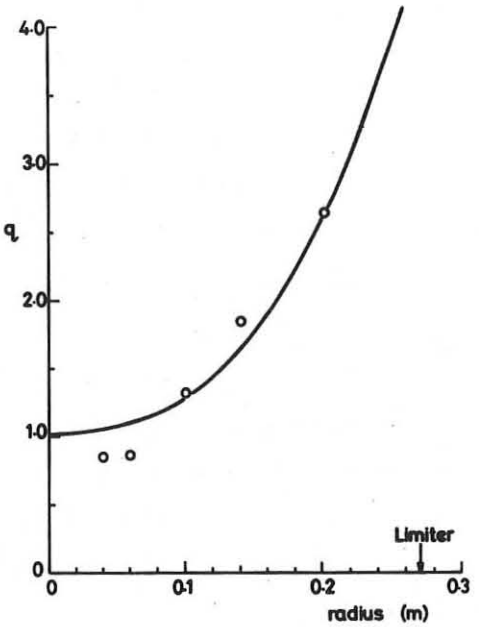

Fig.2 Profile q(r) from scattering [points], and $T_e(r)$ [line].

CLM-P502

plasma without detectable gas or impurity influxes. A second pair of injectors bringing the total to 1.4 MW will be available in January 1978.

The bundle divertor Mk I has operated with $B_T \leq 1.0$ T, $I \leq 50$ kA and modification will allow $B_T \leq 1.5$ T, $I \leq 75$ kA in January 1978. A full power divertor (Mk II) is now designed and should be installed by 1979.

The normal full range of diagnostics are available as illustrated in Fig. 1. The grazing incidence spectrograph (down to 10 Å) provides estimates of impurity concentrations and direct evidence of an outward diffusion of highly ionised species. The electron cyclotron emission is used routinely to measure $T_e(r)$ many times during one pulse (see Fig. 17).

For the first time the photon scattering technique has been used [7] to measure the profile $B_p(r)$ and hence $J_T(r)$ and $q(r)$. The measured values of $q(r)$, circles in Fig. 2, agree well with those derived from $T_e(r)$, assuming $Z_{eff}(r)$ = constant, for a similar discharge.

3. GENERAL BEHAVIOUR

The plasma parameters achieved, though not all at the same time, are as follows; $T_{eo} \leq 1.5$ keV, $T_{io} \leq 0.7$ keV, $n_{eo} \leq 10^{20}$ m^{-3}, $Z_{eff} \rightarrow 1$, $\zeta \rightarrow 4$, $\beta_p \leq 0.6$, $\tau_E \leq 30$ ms (the latter two from diamagnetism). The impurity concentrations for normal to "pure" plasmas are estimated as n_{Ox}/n_e = 1 to 0.1%, n_{Fe}/n_e = 0.4 to 0.02%, n_{Mo}/n_e = 0.2 to 0.01%.

Normal discharges in DITE[8] have always been metal dominated and the operating regime in current and density with gas feed is represented by Region A of Fig. 3, delineated more fully than previously [8]. Within this region the radiated power is an almost constant fraction of the ohmic power, the profiles $T_e(r)$ become theoretically less stable as the density limit is approached and MHD activity has a minimum near the centre of the density range. Also within this region $(Z_{eff} - 1) \propto P_I/n_e$ (Fig. 4), suggesting that the impurity content is proportional to the input power (P_I). Typical experimental profiles $T_e(r)$ are shown in Fig. 5. The peaked high Z (metal) dominated profiles changed to consistently hollow profiles later in the life of the machine. These two profiles illustrate the thermal instability of the centre of the discharge.

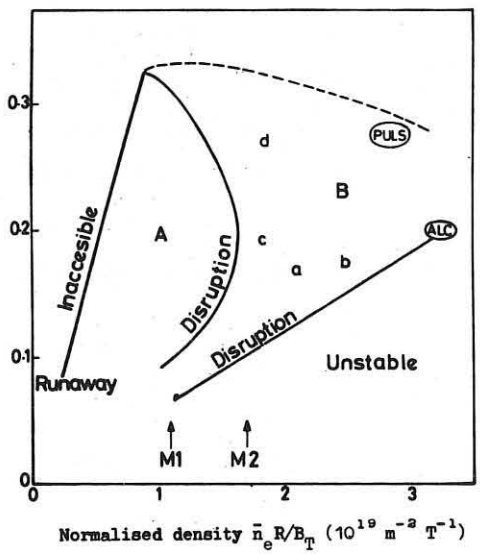

Fig.3 Operating regime, current ($\propto 1/q$) vs. density.

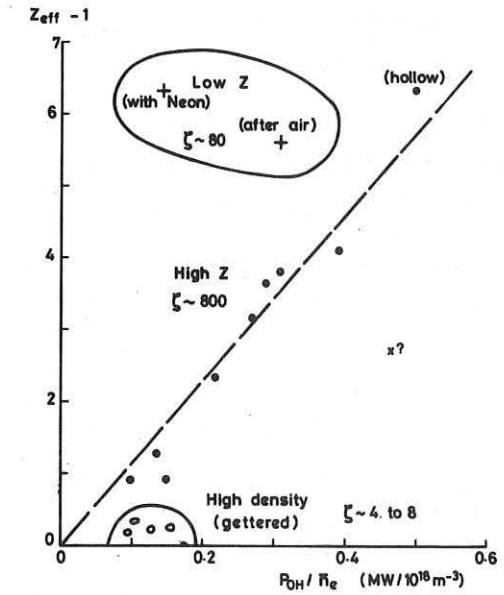

Fig.4 Impurity (Z_{eff} −1) vs. power per particle.

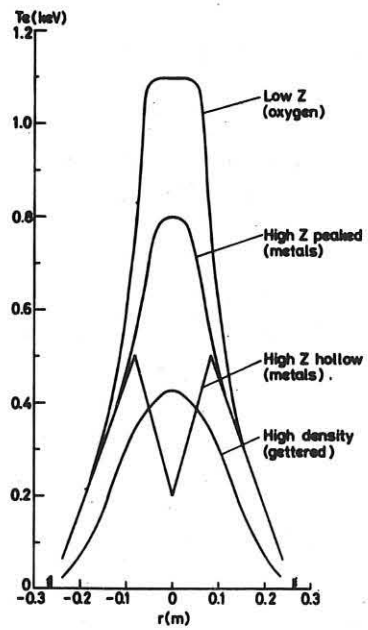

Fig.5 Profiles $T_e(r)$.

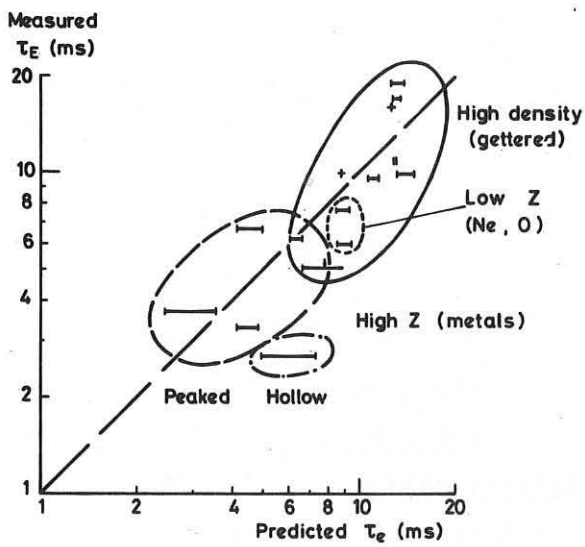

$\tau_{E1} = 2.7\ \bar{n}_e^{0.61}\ a^{1.57}\ B^{0.88}\ A_i^{0.65}$ (ms)

$\tau_{E2} = 5.1\ \bar{n}_e^{0.84}\ a^{2.13}\ (R/a)^{0.91}\ B^{0.49}\ T_{eo}^{0.25}\ A_i^{-0.62}$ (ms)

Fig.6 Comparison with Hugill-Sheffield scalings.

The two other modes of operation of DITE are also shown in Fig. 4 and 5: (1) Small quantities of low Z impurities introduced (e.g. 2% Ne; oxygen after exposure to air) and (2) High density operation with "pure" plasma, $Z_{eff} \sim 1$ achieved after gettering the walls, and corresponding to region B of Fig. 3. It is somewhat surprising that the low Z, high Z and "pure" discharges all fit the Hugill-Sheffield [9] empirical scaling law (Fig. 6).

The bundle divertor removes a bundle of toroidal field lines, localized in major and minor azimuth, from the torus to a separate chamber where it is intersected by a target plate (Fig. 7). The rotational transform connects this bundle to an annular scrape-off region in the torus. The purpose of the divertor is to reduce the impurities by using the following functions: (1) Unload the outgoing plasma and power fluxes from the wall onto the target and this it does with efficiencies of 30% and 60% respectively, (2) Remove the need for a material limiter because of the magnetic separatrix, (3) Screen the central plasma from impurities evolved from the wall by ionizing them in the scrape-off layer and diverting them. This it does with efficiencies of 50% and 80% for low and high Z impurities respectively.

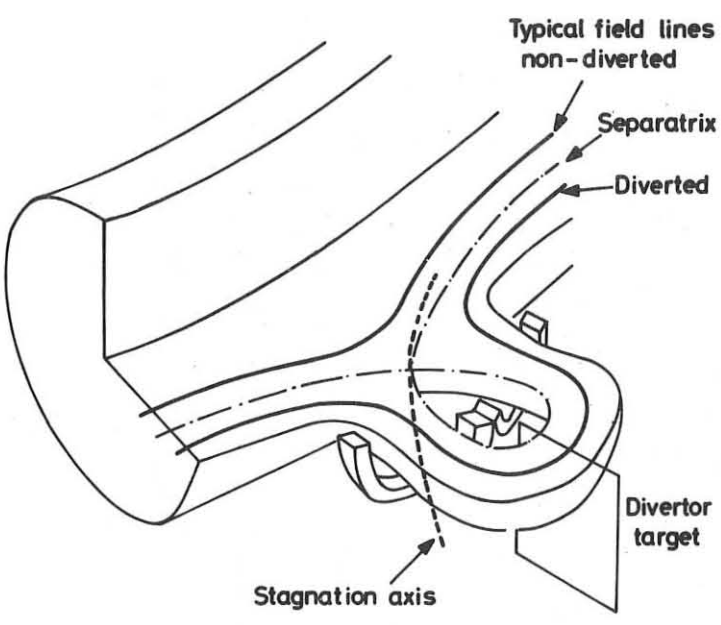

Fig.7 DITE Bundle Divertor.

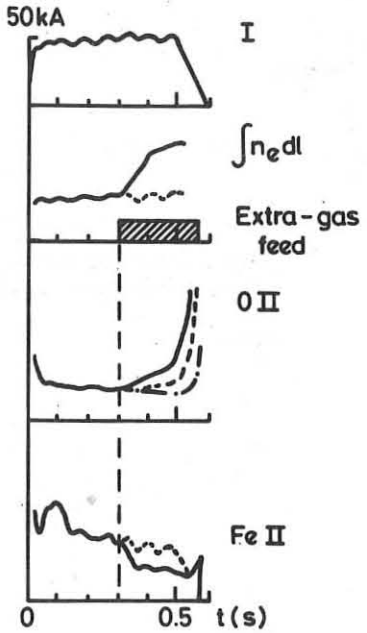

Fig.8 Effect of gas feed on O II and Fe II.

4. PLASMA-SURFACE INTERACTIONS

4.1. Low Z Impurities

Origin: The main contribution is from oxygen, as in most tokamaks, but the level is low. It originates from surface contamination together with some diffusion from the bulk and is desorbed into the plasma by hydrogen recycling near the edge of the plasma.

Effects: Radiative cooling by low Z impurities, which are stripped in the outer regions of the plasma, produces a shrinkage of the current channel. Experiments with artificially high levels, from exposure of the torus to air or the addition of 2% Neon to the hydrogen, show this effect and the resulting high T_{eo} with a flattened central profile out to $q \sim 1$ (Fig. 5).

Normal hydrogen gas feed is largely via the wall and involves increased hydrogen recycling. Even in the normal metal dominated discharges, this increases the desorption of oxygen, as shown in Fig. 8, produces shrinkage of the current channel and ultimately MHD instability.

The maximum density and also containment time in DITE is determined by this oxygen induced disruptive instability. Because the current shrinkage towards instability is related to the balance between radiated and ohmic power, it is not surprising that the density limit scales with ohmic current density ($\propto B/Rq$) as in Fig. 3.

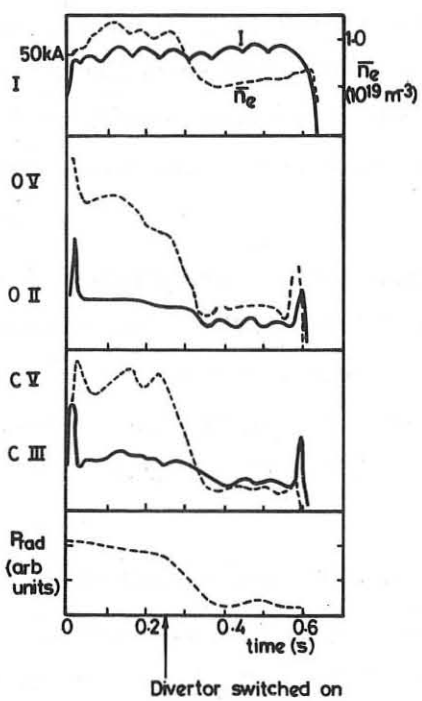

Fig.9 Mid-pulse switch on of divertor.

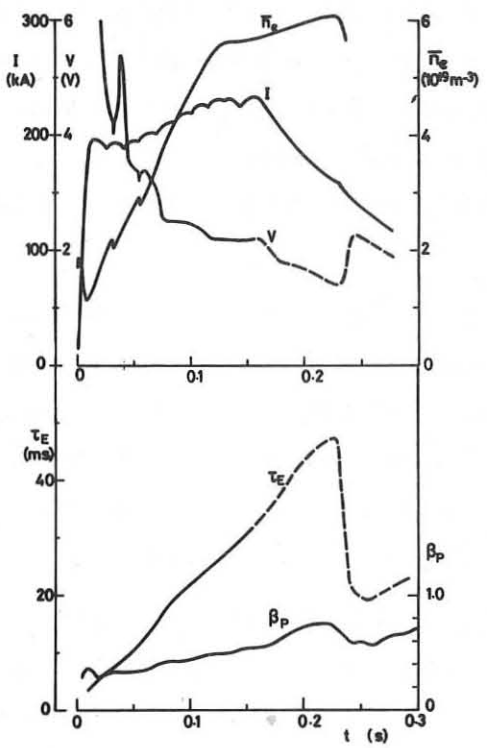

Fig.10 High density discharge.
[dashed lines uncertain]

CLM-P502

Control: The divertor has demonstrated a 50% decrease of the influx of oxygen (Fig. 9) and higher screening efficiency can be expected at higher plasma density.

Gettering only 40% of the torus wall is about 90% efficient in reducing the oxygen influx. The discharge removes oxygen from the ungettered wall and it is trapped in the gettered wall. The reduced oxygen desorption allows more gas feed, increased n_e, (region B of Fig. 3) and longer τ_E (Fig. 10).

Discharge cleaning removes oxygen from the wall. In DITE a few hundred pulses (30 kA, 30 ms) are required each day to obtain operation within the lower density limits (A of Fig. 3). Gettering is simply a quick and more effective way of producing a clean wall.

4.2. High Z Impurities

Origin: Iron, molybdenum and, after gettering, titanium are the dominant high Z impurities. They arise from direct plasma-surface contact involving arcs. Sputtering by hydrogen is totally inadequate to explain the metal content. Sputtering by oxygen appears inconsistent with the decreased metal flux when more oxygen is present and the absence of any change when the oxygen is decreased by gettering without extra gas feed.

Arc marks are clearly observed on the parts of the torus nearest to the plasma and on the limiters. Estimates of the amount of material evaporated by these arcs are not inconsistent with the amount desposited on sample surfaces. There is clear evidence that the influx of iron is reduced by reducing the plasma n and T near the wall. However the interaction will probably be influenced by the violent fluctuation in the plasma near the wall (cf § 6).

Effect: High Z impurities are not fully stripped even at the centre of the discharge and hence radiate from and tend to cool the centre. Measurements showed that the spectrally integrated radiated power is a maximum on axis for all discharges. In some cases the consequent cooling produces a hollow profile $T_e(r)$. The X-ray anomaly factor (ζ) is high corresponding to emission from high Z ions.

Control: Simply increasing the separation between the plasma and the wall by moving the plasma away from the wall or inserting a block limiter, decreases the density and the temperature near the wall and hence the iron influx.

A cold plasma blanket, such as results from gas feed, or from an influx of low Z impurities also effectively increases the separation and thereby reduces the high Z influx as shown in Fig. 8 and 11. The gas feed is more than 90% efficient in reducing the iron influx, resulting in plasmas with $Z_{eff} \sim 1$ and $\zeta \sim 4$.

The divertor unload/limiter function reduces the influx from the wall with 60% efficiency, presumably in part by reducing the n_e and T_e of the plasma in contact with the wall. The screening action of the divertor is about 80% efficient for metals. The fall in total radiation by about 90% and in ζ from 400 to 80, both demonstrate the reduction in metals. The screening action should work for any source of metals whereas the effect of the cold plasma blanket used here is specific to arc sources.

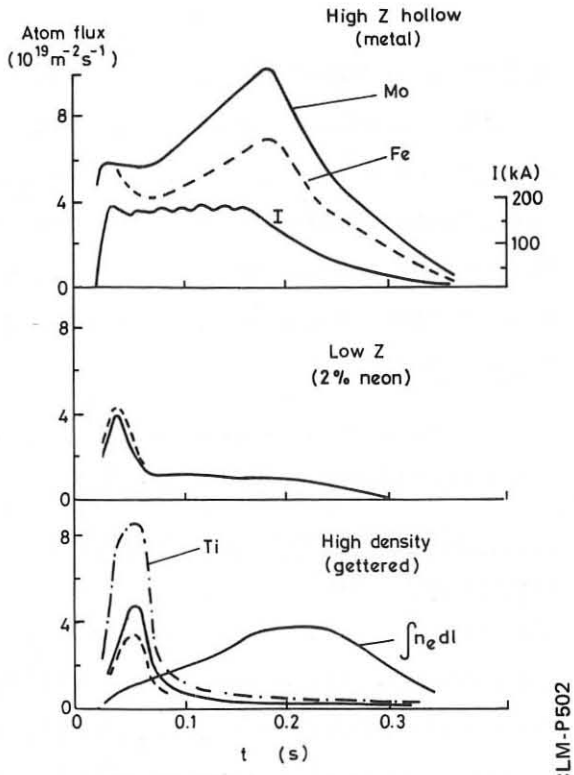

Fig. 11 Effect on metallic fluxes.

4.3. Hydrogen Recycling

Origin: The hydrogen flux into the plasma comes from two sources (i) reflection at the wall of fast neutrals originating from the hot plasma and (ii) desorption of neutrals from the wall surface. Studies using a deuterium filling gas with a hydrogen loaded wall show that these two processes make roughly equal contributions.

Effects: Hydrogen recycling provides the refueling of existing tokamaks because even gas feed is mainly via recycling at the wall. Desorption gives rise to low energy (few eV) neutrals which are ionized in the outer parts of the plasma as shown by the peak in the H_α emission. The reflected neutrals are more energetic ($\sim T_i$) and penetrate further into the plasma, depending on the plasma density. This model and the measured H_α emission against radius agree reasonably with neutral particle transport calculations. However, these various studies have not yet been extended to the highest operating densities, at which we have evidence, from neutral particle analysers, that fast neutrals cannot get out and therefore cannot get into the core of the plasma.

The hydrogen recycling, as we saw in paragraph 4.1, releases oxygen and causes the current channel to contract. Even in the absence of oxygen there would be a limit to the amount of gas which could be absorbed without current contraction.

Control: The divertor unload function reduces the recycling by desorption

and this is shown by the decreased outer peak in $H_\alpha(r)$. The screening function further reduces the influx of slow neutrals. The fast neutrals are affected by neither of these functions at the present low densities. The plasma density falls when the divertor is switched on during a pulse and the increased gas feed required to maintain the density desorbs sufficient oxygen to cancel the screening action. This explains the unchanged Z_{eff} [8].

The effect of gettering on recycling is not fully investigated and the preliminary results are not yet understood.

5. POWER BALANCE AND TRANSPORT

Electrons: The input ohmic power to the electrons is derived by assuming the current density is proportional to $T_e^{3/2}$. The power loss from the electrons by radiation as a function of radius is measured by thermopiles, with some calibration uncertainty, assuming that the power in charge-exchange neutrals is negligible. Typical radial profiles for the three types of discharge, high Z, low Z and high density are shown in Fig. 12. The notable feature is the appreciable reduction of radiated power for the high density "pure" discharges. However the profiles have the same form with a central peak for all three discharge types. This is different from the typical oxygen dominated discharges in TFR which show an outer peak. The divertor, by reducing the high Z impurities, almost removes the central peak for 50 kA

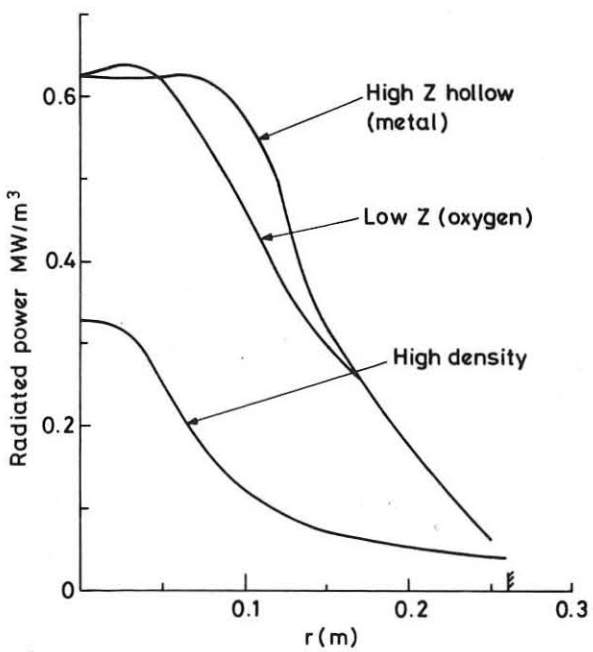

Fig. 12 Profiles of radiated power.

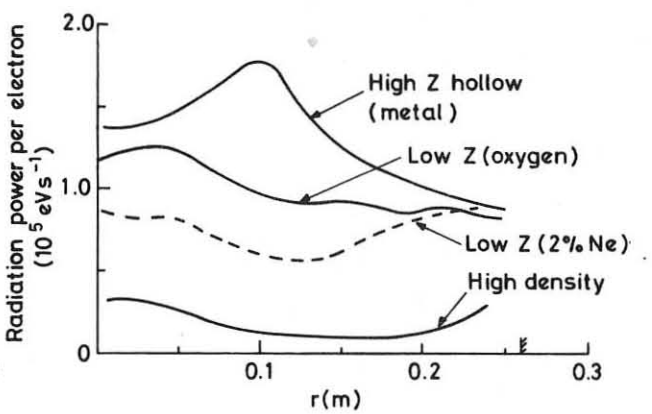

Fig. 13 Profiles of radiated power per electron.

discharges. These various profiles suggest that even in the so called low Z and "pure" discharges, high Z impurities make a major contribution to the radiation losses. Perhaps a better measure of the effect of impurities is the radiated power per electron shown in Fig. 13. Clearly there is a reduction of this parameter from high Z, through low Z to high density discharges.

The difference between the radiated power profiles for low and high Z discharge is much less than the difference between the profiles $T_e(r)$ (Fig 5) and therefore the input power profiles. It appears that the impurities through a small change in the radiated power profile trigger a larger redistribution of the input power.

Before calculating the thermal transport through the electrons, the energy transfer between electron and ions needs to be calculated. This requires a knowledge of the ion temperature profile.

Ions: In earlier experiments we demonstrated near neoclassical profiles of ion temperature for $r/a < 0.4$. In the power balances reported here we have measured only the central ion temperature and compared it with the predictions of neoclassical theory. There is usually reasonable agreement and then we assume the theoretical ion temperature profile, derived using the measured $T_e(r)$, gives the energy transfer between electrons and ions.

Thermal Flux Through Electrons: This has been derived from the above power balances for the three discharge types and the results are shown in Fig. 14. Using the experimental plasma parameters, the theoretical predictions of neoclassical theory [10] are calculated and plotted for comparison. Near the centre of the high Z dominated discharges the comparison is favourable but this is probably fortuitous.

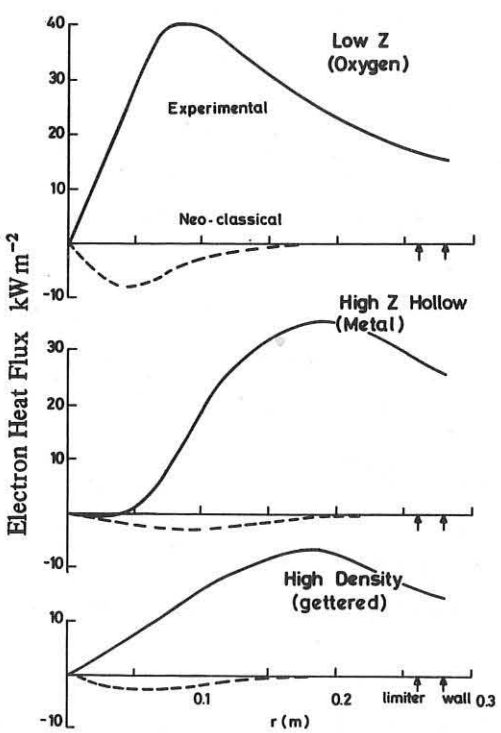

Fig. 14 Profiles of electron heat fluxes compared with neoclassical.

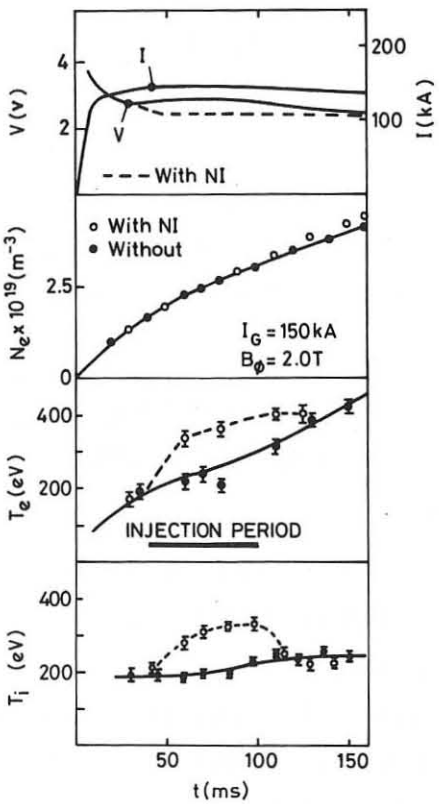

Fig. 15 Electron and ion heating by injection.

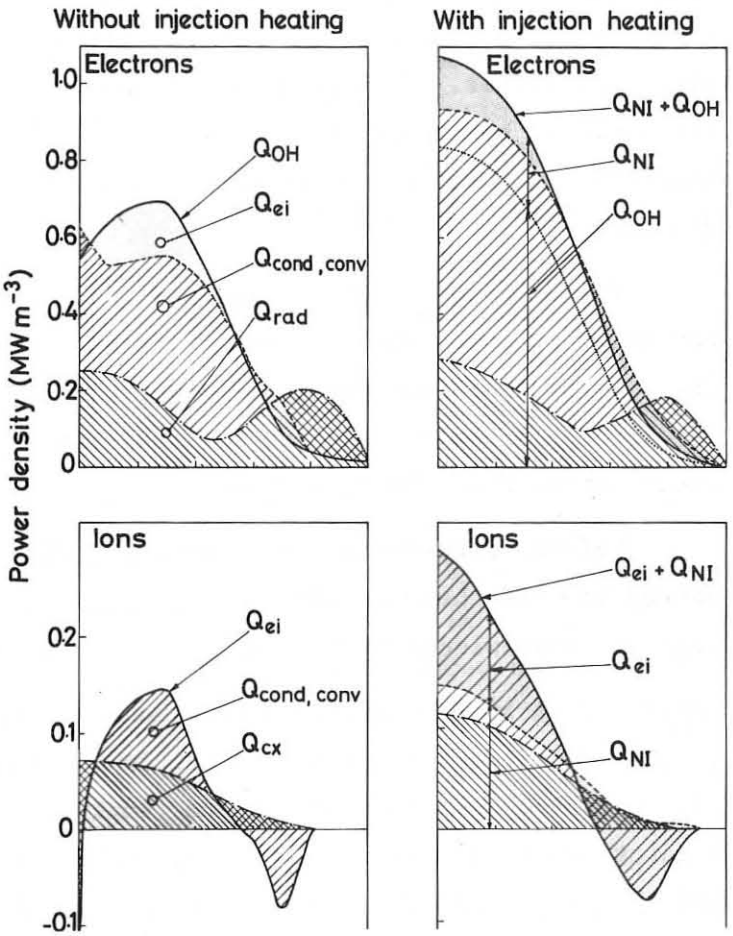

Fig. 16 Power balances for injection into low Z_{eff} discharge.

CLM-P502

Neutral Injection: The three types of discharge have been heated by injection and full power balances performed for the high Z and "pure" cases. In the later case the rise in electron temperature (Fig. 15) can be shown, from the full radial power balance (Fig. 16), to be unambiguously attributable to injection heating. There is no increase in impurities during injection and the plasma parameters return to those without injection. The change in $T_e(r)$ demonstrates the principle of profile control by injection.

6. STABILITY

MHD: Impurities frequently dominate the power balance which determines $T_e(r)$, $q(r)$ and hence the MHD stability (e.g. hollow profiles with $q > 2$, low Z with $q = 1$ and the disruptive density limit).

The theoretical stability of the experimental profiles has been investigated using the Wesson stability code [11]. Most experimentally stable profiles are theoretically stable. But profiles from near the density limit,

which have steeper gradients with flatter centres, tend to be marginally stable or unstable.

During the rise towards high densities there are often pauses in the rise. These are accompanied by increased MHD activity, loss of plasma and an increase in inductance. On some occasion a partial filling of the hollow profile is observed using the sequence of profiles, $T_e(r)$, from the electron cyclotron emission (Fig. 17). This phenomenon appears to be an MHD re-organization of the discharge but it is not yet fully diagnosed or understood.

The plasma near the wall is violently unstable ($\Delta n/n \sim 1$) with $f \sim 200$ kHz.

Micro-instabilities: There is clear evidence from the interferometer for measuring the electron cyclotron emission, that there is strong, narrow band emission at ω_{pe} even from discharge with low runaway levels at high densities.

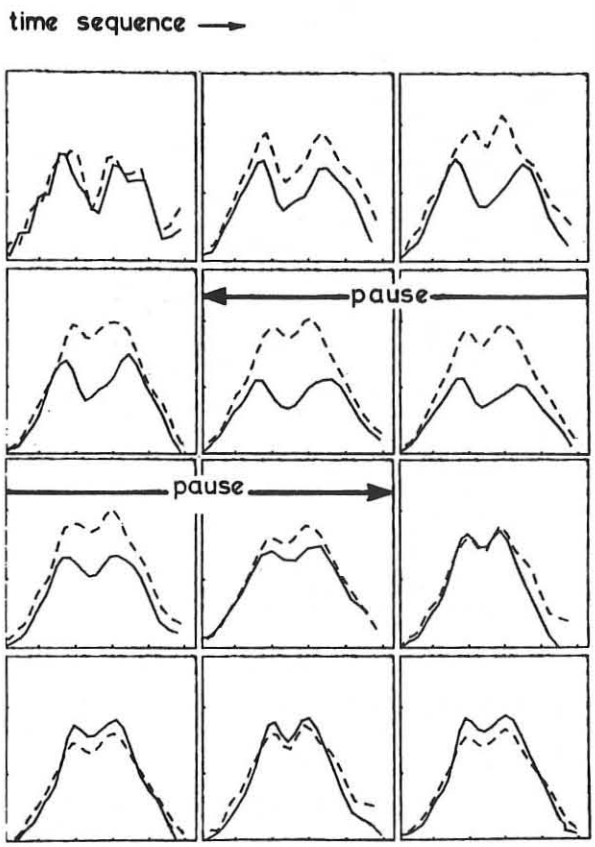

Fig. 17 $T_e(r)$ sequence from the electron cyclotron emission.

——— with pause.
– – – – without pause.

CLM-P502

Drift Waves: The theory of Duchs et al [12] has been used to calculate, using the experimental profiles, the thermal flux to be expected from drift wave turbulent transport. The results for the three types of discharge are compared with experiment in Fig. 18. The theoretical curves are very dependent on the experimental gradients of density. The small changes shown in Fig. 19, which are within experimental errors, are sufficient to produce exact fits of drift wave transport to the observed transport and this implies that such comparisons are at present of doubtful value.

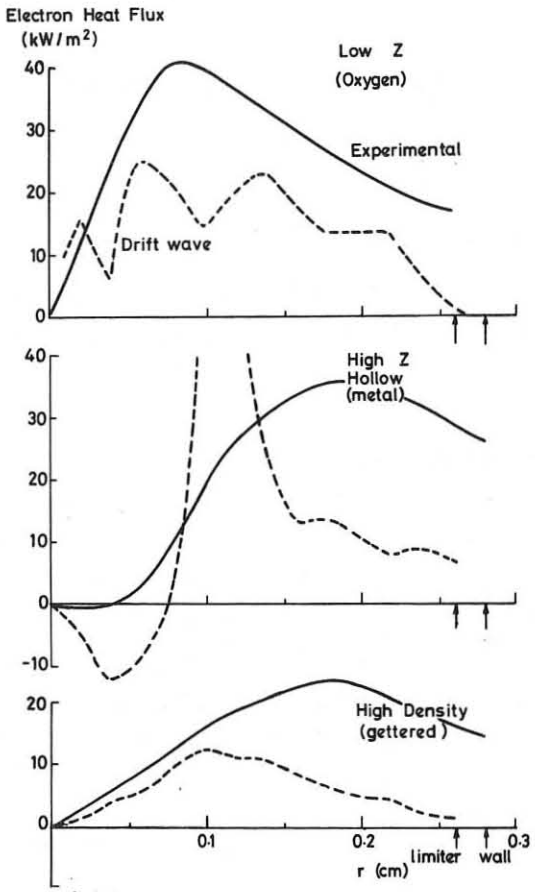

Fig. 18 Comparison of electron heat flux with drift wave theory.

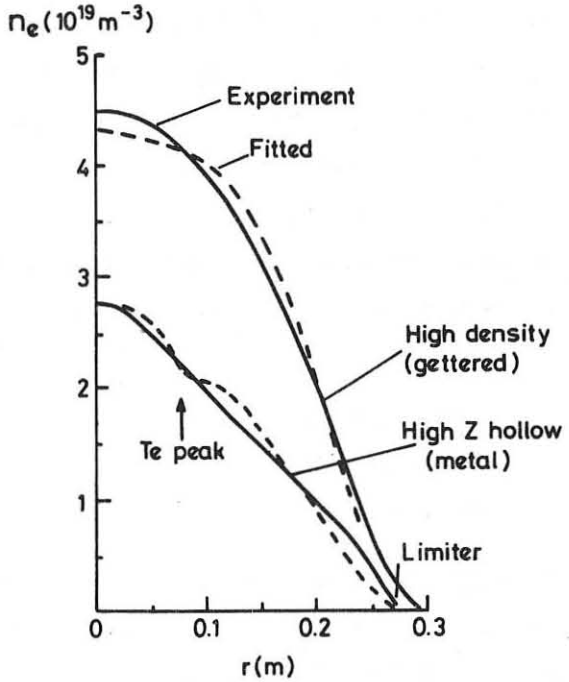

Fig. 19 Fitting to drift wave transport.

CLM-P502

7. DISCUSSION

The DITE results provide a better understanding of the origin, effect and control of impurities and lead to the following conclusions and comments:

(1) The study of transport and stability in impure plasmas may be interesting but may not be relevant to the properties of the pure plasmas required for fusion research.

(2) Relatively pure plasma with $Z_{eff} \sim 1$ and $\zeta \sim 4$ are produced with ease in DITE by a combination of gettering and the cold plasma blanket produced by gas feed.

(3) The DITE divertor controls impurities in a more satisfactory manner but requires testing at higher operating densities, when it should produce similar pure plasmas with $Z_{eff} \sim 1$.

(4) Low ohmic power density machines like DITE, PLT and T10, which all have the same B_T/R, are very sensitive to impurities and larger machines will be even more sensitive. While some of these effects can be off-set by powerful additional heating, it is clearly better to reduce

the impurity level. However, reducing the impurity level reduces the ohmic power input and this emphasises the need for powerful additional heating anyway.

(5) Powerful injection into such plasma should allow a reasonable degree of decoupling between the three main tokamak problems; heating, transport/stability and purity.

(6) Refueling by gas feed is closely coupled to the boundary layer and surface interactions. An alternative independently controllable method needs to be developed particularly for experiments using divertors.

(7) At present in DITE sputtering is not important, compared with arcing, as a source of metal impurities. However, this may not be so with better control of arcing and the higher ion temperature available with powerful injection. Such plasmas must be used to develop methods, such as the divertor and the other type of cold plasma blanket, to control the influx of impurities from sputtering.

The author wishes to acknowledge his indebtedness to all his colleagues on the DITE project.

References

[1] S.J. Fielding, M. Hobby, J. Hugill, G.M. McCracken, J.W.M. Paul, N.J. Peacock, B.A. Powell and P.E. Stott, This conference, Paper 39, Culham Preprint CLM P492.

[2] P.E. Stott, J. Hugill, S.J. Fielding, G.M. McCracken, B.A. Powell, and R. Prentice, This conference, Paper 37, Culham Preprint CLM P492.

[3] S.J. Fielding, G.M. McCracken, S.K. Erents, A. Pospieszczyk and P.E. Stott, This conference, Paper 38, Culham Preprint CLM P492.

[4] J. Hugill, S.J. Fielding, R.D. Gill, M. Hobby, G.M. McCracken, J.W.M. Paul, N.J. Peacock, B.A. Powell, R. Prentice and P.E. Stott, This conference, Paper 39, Culham Preprint CLM P492.

[5] G.M. McCracken, G. Dearnaley, S.J. Fielding, D.H.J. Goodall, J. Hugill, J.W.M. Paul, P.E. Stott, J.F. Turner and J. Vince, This conference, Paper 40, Culham Preprint CLM P492.

[6] R.D. Gill, K.B. Axon, R.S. Hemsworth, J. Hugill, P.J. Lomas, J.W.M. Paul, R. Prentice, P.E. Stott and D.D.R. Summers, This conference, Paper 171, Culham Preprint CLM P492.

[7] M.J. Forrest, P.G. Carolan, N.J. Peacock, Submitted for publication.

[8] J.W.M. Paul, et al, Proc. of 6th IAEA Conference on Plasma Physics and Controlled Fusion Research, Berchtesgaden (1976), Vol 2, 269.

[9] J. Hugill and J. Sheffield, To be published, Nuclear Fusion 18 (1978).

[10] F.L. Hinton, et al, Phys. Rev. Lett. 29 (1972) 698.

[11] J.A. Wesson, To be published, Nuclear Fusion 1977.

[12] D.F. Duchs et al, Nuclear Fusion 17 (1977) 565.

EXPERIMENTS ON ADIABATIC COMPRESSION OF A TOKAMAK PLASMA IN TUMAN -2

V.E.GOLANT

A.F.Ioffe Physical-Technical Institute

Leningrad, USSR

ABSTRACT. The paper presents a review of the results on minor radius compression of a tokamak plasma in the Tuman-2 device ($a = 8$ cm, $R = 40$ cm, $H_o = 4$ kG, $H_{max} = 12$ kG, $I_p = 5$ kA). The experiments showed an effective compression of plasma column and plasma heating during fast increase of a toroidal magnetic field. Oscillations were strongly reduced in compressed column. An essential improvement of energy confinement was found. The maximum value of plasma pressure corresponded to $\beta_T = 2\text{-}2{,}5$. The paper includes also the description of first experiments on the modified Tuman-2A device ($H_{max} = 20$ kG, $I_{pmax} = 15$ kA).

INTRODUCTION. Interest in adiabatic compression of tokamak plasmas is caused by the possibility of its application to the production and heating of plasma column. On the other hand, compression can be an effective method of diagnostics since it provides a means of controlling plasma parameters and their profiles. In recent experiments, two types of compression were realized, i.e. a fast increase of toroidal magnetic field (minor radius compression) /1-4/ and displacement of the plasma column along the major radius (major radius compression) /5/. This paper presents a review of the results on minor radius compression of the tokamak plasma in the Tuman-2 device ob-

tained by the group of the late Dr. M.G.Kagansky [6-8]. It includes also a description of first experiments on the reconstructed Tuman-2A device.

DESCRIPTION OF TUMAN-2 EXPERIMENTS. Tuman-2 was a tokamak type device [9] with major radius R = 40 cm, minor limiter radius a = 8 cm. The value of toroidal magnetic field during ohmic heating was H_o= 3-5 kG, plasma current I_p= 2-6 kA. After ohmic heating period toroidal magnetic field was raised that to provide compression. The maximum value of field after compression was 12 kG, its rise time ~ 120 μs, its decay time ~2 ms.

First experiments were performed at rather poor vacuum condition. They demonstrated an effective compression of a non-stable plasma column and its stabilization after compression [3]. After improvements of vacuum conditions a stable tokamak type discharge was obtained during ohmic heating [6]. The plasma parameters for typical ohmic heating regime at H = 4 kG, I_p= 5 kA were following: average plasma density $\bar{n} = (6-8).10^{12}$ cm^{-3}, maximum electron temperature T_e= 100-150 eV, ion temperature $T_i \approx$ 30 eV, energy confinement time τ_E = 150-200 μs, Z_{ef}=1.5-2, β_I = 0.5-0.7. The typical compression experiments were performed by increasing magnetic field from 4 up to 12 kG (compression degree α = 3). Transverse magnetic field was increased during compression that to prevent the outward shift of plasma, caused by the rise of β_I. The time behaviour of some plasma cha-

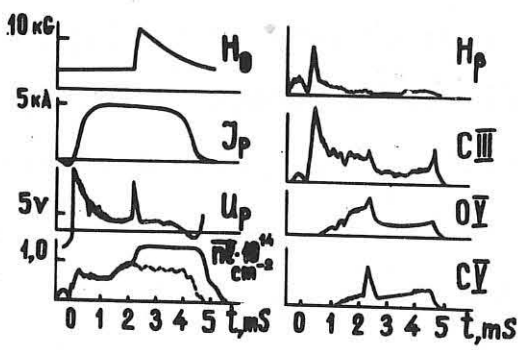

Fig. 1

racteristics is shown in Fig.1. The plasma current I_p was kept constant by external circuit. The loop voltage U_p shows an inductance spike connected with current channel compression. The $n\bar{\ell}$ curve was obtained from 4 mm microwave interferometer measurements. Temporal behaviour of spectral lines: H_β, CIII, OV and CV permitted to estimate electron temperature, amount of impurities and hydrogen flux. All these data together with data obtained by laser scattering and charge exchange analysis gave information about plasma compression and heating.

PLASMA COMPRESSION. The data on plasma density compression can be taken from microwave measurements /6/. They give the alteration of quantity $n\bar{\ell} = \int_{-a}^{a} n dx$. During compression corresponding to the "frozen" condition the value $n\bar{\ell}$ must increase $\sim\sqrt{a}$. The experimental curves show an increase close to this prediction (see Fig.1). It must be mentioned that $n\bar{\ell}$ did not decrease after compression during decay of magnetic field. This implies the accumulation of a plasma which can be caused by slowing down of plasma diffusion. This conclusion agrees with ~2 fold decrease of hydrogen and impurities flux deduced from spectroscopical and charge exchange neutrals measurements.

Some data on density profile during compression can be obtained from spectral line intensity measurements if ionization time of radiating state is essentialy longer than the time of compression /7/. Such condition was realized for OV line in a discharge regime with a reduced current (I_p= 2.5 kA, n = = 1.5×10^{12}cm^{-3}, T_{eo}= (40-50)eV). The profiles of OV intensity before and after 3 fold compression of this discharge are presented in Fig.2. The figure shows the contraction of the intensity profile and 5 fold rise of its amplitude during comp-

ression. This corresponds well to the "frozen-in" condition ($\mathcal{J} \sim n\bar{n}_c \ell \sim \alpha^{3/2}$).

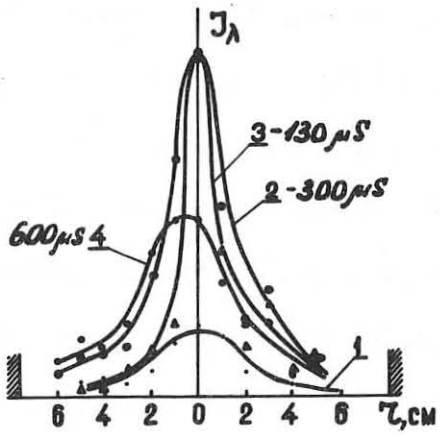

Fig. 2

CURRENT CHANNEL COMPRESSION. The data on current compression can be deduced from inductance spike on the loop voltage curve [8]. The well known formula for toroidal plasma inductance leads to the simple relationship between alteration of loop voltage and current channel radius (a_I). Experimental curves of loop voltage at different compression degree are shown in Fig.3a. Fig.3b presents comparison between experimental data and calculations for current profile "frozen" into toroidal magnetic field ($a_I \sim 1/\sqrt{H} \sim \alpha^{-1/2}$). It can be seen that during the first half of compression period the calculations agree well with experiments. The discrepancy in later stage can be explained by classical diffusion of poloidal magnetic field ($D_H = c^2/4\pi\sigma \sim 4\times10^3$ cm^{2}s^{-1} for compressed state).

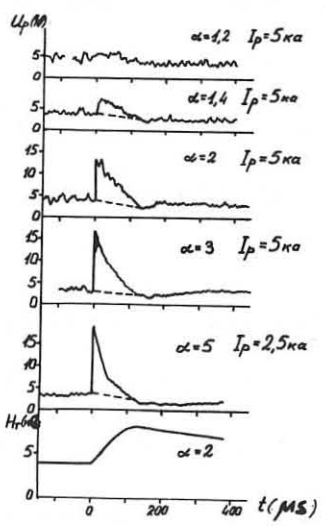

Fig. 3a

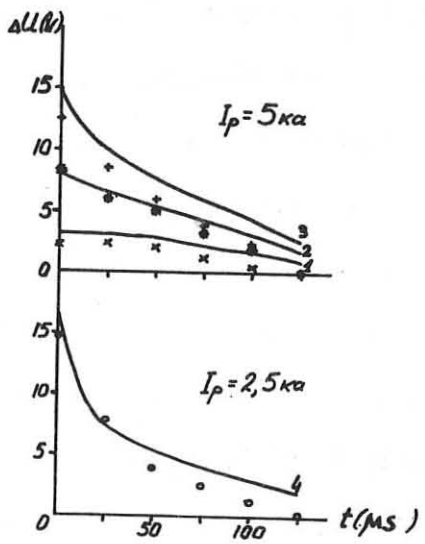

Fig. 3b

The data on field diffusion were obtained also from other observations /8/, for instance, the absence of current compression by small increase of magnetic field (see Fig.3 at α =1.2), the early break of compression for unstable regime with smaller conductivity. These data confirmed the classical value of field diffusion coefficient in the conductivity range σ =(1-5)x10^{15} CGSE.

DAMPING OF PLASMA OSCILLATIONS. A strong decrease of plasma oscillation amplitude was observed as a result of plasma compression /8/. This effect can be seen on oscillograms of U_p, $n\bar{\ell}$, CIII and OV intensity (Fig.1,3) and strongly pronounced on magnetic probe signals (Fig.4). It must be mentioned that the oscillation amplitude before compression on the outer side of torus was larger than on the inner side. It is in accordance with larger H_β intensity which shows stronger plasma-wall interaction. The damping of oscillations after compression equalizes their amplitudes and make the H_β profile symmetrical. This observation leads to the assumption that the oscillations are connected with the resistive balloon mode on the cold plasma periphery. If this assumption is true the damping of oscillations after compression can be caused by heating of electrons on periphery of current channel /8/.

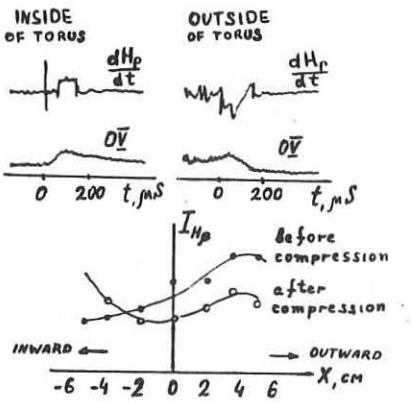

Fig. 4

PLASMA HEATING. The data on electron heating during compression were obtained from conductivity, laser scattering and spectral line intensity measurements. Fig.5 shows the rise of

conductivity (σ/σ_0) [6]. It can be seen that the increase of σ after compression was higher than it follows from the adiabatic law ($T_e \sim \alpha^{2/3}$; $\sigma \sim T_e^{3/2} \sim \alpha$). It is difficult to explain the discrepancy by increase of Z_{ef} since the impurity flux drops after compression. Therefore the obtained conductivity rise must be caused by electron heating.

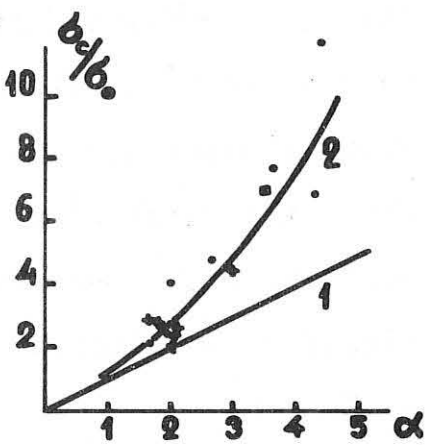

Fig. 5

Laser scattering measurements [6] gave the most reliable data on electron heating near the axis of plasma cross section (at $r < 2$ cm) [6]. The maximum electron temperature measured by scattering for typical regime before compression was $T_e = (110 \pm 20)$eV, just after compression $T_e = (190 \pm 30)$eV and 320 μs later $T_e = (280 \pm 40)$eV.

The data on electron temperature profile were deduced from spectral line measurements [7]. The profile during the period of ohmic heating was determined by location of OV and CIII intensity maxima. After compression it became possible to use the burnout of CV line caused by ionization, since the ionization time is determined by T_e. The measurements of burnout time at different chords were used for determination of T_e profile. Spectroscopic data on T_e spatial distribution along major radius before and after 3 fold compression together with laser data are pre-

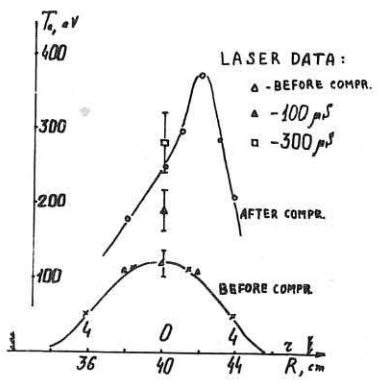

Fig. 6

sented in Fig.6. It can be seen that the temperature profile contracts during compression. The profile became asymmetric, the spatial decay of T_e was steeper on the outer side of the torus. The electron temperature rise after compression $T_{ec}/T_{eo} \approx 3.5$ was considerably larger than adiabatic one ($T_{ec}/T_{eo} = \alpha^{2/3} \approx 2$).

The data on ion heating were obtained from charge exchange particle analysis /10/. The ion temperature for typical regime of compression increased from 30 up to 55 eV in agreement with the adiabatic law.

The estimate of plasma pressure based on measured T_e profile, ion heating and density compression data leads to $\beta_I = 8\pi nT/H_I^2 = 2\text{-}2.5$. This large value ($\beta_I > 1$) can cause the observed asymmetry in T_e distribution on major radius (Fig.6). It can be shown that this asymmetry approximately corresponds to the displacement of magnetic surfaces predicted by equilibrium theory /7/.

ON THERMOINSULATION OF COMPRESSED PLASMA. It has been shown that the rise of electron temperature during compression is larger than predicted by adiabatic law and that after compression the temperature continues to increase during some time. The estimates based on these data lead to the energy confinement time in compressed state $\tau_E = 600\text{-}800$ μs, i.e. 3-5 times longer than in the ohmic heating period /6,7/. It can be mentioned that this result distiguishes the Tuman-2 experiment from the major radius compression experiment on ATC in which the stored energy and its confinement time decreased during compression /11/. The difference can be caused by contact of the plasma column with the limiter during compression on ATC.

It is interesting to compare the experimental value of τ_E with scaling laws obtained from different tokamak experiments $\tau_1 = 3.6\times10^{-8}a^2H_\varphi$ /12/, $\tau_2 = 6\times10^{-19}\bar{n}a^2\sqrt{q/Z_{ef}}$ /13/ (τ - sec, n - cm^{-3}, H - G, a - cm). The comparison for ohmic heating period (a_{ef}= 6 cm) and for compressed state (a_{ef}= 3.5 cm) is presented in the table (the values of a_{ef} are taken from T_e profile). It can be seen that the experimental value of τ_E for compressed state is 3-6 times longer than τ_1 and τ_2 and only 2 times shorter than the time of neoclassical heat transport τ_q.

Comparison of τ (ms)

	τ_E	τ_1	τ_2	τ_q
Ohmic heating	0.15-0.2	0.22	0.2	3
Compression	0.6-0.8	0.13	0.2	1.5

An observed improvement of thermoinsulation during compression may be caused by removal of the plasma column from the limiter. This effect was pointed out in /14/. Another possible reason is connected with the decrease of transverse energy transport caused by the damping of plasma oscillations.

EXPERIMENTS ON TUMAN-2. Recently the Tuman-2 device was considerably reconstructed to provide higher magnetic fields (up to 20 kG after compression), higher currents and better vacuum conditions. The experiments on the modified device Tuman-2A were started in 1977. A stable regime of ohmic heating was achieved at H = = 6-7 kG, $I_p \approx 12$ kA. The maximum plasma density measured by 2-mm interferometer in ohmic heating period was $n \approx 2\times10^{13}cm^{-3}$, the maximum electron temperature as determined by spectroscopical and soft X rays techniques was ~300 eV. The behaviour of

plasma characteristics during 2 fold increase of toroidal magnetic field (τ_c = 0.5 ms) is illustrated by oscillograms shown in Fig.7. Some of them are similar to those obtained in previous experiments (Fig.1). The inductance spike on U_p curve and increase of $\bar{n}\ell$ lead to a conclusion that compression is close to "frozen" condition. The decrease of U_p after compression and the rise of OVII intensity show an essential heating of electrons. More detailed investigation of compression is now in progress. Its programme includes the study of density and temperature profiles, energy losses and plasma oscillations during and after compression. We hope that these experiments together with compression experiments on the Tosca device /4/ will clear up the matter of plasma thermoinsulation in compressed state.

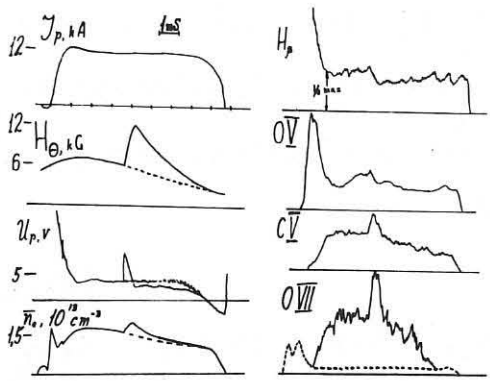

Fig. 7

The next step in adiabatic compression experiments will be connected with the larger instalation Tuman-3, the construction of which is now in finale stage. The dimensions of its chamber will be a = 23.5 cm, R = 55 cm, the magnetic field before compression H_o = 10 kG, after compression H_c = 30 kG. The programme includes three stages of heating: first - ohmic heating (I_{pmax} = 150 kA), second - high frequency heating in the ranges of electron cyclotron and low hybrid frequency and third - adiabatic compression in minor and major radius (the maximum compression degree α = 5). Plasma density and tempe-

rature are expected to be $n \approx 10^{14}$ cm^{-3}, $T \gtrsim 3$ keV.

The author wish to thank the staff of the Tuman group and especially Drs. S.G.Kalmykov, S.V.Lebedev and K.G.Shakhovets for numerous discussions and assistance in preparing of this paper.

REFERENCES

1. Ivanov D.P., Parfenov D.S. Plasma Phys. and Contr.Nucl.Fus. Res. 1965, v.2, IAEA, Vienna (1966), p.659.
2. Gladkovsky I.P. et al. Plasma Phys. and Contr.Nucl.Fus.Res. 1968, v.1, IAEA, Vienna (1969), p.277.
3. Berezovsky E.L. et al. Proc. of the 3 Int.Symp. on Toroidal Plasma Confinement, Munich, 1973; Zh.Techn.Fiz. 45, 555, 1975.
4. Cima G. et al. Plasma Phys. and Contr.Nucl.Fus.Res. 1976, v.1, IAEA, Vienna (1977), p.335.
5. Bol K. et al. Phys.Rev.Lett. 29, 1495, 1972; Plasma Phys. and Contr. Nucl.Fus.Res. 1974, v.1, IAEA, Vienna (1975)p.77.
6. Berezovsky E.L. et al. Proc. of the 7 Europ.Conf. on Contr. Fus. and Plasma Phys., Lausanne (1975), pp 4,5.
7. Kagansky M.G. et al. Plasma Phys. and Contr.Nucl.Fus.Res. 1976, v.1, IAEA, Vienna (1977), p.387.
8. Kagansky M.G., Kalmykov S.G. Fiz.Plazmy 3, 1977.
9. Anisimov A.I. et al. Plasma Phys. and Contr.Nucl.Fus.Res. 1971, v.3, IAEA, Vienna (1972), p.543.
10. Berezovsky E.L. et al. Zh.Techn.Fiz. 46, 1575, 1976.
11. Daughney C.C., Bol K. Nucl.Fus. 17, 367, 1977.
12. Gorbunov E.P. et al. Nucl.Fus. 10, 43, 1970.
13. Berry L.A. et al. Plasma Phys. and Contr.Nucl.Fus.Res. 1976, v. 1, IAEA, Vienna (1977), p. 49.
14. Dnestrovsky Yu.N. et al. Pisma v Zh.Ehksp.Teor.Fiz. 13, 697, 1971.

Ohmic Heating Experiments in the W VII A Stellarator

W VII A Team

Max-Planck-Institut für Plasmaphysik, EURATOM-Ass.
D-8046 Garching, Federal Republic of Germany

Abstract:

The confinement of plasma in W VII A was studied in the parameter regime: $B_o = 20 - 35$ kG, $t_o = 0.055 - 0.23$, density $\bar{n}_e = .5 - 2.5 \times 10^{13}$ cm^{-3} and temperatures between $kT_e = 300 - 700$ eV, $kT_i = 150 - 300$ eV. In stationary discharges up to 500 ms, energy confinement times from 2 - 10 ms were found. $T_i(r)$ profile measurements show asymmetries. Particle confinement times are derived from H_α -measurements. The stellarator field stabilizes the discharge at $q(a) = 2$, where stationary operation is possible.

Introduction

The first experimental results of the W VII A stellarator were presented at the Berchtesgaden conference 1976 /1/. Since that time several technical improvements made it possible to expand the attainable parameter range. The magnetic field could be increased up to 3.5 T. With a feedback control system of the ohmic heating transformer the plasma current during the discharge could be varied in a programmable way. So stationary discharges and a maximum pulse length of 650 ms could be achieved. Also the horizontal position of the plasma column was controlled using the signals from magnetic coils or X-ray diodes. In order to maintain the density for these long pulses and to build up higher electron densities a constant influx of neutral hydrogen was necessary. This seems to indicate that recycling rates are not high enough. A system of fast acting valves consisting of a combination of mechanical and piezoelectric valves was used to program the neutral hydrogen flux $\Gamma(t)$ within a range of 10^{18}-10^{21} atoms/s.

Diagnostics

The main parameters of the W VII A device are given in Fig. 1. This diagram also includes the diagnostic methods which have been used:

- The line density is measured by 2 mm microwaves.
- The temperature and density profiles $T_e(r)$, $n_e(r)$ are measured along a vertical line by Thomson scattering methods. This yields a scan through the elliptical plasma cross section under 45° to the major axis of the ellipse.
- Radial scans of impurity line emission were obtained with a normal incidence VUV spectrometer.
- Also the temperature profile of ions was measured with a movable particle energy analyzer. A 18 kV neutral beam was used to measure the ion temperature in the plasma center.
- H_α-light emission was measured across the plasma radius and at several positions around the torus in order to obtain the neutral particle density and the plasma particle confinement time.
- Calorimetric measurements at the limiter and bolometric measurements of the energy flow to the wall show that about 20% of the ohmic heating power is going to the limiter and 80% of the power is delivered to the wall.
- MHD activity of the plasma is recorded by 12 magnetic pick-up coils around the minor and major circumference of the torus.
- X-ray emission is investigated with diodes, the time dependent signals of the floating limiter segments and probe signals at the edge of the plasma complete the picture of transient phenomena.

Parameter Range

After one hour of cleaning discharges in a stationary magnetic field of 4 kG and a heating power of 5 kW (50 Hz) reproducible operation with pulsed discharges is possible. Preionization is made by a plasma gun and an additional 108 MHz (3 kW) rf pulse of 10 - 20 ms duration. Normal filling pressure of H_2 is 10^{-4} - $6 \cdot 10^{-4}$ torr.

The parameter range investigated so far is:

magnetic field	$B_o = 2.0 - 3.5$ T
external transform	$\iota_o = 0.23$ (2.5 - 3 T)
	$\iota_o = 0.11$ (2.5 - 3.5 T)
	$\iota_o = 0.055$ (3.0 - 3.5 T)
	$\iota_o = 0.68$ (2.0 T)
density regime	$n_e = 5 \times 10^{12} - 5 \times 10^{13}$ cm^{-3}
	$kT_e(o) = 200 - 700$ eV
	$kT_i(o) = 150 - 350$ eV
	$nkT \leq 2 \times 10^{16}$ eV/cm^3

The plasma current was varied between 11 and 40 kA.

Several limitations prevented the extension of the parameter range. In the stationary phase of the discharge the loop voltage could not be increased beyond 5 V because of technical reasons thus limiting the available ohmic heating power. The attempt to reduce the external rotational transform ι_o to zero failed because of a small radial stray field < 10 G, which shifts the plasma column in vertical direction. Below $\iota_o \approx 0.01$ this shift destroys the discharge. This stray field is generated by eddy currents which are induced by the ohmic heating transformer.

Energy Confinement

The gross energy confinement time of the electrons $\tau_{E'}(r)$ ($\tau_{E'} = \frac{\frac{3}{2}\int n_e kT_e \, dV}{P_{OH}}$)

and the total energy confinement time $\tau_E = \frac{\frac{3}{2}\int nk(T_e + T_i) \, dV}{P_{OH}}$

are calculated from the measured n_e, T_e, T_i profiles. The ion temperature profiles are rather flat and similar to the density profiles, therefore, $T_i \sim n_e$ was used in all cases where only $T_i(o)$ was measured. The diamagnetic loop, which measures the total plasma energy content, gives values of τ_E which are about 20% higher than those from the profile measurements. The measured profiles are fitted by functions of the type $T_e(r) = \frac{T_e(o)}{1 + (\frac{r}{r_o})^{\alpha}}$.

A comparison of discharges with $\iota_o = 0.055, 0.11, 0.23$ shows a pronounced difference in the shape of the profiles. At $\iota_o = 0.23$ the profiles are flat in the plasma centre and more peaked in the case $\iota_o = 0.055$ (Fig.2). At nearly same plasma current and plasma density the central temperature reaches larger values for $\iota_o = 0.055$. In spite of this effect the energy content and the energy confinement times are nearly the same.

The enhanced transport mechanism which flattens the profiles in the stellarator case $\iota_o = 0.23$ is attributed to the sawtooth oscillations observed in the plasma centre. This is supported by several observations:

1. The thermal electron conductivity D_E derived from the energy balance
$$D_E = \frac{\int (P_{OH} - P_{ei}) \, dV}{4\pi^2 R \, r k \frac{dTe}{dr}}$$
shows a minimum at the radius with $q = 1$ (see Fig.3).

2. The flat area in most cases extends to the $q = 1$ surface.

3. The energy confinement time for the volume $q \leq 1$ as derived from the observed amplitude of the sawtooth oscillations shows that a significant part ($\leq 50\%$) of the energy losses of the electrons is due to these oscillations (Fig.4).

The explanation for the flat temperature profiles is the anomalous loss which limits the current density and also the heating power in the centre so that $q(o) \approx 1$ is always maintained.

The minimum values of the thermal conductivity $D_E(r)$ are between 1×10^3 and $1 \times 10^4 \, cm^2/s$; these data are close to those found in Ormak and TFR, although the temperature T_e is larger in these machines. Pseudoclassical thermal conductivity does not fit the observed data. The measured values of D_E (which are upper limits since radiation losses have been neglected) roughly scale with $n_e^{-0.8}$ and decrease with increasing temperature. A dependence on the stellarator field could not be observed for the studied ι_o values at currents between 15 and 35 kA. The gross energy confinement time of the electrons $\tau_E'(r)$ only varies by $\leq 25\%$ over the plasma radius $\tau_E'(a) \leq \tau_E(o)$. Because of the condition $q = 1$ in the centre $\tau_E(o)$ can be

connected to $kT_e(o)$ and $n_e(o)$. The plasma data in the centre therefore determine an upper limit for the electron confinement time (Fig.5).

When the plasma current is increased the total energy confinement time τ_E decreases beyond a critical current which corresponds to a total rotational transform of $\iota_p(a) \approx 0.2$ and $\iota_o + \iota_p(o) = 1$ (Fig.6) for ι_o is 0.055.

In the case $\iota_o = 0.055$ the decrease is accompanied by growing MHD modes of the type m = 2, n = 1. $\iota(a) = 0.5$ could not be reached without current disruption. With higher external rotational transform $\iota_o = 0.23$ the decrease of τ_E with current begins beyond $\iota(a) = 0.5$. Only a low activity of m = 2, n = 1 and m = 3, n = 2 modes is observed, in this case the increasing effect of the enhanced transport due to internal disruptions within the q = 1-surface is believed to be responsible for the deteriorations of the confinement. Beyond the critical current the energy content of the plasma drops again at low external rotational transform whereas in the equivalent case with $\iota_o = 0.23$ the energy content W reaches higher values (see Fig.6, upper picture). This is another indication that in both cases different loss mechanisms are causing the deterioration of the confinement.

In a small region around $\iota(a) = 0.5$ the confinement time drops by a factor of 2. No enhanced fluctuations are observed at the same time, therefore, a stationary loss in combination with island formations may be the reason for this loss.

The energy confinement time is an increasing function of the electron density (Fig.7). The plasma parameters are changed by varying the neutral gas inflow $\overline{\Gamma}(t)$ with all other parameters kept fixed ($B_o = 3$ T, $\iota_o = 0.23$, $I_p = 26$ kA). The temperatures of ions and electrons approach each other with increasing density, therefore, a scaling of the confinement time should include a dependence on temperature. Evaluation of all data from the profile measurements showed a scaling of τ_E with $n_e^{0.8}$ (n_e is the space averaged density.) This scaling was found in a regime from $\bar{n} = 0.5 - 2.5 \times 10^{13}\,\mathrm{cm}^{-3}$, but temperature dependence was neglected. The absolute values of τ_E vary between 2 and 10 ms. The optimum values always obtained at the lowest possible currents are nearly equal for all cases of external rotational transform ($\iota_o = 0.055 - 0.23$). Although ι_o varies by a factor of 4 the stellarator field only

A comparison of discharges with $\iota_o = 0.055, 0.11, 0.23$ shows a pronounced difference in the shape of the profiles. At $\iota_o = 0.23$ the profiles are flat in the plasma centre and more peaked in the case $\iota_o = 0.055$ (Fig.2). At nearly same plasma current and plasma density the central temperature reaches larger values for $\iota_o = 0.055$. In spite of this effect the energy content and the energy confinement times are nearly the same.

The enhanced transport mechanism which flattens the profiles in the stellarator case $\iota_o = 0.23$ is attributed to the sawtooth oscillations observed in the plasma centre. This is supported by several observations:

1. The thermal electron conductivity D_E derived from the energy balance
$$D_E = \frac{\int (P_{OH} - P_{ei})\, dV}{4\pi^2 R\, r k \frac{dTe}{dr}}$$
shows a minimum at the radius with $q = 1$ (see Fig.3).

2. The flat area in most cases extends to the $q = 1$ surface.

3. The energy confinement time for the volume $q \leq 1$ as derived from the observed amplitude of the sawtooth oscillations shows that a significant part ($\leq 50\%$) of the energy losses of the electrons is due to these oscillations (Fig.4).

The explanation for the flat temperature profiles is the anomalous loss which limits the current density and also the heating power in the centre so that $q(o) \approx 1$ is always maintained.

The minimum values of the thermal conductivity $D_E(r)$ are between 1×10^3 and $1 \times 10^4 cm^2/s$; these data are close to those found in Ormak and TFR, although the temperature T_e is larger in these machines. Pseudoclassical thermal conductivity does not fit the observed data. The measured values of D_E (which are upper limits since radiation losses have been neglected) roughly scale with $n_e^{-0.8}$ and decrease with increasing temperature. A dependence on the stellarator field could not be observed for the studied ι_o values at currents between 15 and 35 kA. The gross energy confinement time of the electrons $\tau_E'(r)$ only varies by $\leq 25\%$ over the plasma radius $\tau_E'(a) \leq \tau_E(o)$. Because of the condition $q = 1$ in the centre $\tau_E(o)$ can be

connected to $kT_e(o)$ and $n_e(o)$. The plasma data in the centre therefore determine an upper limit for the electron confinement time (Fig.5).

When the plasma current is increased the total energy confinement time τ_E decreases beyond a critical current which corresponds to a total rotational transform of $\iota_p(a) \approx 0.2$ and $\iota_o + \iota_p(o) = 1$ (Fig.6) for ι_o is 0.055.

In the case $\iota_o = 0.055$ the decrease is accompanied by growing MHD modes of the type m = 2, n = 1. $\iota(a) = 0.5$ could not be reached without current disruption. With higher external rotational transform $\iota_o = 0.23$ the decrease of τ_E with current begins beyond $\iota(a) = 0.5$. Only a low activity of m = 2, n = 1 and m = 3, n = 2 modes is observed, in this case the increasing effect of the enhanced transport due to internal disruptions within the q = 1-surface is believed to be responsible for the deteriorations of the confinement. Beyond the critical current the energy content of the plasma drops again at low external rotational transform whereas in the equivalent case with $\iota_o = 0.23$ the energy content W reaches higher values (see Fig.6, upper picture). This is another indication that in both cases different loss mechanisms are causing the deterioration of the confinement.

In a small region around $\iota(a) = 0.5$ the confinement time drops by a factor of 2. No enhanced fluctuations are observed at the same time, therefore, a stationary loss in combination with island formations may be the reason for this loss.

The energy confinement time is an increasing function of the electron density (Fig.7). The plasma parameters are changed by varying the neutral gas inflow $\overline{\Gamma}(t)$ with all other parameters kept fixed ($B_o = 3$ T, $\iota_o = 0.23$, $I_p = 26$ kA). The temperatures of ions and electrons approach each other with increasing density, therefore, a scaling of the confinement time should include a dependence on temperature. Evaluation of all data from the profile measurements showed a scaling of τ_E with $n_e^{0.8}$ (n_e is the space averaged density.) This scaling was found in a regime from $\bar{n} = 0.5 - 2.5 \times 10^{13}\,cm^{-3}$, but temperature dependence was neglected. The absolute values of τ_E vary between 2 and 10 ms. The optimum values always obtained at the lowest possible currents are nearly equal for all cases of external rotational transform ($\iota_o = 0.055 - 0.23$). Although ι_o varies by a factor of 4 the stellarator field only

changes by a factor of two. Even in the case of low rotational transform 0.055 the stellarator field is larger by a factor of 2 than the poloidal field of the plasma current. This might explain the relatively high confinement times in comparison with equivalent tokamak data (equivalent density, plasma cross section, magnetic field, etc.)

Ion Temperature Measurements and Ion Energy Confinement

The maximum ion temperature $T_i(o)$ has been derived from the slope of the energy spectrum of the charge exchange (CX) flux ϕ as measured by a 5 channel particle energy analyzer. Model calculations with the Düchs-code of the outgoing CX flux have been compared with the measured slope of ϕ (E) at large energies (Fig. 8). To obtain agreement between the calculated and the measured slope it is necessary to assume an ion temperature $T_i(o)$ which is up to 10% above the ion temperature as obtained from the slope of $\ln \phi / \sqrt{E}$. Measured values of $T_i(o)$ are in the range of 150 to 320 eV for electron densities $n_e(o)$ from 1.5 to 5.0×10^{13} cm^{-3}. Injecting a neutral particle beam across the plasma and detecting the CX flux perpendicular to the beam allows one to measure $T_i(o)$ also from the increase of the CX signal. A hydrogen beam of 18 kV accelleration voltage increases the neutral density by about 1×10^{9} cm^{-3} over a width of 3 cm along the observation line. The flux spectrum shows very intense lines at 6 keV and 1 keV. The origin of these is the extraction of H_3^+ ions (mass 3) and most probably water or CH_4 ions (mass 18 or 16). The presence of the lines allows only a rough determination of the temperature which does not contradict the passive measurement.

A radial profile of T_i has been measured by measuring the CX flux spectra at different inclination angles of the detector. Taking into account the corrections for an elliptical plasma cross section it turns out that $T_i(r)$ follows the density profile, but only in the upper half of the plasma diameter (Fig. 9). Below the plasma centre the measured temperature is almost constant. This is due to the downward drift of the high energetic ions (>1 keV) which are trapped in the helical mirrors. Between successive collisions these ions drift over a distance of about 3 cm.

Absolute measurement of the CX flux at high energies allows the determination of the central neutral density $n_H(o)$. The calculated flux $\phi_{1000} = n \cdot n_i \cdot f_i(E) \langle \sigma v \rangle_{cx} \cdot$ Vol

has been compared with the measured flux at E = 1000 eV which leads to a neutral density of the order of 10^{-8} cm^{-3}. Adjusting the outgoing flux of the model calculations to the measured ϕ_{1000} leads to a central neutral density $n_H(o) = 5 \times 10^{7}$ cm^{-3} to 5×10^{8} cm^{-3}. Large n_e leads to low $n_H(o)$. The energy of the recycling particles in the model calculation has been varied from $E_o = 0.05$ eV to 5 eV. This energy effects the neutral density profiles and consequently the low energy part of the CX flux spectrum. Comparison with the measurements (Fig.8) demonstrates that only for $E_o \lesssim 1$ eV can the measured curvature of the spectrum at low energies be reproduced.

The energy confinement time of the ions as experimentally obtained from $1/\tau_i(r) = \int_o^r P_{ei}\, r dr \,/ \int_o^r \frac{3}{2} n_i k T_i\, r dr$ is typically 5 to 15 ms in the plasma centre and generally three times larger at the boundary. The neoclassical heat conduction χ_i together with an effective plasma radius a_{eff} leads to the neoclassical confinement time $\tau_{nc} = a^2_{eff}/\chi_i$ of about 100 ms for the centre ($a_{eff} = 6$ cm) and about 200 ms for the boundary ($a_{eff} = 10$ cm). These are roughly a factor 10 above the measured confinement times. To explain the measured energy losses in the centre by CX a neutral particle density of about 10^{9} cm^{-3} would be necessary. This is an order of magnitude above the measured neutral density. Thus the energy losses of the ions in the central region cannot be explained by neoclassical heat conduction alone. In the outer region the energy losses can possibly be attributed to the CX losses because of the increase of the neutral density.

Particle Confinement

We have made some attempts to measure the particle confinement time in the W VII A device. At present we can give some estimates and point out the problems. The average particle confinement is given by $\frac{dne}{dt} = -\frac{ne}{\tau_p} + \sum$ ionization rates. We assume, that the dominating ionization rate is due to hydrogen. This is supported by absolute measurements of impurity content and low Z_{eff} values.

Measuring the absolute intensity of H_α -light, the ionization rate can be calculated using the rate coefficients for excitation and ionization given by Johnson and Hinnov. /2/. Since ionization rates depend strongly on radial and azimuthal position we have

tried to measure the ionization rate at all available ports around the machine. All large scale devices nowadays use pulsed gas inlet systems because of low recycling or to build up higher electron densities. These gas inlet systems are strong local sources, which have to be taken into account for the estimation of $\bar{\tau}_p$.

To measure the radial distribution of H_α -light we have imaged the elliptical cross-section of the plasma through a horizontal port on to an array of 25 light pipes which are scanned within 2.5 ms by a mechanical chopper. A rotation of 90° of this array allows us to get information on intensity distribution in azimuthal direction to some extent.

We also are able to view along radial chords at four additional ports. The experimental results indicate in many cases asymmetric radial profiles of H_α -emission, which can change during the discharge. For some of the discharges the asymmetry could be attributed to sources such as an antenna which was located at this port acting as a limiter. The asymmetric port of the emission may be as high as 30% of the total emission at one port.

With a gas inlet system at the measuring port a very pronounced localized asymmetry was found toward the gas inlet. Also the intensity of the centre chord was up by a factor of 6 compared to a measurement without gas inlet at this position.

From these measurements we have estimated that with gas inlet the emission per unit volume is about a factor of 20 higher compared to the emission without gas inlet. The limiter was found to cause comparable emission. Rotating the light pipe array by 90 degrees we found this increased intensity to fall off along the machine with about 30 cm halfwidth.

Considering three gas inlet systems which are being used, the limiter and the measured decay length, we estimate that about 2/3 of the particle production takes place at the gas inlets.

We present in the following Table some first results on particle confinement time τ_p and compare it to particle exchange time τ_A, defined by $\tau_A = \frac{\int ndV}{\bar{\Gamma}(t)}$, where $\int ndV$ is the total number of particles and $\bar{\Gamma}(t)$ is the total external flux.

τ_A should give an upper limit of the particle confinement time, since recycling is neglected. The energy confinement time τ_E and peak electron densities $n_e(o)$ are also shown.

$t_o = 0.23$	$B_o = 3$ T	$I_p = 26$ kA	# 7958 - 8053
$n_e(o)$ I cm^{-3} I	τ_A I ms I	$\bar{\tau}_p$ I ms I	τ_E I ms I
1.2×10^{13}	15	5.3	2.9
1.8×10^{13}	26	8.7	3.2
3.5×10^{13}	44	11.3	6.1

$\bar{\tau}_p$ is about a factor of 3 smaller than τ_A. It increases with electron density as do the other quantities. $\bar{\tau}_p$ is about a factor of 2 higher than the energy confinement time τ_E. Note that this is different from W II b /3/, where $\bar{\tau}_p$ was neoclassical and a factor of 10 above τ_E. Defining a recycling coefficient $\tau_A = \frac{\bar{\tau}_p}{1-\varsigma}$, ς is found to be around 0.7.

From Abel inverted symmetric radial profiles of H_α emission we can calculate the neutral particle density as a function of radius using electron temperature and density from laser measurements. We find it to be $\sim 3 \times 10^9 cm^{-3}$ at the limiter radius and to decrease an order of magnitude towards the centre. Because most of the intensity originates from the outside, we cannot get numbers for the central part of the plasma $r \leq 4$ cm by Abel inversion. Absolute measurements of the flux from charge exchanged neutrals give numbers for $n_o \approx 10^8 cm^{-3}$ for the central part which is to be consistent with the neutral density obtained from H_α measurements.

Impurity Content

For various values of t_o and n_e the behaviour of Z_{eff} was studied. The measurements of Z_{eff} by means of the conductivity, the VUV spectroscopy and X-ray fluxes yield very similar results. This is shown in Fig. 10 . t_o was varied from 0.055 to 0.23. The central electron temperatures were from 0.3 to 0.6 keV and the toroidal magnetic field between 2.5 and 3.5 T. The upper part shows the spread of Z_{eff} as a function of the line density, which was obtained from the central channel of a 2 mm microwave interferometer. This spread of Z_{eff} between 1 - 6.5 increases with decreasing

electron density. However, there is no direct connection between an increase of Z_{eff} with decreasing density. Also no clear dependence of the Z_{eff} values on the external rotational transform exists.

The low Z_{eff} values at low electron densities are not caused by slide or runaway electrons, as has been verified by the X-ray measurements. In general, the features of the upper figure are confirmed by the measurements of the X-ray flux through 50 μ Be and the determination of the impurity content by means of the impurity line (1032 A) of O^{5+}.

For certain discharges the Z_{eff} evaluated from the X-ray flux is overestimated because of the presence of line radiation (Fe and Mo L-lines). But usually this radiation was less than 30% of the total continuum radiation. Since the cross sections needed for the calculation of the X-ray continuum radiation for the Molybdenum impurity are unknown for electron temperatures below 0.5 keV, a Z_{eff} value, assuming Molybdenum as only impurity, has not been determined. However, these Z_{eff} values should be between the iron and the oxygen Z_{eff}'s.

The lower part of the figure shows the Z_{eff} value obtained by VUV spectroscopy at a radius $a \approx 8$ cm. Oxygen was the dominating impurity as verified by the VUV measurements. This may explain the fact that the Z_{eff} values from the X-ray fluxes assuming oxygen present as impurity are close to the conductivity Z_{eff}.

The dependence of the impurity content on the electron density is represented differently in Fig. 11. The points connected by a continuous line are obtained in one single discharge. This shows again that there seems to be no direct relation between Z_{eff} and the electron density.

The oxygen density was determined in the usual way by radially scanning the minor cross section of the plasma at the different oxygen lines. Fig. 12 shows the distribution of O^{1+} to O^{6+} across the minor radius after taking into account the elliptic plasma cross section in the Abel inversion. The results are similar to those from TFR (Laussanne 1975), except for differences due to the flattening of the electron temperature at lower values ($\sim$0.4 keV). The broadening and the shifting inwards of the peaks of the different ionization stages across the minor radius does not agree

with Coronal equilibrium calculations which shows that diffusion mechanisms must be taken into account.

In about 50% of the radial scans of O-line emission a strong asymmetry is observed which could not be explained by the geometry of the magnetic surface. This asymmetry is mainly found in the low ionization stages O^{1+} - O^{5+} and decreases in the higher stages (Fig. 13). Also during one discharge the asymmetry changes. The plasma profiles [$T_e(r)$, $n_e(r)$] did not show asymmetries in these discharges, but it seems that the asymmetry of the oxygen emission is mainly localized to the magnetic surface with $q = 2$. It is believed that this originates from the interaction between the low ionization stages oxygen and the neutral oxygen and hydrogen /4/. Asymmetries of the H_α-light emission observed in the same plane support this idea.

MHD Stability and Sawtooth Oscillations

The stability of the plasma column against the kink and tearing mode was studied with a numerical code[+], which solves the equation for marginal stability. Cylindricial approximation was made for the plasma column, the only stellarator effect included was an additional term in the rotational transform $\iota_p(r) \rightarrow \iota_p + \iota_o = \iota(r) \cdot \iota_p(r)$ is the rotational transform of the current. As already shown by Johnson et al. /5/ and Shafranov et al. /6/ for the stability of kink modes, the external transform ι_o also has a stabilizing effect on the tearing mode. For a given current profile $j_z(r)$ the unstable zones become more narrow with increasing stellarator field. Also the region where different tearing modes overlap (e.g. m = 2/ n = 1 and m = 3 / n = 2) narrows with increasing stellarator field. Thus, the stabilizing effect of the stellarator field is twofold: the unstable regions around $\iota(a) = 0.33$ and 0.5 are shifted to lower $\iota_p(r)$, which means lower plasma currents and lower free energy in order to drive the kink and tearing modes. The other effect is the narrowing of the unstable zones. Both effects may explain, why the transition through $\iota = 0.5$ is possible with an external stellarator field.

We have found experimental evidence for the theoretical picture mentioned above. A first striking feature is the disappearance of m =2, n = 1 modes when $\iota(a)$ gets

[+] The code was developed by K. Lackner.

above 1/2. As expected when the current profile changes to a more square profile the m = 2, n = 1 reappears. For $\iota_o = 0.23$ this can be seen in Fig. 14 . The expected change in the current density profile during the internal sawtooth disruption causes also changes in amplitude and frequency of the modes. The sawtooth disruption can be seen on the lower trace as measured by the soft X-ray flux. The several MHD modes present are identified by a proper series connection of the B_θ-coils. The third trace from above shows a weak ($\approx$1.4 ‰) m = 3, n = 2 tearing mode which diminishes its amplitude $\approx$ 1/2 ms before the disruption. This is supposed to be caused by a peaking of the current channel towards the centre. Just before and after the disruption a stronger (3‰) m = 2, n = 1 kink mode appears. This suggests a flattening of the current channel (square profiles) which would make the m = 2 more unstable . During this discharge $\iota(a) \approx 0.58$.

At lower $\iota(a)$ the m = 2, n = 1 mode is mainly absent except in a very small region around the resonant $\iota(a) = 1/2$ with a small amplitude ($\approx$1‰). A similar behaviour of other modes near resonant $\iota(a)$ values is also found during the current rise.

For lower values of ι_o the plasma is more unstable. Strong m = 2, n = 1 modes are present, depending on the electron density (this conference, paper presented by A.Weller). Coupling of m = 1, n = 1 with the m = 2, n = 1 may occur; larger sawtooth disruptions at q = 1 are preceded by sawteeth starting around the q = 2 surface (predisruptions). At even lower ι_o values soft current disruptions and major current disruptions occur (Fig. 15). The upper part shows the dependence of the relative sawtooth amplitude versus density. Apart from $n_e \lesssim 2 \cdot 10^{13}\,cm^{-3}$, the behaviour of $\Delta A^{\nu} / A$ versus n_e is the same as for $\iota_o = 0.23$ up to $n_e = 3.5 \cdot 10^{13}$. Above this density the m = 2 modes become progressively larger while the $\Delta A^{\nu} / A$ becomes progressively smaller. This indicates an additional transport caused by the m = 2 mode, which has meanwhile coupled itself with and forced its frequency upon the m = 1 mode. With the increase of the m = 2 is also linked the appearance of predisruptions and soft current disruptions at $\iota_o \approx 0.027$ (lower picture).

The enhanced transport is also noticed when passing through or close to rational values of $\iota(a)$. This can be seen from increases of the impurity content (Fe and O), of the Langmuir probe signals (electron and ion currents) and of the

HF emission (correlated with sawtooth disruptions).

At the limiter voltage and current bursts are detected; side-on light signals show simultaneous maxima. Also the bolometer signals are correlated with the transition through rational $\iota(a)$, showing an enhanced flux to the wall. In general, this coincides with an increase of MHD activity. But close to rational values of $\iota(a)$ the resonant mode may disappear completely. It is believed that then the mode, however, remains present but stationary.

Summary and Conclusions

The installation of a current feedback system for the ohmic heating transformer made it possible to study stationary discharges for more than 400 ms. The impurity content in the main body of the plasma was found to be rather low at densities above $n = 10^{13}\,cm^{-3}$. An increase of impurity content during the discharge could not be observed. The comparison of discharges at several values of the external transform showed the following picture:

1. With increasing external transform and plasma current the profiles are flattened due to the increasing effect of the internal disruptions.

2. The energy confinement time increases with density as long as the temperature is not reduced too much. In the regime of $\bar{n} = 0.5 - 2.5 \times 10^{13}\,cm^{-3}$ the confinement time reaches values between 2 and 10 ms. A dependence on the external transform could not be found in the parameter range with $\iota \cdot I_p \geq 8$ kA.

3. Above a critical current the confinement time drops. For $\iota_o = 0.055$ this reduction is accompanied by growing MHD modes ($m = 2, n = 1$). Similar to ORAMK this decrease starts at $\iota_p(a) = 0.2$ ($q(a) = 5$). For $\iota_o = 0.23$ low MHD activity is observed, so the reason for this reduction may be due to the dominating mechanism of the internal disruptions with $q = 1$ approaching towards the plasma edge.

4. Edge effects sharply localized at $\iota(a) = 0.5$ deteriorate the confinement at high external transform. Nevertheless, stationary discharges can be maintained at $\iota(a) = 0.5$. This demonstrates the stabilizing effect of the

stellarator field on MHD activity and plasma equilibrium.

First measurements of the particle confinement time by H_α -light emission showed that the particle confinement time is nearly twice the energy confinement time. The difficulty in evaluating the confinement time consists in the local sources of hydrogen.

The measurements of ion temperature showed values between 150 and 300 eV. An asymmetry of the radial temperature profiles was found which may be caused by super-banana particles trapped in the helical mirrors. Neutral particle density in the plasma centre is found to be of the order of $10^8/cm^3$.

Unsolved so far is the origin of the asymmetric profiles of oxygen light and H_α-light emission. Also the mechanism of the plasma loss at $\iota(a) = 0.5$ is not yet understood. The experiments show, that the stellarator field modifies the plasma profiles and the stability appreciably.

Although a direct comparison with tokamak operation in W VII A was not yet possible, the measured confinement times show higher values than found in tokamaks with similar plasma cross sections and in the same density regime.

References

/1/ W VII A team, Proc. 6th Conf., Berchtesgaden, II, IAEA, Vienna (1977), 81

/2/ L.C. Johnson and E. Hinnov, J. Quant. Spect. Rad. Transf. 13 (1973) 333

/3/ H. Hacker et al., Proc. 5th Conf. Tokyo (1974, II, IAEA, Vienna (1974) 3

/4/ W. Engelhardt, IPP, private communication

/5/ L.E. Zahkharov, V.D. Shafranov, Proc. 6th Conf. Berchtesgaden, II, IAEA, Vienna (1977) 155

/6/ M.D. Kruskal, J.L. Johnson, M.B. Gottlieb, and L.M. Goldman, Phys. Fluids 1 (1958) 421

W VII A - Stellarator

Major radius R_0 = 2 m	Rotational transform	$0 < \iota_0 \leq 0.23$	
Vacuum tube r_i = 0.17 m	Shear	$\frac{\Delta\iota_0}{\iota_0}$	$= 10^{-2}$
Limiter radius r_l = 0.135 m	Toroidal field		≤ 3.5 T
Helical Windings l = 2, m = 5	Air Core transformer	Φ	= 2.2 Vs

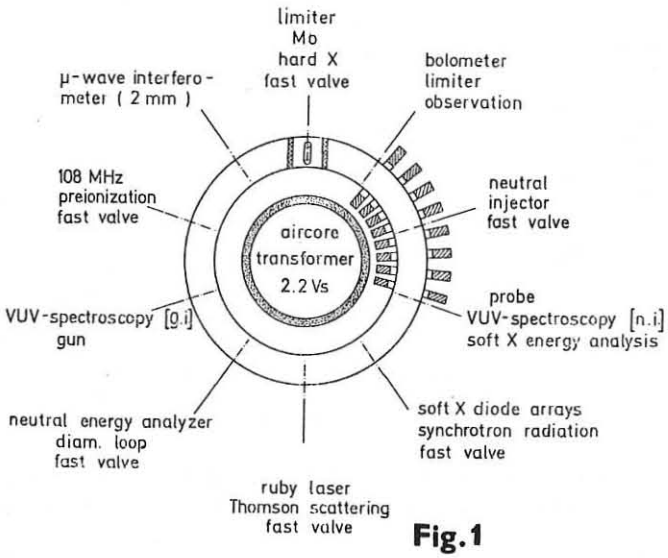

Fig. 1

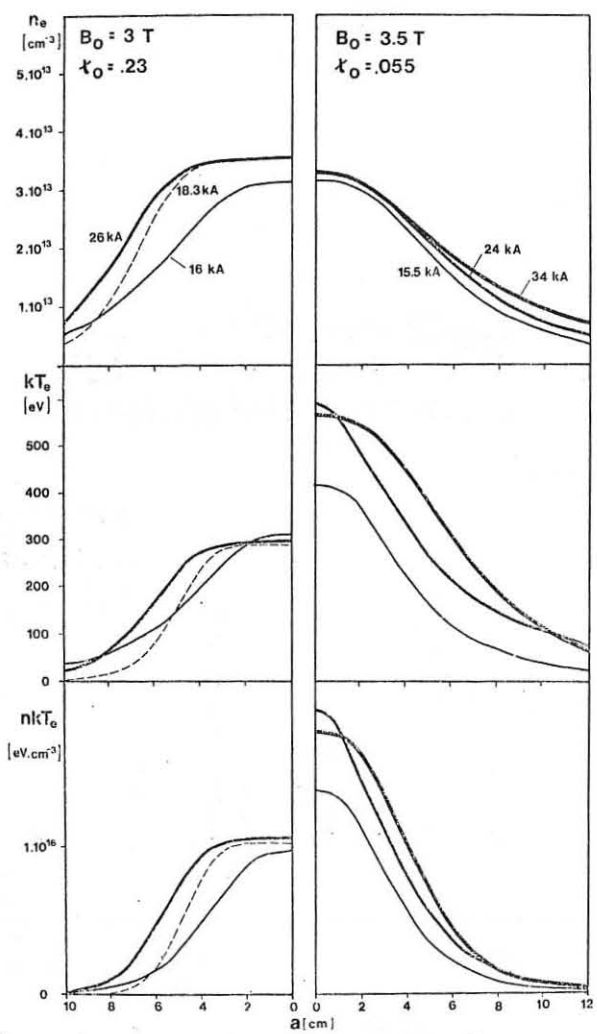

Fig. 2

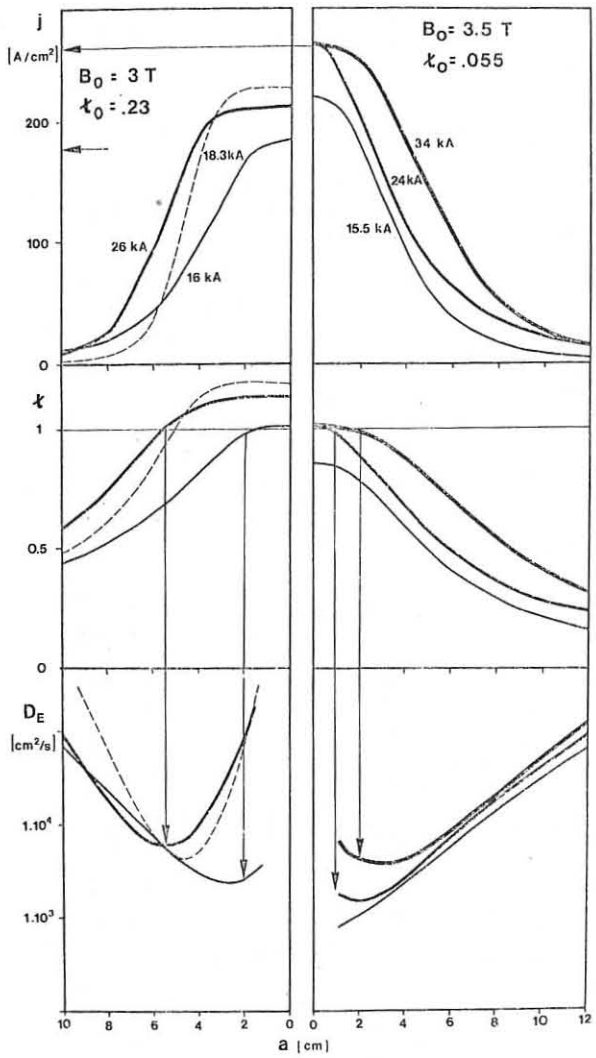

Fig. 3

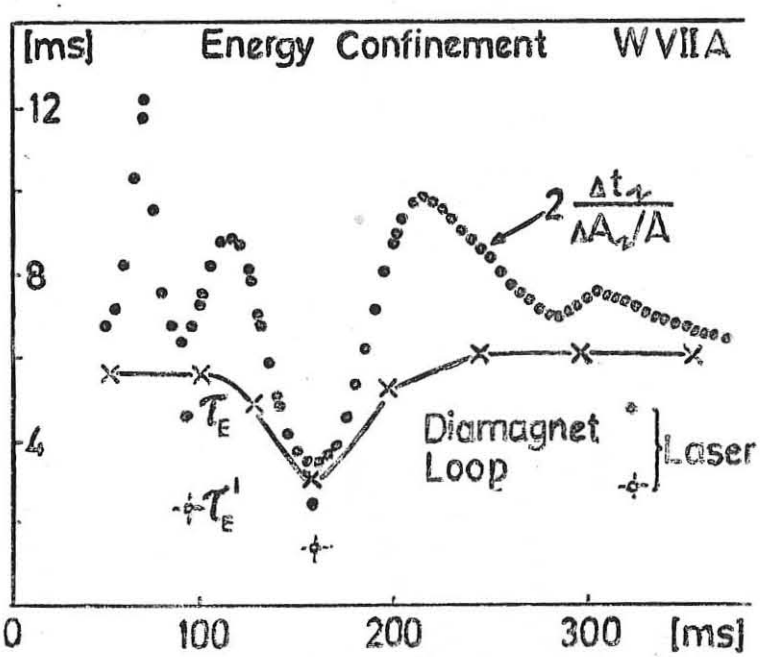

Fig. 4

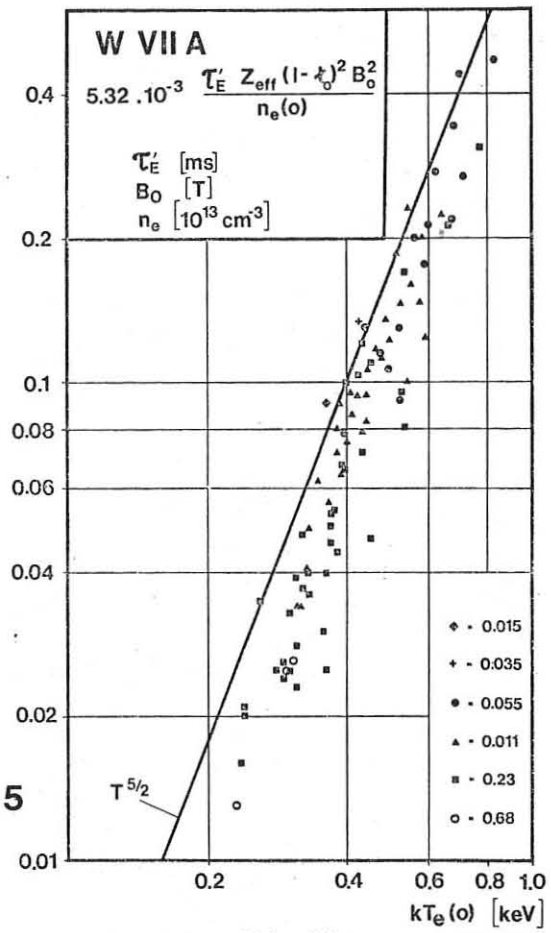

Fig. 5

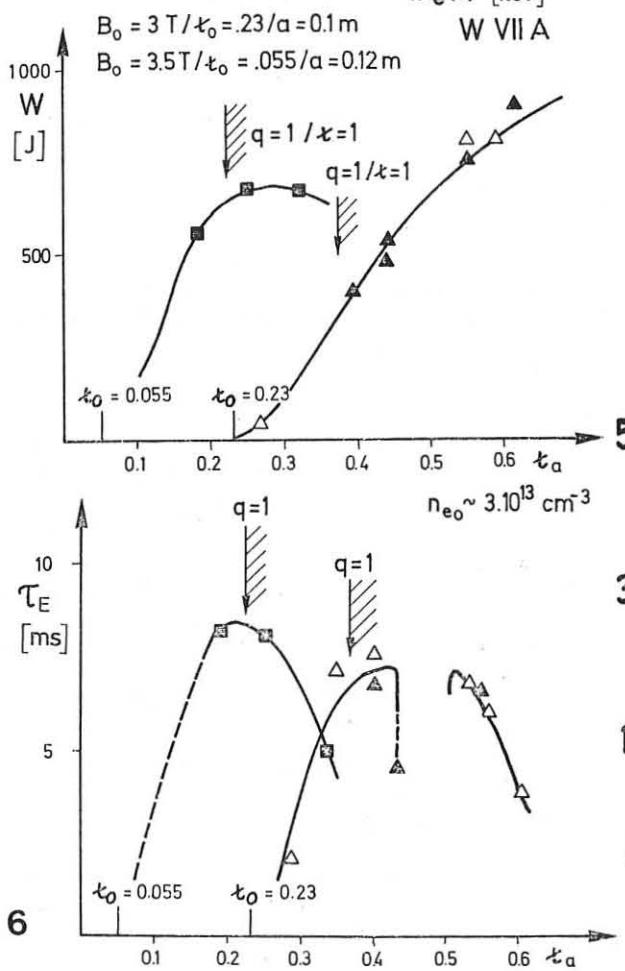

Fig. 6

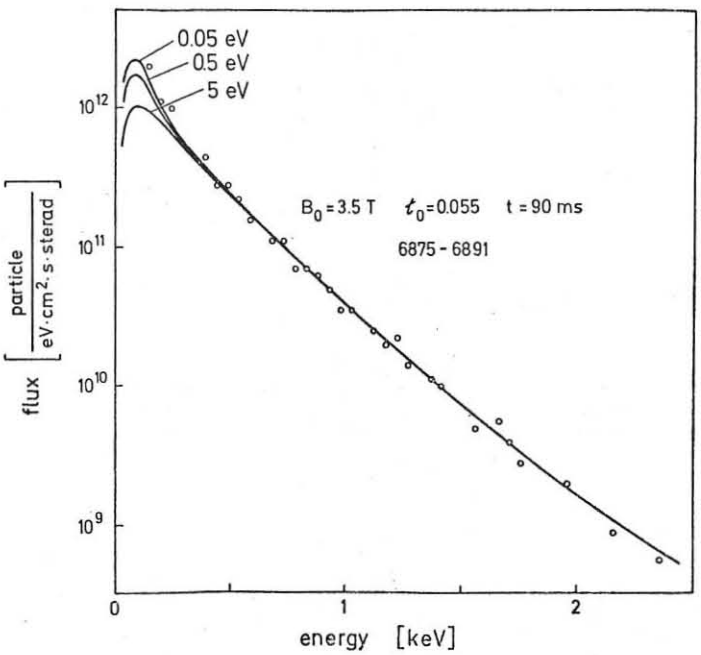

Energy spectrum of measured cx-flux compared with computations for various energies of the recycling particles

Fig. 8

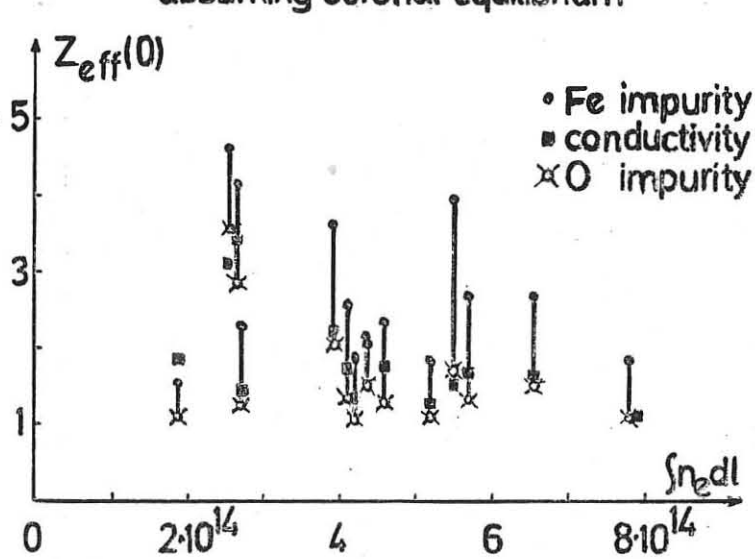

Fig. 10b

Z_{eff} from conductivity for various t_o

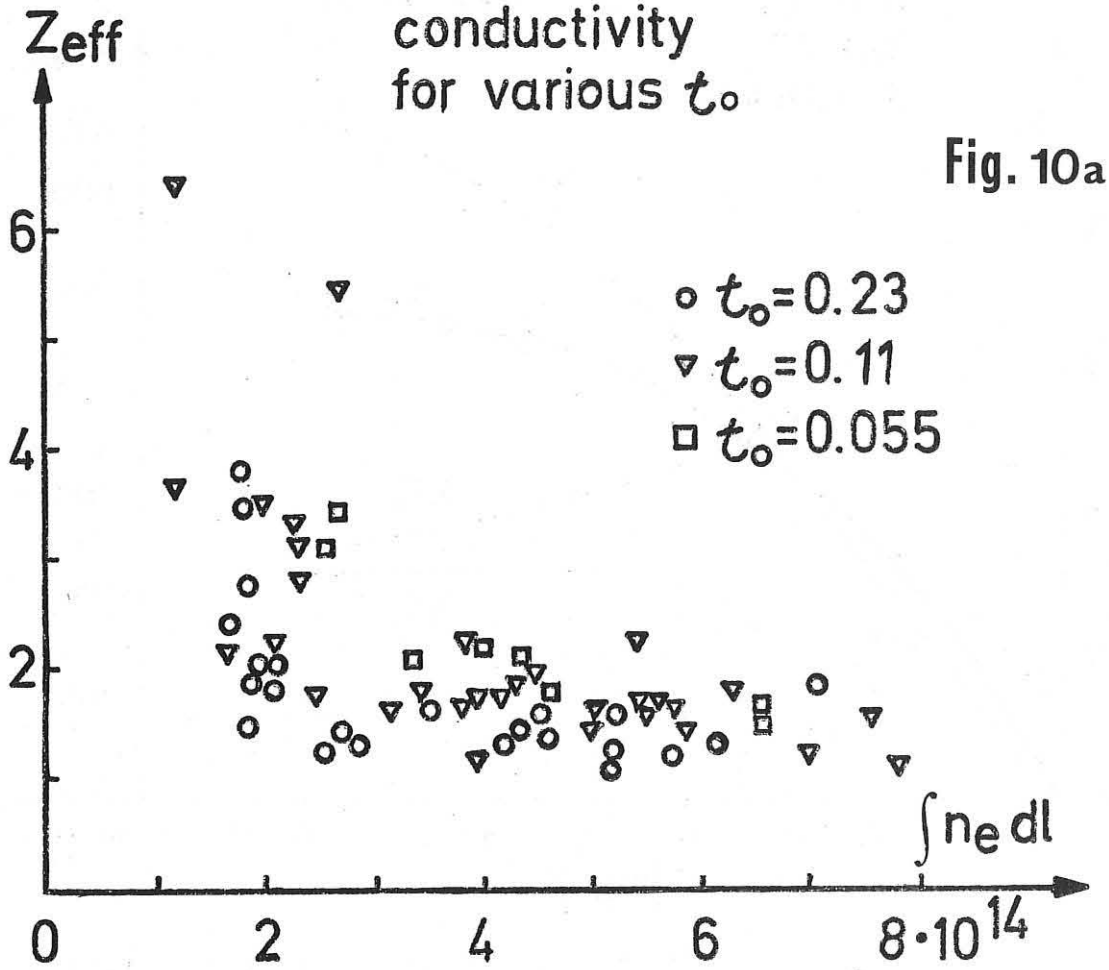

Fig. 10a

Z_{eff} from OVI (1032 Å) for various t_o

$Z_{eff} = \frac{1}{n_e}(n_{H^+} + 20 \cdot n_{O5+})$

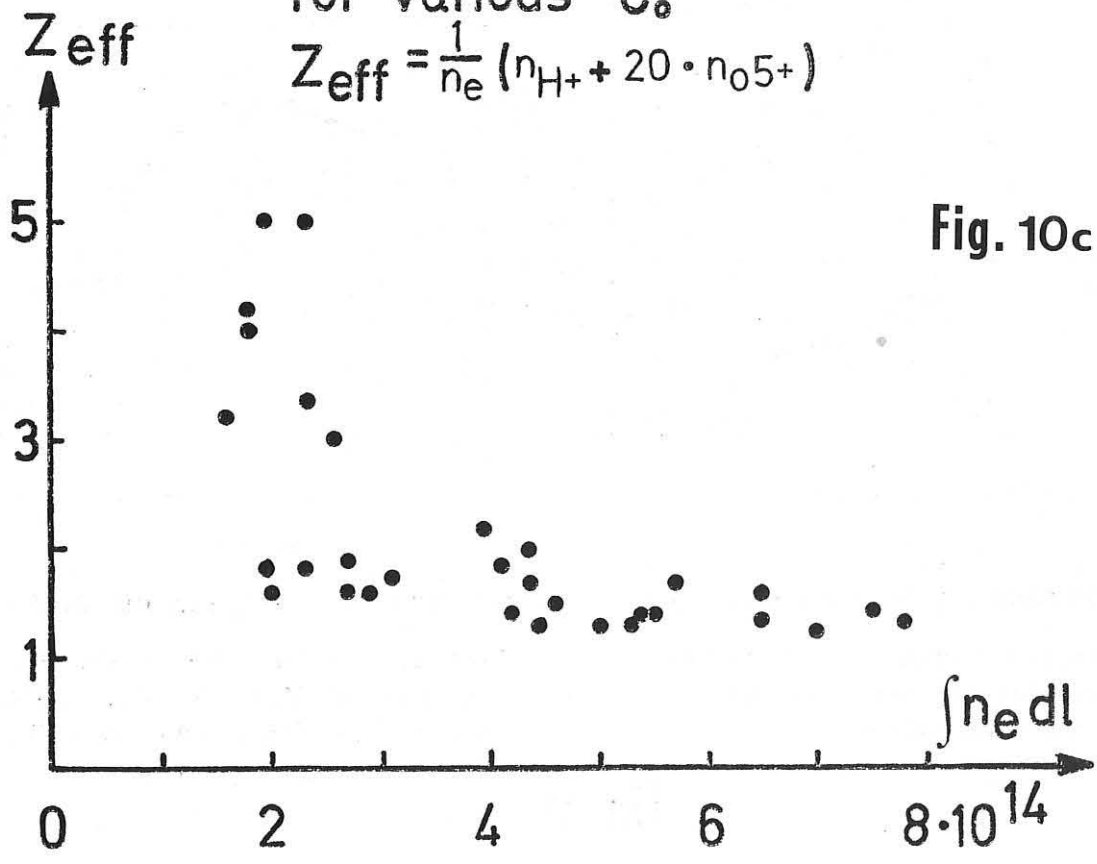

Fig. 10c

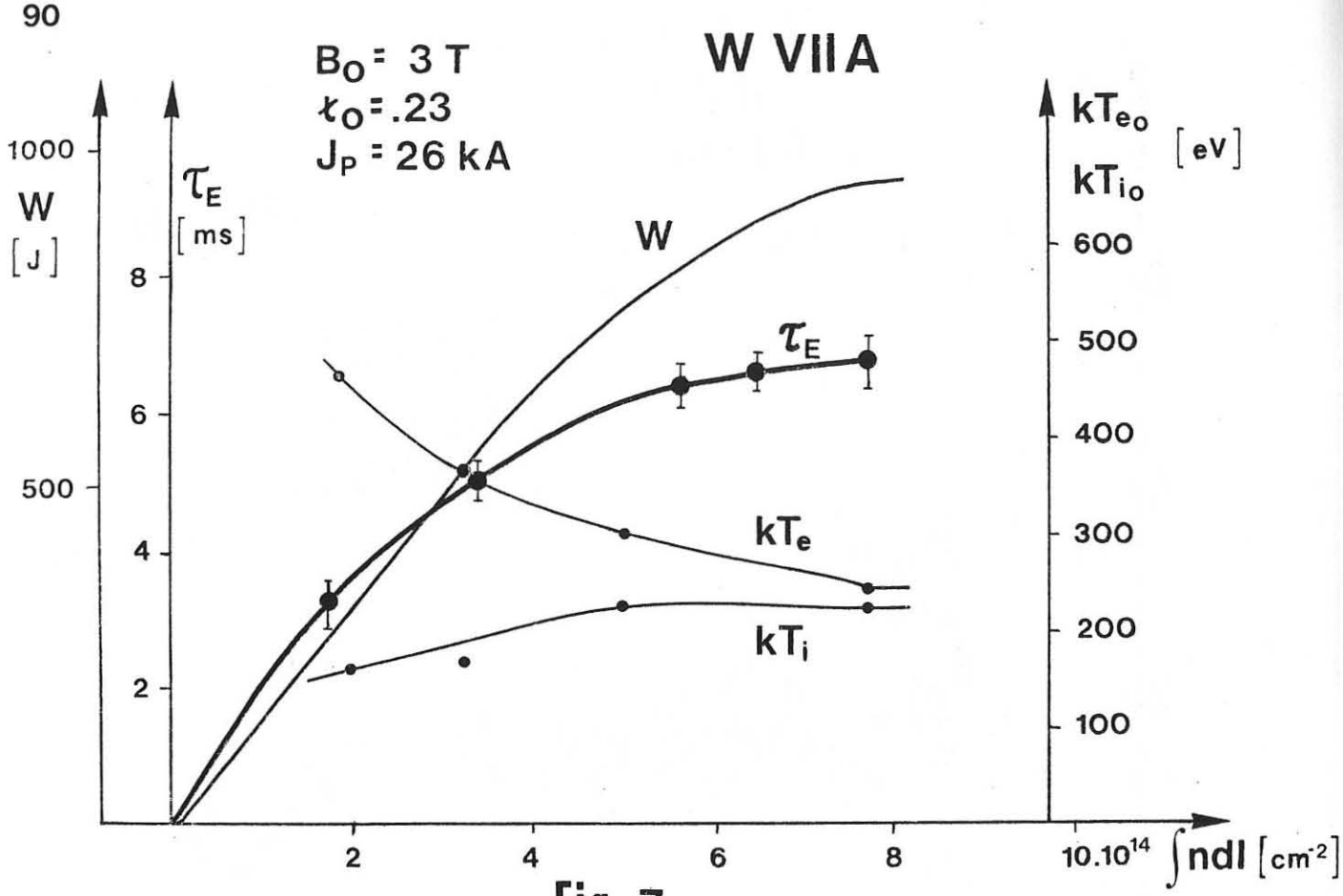

Fig. 7

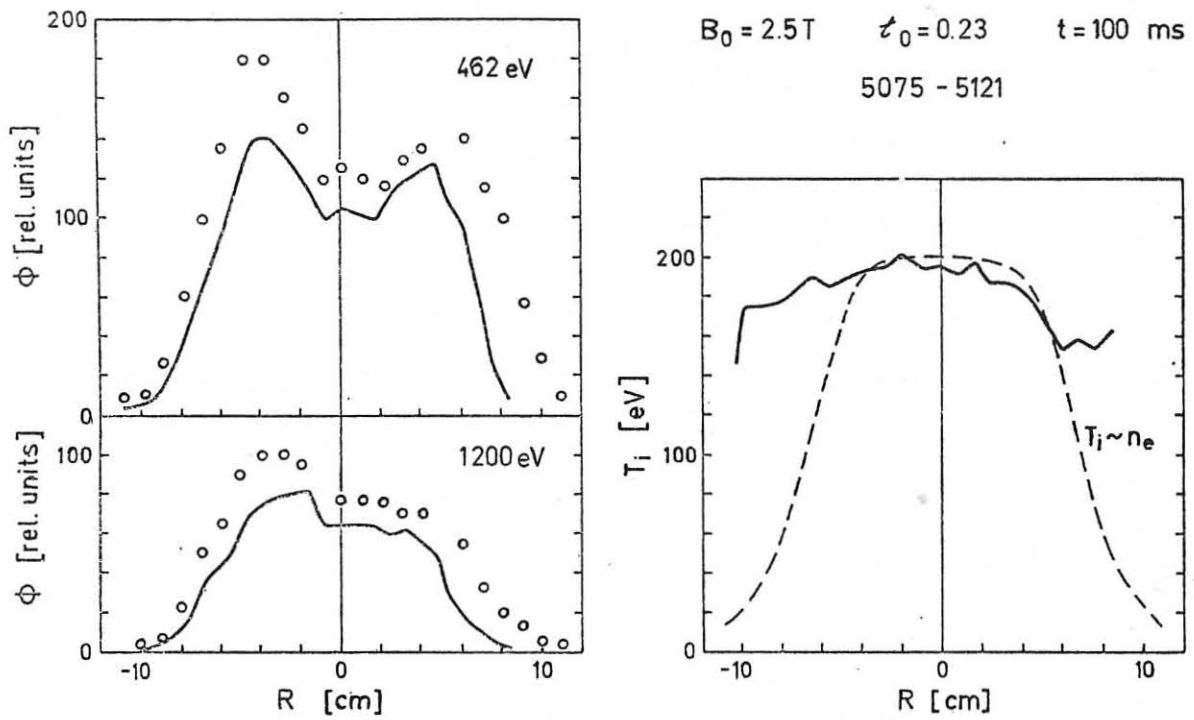

Measurement of the radial cx-flux profile and ion temperature profile

The measured angular profile (o) of the cx-flux has been converted into the radial profile (—)

The radial profile of the ion temperature as evaluated from the radial profiles of the cx-flux. The dashed line represents the electron density profile

Fig. 9

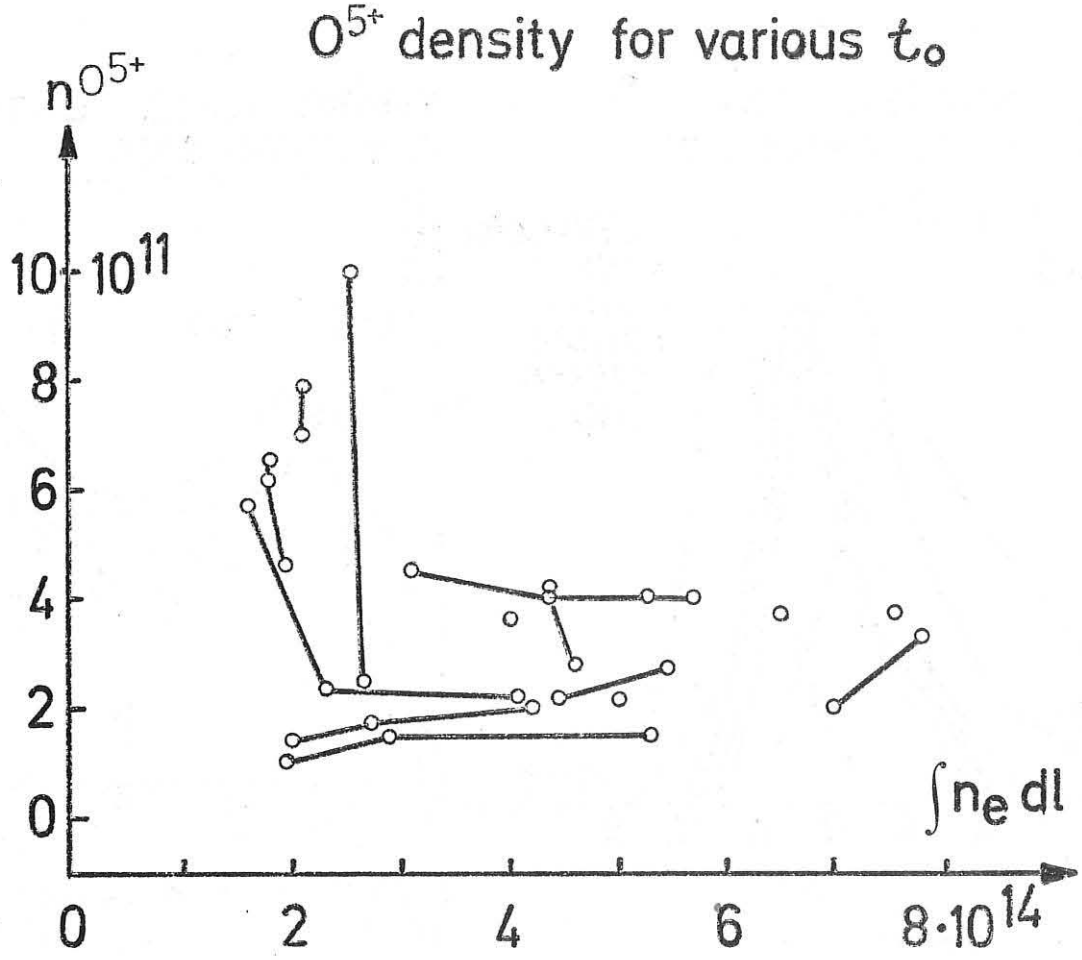

Fig. 11

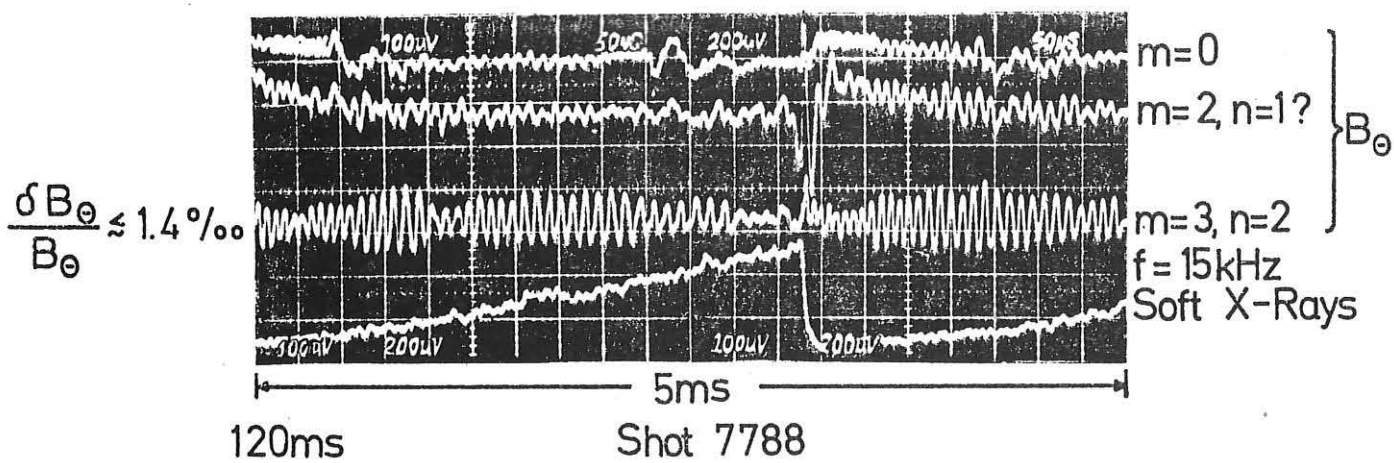

Signals of B_Θ-coils (m=0,2,3 - components selected by series connections) and Soft X-Signal for $t_o = 0.23$ and $n_{e,o} \approx 6 \cdot 10^{13}\,cm^{-3}$ ($I_p = 25.5kA$, $T_{e,o} = 245eV$, $t\,(a) = 0.58$)

Fig. 14

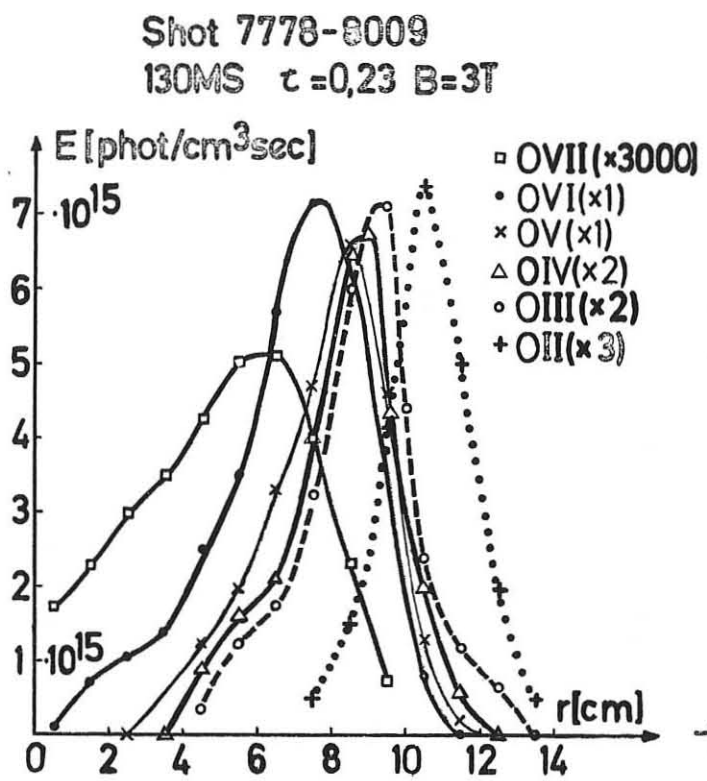

Fig. 12

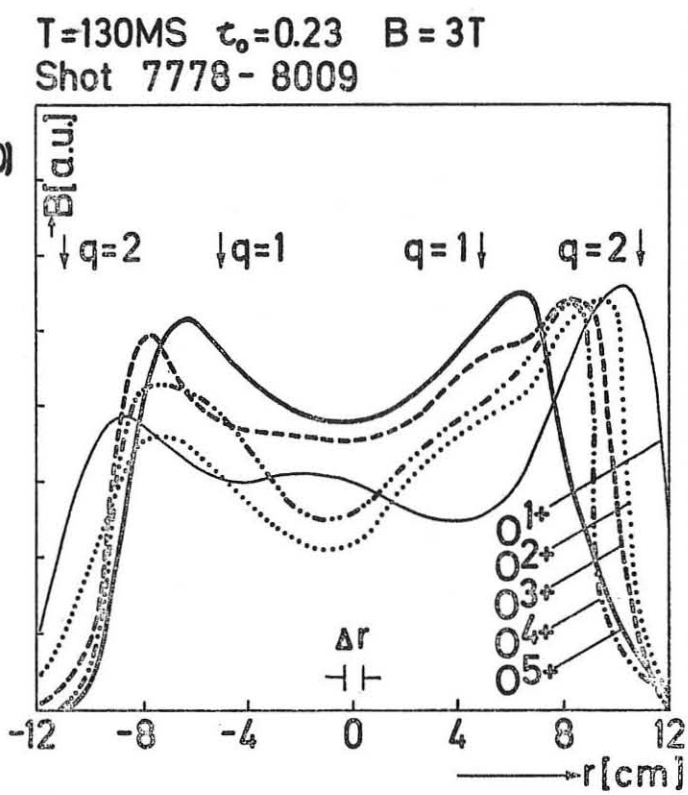

Radial scan of oxygen line emission transformed to circular geometry

Fig. 13

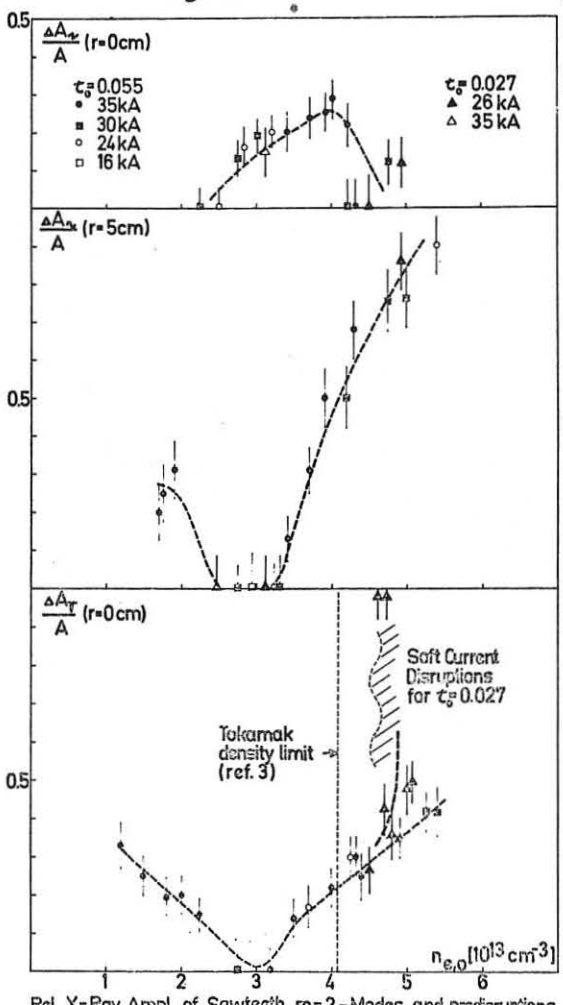

Rel. X-Ray Ampl. of Sawteeth, m=2-Modes and predisruptions for $\tau_s = 0.055; 0.027$ as a function of the central density

Fig. 15

HEATING AND CONFINEMENT IN THE CLEO STELLARATOR

D.W. Atkinson, D. Bartlett, J. Bradley, A.N. Dellis, S.M. Hamberger
D.J. Lees, J.B. Lister, W. Millar, L.E. Sharp and P.A. Shatford

Euratom/UKAEA Fusion Association,
Culham Laboratory, Abingdon, Oxon, England

INTRODUCTION

CLEO is a conventional stellarator, having 7-field periods of $\ell = 3$ helical windings wound on a 25 mm thick, stainless steel torus of mean major radius 90 cm and bore 28 cm. When the lobes of the outermost closed magnetic surface (trefoil-shaped) are defined by the 13 cm radius tungsten limiters, the resulting plasma boundary has a mean radius $a \approx 10$ cm.

Recent modifications have for the first time allowed operation at the full helical winding current (120 kAT) with maximum toroidal field $B_\phi = 20$ kG; with the separatrix just inside the limiters the maximum rotational transform due to the vacuum fields is $\iota_0 = 0.6$. The computed magnetic surfaces have been confirmed by experiment using a low velocity electron beam. Most of the results reported here use this field configuration ($I_{eq} \equiv \frac{a^2}{2R} \iota_0 B_\phi \leq 66$ kA), in contrast to that reported earlier[1,2] for which restrictions on the helical winding current limited the transform to $\iota_0 \approx 0.3$ at $B_\phi = 12.7$ kG ($I_{eq} = 21$ kA).

Many of the trends reported here, e.g. the improvement in confinement at low currents, were suggested in the earlier results but the limited operating range did not allow them to be positively confirmed.

Ohmic heating currents lasting up to 0.2 s are obtained using a series of up to 6 electrolytic capacitor banks discharged into a 12-turn primary winding on a two-limbed iron transformer core (0.8 Vs).

The principal diagnostics include: a single-channel 2 mm microwave interferometer producing a direct reading display of mean density; photon scattering (5 J ruby laser) for profiles of T_e and n_e, measured at

R = 90 cm along a vertical radius above the horizontal median plane; soft X-ray emission from minor radii between r = ± 7 cm (vertically) using uncooled Si detectors and foil absorbers; energy spectra of neutral particles emitted both radially and tangentially; horizontally viewed electromagnetic emission spectra from 30 to 300 GHz (cyclotron radiation) using Fourier transform spectroscopy; absolute H_α emission from plasma regions both close to and remote from a limiter; quartz and grazing-incidence vacuum ultra-violet line emission; and a sensitive multi-channel 2 mm interferometer used to study density fluctuations in the outer plasma regions.

OPERATION WITH OHMIC DISCHARGES

'Clean' vacuum conditions are obtained by continuous titanium gettering over about half the internal surface of the torus between discharges, rapid discharge cleaning being necessary only following initial pump-down The normal operating base pressure is $\sim 5 \times 10^{-8}$ torr, the residual gas consisting mainly of water vapour.

Operation at the significantly larger poloidal fields than were previously available[1,2] allows the ready production of well-behaved, long duration discharges whose boundary is close to the computed separatrix. This contrasts with the operation at lower I_{eq} when it was found necessary to apply a programmed vertical field proportional to the current I_g in order to obtain equilibria. This is now attributed to the effect of a leakage field from the transformer on the magnetic surfaces, whose effect becomes weak at low I_g and high I_{eq}.

Hydrogen gas is admitted from three pre-programmed electromechanical valves. Breakdown occurs readily for initial pulsed fillings of $\sim 10^{-4}$ torr H_2 and low loop voltages ($V \leqslant 15$ V) with little evidence of runaway production, as inferred from the absence of hard X-ray and non-thermal e.m. emission. The low wall recycling rate resulting from the gettered surface allows the subsequent density to be controlled by a carefully distributed gas influx. The maximum rate of density increase depends on the gas current, too great a neutral influx quenching the discharge. For typical pulse lengths ~ 150 - 200 ms maximum mean densities achieved in this way range from $\bar{n}_e \sim 3 \times 10^{13}\,cm^{-3}$ at $I_g = 10$ kA to $\sim 6 \times 10^{13}\,cm^{-3}$ at 25 kA, while much lower, steady densities, e.g. $\bar{n}_e \sim 5 \times 10^{12}\,cm^{-3}$, can be made reproducibly and free of runaways.

Some typical oscillograms illustrating two operating conditions are shown in Fig.1(a) and (b), Fig.1(b) showing the effect of too great a gas influx which quenches the discharge.

The results quoted here have all been obtained with the vacuum magnetic fields chosen so as to place the separatrix just inside the limiter; under these conditions the H_α emission is not enhanced at the limiter, indicating the detachment of the plasma from the material wall (i.e. the plasma is defined by a magnetic limiter). This implies that the ionization is essentially uniform azimuthally and thus allows a reasonable estimate of the total hydrogen ionization rate, and thus the particle confinement time τ_p, to be obtained.

Electron density and temperature profiles (Fig.2) are obtained by optically imaging different parts of the ruby laser beam which traverses a vertical diameter at $R = 90$ cm on to the entrance slit of the receiving spectrograph; this allows measurements between the horizontal axis and the upper plasma boundary with a spatial resolution of ~ 1 cm. The density distribution is always fairly flat, and similar to those found earlier with the separatrix outside the limiter, while the temperature profile is narrower.

Under some conditions, difficulty has been found in fitting the observed scattered spectra to simple Maxwellian distributions, a significantly higher temperature 'tail' being apparent — this effect is not seen near the centre of the plasma ($r = 0$) but is quite pronounced at radii $\sim 2 - 4$ cm. Since we have not yet resolved whether this is due to a genuine non-Maxwellian electron distribution or due to instrumental error, we show in Fig.2(a) two limiting profiles which are consequences, (i) of fitting the best Maxwellian to the data, representing an *upper* limit on the true temperature; (ii) of neglecting the signals in the outer channels (i.e. those associated with the higher energy electrons) and so finding a *lower* temperature limit. The resulting profiles are shown in Fig. 2(a). In what follows we shall, for the sake of caution, assume that the temperature profile has the narrower shape (ii), so that, e.g., energy confinement times based on this profile may well be an underestimate.

Notice that the temperature profile can be measured with the laser only along a vertical chord at $R = 90$ cm, while the maximum current density,

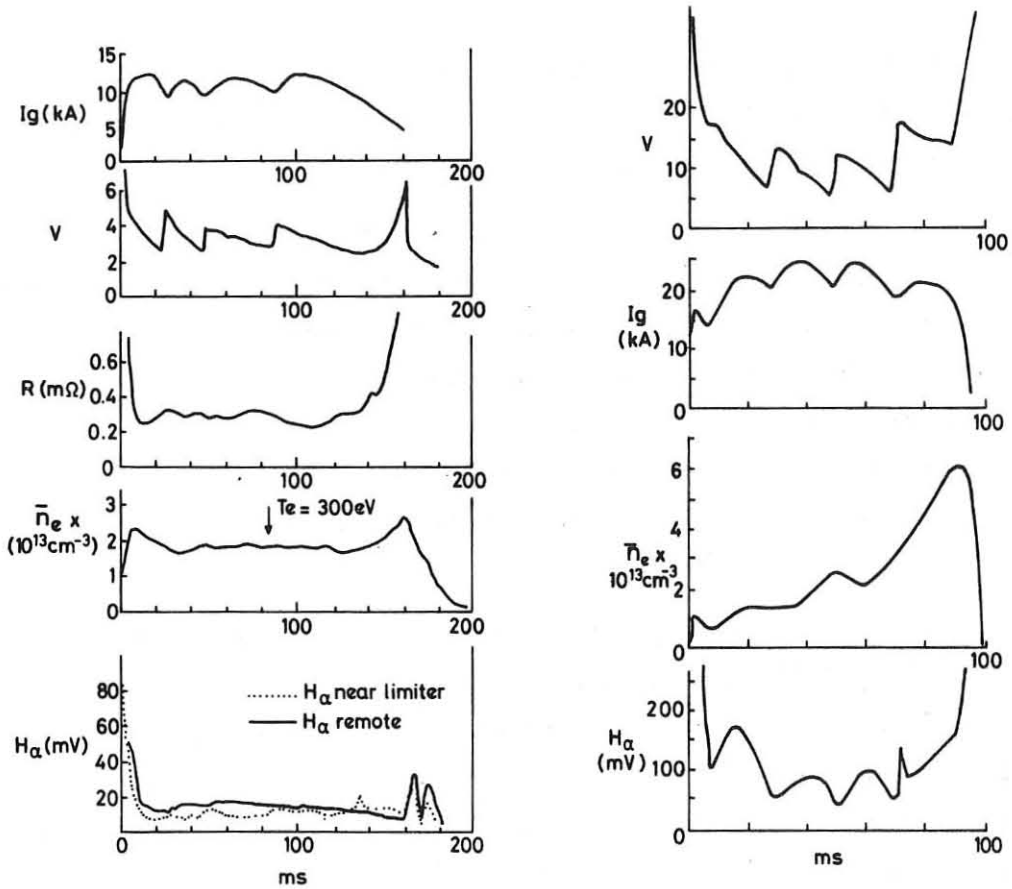

Fig.1
Oscillograms under two typical conditions
(a) Shot 4599. $B_\phi = 18$ kG, $t_0 = 0.6$, one gas valve only.
(b) Shot 3389. $B_\phi = 16$ kG, $t_0 = 0.6$, with auxiliary gas puffing 30 ms after discharge initiation.

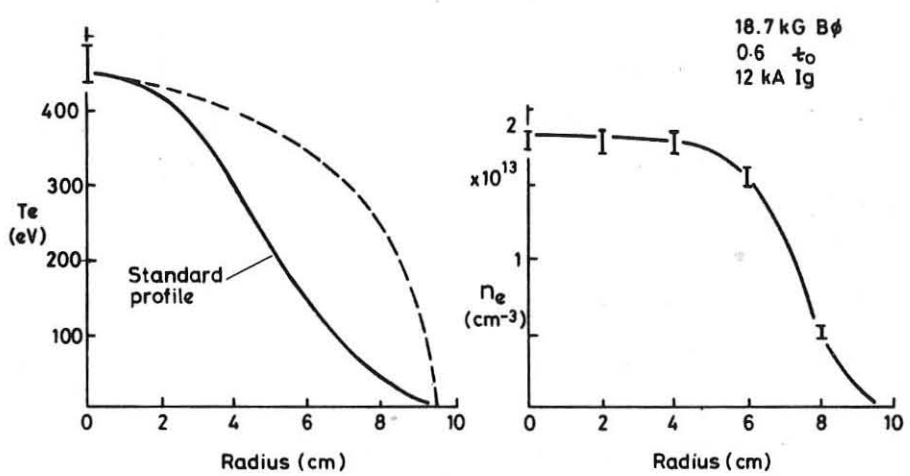

Fig.2
Radial profile of (a) electron temperature
(b) electron density; $B_\phi = 18.7$ kG, $I_g = 12$ kA and $t_0 = 0.6$.

CLM-P505

(corresponding to the self-consistent magnetic axis) could occur at $R > 90$ cm, so that the laser measurement may well underestimate the peak temperature when the profile is not flat.

The approximate effect of the azimuthal current on the total rotational transform is shown in Fig.3 for $B_\phi = 18.7$ kG and current direction such as to add to the transform; the contribution due to the current is based on type (ii) temperature profiles together with the usual assumptions on current distribution.

HEATING AND CONFINEMENT

Confinement times have been derived in the following way for the parameter ranges given in Table I.

τ_{Ee} is the simple electron energy replacement time defined by

$$\frac{d}{dt}(W_e) + \frac{W_e}{\tau_{Ee}} = I_g\left(V - I_g \frac{dI_g}{dt}\right)$$

where

$$W_e = 3\pi^2 R_0 \int_0^a r\, n(r)\, T_e(r)\, dr = A \bar{n}_e \hat{T}_e$$

is the total electron energy, $n(r)$ and $T(r)$ have the forms given by Fig.2, $\bar{n}_e$ and $\hat{T}_e$ are respectively the mean electron density (from interferometry) and central temperature (laser), A then being a shape factor taken as constant. In general the time dependent terms in the above relation were very small. Notice that, as defined, τ_{Ee} excludes ion energy and includes inelastic collisions and radiative power losses in the power input term.

TABLE I

Parameter	Range
Mean density $\bar{n}_e$ (cm^{-3})	$3 \times 10^{12} - 6 \times 10^{13}$
Central electron temperature T_e (eV)	100 - 1000
Ion temperature T_i (eV)	80 - 300
Toroidal field B_ϕ (kG)	14 - 20
Vacuum transform at separatrix ι_0	0.6
Plasma current I_g (kA)	8 - 25
*Collisionality $\frac{\nu}{\nu^*} = \frac{R}{\bar{\tau}\,\bar{\lambda}_{mfp}}$ (electrons)	$10^{-4} - 3 \times 10^{-1}$
Collisionality " " (ions)	$10^{-3} - 10^{-1}$
Electron drift/thermal velocity $\overline{v_d/v_e}$	0.01 - 0.3
Equivalent current I_{eq}	46 - 66

*Averaged over $|r| \leq 5$ cm, assuming $Z = 1$

Generally it is found that both energy and particle confinement improve as the current decreases and as the density increases. As a result of this, roughly similar temperature and density can be obtained for a wide range of ohmic heating current (in contrast to the usual situation in a tokamak where the heating and confining currents cannot be separated). This trend is illustrated in Fig.4, which shows the electron energy replacement time τ_{Ee} for various currents for two sets of plasma conditions. At the largest currents used τ_{Ee} approaches values typical of stellarators with $I_g \sim I_{eq}$, i.e. about those for the equivalent tokamak[2,3]. The range of values corresponding to the empirical tokamak scaling law of Hugill and Sheffield[4] for the total energy confinement time

$$\tau_E(\text{ms}) = 2.7\, n_{13}^{0.61}\, a^{1.57}\, B_3^{0.88}$$

($n_{13} = n_e \times 10^{-13}$, a = radius in m, $B_3 = B_\phi$ in kG) are shown for comparison. However, at the lowest currents used, where the vacuum fields dominate the transform, the energy confinement increases to significantly higher values.

The effect on τ_{Ee} of increasing the magnetic field strength for low current discharges at roughly similar density and temperature, is shown in Fig.5. This strong dependence (approximately $\tau \propto B_\phi^2$), is not, however, found when larger currents ($\geqslant 20$ kA) are used (dashed error bars).

The overall effect of different densities, current and temperature conditions can be seen by plotting τ_{Ee} against the drift parameter $\xi \equiv v_d/v_e \propto I/n\,T_e^{\frac{1}{2}}$. This is shown in Fig.6, which uses data from ~ 150 discharges with the same t_0, but with other parameters as in Table I. This plot, which is qualitatively like that found in TORSO[1,5] indicates a clear trend towards poorer confinement at large drift parameters.

Particle confinement times, obtained using hydrogen ionization rates derived from the H_α emission and neglecting any contribution from impurities, are shown plotted in the same way in Fig.7. These exhibit essentially the same trend, but with absolute values considerably longer than τ_{Ee}.

Ion temperatures, derived in the usual way from the neutral particle analyzers, vary between 80 and 300 eV. For most operating conditions the measured values are within a factor of two of estimates based on the usual Artsimovich scaling law, but at lower densities there is some indication of enhanced ion-heating, (Fig.8).

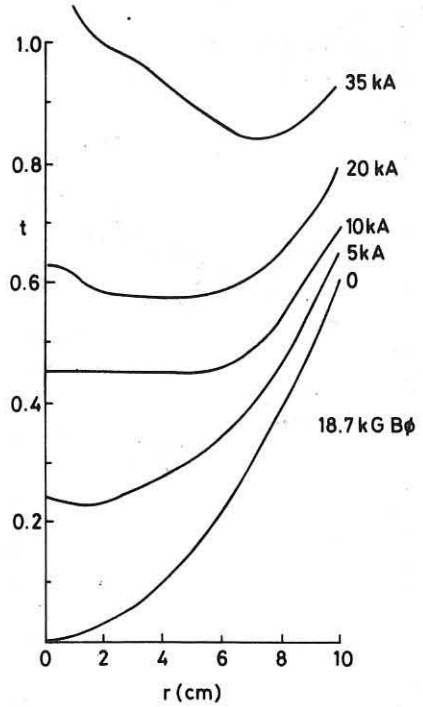

Fig.3
Radial dependence of rotational transform for B_ϕ = 18.7 kG and different values of plasma current, based on standard profile of Fig.2(a).

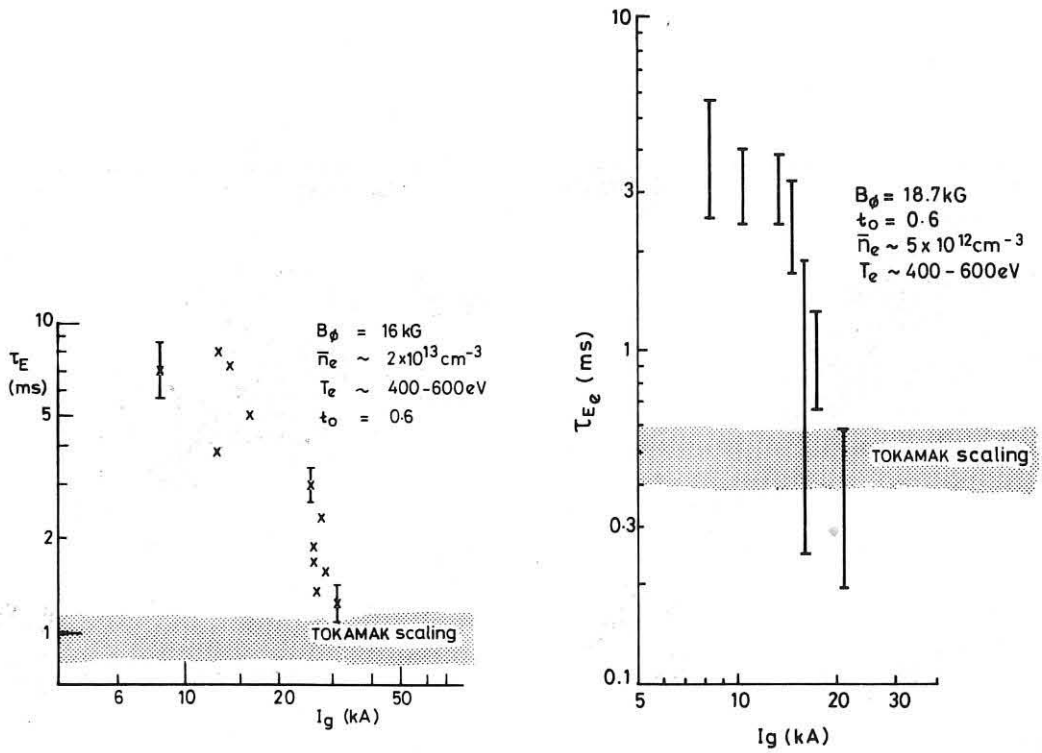

Fig.4
Variation of energy replacement time τ_{Ee} with plasma current for two different conditions of density and temperature.

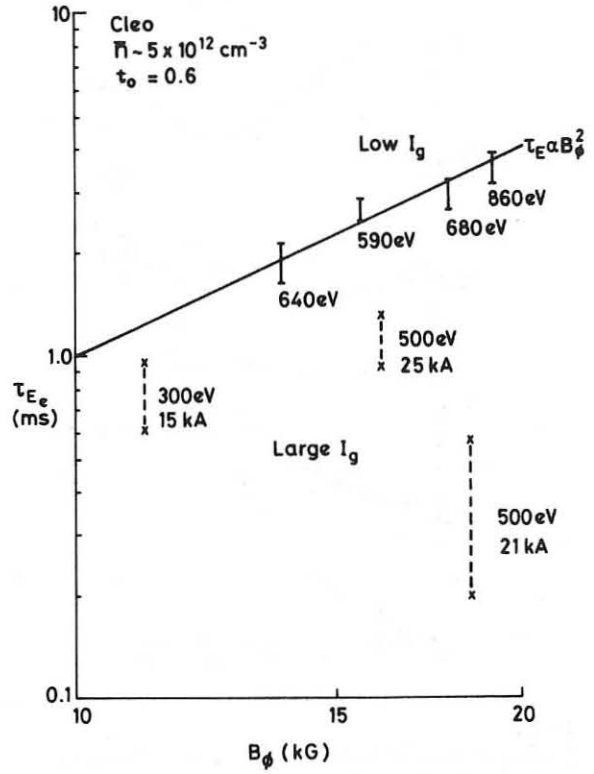

Fig.5
Variation of electron energy replacement time with toroidal field.

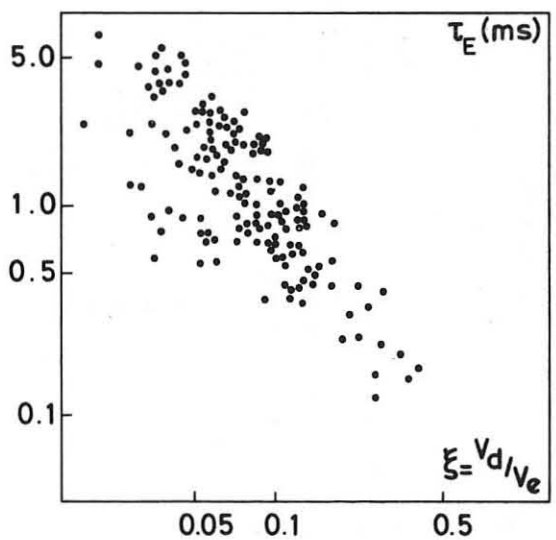

Fig.6
Variation of electron energy replacement time with mean drift parameter $\overline{v_d/v_e}$.

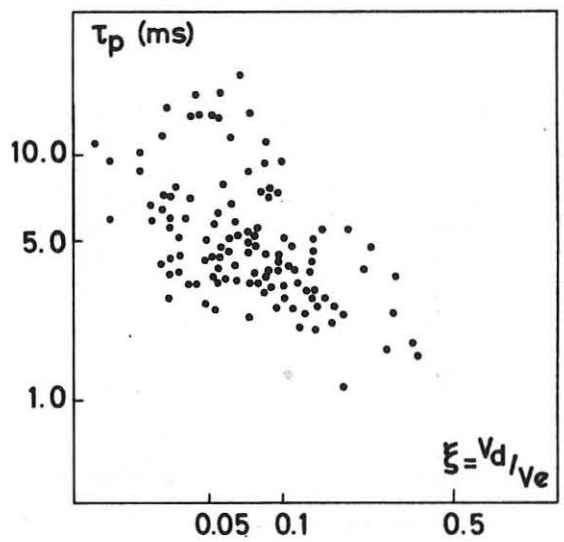

Fig.7
Variation of particle containment time with mean drift parameter $\overline{v_d/v_e}$.

A comparison with the pseudo-classical scaling law, which should result in the proportionality

$$W \propto I_g(I + I_{eq})$$

is shown in Fig.9, where the earlier data has been indicated by different symbols. This plot suggests that the apparent pseudo-classical dependence found in the early data was fortuitous, and resulted from the experimentally unavoidable inter-dependence of density and current which no longer applies under present conditions.

Some representative plasma conditions are shown in Table II.

TABLE II

Shot Number	3514	4400
B_ϕ (kG)	15.7	18
τ_0	0.6	0.6
$\bar{n}_e$ (10^{13} cm^{-3})	1.8	0.5
$\hat{T}_e$ (eV)	540 ± 40	620 ± 80
T_i (eV)	170	120
V_R (V)	2.4	2.8
I_g (kA)	12.0	10.5
τ_{Ee} (ms)	9.5 ± 1.1	3.2 ± 0.5
Z_R	3.2	4.0
τ_p (ms)	~ 34	~ 30
$\beta_{\phi e}$	1.6 ± 10^{-3}	4×10^{-4}
τ_{Ee}/τ_{Bohm}	~100	~40

PLASMA PURITY AND RESISTANCE

Absolute measurements of the soft X-ray emission spectra, made by pulse height analysis using the cooled detector, are shown in Fig.10 for a typical discharge condition. The emission is only slightly above that expected for pure hydrogen bremsstrahlung with the profiles used, the X-ray anomaly factor being $A_x = 4.3$ corresponding to $Z_{eff} \leqslant 1.05$ (assuming the increase is due to oxygen recombination radiation). The value of electron temperature derived from the slope is somewhat higher than that measured by the laser at $R = 90$ cm, consistent with a horizontal displacement of the central (hottest) region.

A comparison with the pseudo-classical scaling law, which should result in the proportionality

$$W \propto I_g(I + I_{eq})$$

is shown in Fig.9, where the earlier data has been indicated by different symbols. This plot suggests that the apparent pseudo-classical dependence found in the early data was fortuitous, and resulted from the experimentally unavoidable inter-dependence of density and current which no longer applies under present conditions.

Some representative plasma conditions are shown in Table II.

TABLE II

Shot Number	3514	4400
B_ϕ (kG)	15.7	18
τ_0	0.6	0.6
$\bar{n}_e$ (10^{13} cm^{-3})	1.8	0.5
$\hat{T}_e$ (eV)	540 ± 40	620 ± 80
T_i (eV)	170	120
V_R (V)	2.4	2.8
I_g (kA)	12.0	10.5
τ_{Ee} (ms)	9.5 ± 1.1	3.2 ± 0.5
Z_R	3.2	4.0
τ_p (ms)	~ 34	~ 30
$\beta_{\phi e}$	1.6 ± 10^{-3}	4×10^{-4}
τ_{Ee}/τ_{Bohm}	~ 100	~ 40

PLASMA PURITY AND RESISTANCE

Absolute measurements of the soft X-ray emission spectra, made by pulse height analysis using the cooled detector, are shown in Fig.10 for a typical discharge condition. The emission is only slightly above that expected for pure hydrogen bremsstrahlung with the profiles used, the X-ray anomaly factor being $A_x = 4.3$ corresponding to $Z_{eff} \leqslant 1.05$ (assuming the increase is due to oxygen recombination radiation). The value of electron temperature derived from the slope is somewhat higher than that measured by the laser at $R = 90$ cm, consistent with a horizontal displacement of the central (hottest) region.

The above result also agrees with an estimate of the oxygen impurity concentration based on the absolute emission of the O VIII resonance line at 23 Å, viz $N_{oxygen} \nmid 2 \times 10^{10}\,cm^{-3}$, so that $Z_{eff} \leqslant 1.1$. Photographic records of grazing incidence emission lines show a very low level of metal impurity.

The measured plasma resistance, however, generally shows a resistive anomaly Z_R between 2 and 4 times larger than that calculated for pure hydrogenic plasma (Z = 1) with local conductivity given by the Spitzer value based on the measured central electron temperature and the assumed profile, but taking no account of e.g. trapped particle effects. The greatest resistive anomaly occurs at low currents and high temperatures; unfortunately the T_e profiles are not sufficiently accurately known to determine whether this anomaly is real.

ELECTRON CYCLOTRON EMISSION

Electromagnetic emission spectra encompassing the first three harmonics of the electron cyclotron frequency are obtained, with 14 ms time resolution, using the mechanically scanned interferometer system described elsewhere[6]. A typical spectrum is shown in Fig.11, and is consistent with a thermal electron distribution without enhancement due to collective effects. The peak electron temperature derived from the second harmonic component of the emission is always proportional (within ± 25%) to the central temperature measured by the laser; however, using the precise resonance condition $\omega = 2\omega_{ce}$ to find the position corresponding to this peak, shows it to occur some 2 - 3 cm outwards from the geometric axis, i.e. at R = 92 - 93 cm. Even at densities as low as $n_e \approx 5 \times 10^{12}\,cm^{-3}$, provided low loop voltages ($V \leqslant 15$ eV) are used, non-thermal effects due to runaways disappear in less than 50 ms after the discharge is initiated. When steady conditions are maintained throughout the pulse the emission remains constant, showing that the electron temperature, within the 14 ms time resolution available, remains the same.

Temperature profiles derived on the usual assumption that the plasma everywhere radiates as a black body are shown in Fig.12, with appropriate laser temperature data (normalized) for comparison. However, at the low densities for which this diagnostic has so far been employed ($n < 2 \times 10^{13}$ cm^{-3}) the plasma is insufficiently locally absorbing, except perhaps at

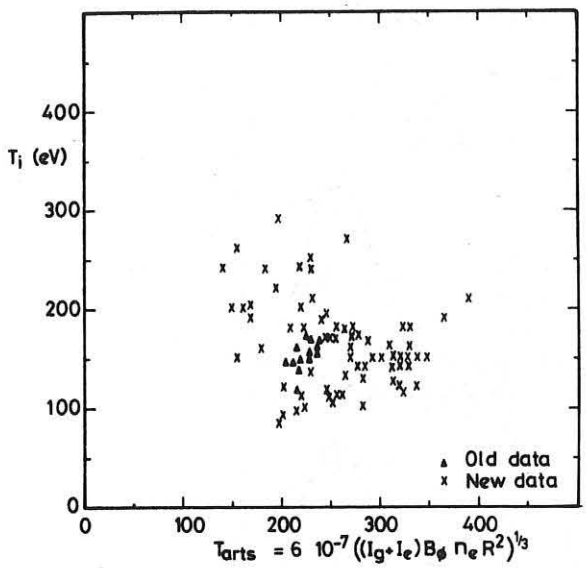

Fig.8
Ion temperature T_i versus the Artsimovich scaling parameter. The full line is drawn through the previous experimental data[1,2] and lies a factor of two below the true Artsimovich scaling.

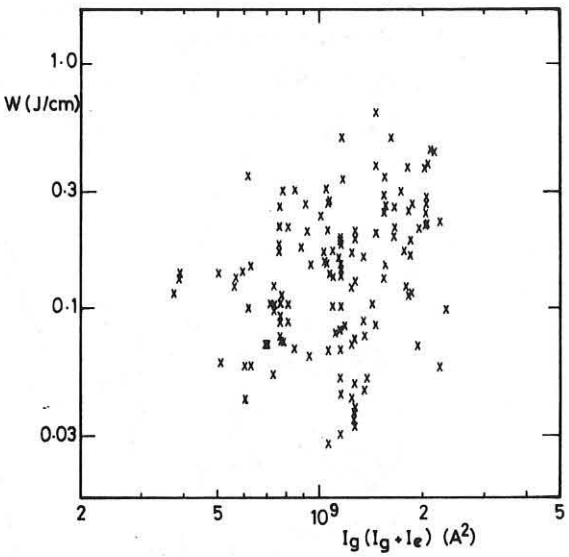

Fig.9
Electron energy per unit length W_e versus the pseudo-classical scaling parameter. I_E is the equivalent current due to the vacuum transform

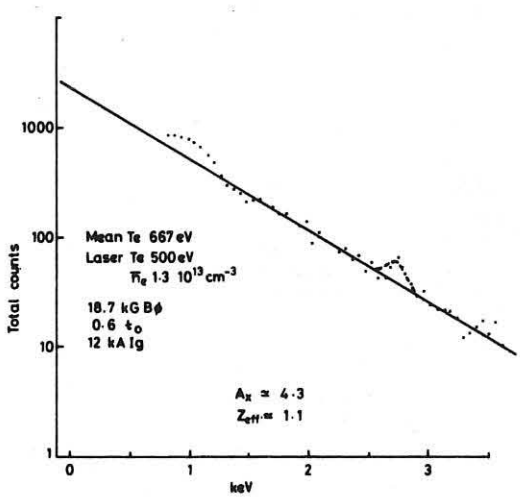

Fig.10
Spectrum of soft X-radiation as measured by Si(Li) cooled detector.

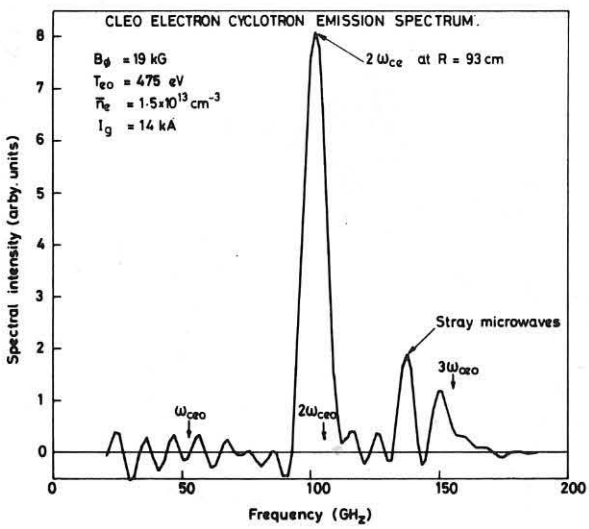

Fig.11
Typical electron cyclotron emission spectrum for the conditions B_ϕ = 19 kG, T_e = 475 eV (by photon scattering), $\bar{n}_e = 1.5 \times 10^{13}$ cm^{-3}.

CLM-P505

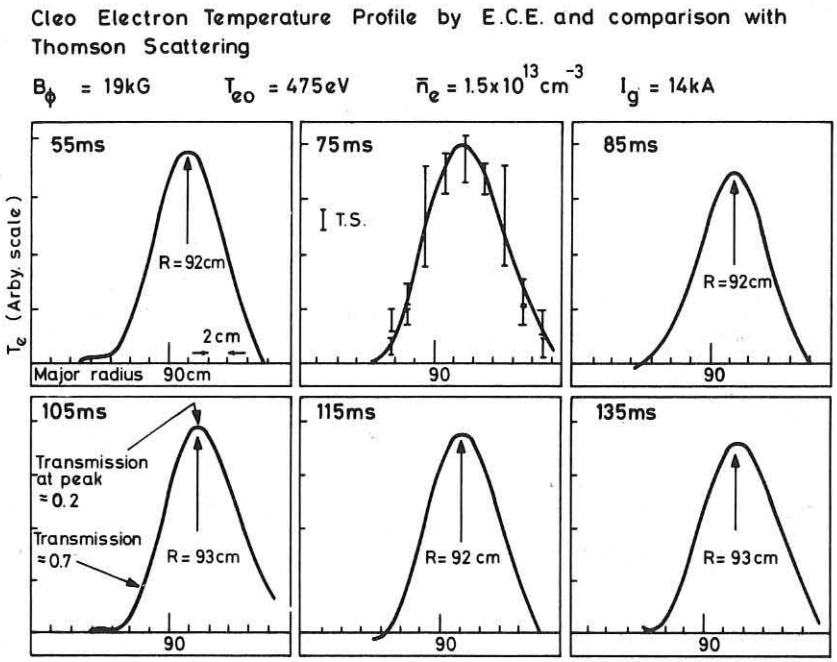

Fig.12
Time resolved radial profiles of electron temperature derived from electron cyclotron emission. A comparison is made between the profile at 75 ms and the data used for Fig.3(a).

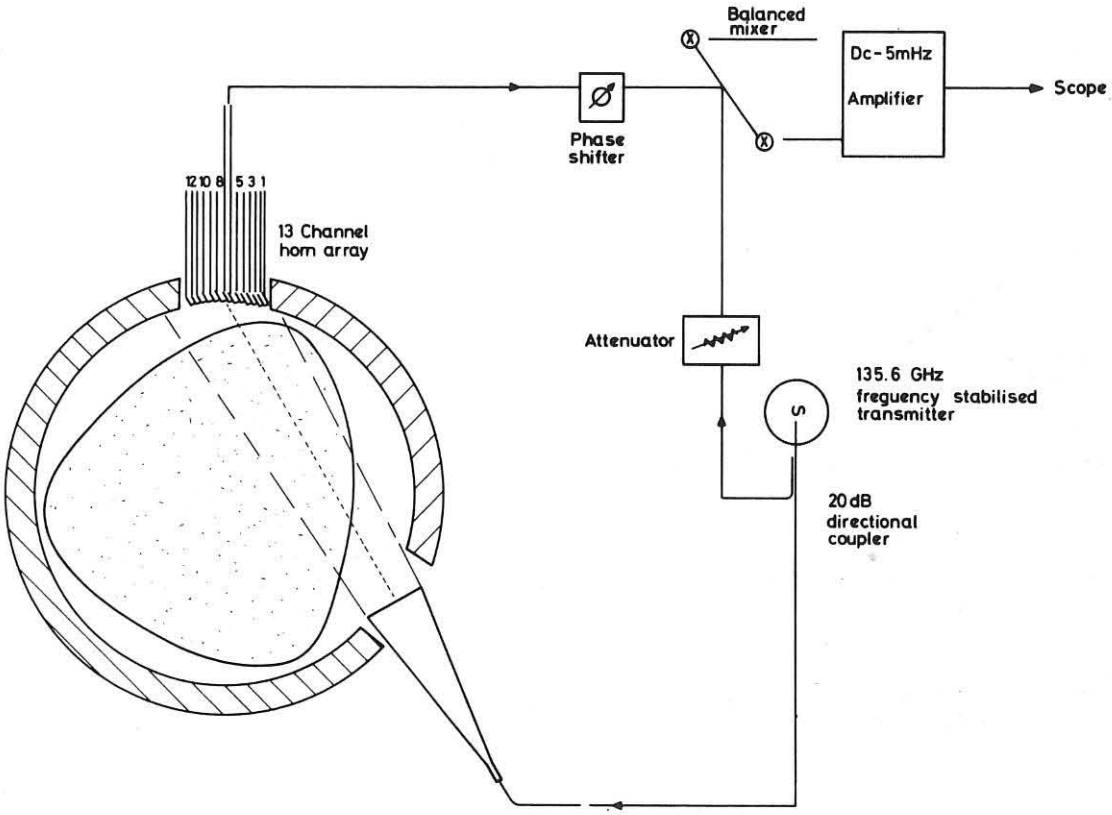

Fig.13
Schematic arrangement of the apparatus for measuring density fluctuations.

CLM-P505

the centre, for this apparent agreement to be relied on, since the low opacity in the outer regions can lead to an under-estimate of the profile width.

DENSITY FLUCTUATIONS

The arrangement shown schematically in Fig.13 has been installed to observe density fluctuations in the outer region of the plasma in an attempt to examine these as a possible cause of the enhanced diffusion at higher plasma currents. A 2 mm microwave beam about 7 cm wide traverses the plasma, entering as an essentially plane wave and emerging with phase variations across the beam caused by the fluctuations. The phase is recorded with time resolution $\sim 10^{-6}$ s at up to 8 positions across the beam by a set of 13 receiving antennae, wavelength and frequency spectra of the fluctuations being related to appropriate time and position correlations of the received signals.

A preliminary example of recorded signal is shown in Fig.14 for seven such channels. There appears to be more than one type of fluctuation present simultaneously, e.g. the signals show coherent, harmonic oscillations at $\sim$20 kHz, well correlated for transverse distances > 3 cm, and with amplitudes $\delta n/n \sim 3\%$ which disappear when the current decays in the afterglow, while at the same time incoherent oscillations, with much smaller scale length and broad frequency spectra (up to 120 kHz) can be observed. Magnetic probes outside the plasma show that the 20 kHz density oscillations are well correlated with fluctuations in the poloidal field, with $\delta B_\theta/B_\theta \sim 1\%$.

DISCUSSION AND CONCLUSIONS

Although there inevitably remains some residual uncertainty about the absolute values of the electron energy replacement time resulting from uncertainty in interpreting the laser scattering data, the general trends are clear, namely:

1. That the energy confinement is improved when operating at low ohmic heating currents, i.e. with the vacuum magnetic fields essentially determining the particle confinement in the outer regions.
2. The confinement at a given (low) current improves significantly with the magnetic field strength, when the plasma density and temperature are held approximately constant.

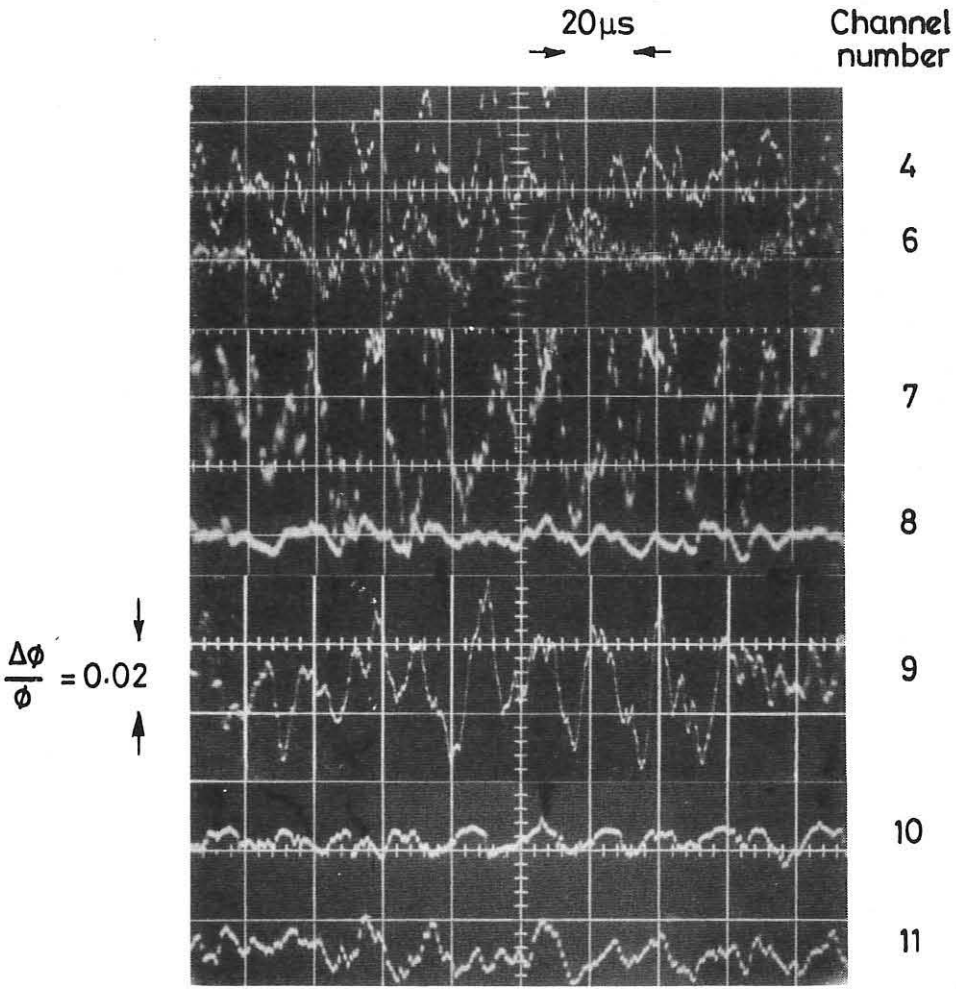

Fig.14
Oscillograms of raw data produced by the arrangement in Fig.13. The phase changes are shown for 7 separate channels. Abscissa 20 μs/div.

CLM-P505

3. The confinement is noticeably worse when the drift parameter v_d/v_e, is larger, although no physical explanation is as yet available to justify this dependence.

4. There is a variety of fluctuations present in the outer density region, whose relation (if any) to the confinement has yet to be explored.

5. The plasma, presumably as a result of the surface gettering, appears to be almost free of impurity. However, under some conditions of current and temperature the measured plasma resistance is higher than expected. Further work is needed to ascertain whether there is a genuine resistive anomaly or whether this reflects a constriction of the current narrower than can be explained by the temperature profile data presently available.

6. Because the temperature gradients are not yet sufficiently well known to derive experimental heat conductivities it is not meaningful to make proper comparison with neo-classical transport theory.

7. Operation over a much wider range of parameters than was previously possible shows that the confinement is no longer consistent with the semi-empirical pseudo-classical scaling law found at high current operation and a very restricted parameter range[1] (see Fig.9).

ACKNOWLEDGEMENTS

The team wish to thank R.J. Bickerton for his constant encouragement, K. Axon and R.D. Gill for the soft X-ray spectrum and its interpretation, and A. Costley and the National Physical Laboratory, Teddington, England, for the loan of the scanning microwave interferometer.

REFERENCES

(1) ATKINSON, D.W. et al. Plasma Physics and Controlled Nuclear Fusion Research, 1976, vol.II.

(2) ATKINSON, D.W. et al., Phys. Rev. Lett., 37, 1616 (1976).

(3) BLAUMOSER et al., WVII A Team, Plasma Physics and Controlled Nuclear Fusion Research, 1976, IAEA, vol.II, p.81.

(4) HUGILL, J. and SHEFFIELD, J., Nuclear Fusion (to be published)

(5) HAMBERGER, S.M. et al., Phys. Rev. Lett., 37, 1345 (1976).

(6) COSTLEY, A.E. and TFR Group, Phys. Rev. Lett., 38, 1477 (1977).

OHMIC HEATING EXPERIMENTS IN THE L-2 STELLARATOR

I.S. Shpigel'

Lebedev Physical Institute USSR Academy of Sciences, Moscow USSR

1. A SHORT DESCRIPTION OF THE L-2 STELLARATOR

The L-2 stellarator is a contemporary confinement device with a vacuum chamber bakeable to 300°C and an oil-free vacuum system, with a pumping speed of 150 litre/sec. Its basic charasteristics are shown in Table 1.

TABLE 1

Vacuum chamber major radius R = 100 cm

Vacuum chamber minor radius r = 17,5 cm

Average radius of last closed magnetic surface a = 11,5 cm

Maximum toroidal magnetic field B = 20 kG

Helical winding multiplicity l = 2

Number of helical winding pitches N = 7

Number of magnetic field periods $lN = 14$

Rotational transform on axis $\iota(o) = \frac{L(o)}{2\pi} = 0,2$

Rotational transform on last closed magnetic surface

$$\iota(a) \simeq 0,7 - 0,8$$

Shear $\theta = \frac{a^2}{R} \frac{d\iota}{dr} \simeq 0,5$

Base pressure in vacuum chamber 1 - 2×10^{-8} torr

Interval between discharges 2 - 3 minutes

The construction of L-2 embodies a number of features.

The vacuum chamber, which does not have an insulating break, is made of stainless steel 0,125 cm thick. During ohmic heating of the plasma, an induced current flows through the chamber. However, because of the relatively large resistance of the chamber (4×10^{-3} ohm) the chamber

current is negligibly small. The vacuum chamber is fitted with 28 ports with metal vacuum seals. The ports are distributed in seven toroidal cross-sections: 14 vertical ports (on the top and bottom of the chamber) have an inner diameter of 6cm, and of the 14 horizontal ports, the seven outside ports have an inner diameter of 9 cm, while the 7 inside ports have an inner diameter of 2 cm.

Since the chamber has limited mechanical strength, it is not used to support the helical winding. The helical winding is attached by an external, insulating structure made up of four U-shaped rings. The helical conductors are arranged in an uniform angle spiral with an angle of 57^{o} with respect to the toroidal direction.

Such a large helical winding angle requires some increase in the helical current in order to keep the last closed magnetic surface inside the vacuum chamber. In this case the separatrix has a relatively small ellipiticity (ratio of semiaxes 1:1,5). Furthermore, the rotational transform depends strongly on radius, which is usually a characteristic of $\ell = 3$ helical windings. Thus, the large pitch angle of the helical winding produces the finite rotational transform on axis $\iota(o) \approx 0{,}2$ characteristic of an $\ell = 2$ winding as well as the large shear ($\theta = 0{,}5$) characteristic of an $\ell = 3$ winding.

We did not succeed in experimentally attaining the calculated value of $\iota(a) = 1{,}06$ at a last closed magnetic surface and mean radius of 12,6 cm because an m = 1, n = 1 disturbance, caused by the finite accuracy of assembly, dis-

rupts the surfaces in the outer region. As a result, the mean radius for ε = 0,228 is a = 11,5 cm, with a rotational transform $\iota(a)$ = 0,78 on the last closed surface.

An O-shaped iron core with a flux of 0,18 volt-sec (without back-biasing) was used to produce the ohmic heating current. The experiments were conducted without a material limiter.

Figure 1 is a schematic of the diagnostic layout of L-2.

The complement of diagnostics allows the basic plasma parameters to be determined in several different ways.

A mini-computer serves as a data acquistion system and also performs preliminary data reduction in the interval between shots.

2. GENERAL DISCHARGE CHARACTERISTICS

1. Pre-ionization was effected by UV radiation from a powerful quartz lamp shining into one of the ports and a short pulse of poloidal magnetic field.

The duration of the pre-ionization current pulse was 1-2msec. The presence of the vacuum magnetic field structure produced by the helical winding allowed a plasma with an average electron density of 10^{11}-10^{12} cm^{-3} to exist at the moment of main current start-up (i.e., 10msec after pre-ionization). This value of initial electron density, under typical discharge conditions in hydrogen ($p=2.10^{-5}$ to 2.10^{-4} torr) ensured the subsequent growth of the average electron density to a maximum value of $\bar{n}_e \simeq 5.10^{12}$-$2.10^{13}$ cm^{-3} in 1-2msec with very little runaway electron production.

2. One of the important parameters in plasma ohmic heating is the value of the limiting plasma current [1]. In order to determine this limit a half-sine-wave current was induced in the plasma. By varying the voltage on the capacitor banks feeding the ohmic heating transformer primery winding, it was possible to vary the plasma current over a wide range. However, experiments showed that there is a sharp limit on the value of the plasma current that can be excited. This critical current I_{cr} was found to be proportional to the toroidal field strength and independent of the filling pressure (see figure2). Evidently, the limiting of the plasma current is caused by the development of a fundamental mode of MHD instability, which causes the plasma column to interact strongly with the chamber walls. The resultant influx of neutral atoms cools the electrons, the conductivity falls, and as a result, the current decreases.

In figure 3 are shown two series of oscillograms, obtained from discharges with less-than-critical and critical currents.

It is clear that when the current reaches I_{cr}, the instability leads to extensive plasma-wall contact. The density sharply increases, and peaks again appear in the hydrogen and impurity lines.

Direct evidence of the instability was obtained from measurements with a system of sinusoidal and cosinusoidal helical windings with multiplicities m=n=1. This system would only respond to the fundamental mode. The measurements showed that when the plasma current attains the critical value, a short, unipolar pulse appears on the diagnostic windings.

It should be noted, hower that the skin time of the vacuum chamber is ≃ 150-200 microseconds, which limits the high--frequency response of the diagnostic windings and thus distorts the true signal. Analysis of the signals from both windings shows that spatial phase of the disturbance is fixed, thus indicating that there is a plasma-current-independent perturbation in the stellarator magnetic field structure. We cannot exclude the possibility that this perturbation leads to the destruction of outer magnetic surfaces, the reduction of the radius of the vacuum surfaces, and the reduction of the plasma edge rotational transform to $t(a) = 0{,}78$.

3. The ohmic heating experiments were conducted with $\varepsilon = 0{,}228$, i.e. for that value of the ration of toroidal field current to helical winding current which places the lost closed magnetic surface inside the vacuum chamber. Therefore, a material limiter was not used to limit the plasma dimensions. As has been noted, the winding law used leads to an inward shift in major radius of 2,5-3 cm from the vacuum chamber axis. The magnetic axis is thus a flat circle of major radius R ≃97,0-97,5. The self-field of the plasma current shifts the magnetic structure (and therefore the plasma column) outward in major radius. As is well-known, the magnitude of the shift depends on the rotational transform: $\Delta r \simeq R \frac{B_\perp}{B} \frac{1}{t}$ where $B_\perp$ is the perpendicular field of the plasma current, and B is the toroidal field. The maximum shift occurs on the magnetic axis, and the minimum shift occurs on the last closed surface. For the experimental values $\frac{I_p}{B} \simeq 0{,}9\text{-}1{,}8$, the shift on axis is $\Delta r(0) \simeq 1{,}5\text{-}3$ cm, while the shift on the last closed surface is $\Delta r(a) \simeq 0{,}4\text{-}0{,}7$ cm.

In view of the small edge shift $\Delta\tau(a)$, an additional vertical field to compensate the $B_\perp$ due to the plasma current was not used.

3. OHMIC HEATING WITH QUASI-STATIONARY CURRENT

1. The basic ohmic heating experiments were performed with $\varepsilon = 0{,}228$ and a quasi-stationary current. Typical discharge oscillograms are shown in figure 4. Shown here are oscillograms of the plasma current I_p, the loop voltage, average electron density, and line intensities of hydrogen and impurity atoms. As can be seen, the current, loop voltage, and average electron density reach steady-state values 2-3 msec after the initiation of the discharge. The H_α and CIII lines behave similarly, and only the OVI line peaks and then falls to a low level after 5-6msec. Towards the end of the discharge, at 17msec in this case, the chordal average electron density reaches $(9\text{-}10).10^{12}\,\mathrm{cm}^{-3}$.

For the regime B=12 kG, I_p = 14 kA, and $p=4.10^{-5}$ torr, the ohmic heating power input does not exceed 25-30 kW in the steady-state portion of the discharge (see fig. 5). The time development of the central electron and ion temperatures, $T_e(0)$ and $T_i(0)$, and the average plasma energy is shown in fig. 6. The ion temperature was determined by analysis of charge-exchange neutrals averaged over a 1msec time interval, the electron temperature was determined by analysis of soft X-ray spectra in the range 1,2 to 4 keV averaged over 7msec, and the plasma energy density was determined from diamagnetic loop measurements with the assumption of a last closed surface average radius of 11,5 cm.

2. The dependence of the plasma temperature on density is particularly interesting. Fig. 7 shows the dependence of electron and ion temperature on average plasma density. As can be seen, for $\bar{n}_e = 4\text{-}5.10^{12}\,cm^{-3}$, the central electron temperature reaches 800 eV. However, as the density increases, Fe(0) decreases to 200 eV at $\bar{n}_e \simeq 16.10^{12}\,cm^{-3}$. The dependence of W, the energy stored in the plasma, and τ_E, its confinement time, on average electron density for B = 12 kG, I_p = 14 kA is shown in fig. 8. Here is plotted the confired plasma energy, as determined directly from diamagnetic measurement (W_d), as calculated from the central electron and ion temepratures and average electron density. In the calculations it was assumed that the radial dependence of these quantities is parabolic. As can be seen, the measured and calculated energy densities W_d and W_s agree in the density range $\bar{n}_e = 7\text{-}15.10^{12}\,cm^{-3}$. Significant disagreement occures for $\bar{n}_e < 7.10^{12}\,cm^{-3}$ in which case the energy determinedfrom diamagnetic measurements increases, while the calculated energy, W_s, falls. This discrepancy can be explained as a consequence of the contribution of suprathermal electrons to the diamagnetic signal [2]. The energy and relative number of suprathermal electrons increases as the plasma density decreases. The agreement between W_d and W_s which occurs for $\bar{n}_e \simeq 7\text{-}15.10^{12}\,cm^{-3}$ indicates that the true distributions $T_e(r)$, $T_i(r)$, and $n_e(r)$ are little different from the parabolas assumed in the calculations. In experiments on Cleo [3] and W-7a [4] it was found that the profiles were significantly wider than parabolic.

3. In the majority of ohmic heating experiments on tokamaks, the ion temperature in the center of the plasma coincides

with that given by the Artsimovich formula [5]:

$$T_i(0) \simeq 6.10^{-7} [I B R^2 \bar{n}_e]^{1/3} ev \ (A, G_s, cm)$$

For tokamak experiments, the plasma current I_p is used for I in the formula. In the case of a stellarator, one would expect that the thermal insulation is determined by the total poloidal field, including the contribution of the stellarator magnetic field. The equivalent current due to the stellarator field, I_{St}, is determined by the geometry and the rotational transform on the lasted closed surface, $t_{St}(a)$, and is given by $I_{St} = \frac{5a^2 B}{R} t(a)$. For the L-2 stellarator with $\varepsilon = 0{,}228$, $I_{St} \simeq 5{,}1$ B amperes, with B in gauss. The total current which determines the thermal insulation of the plasma and ion temperature through the Artsimovich formula is then $I_\Sigma = B(S + 5{,}1)$ amperes, where B is in gauss and $S = Ip/_B$. In our experiments the ratio S is in the range 0,9-1,8. As can be seen from these ratios, the contribution of the stellarator field to the thermal insulation exceeds that of the plasma current by a factor of 2-5.

In figure 9 are plotted measured central ion temperatures as a function of the parameter $\xi \sim [I_\Sigma B \bar{n}_e]^{1/3}$. As can be seen, the temperature rises proportionally with ξ. However, the absolute magnitude of $T_i(0)$ is two times less than that predicted by the Artsimovich formula.

Fig. 10 shows the dependence of the ion temperature on the ratio $S = \frac{I_p}{B}$ for three different values of toroidal filed B. The very strong dependences $T_i(0) = f(S)$ and $T_i(0) = f(B)$ are very striking. Thus, for $S = 1{,}1$, the ion temperature is 65 eV for B = 9,2 kG and 120 eV for B= 16,4 kG.

It should be noted that simultaneously ξ increases by a factor of $\left(\frac{16,4}{9,2}\right)^{2/3}$ which is approximately the factor by which the ion temperature rises.

Thus, while the ion temperature in L-2 has the same functional dependence as the ion temperature in tokamaks, its magnitude is two times smaller than that predicted by the Artsimovich formula with the substitution of $I = I_\Sigma = I_p + I_{st}$ for $I = I_p$.

4. Analysis of the experimental data allows us to conclude that when $\frac{dI_p}{dt} = 0$ the electron density, light impurity line intensity, central electron temperature, and electron temperature determined from conductivity measurements all remain constant for the duration of the falt-top current pulse. If the impurity contribution to the charged particle population is neglected, it is possible to derive from the data a source function. Assuming stationary source and electron densities, it is then possible to determine the local and integral electron confinement time.

For known or given profiles of $n_e(r)$ and $T_e(r)$, it is possible to calculate, in the case of multiple charge exchange, the neutral hydrogen density profile $n_0(r)$ [6*]. The absolute scale can be determined to within $\pm$ 50% from absolute measurements of the neutral hydrogen flux or of the H_α line intensity. The first set of measurements gives the neutral density in the central region with greater accuracy while the second set gives the neutral density at the plasma edge.

Fig. 11 shows the calculated profile $n_0(r)$, with abso-

---

*In the present calculation, it is assumed that $n_e(r)$ and $T_e(r) \sim 1 - \frac{r^2}{a^2}$.

lute value at $r = 0$ determined by charge exchange measurements. Also shown is the neutral density, $n_0(a)$, determined from spectroscopic measurements. As can be seen, the charge exchange and spectroscopic measurements are in close agreement. This justifies the assumptions made in calculating $n_0(r)$.

In the same figure is also shown the radial dependence of the particle confinement time, $\tau_p(r)$, which is calculated neglecting the impuritiy contribution to the electron population and under the assumption of steady-state $n_0(r)$ and $n_e(r)$. The particle confinement time at a radius of 0,9a = = 10 cm is 15msec. for B = 12,4 kG.

In figure 12 is shown the toroidal field dependence of the particle confinement time on-axis and at a radius of 0,9a = 10 cm. The calculations were done under the assumptions already described. The analysis shows that the particle confinement time is proportional to the magnetic field raised to a power greater than 1, and that for B = 16,4 kG $\tau_p(0,9a) \simeq$ $\simeq$ 20-22msec. The dependence of $\tau_p(0,9a)$ was determined at a current of 10 - 14 kA, and that of $\tau_p(0)$ for currents 8 to 22 kA.

5. An important characteristic of the thermal insulation of the plasma is the energy confinement time $\tau_E = \frac{W}{P - \frac{dW}{dt}}$, where $W = \frac{3}{2}\int n_e(T_e+T_i)dV$ is the energy contained in the plasma and $P = I_p U$ is the ohmic heating power.

In figure 13 is shown the dependence of the energy confinement time on toroidal magnetic field for I_p = 12-13 kA, as determined from diamagnetic measurments and as calculated using the average electron density, central ion and electron temperatures, and the assumption of parabolic profiles. The

confined energy increases from 120 to 350 joules, i.e., by a factor of three, as the magnetic field is increased from 9 to 16,5 kG. The dotted curve represents the pseudoclassical prediction for energy confinement [7,8] $W \sim I_p (B_{st} + B_I)$ calculated with the coefficient $c^2 = 10$. The difference between the two confined energies determined from diamagnetic measurements and calculated from $\bar{n}_e$, $T_e(0)$, and $T_i(0)$ is relatively small, and their dependence on the toroidal field coincides both functionally and in magnitude with the pseudoclassical predictions (dotted line in fig. 13) in which the total poloidal field $B_z = B_{st} + B_I$ is included.

The $P(B)$ and $W(B)$ data allow us to construct $\tau_E(B)$, which is also shown in fig. 13. The energy confinement time increases faster than linearly with the magnetic field. The magnitude of τ_E for B=12 kG agrees with the empirical law $\tau_E = 4.10^{-8} a^2 B_z$ [9].

If the magnetic field is held constant as the current is raised, τ_E at first rises, but after reaching a maximum value [at $S = 1,3$], falls (see fig. 14). The ohmic losse P (see Fig. 5) in the interval of current variation S = 0,9-1,3 remains practically constant, but with further increasing current P increases sharply, reaching 100-200 kW at $S = 1,8$.

Under the same conditions the behaviour of $W(I_p)$ differs significantly from that of the ohmic heating power. At first, the plasma energy grows almost proportionally with the current, but at $S = 1,3$ (I_p = 17 kA) the growth of plasma energy stops, and with further increase in current the energy begins to decrease. At a current of 20-22 kA the energy confined in the plasma is about one-half the maximum value. In contrast to P and W the

seen, the results obtained on these three device fall on a straight line proportional to this parameter. The slope of the line is one-half the slope of the corresponding line for tokamaks.

It is striking that the energy confinement times of these three devices differ markedly. Fig. 16 shows the dependence of τ_E on α, the ratio of the average electron drift velocity $\bar{v}_{dr} = \frac{I_p}{e\int n_e dS}$ to the average electron thermal velocity $\bar{v}_{th}$. As can be seen, the energy confinement time increases as α decreases. In [10] it is shown that the particle confinement time depends significantly on the value of α. Such a strong dependence of τ_E on α indicates a significant transport of energy out of the plasma by convection.

In all of the stellarator experiments it has been noted that an arbitrarily large ohmic heating current cannot be obtained. The current is limited by Kruskal-Shafranov condition that the total rotational transform $t_\ell \lesssim 1$. This means that, in spite of its effectiveness, the ultimate capabilities of ohmic heating in stellarators are limited. Further progress in attaining better plasma parameters must be achieved through use of current-less heating.

CONCLUSION

1. The goal of this paper was to give a review of the current status of experiments on the L-2 stellarator and to compare the L-2 results with those of other stellarators. In these experiments high density plasmas with $\bar{n}_e \simeq 5\text{-}20.10^{12}\,\mathrm{cm}^{-3}$ are obtained. The central electron temperature is 800-200 eV, while the ion temperature is 60-120 eV. The energy confinement

central electron temperature changes only slightly as the current is raised from 12 to 22 kA. It may be possible to explain the dependence shown in Fig. 14 by supposing that, for currents greater than 16-17 kA ($S > 1,3$), the plasma column shrinks, due to the development of instabilities in its outer regions. This leads to a constriction of the current channel, an increase in gas influx from the walls, an increase in power input, and, as a result, a reduction in τ_E . At the same time $T_e(0)$ can remain unchanged, since, although the energy confinement time decreases, the power input to the plasma increases significantly (2-4 times).

4. COMPARISON OF EXPERIMENTAL RESULTS FROM THE L-2, CLEO, AND W-7A STELLARATORS

Data presented in this and in an earlier paper [1] indicate the confinement of the L-2 stellarator plasma is good.

The long energy confinement time of 6-12msec achieved in L-2 can be attributed to the significant contribution of the poloidal component of the stellarator field to the thermal insulation of the plasma. As has already been shown, for $S \simeq 1,0$--$1,2$, this component is about five times larger than the poloidal field of the current, and for I_p = 15 kA, it reaches B_{st} = 1,2 kG. Other work [1,3,4] has also shown the importance of the stellarator poloidal field.

However, in stellarator experiments [1,3,4,6] the ion temperature has been found to be about one-half the value expected from the Artsimovich formula. In figure 15 the central ion temperatures of the Cleo, W-7A, and L-2 stellarators are plotted versus the parameter $[B R^2 \bar{n}_e (I_{st} + I_p)]^{1/3}$. As can be

time reaches 8-12msec. The energy density averaged over the plasma cross-section is $6\text{-}7.10^{15}$ eV/cm^3 for a total plasma energy of 350 joules. All of these results were obtained at relatively low magnetic fields of B=9-16 kG with an ohmic heating current of 10-20 kA.

2. The results listed above show that the plasma temperatures and energy confinement times attained in L-2 can only be attributed to a significant influence of the poloidal component of the stellarator field.

The presence of a significant rotational transform created by the helical winding on the one hand increases the MHD stability of the plasma column for values of totoal rotational transform $t_z < 1$, but at the same time limits the plasma current, and therefore the ohmic heating power input to the plasma. This limits the maximum electron and ion temperatures.

3. Analysis of the Cleo [3,11] and W-7A [4] experiments in which the stellarators were operated as tokamaks with out stellarator fields shows the importance of the poloidal stellarator field.

These experiments showed that when these devices were operated as tokamaks, the plasma parameters were significantly lower than those achieved in stellarator operation. The conclusions drawn in the papers [3,4,11] unequivocally show the significant contribution of the poloidal stellarator field to energy confinement.

4. Along with this, it is necessary to note the relatively low ion temperature, one-half the Artsimovich value, obtained in these stellarators. A possible explanation of this may be enhanced losses due to charge exchange or diffusion.

Experiments on the Levitron [10] have shown the importance of convective losses. Certainly the presence of an electron drift velocity due to current flow effects the particle and energy confinement times.

In conclusion, it is the author's pleasant duty to express his deep gratitude to the members of the L-2 stellarator group for many useful discussions.

REFERENCES

[1] D.K. Akulina, E.D. Andryukhina et al. in Plasma Physics and Controlled Nuclear Fusion Research (proc. VI Int. Conf, Berchtesgaden, 1976), 2, 115, IAEA, Vienna (1977)

[2] V.V. Sannkov, Yu.A. Sokolov. Fizika Plasmy, 2, 204 (1976)

[3] D.W. Atkinson, J. Bredley et al. in Plasma Physics and Controlled Nuclear Fusion Research (Proc. VI Ing. Conf., Berchtesgaden, 1976) 2, 71, IAEA, Vienna (1977)

[4] M. Blaumoser, G. Gattanei et al. in Plasma Physics and Controlled Nuclear Fusion Research (Proc. VI Int. Conf., Berchtesgaden, 1976), 2, 81, IAEA, Vienna (1977)

[5] L.A. Artsymovich, M.P. Petrov. J.E.T.Ph.Lett., 11,142(1970)

[6] D.K. Akulina, E.D. Andryukhina et al., VIII European Conf. on Contr. Fusion and Plasma Physics, '129', Prague (1977)

[7] A.G. Dikii, Yu.K. Kusnetsov et al. in Plasma Physics and Controlled Nuclear Fusion Research (Proc. V Int. Conf., Tokyo, 1974), 2, 45, IAEA, Vienna (1975)

[8] H. Hacker, G. Parcher et al. in Plasma Physics and Controlled Nuclear Fusion Research (Proc. VI Int. Conf., Tokyo, 1974), 2, 3, IAEA, Vienna (1975)

[9] E.P. Gorbunov, S.V. Mirnov, V.S. Strelkov. Nuclear Fusion, 10, 43, 1970

[10] M.W. Alcock, D.E.T.F. Ashby et al. in Plasma Physics and Controlled Nuclear Fusion Research (Proc. VI Int. Conf., Bechtesgaden, 1976), 2, 305, IAEA, Vienna (1977)

[11] D.W. Atkinson, A.N. Dellis et al. Phys. Rev. Lett., 37, 1616 (1976)

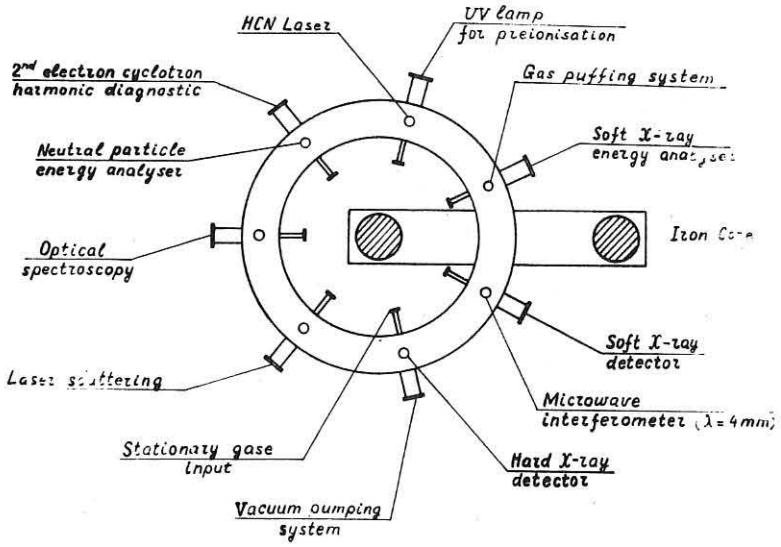

Fig. 1. Schematic of diagnostic apparatus

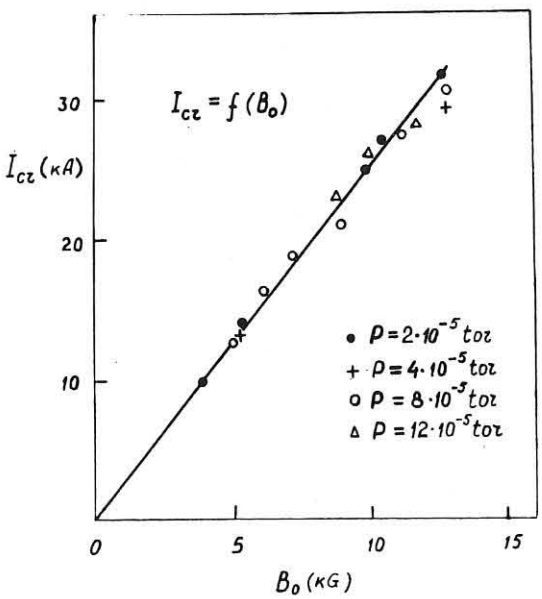

Fig. 2. Dependence of critical current on magnetic field for $\mathcal{E} = 0{,}228$

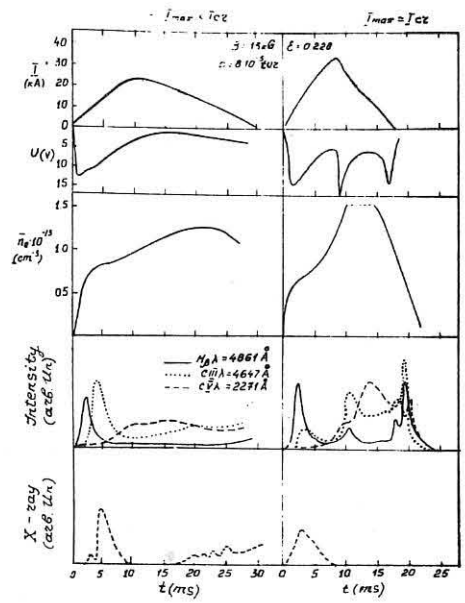

Fig. 3. Oscillograms of (from top to bottom) plasma current I_p, loop voltage U, average electron density $\bar{n}_e$, H_α line intensity, CIII and CIV line intensities, and hard X-ray signal ($h\nu > 50$ keV) for the cases $I_{max} < I_{cr}$ and $I_{max} \approx I_{cr}$.

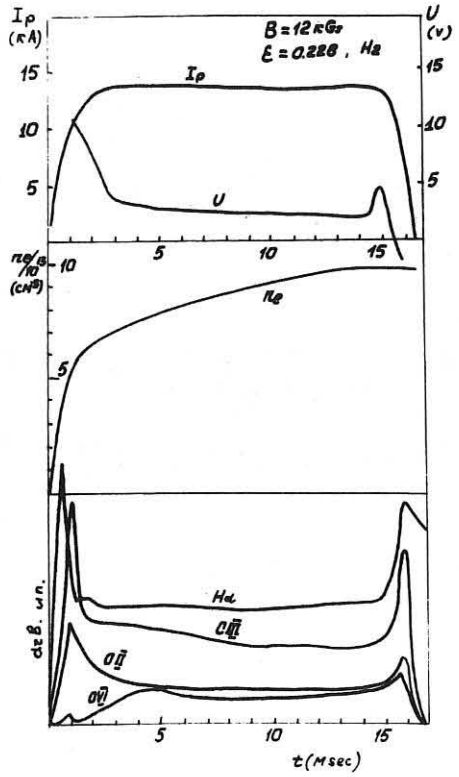

Fig. 4. Oscillograms of discharge with flat-top current.

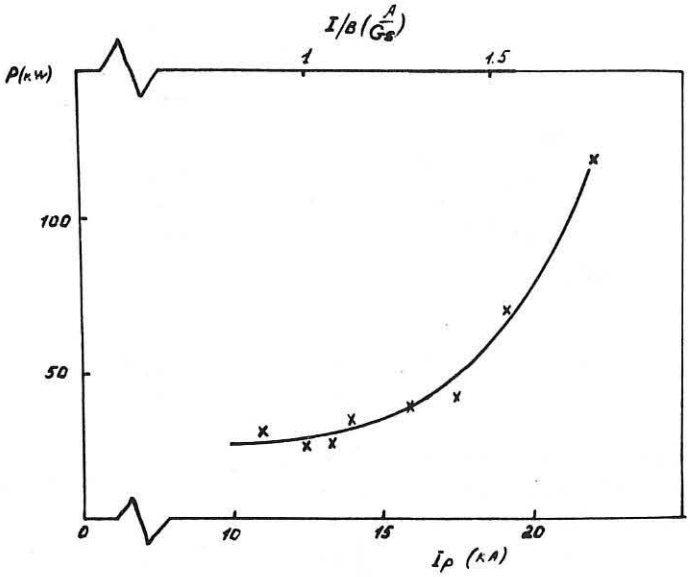

Fig. 5. Ohmic heating power versus plasma current I_p for B = 12,4 kG

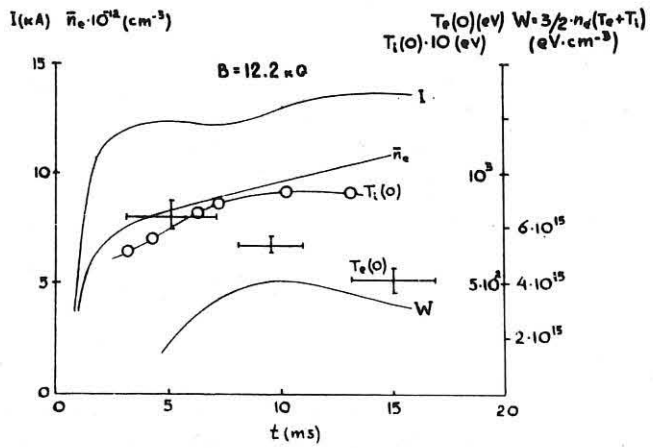

Fig. 6. Time dependence of I_p , $\bar{n}_e$, average energy density W, and ion and electron temperatures in central region.

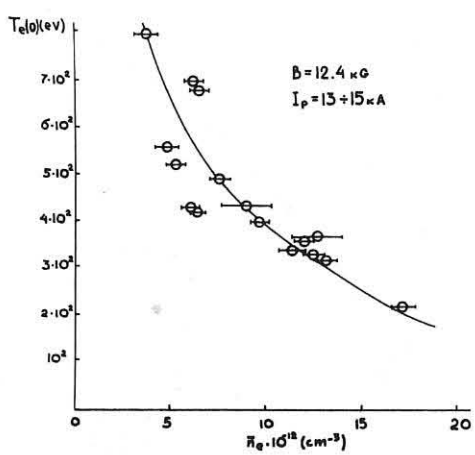

Fig. 7. Central electron temperature $T_e(0)$ versus $\bar{n}_e$. Horizontal lines indicate range of variation over which $\bar{n}_e$ is averaged.

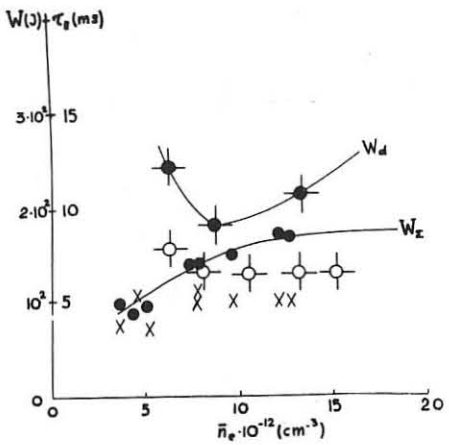

Fig. 8. Total plasma energy W_d (diamagnetic) and W_S (calculated from measured $T_e(0)$, $T_i(0)$, and $\bar{n}_e$), $\tau_d = \frac{W_d}{P}$ - ⊙ , and $\tau_s = \frac{W_s}{P}$ (x) versus mean electron density

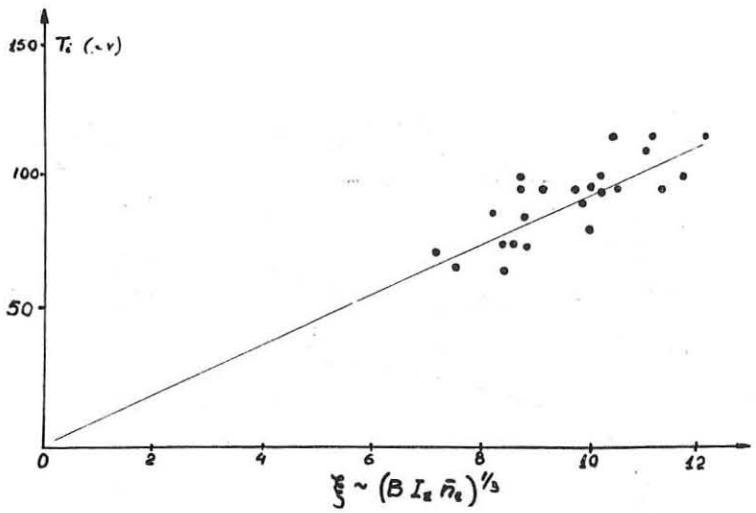

Fig. 9. $T_i(0)$ versus $\xi \sim (B I_\varepsilon \bar{n}_e)^{1/3}$

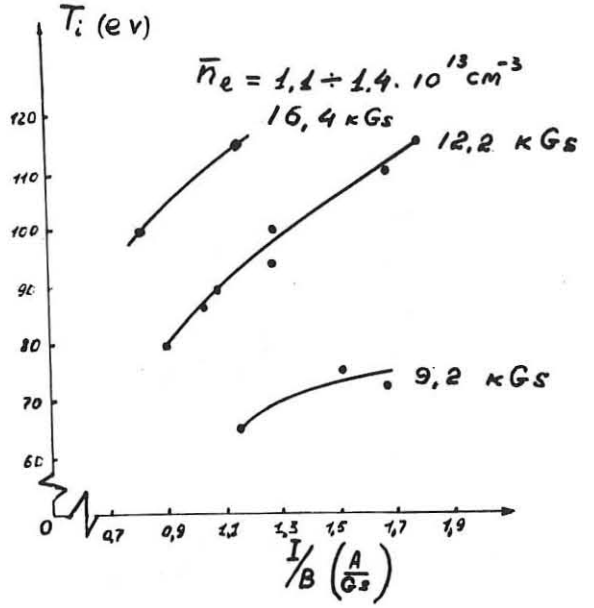

Fig. 10. $T_i(0)$ versus $\frac{I_p}{B}$ for B = 9,2, 12.2, and 16,4 kG. Mean electron density $1,1\text{-}1,4.10^{13}\,cm^{-3}$

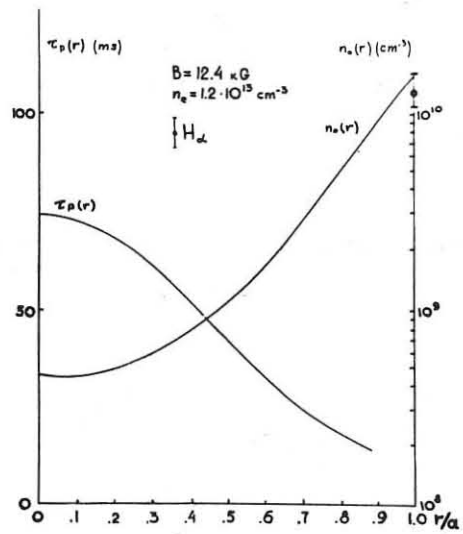

Fig. 11. Radial profiles of neutral hydrogen density $n_0(r)$ and electron confinement time $\tau_p(r)$. $\tau_p(r)$ calculated under assumption of pure hydrogen plasma. $\bar{\phi}$ - experimental value of $\tau_p(a)$, determined from absolute measurements of H_α intensity

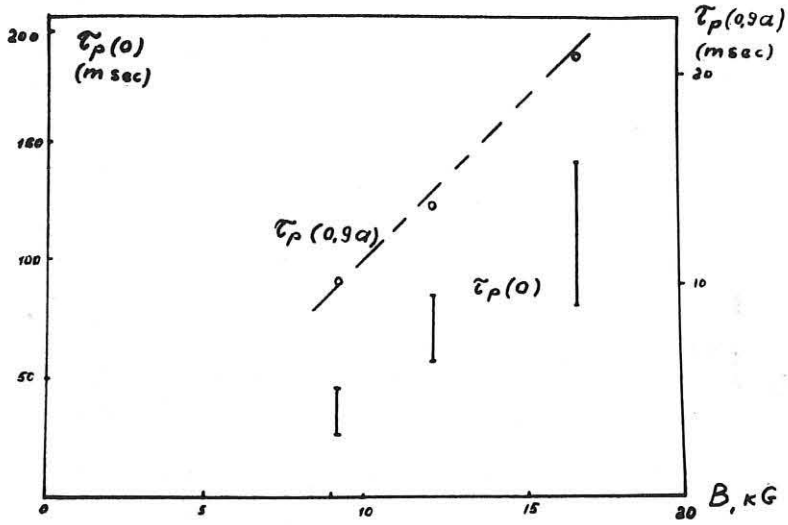

Fig. 12. Central $(\tau_p(0))$ and radially averaged (over $r = 0$ to $r = 0,9\ a = 10$ cm) particle confinement time versus magnetic field

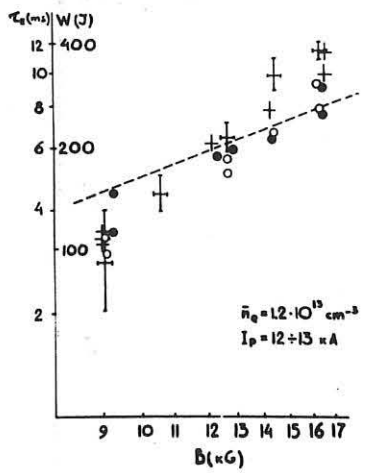

Fig. 13. Energy confinement time τ_E and total plasma energy W versus magnetic field B. $\dagger$ and $+$ show τ_E and W_d as determined from diamagnetic measurements. O and $\bullet$ show τ_E and W_s as calculated from measured $T_e(0)$, $T_i(0)$, and $\bar{n}_e$ with assumption of parabolic profiles

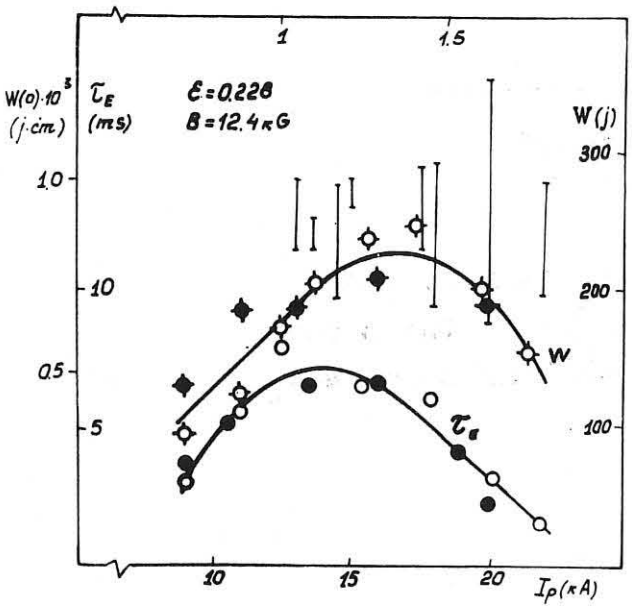

Fig. 14. Total plasma energy W, energy confiment time τ_E (O , $\dagger$ - $\bar{n}_e = (7\text{-}8) \cdot 10^{12}$ cm^{-3}, $\bullet$, $+$ - $\bar{n}_e = (11\text{-}12) 10^{12}$ cm^{-3}) and energy density in the central region (|) versus plasma current

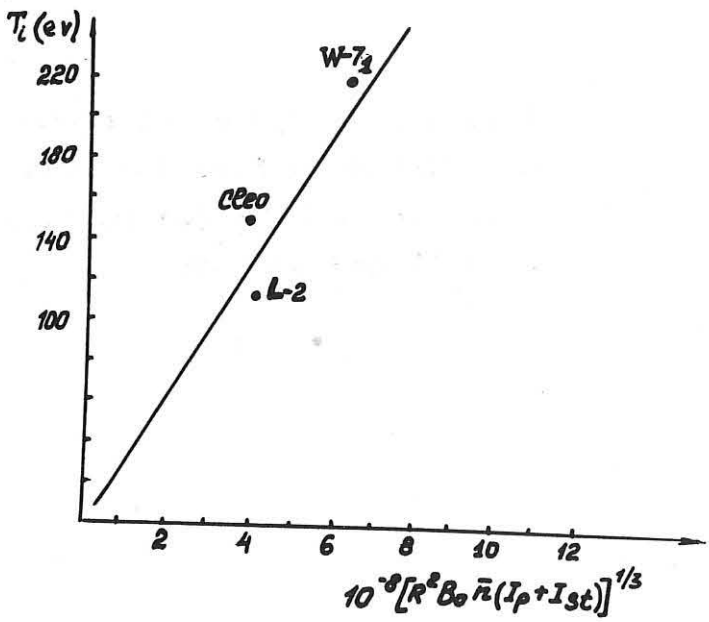

Fig. 15. Ion temperature in central region versus the parameter $[BR^2 \bar{n}_e (I_p + I_{st})]^{1/3}$.

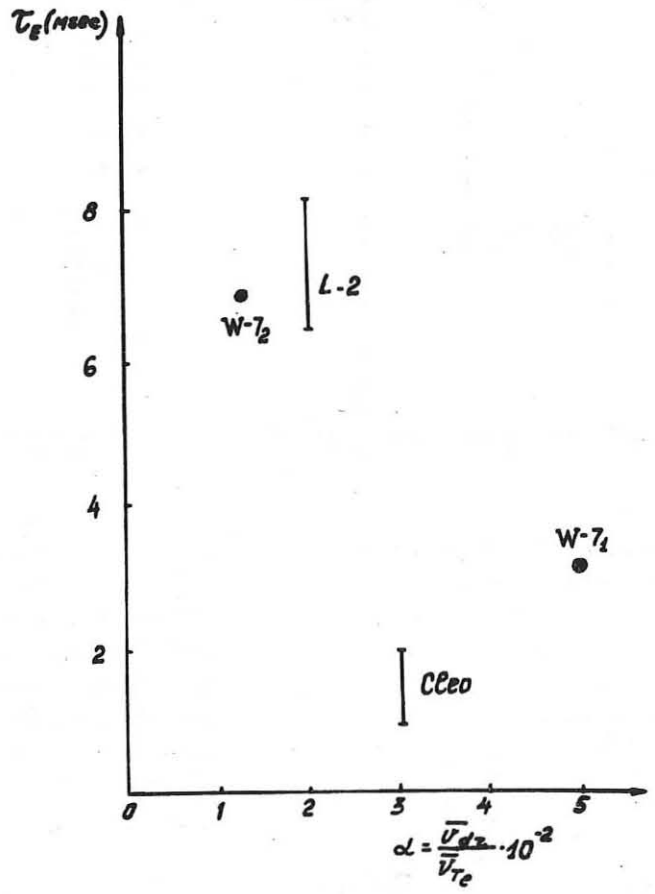

Fig. 16. Energy confinement time in L-2, W-7A, and Cleo as a function of $\alpha = \frac{\bar{v}_{dz}}{\bar{v}_{th}}$. The point $W\text{-}7_1$ is without gas puffing, and the point $W\text{-}7_2$ is with gas puffing

THE MIRROR MACHINE PROGRAM IN THE USA

by

F. H. Coensgen

Lawrence Livermore Laboratory, University of California

Livermore, California USA

ABSTRACT: As the result of recent experimental progress, theoretical advances, and the emergence of new approaches to the improvement of mirror confinement, the mirror approach has become the principal alternative to the tokamak in the USA magnetic fusion program. Emphasis is now centered on the Tandem Mirror and Field-reversed Mirror Concepts, which theoretically can obtain Q values of five or more.

INTRODUCTION: Recent progress in the mirror fusion program (see Table 1) includes a series of favorable advances in the 2XIIB experiment and the

Table 1. Recent Highlights in the Mirror Fusion Program

July 1975	2XIIB plasma stabilized; lifetime increased 10-fold; mean ion energy of 13 keV.
July - December 1975	Theory of 2XIIB stabilization developed; predictions of this theory guide Mirror Fusion Test Facility (MFTF) design.
October 1975	Simple method of "startup" in a dc magnetic field demonstrated: neutral injection on a cold-plasma stream.
February 1976	High β achieved (peak $\beta \approx 1.2$ to 1.6); raises hope for field-reversal concept.
March - September 1976	MFTF proposed and approved by ERDA.
July 1976 - April 1977	Tandem mirror idea for high-Q reactor introduced, favorably evaluated at LLL. TMX proposed and approved.
December 1976 to date	2XIIB field-reversal experiments yield 50% greater diamagnetic signal and maximum electron temperature to 140 eV; neutral-beam current being increased beyond 500 A for further experiments.

development of a theoretical model that accounts for observed plasma behavior in 2XIIB and other mirror experiments. This theory provides scaling laws for extrapolating of present experiments to larger devices.

These advances, together with the emergence of new approaches to the improvement of mirror confinement, have led to increased planning and construction of magnetic mirror systems in the USA. The USA mirror program (shown in Table 2) includes several university experiments as well as

Table 2. USA Mirror Research Facilities.

Cornell University — Field-reversal experiments in a mirror machine using energetic electron beams to form electron rings. Working on production of intense bursts of energetic ions to be used in field-reversal experiments to either directly reverse the field in a mirror machine or to produce the reversal by subsequent compression of the trapped ion ring.

Massachusetts Institute of Technology — Investigating a possible means of stabilizing the drift cyclotron loss cone (DCLC) mode. Idea is based on Ioffe's interpretation of PR-6 and -7 results. In the MIT experiment, electron beams will be used to generate rf fields within the plasma that will heat a portion of the electrons until they become magnetically confined and serve to produce a depression in the ambipolar potential. It is expected that low-energy ions trapped in this depression will partially fill the loss cone and thus suppress the DCLC instability mode.

University of California at Berkeley — Constructing a new, multiple mirror facility that is fully stabilized against MHD interchange mode and in which the density decay time is long enough to observe any residual MHD instability. The loss cone is nearly full in this device, which should suppress mirror-associated microinstabilities.

University of California at Irvine — Planning an experiment to test the possibility of stabilizing the MHD interchange modes by "line tying" only the plasma boundary through a cold-plasma blanket that surrounds the hot plasma.

University of California at Los Angeles — Planning to produce a collisionless, mirror-confined plasma with radial density gradients confined to a surface region to test the prediction that the DCLC mode will be localized in boundary region.

Table 2. Continued

University of Wisconsin — Planning to build a tandem mirror experiment in which the ions are heated by low-frequency rf rather than by neutral beams.

Lawrence Livermore Laboratory — Operating the neutral-beam-injected 2XIIB experiment. Constructing a tandem mirror experiment (TMX) to be completed by October 1978. Constructing the Mirror Fusion Test Facility (MFTF) to be completed in 1981.

Los Alamos Scientific Laboratory — Operating a field-reversed theta pinch which produces field reversal for 20 μs or more and which shows increased electron temperature when the field lines close.

Naval Research Laboratory — Pursuing two field-reversal experiments. In one, a 50- to 70-ns burst of 1-MeV ions is to be cusp-injected into a low-ratio mirror field. In the other, an electron ring is formed by injection of a burst of relativistic electrons that induce an ion "back current." The electron current decays in 60 ns, leaving an ion ring current that reverses the magnetic field. Field reversal persists for a time (5 μs) consistent with resistive diffusion and cross-field diffusion times.

Oak Ridge National Laboratory — Operating electron bumpy torus (EBTI), which is a toroidal mirror experiment. Increasing rf power to convert EFTI to EBTS and planning a larger experiment called EBT II.

United Technologies Corporation — Preparing an experiment to explore stabilization of the DCLC instability. Electron cyclotron resonant heating is used to generate a population of energetic, magnetically confined electrons that will depress the plasma potential in the plasma interior to confine low-energy stabilizing ions.

installations at the Lawrence Livermore Laboratory (LLL), Los Alamos Scientific Laboratory, Naval Research Laboratory, Oak Ridge National Laboratory, and the United Technology Corporation.

As a candidate for a fusion power plant, a mirror system offers a number of advantages, including high beta, the possibility of steady-state operation, small unit size, and natural divertor action along the open field lines. This divertor action precludes buildup of impurities, somewhat reduces wall loading, and makes practical the direct conversion of the energy of escaping plasma and charged reaction products to electricity.

The major disadvantage is the relatively poor particle confinement, leading to a power amplification factor Q of about unity even if stability is achieved. Augmented by a blanket of uranium or thorium, such a system might provide an attractive fissile fuel breeder or hybrid fission-fusion reactor.[1] As a pure-fusion reactor, it would have to operate as a driven power amplifier with a large recirculating power fraction requiring very efficient energy recovery and high heating efficiency in order to produce net power.

Emphasis in the mirror program is now centered on new concepts that theoretically can obtain Q values significantly larger than that of previous mirror reactor designs. Q is defined as the ratio of fusion power output to the injected neutral-beam power required to sustain the plasma density and temperature. From among the possibilities[2] for enhancing Q in mirror machines, the Tandem Mirror and the Field-reversed Mirror Concepts have been selected as the basis for the LLL mirror program. Theoretically, both concepts can obtain Q values of five or more. During the next 5 years, the largest USA mirror facilities will be 2XIIB, a tandem mirror experiment (TMX), and a large mirror facility called the Mirror Fusion Test Facility (MFTF). The specifications of these three machines, which will all be located at LLL, are compared in Table 3.

Table 3. LLL Mirror Facilities.

	2XIIB	TMX (end plugs)	MFTF
Magnetic field (midplane)	7 kG	10 kG	20 kG
Field duration	10 ms	Seconds	dc (superconducting)
Length between mirrors	1.6 m	1.15 m	3.2 m
Injection current	600 A maximum	550 A/plug maximum	750 A (sustaining beams)
Beam accelerating voltage	20 kV	20 kV (some 40 kV)	80 kV
Beam duration	10 ms	25 ms (first beam set)	500 ms (later, seconds)
Date operational	Operating	October 1978 (proposed)	October 1981 (proposed)

RECENT PROGRESS: Experimental progress at LLL was made possible by modifying the 2XII experimental facility to incorporate a system of 12 neutral beams,[3] each designed to inject 50 A of deuterium atoms into the contained plasma at energies of up to 20 keV in 10-ms pulses. First experiments with the new 2XIIB facility were carried out in January 1975. Research centered about identifying and eliminating the source of microinstability that had limited confinement times to a few hundred microseconds. Experimental evidence[4] pointed to the drift cyclotron loss-cone (DCLC) instability. Following the lead of an earlier theory[5,6] and experiments,[7] a low-energy plasma stream was injected along magnetic field lines into the contained energetic plasma in an attempt to partially fill the loss cone and stabilize the DCLC mode at a low level of turbulence. In a period of a few months (see Table 1), the principal issues of the Mirror Program — control of microinstability, scaling of $n\tau$ with energy, and startup in a dc magnetic field — were addressed with favorable results. Details of this work are reported in Refs. [8] through [11].

An alternative technique of providing cold ions for suppression of the DCLC mode uses electron cyclotron resonant heating (ECRH) to heat electrons in the mirror trap. The presence of the hot electrons modifies the ambipolar potential so that the cold ions are trapped in a local potential well, filling the loss cone sufficiently to stabilize the DCLC mode. This approach produced apparent stabilization for 50 to 100 μs in the PR-6 trap at the Kurchatov Institute.[12] In the USA, similar investigations (see Table 2) are underway at the United Technologies Research Center and at the Massachusetts Institute of Technology (MIT). In the MIT experiment, the ECRH is replaced by rf fluctuations driven by electron beams.

Concurrently with the 2XIIB experimental program discussed above, the quasi-linear theory[13,14] of the DCLC mode was developed at LLL. The DCLC mode is driven by the plasma density gradient coupled with a loss cone ion energy distribution. It can be stabilized either by reducing the density gradient or by partially filling the ambipolar potential hole in the ion energy distribution with a warm-ion plasma. Warm-plasma stabilization has been tested successfully in 2XIIB but has the disadvantage of increasing the electron energy loss rate, hence, lowering T_e. As the density gradient is reduced, the amount of warm plasma necessary for stability decreases, so the electron temperature can increase.

Tho quasi-linear theory also predicts the long-standing experimental observation that the stability condition is easiest to satisfy at high

values of beta. Plasmas of reactor size and density are predicted to be completely stable to the DCLC mode with the possible exception of boundary effects.

MIRROR FUSION TEST FACILITY (MFTF): Testing the predicted geometric scaling of T_e [and $(n\tau)_E$] with the density gradient is a primary physics objective of the MFTF. To achieve values of $(n\tau)_E$ significantly larger than those attained in 2XIIB and to provide a convincing test of predicted scaling, it is necessary to increase both electron and ion energies. A NbTi superconducting Yin-Yang magnet provides a 20-kG, minimum-B magnetic field (40 kG at the mirrors). Startup is accomplished as in 2XIIB by injecting pulsed beams into a transient cold plasma provided by an array of streaming guns. After startup, the plasma will be sustained by injecting 750 A of deuterium atoms with energies up to 80 keV for a period of 0.5 s. The injection period is long enough to achieve steady-state plasma conditions but not sufficient to attain equilibrium particle reflux from the walls, which are initially clean titanium surfaces providing high-speed pumping during the startup phase. Twenty-four 80-keV neutral beams provide the 750-A sustaining current, and twenty-four 20-keV, 10-ms, 2XIIB-type neutral beams inject a current of 1000 A into the cold-plasma stream for startup. MFTF plasma parameter goals are: density $\approx 10^{14}$ cm^{-3}, mean ion energy $\approx$50 keV, electron temperature $\approx$1 keV, and confinement $(n\tau)_E \approx 10^{12}$ $cm^{-3}\cdot s$. Successful completion of the MFTF requires development of reliable, high-current, 80-keV neutral beams; methods of disposal of intense flux of energetic particles; steady-state, high-speed, high-capacity pumping techniques; reliable, large-scale, complex, superconducting magnets; and reliable control systems for all beams, magnets, machine, and safety monitors.

TANDEM MIRROR EXPERIMENT (TMX): A tandem mirror system[15,16] consists of a solenoidal central magnet that is terminated at each end by conventional mirror cells that by virtue of their high positive potential act as electrostatic "end plugs" to prevent plasma leakage out the ends of the solenoid. In TMX, each end plug is essentially a duplicate of the 2XIIB experiment, except that the energy of four of the neutral beams in each plug has been increased to 40 keV and duration of all beams has been increased to 25 ms. The particles lost from the central solenoid are replaced by injection of gas or low-energy neutral beams that are ionized and heated by the hot electrons. The electrons are, in turn, heated by the energetic ions in the plugs. Electron temperature is the same in both

plugs and the center cell. The system is characterized by $E_p >> T_e > T_c$, where E_p is average ion energy of the plugs and T_c is the ion temperature in the central cell.

If the density in the plugs is greater than that in the solenoid, the requirement of quasi-neutrality establishes a potential difference ϕ_i between the two regions that confines the center-cell plasma ions. Electrons are confined by a net positive potential ϕ relative to ground; this potential adjusts to equalize the electron losses with the combined ion loss from the plugs and the solenoid.

Projected TMX plasma parameters are: $T_e \approx 0.2$ keV, $\Phi \approx 1.1$ keV, plug density $n_p = 5 \times 10^{13}$ cm^{-3}, mean plug ion energy $E_p \approx 26$ keV, plug beta $\beta_p \approx 0.5$, central density $n_c \approx 1.2 \times 10^{13}$ cm^{-3}, center cell ion temperature $T_c \approx 80$ eV, confining ion potential $\phi_i \approx 290$ eV, center beta (ion + electron) $\beta_c \approx 0.54$, center magnetic field = 0.50 kG, plug center field $B_p \approx 10$ kG. Magnet and current parameters of the end plugs are given in Table 3. Experiments using 20-keV beams to independently heat the center cell are also being prepared. With these beams, the principal parameter changes are that T_e increases to 290 eV and center-cell ion energy increases to 280 eV.

The purpose of TMX is to provide a proof-of-principle evaluation of the Tandem Mirror Concept as rapidly as possible. To accomplish this, there are three main physics objectives of the experiment: to demonstrate the establishment and maintenance of a potential well between two mirror plasmas, to develop a scalable magnetic geometry while keeping macroscopic stability at high beta, and to investigate the microstability of the plug-solenoid combination. In the first experiments, low-energy ions required to stabilize the DCLC mode in the end plugs will be provided by plasma losses from the center cell. If the above goals are met, TMX should demonstrate the enhancement of confinement by the electrostatic barriers and determine the limitation on beta in the central cell.

Plasma containment in tandem mirror systems is directly dependent upon plasma containment in the end plugs. Thus, in scaling TMX to the large sizes required for fusion power plants, the most important question is stability of the end plugs. The MFTF experiment discussed above will provide a definitive test of the relevant scaling laws.

FIELD-REVERSED MIRROR (FRM): The FRM is an entirely different mode of operation of a mirror machine. In the field-reversed state, the plasma diamagnetic current is strong enough to cause magnetic lines in the center of the

system to close upon themselves. Plasma confined on these closed lines would assume a toroidal shape embedded in a system of open lines that would act as a natural divertor, shielding the toroidal volume from accumulation of impurity ions. The FRM is similar to the Astron, the toroidal Z-pinch, and the reversed-field theta pinch. It differs from the Astron in that the current is carried by the plasma rather than by an independent axis encircling the electron current layer. In contrast to toroidal pinches, the current would be carried by the ions (at least initially), and there is the possibility that the FRM could be maintained continuously by neutral-beam injection.

In the fluid (guiding-center) limit, the FRM is similar to the toroidal Z-pinch with no stabilizing field. Theoretically, such configurations are MHD unstable.[17] On the other hand, field-reversed Astron configurations[18] and reversed-field theta pinches[19] have been established experimentally and appear to be stable for periods much longer than the respective MHD instability growth times. It is speculated that stability in these cases is attributable to the small plasma radii as measured in gyroradii of the energetic component carrying the current and to the fact that the aspect ratio is near unity, a domain that is not accessible in tokamaks. These conditions violate both the limits of validity of the fluid theory and the limiting geometries amenable to stability analysis.

The unexpectedly high values of beta ($\beta > 1$) obtained in 2XIIB (Table 1) have raised the possibility of obtaining field reversal by neutral-beam injection into a mirror field. Measured flux changes through a loop encircling the plasma and in an array of small loops outside of the plasma volume establish that the circulating diamagnetic current in 2XIIB is intense enough to cancel the externally produced field within the plasma. Independent measurement of plasma ion energies and electron temperature indicate that these currents must be produced by the ions.

Values of the field-reversal parameter $\Delta B/B$ have been derived from experimental data and the "best values" exceed unity. These results are encouraging but inconclusive. Data from the experiment are compared to plasma parameters calculated using a two-dimensional (r-z) particle simulation code, SUPERLAYER.[20] There is reasonable agreement with 2XIIB values of n, $\Delta B/B$, and beta. Although comparison shows the necessity for including turbulence in the code, it indicates that the field-reversal parameter $\Delta B/B$ has approximately a three halves power dependence on T_e and is linearly dependent on the injected current. It is hoped that field

reversal will be conclusively demonstrated in 2XIIB either in the present system or in a later modification with increased beam power.

Even if field reversal is achieved in 2XIIB where the plasma radius is only one to two gyroradii, there will remain issues of scale size because a viable, reversed-field mirror reactor[21] will require a minor radius of 5 ion gyroradii (in vacuum field) and a major radius of 10 to 15 gyroradii. If closure of the magnetic field lines improves $n\tau$ by as much as a factor of ten (to 10^{13}), the MFTF beam system is more than adequate to maintain a toroidal plasma of 15 ion gyroradii major radius. Thus, MFTF could be the ideal place to explore the issues of MHD stability, microinstability, and transport in plasmas of the size required for field-reversed reactors.

A conceptual central power plant design[21] based on the FRM incorporates a linear chain of modules of approximately the MFTF size. Each module injected with 200-keV neutral beams would produce 10 MW of electric output.

SUMMARY: 2XIIB experiments have demonstrated the possibility of stable plasma confinement in magnetic mirror geometry. A theoretical model has been developed which predicts observed plasma parameters of 2XIIB and which can be used to extrapolate 2XIIB results to the larger systems required for fusion reactors. This theory has been used in the design of an experimental MFTF, which should obtain an order of magnitude improvement of $n\tau$ over present mirror machines and provide a definitive test of the theory. Several university and USA national laboratories already have programs, and others are starting programs to investigate alternative approaches to stabilization and development of concepts to enhance the Q of confinement systems based on magnetic mirrors. The breadth and depth of the effort indeed substantiates the statement that the mirror approach has become the principal alternative to the tokamak in the USA magnetic fusion program.

REFERENCES:

[1] J. D. Lee et al., in Proc. Second Topical Meeting Technology Controlled Nuclear Fusion, Richland, Washington, 1976 (ANS, CONF-760935, 1976).

[2] D. E. Baldwin, "Energy Confinement in Mirror Plasma," (to be published in Comments Plasma Phys. and Controlled Fusion).

[3] W. R. Baker et al., in Proc. Fifth International Conf. Plasma Physics and Controlled Nuclear Fusion Research, Tokyo, 1974 (IAEA, Vienna, 1975), Vol. 1, p. 329.

[4] W. C. Turner, in Proc. Third International Congress on Waves and Instabilities in Plasmas, Ecole Polytechnique, France, 1977 [to be published in J. Phys. (Paris)].

[5] R. F. Post and M. N. Rosenbluth, Phys. Fluids 9, 730 (1966).

[6] R. F. Post, in Proc. International Conf. Plasma Confinement in Open-Ended Geometry, Gatlinburg, 1967 (ORNL, CONF-671127, 1967), p. 309.

[7] F. H. Coensgen et al., in Proc. Fifth Conf. Plasma Physics and Controlled Nuclear Fusion Research, Tokyo, 1974 (IAEA, 1975), Vol. 1, p. 323; also Yu. V. Gott et al., same Proc. Vol. 1, p. 341.

[8] F. H. Coensgen et al., Phys. Rev. Lett. 35, 1501 (1975).

[9] F. H. Coensgen et al., Phys. Rev. Lett. 37, 143 (1976).

[10] B. G. Logan et al., Phys. Rev. Lett. 37, 1468 (1976).

[11] F. H. Coensgen et al., in Proc. Sixth International Conf. Plasma Physics and Controlled Nuclear Fusion Research, Berchtesgaden, Germany, 1976 (IAEA, Vienna, 1976), CN-35/C1.

[12] M. S. Ioffe, B. I. Kanaev, V. P. Pastukhov, and E. E. Yushmanov, Sov. Phys. JETP 40, 1064, (1975).

[13] D. E. Baldwin, H. L. Berk, and L. D. Pearlstein, Phys. Rev. Lett. 36, 1051, (1976).

[14] H. L. Berk et al., in Proc. Sixth International Conf. Plasma Physics and Controlled Nuclear Fusion Research, Berchtesgaden, Germany, 1976 (IAEA, Vienna, 1976), CN-35/C2.

[15] G. I. Dimov, V. V. Zakaidakov, and M. E. Kishinevsky, Fiz. Plasmy 2, 597 (1976).

[16] T. K. Fowler and B. G. Logan, "The Tandem Mirror Reactor," to be published in Comments Plasma Phys. and Controlled Fusion.

[17] R. N. Sudan and M. N. Rosenbluth, Phys. Rev. Lett. 36, 972 (1976).

[18] J. J. Bazura et al., Phys. Rev. Lett. 29, 256 (1972).

[19] A. G. Eskov et al., in Proc. Seventh European Conf. Controlled Fusion and Plasma Physics, Lausanne, 1975 (CRPP, 1975), Vol. I, p. 55.

[20] J. A. Byers, Lawrence Livermore Laboratory Rept. UCRL-79936 (1977); to be published in Phys. Rev. Lett.

[21] W. C. Condit et al., in Proc. Second Topical Meeting Technology of Controlled Nuclear Fusion, Richland, Washington, 1976 (ANS, CONF-760935, 1976), p. 107.

This work was performed under the auspices of the U. S. Energy Research and Development Administration under contract No. W-7405-Eng-48.

TOROIDAL HIGH-BETA SYSTEMS

C. Bobeldijk
Association Euratom-FOM, FOM-Instituut voor Plasmafysica
Rijnhuizen, Jutphaas, The Netherlands

Abstract. Toroidal axisymmetric systems which aim at the confinement of high-β plasmas can be divided into two categories by means of the Kruskal-Shafranov limit. The reversed field pinches operate at currents above this limit; their stability is governed by shear and wall stabilization. The screw pinch and high-β tokamak operate in the tokamak mode where the plasma current is below the K.S.-limit. Experimental results of both categories are discussed.

Introduction. Toroidal high-β systems include reversed field pinches (RFP), screw pinches and/or high-β tokamaks, non-axisymmetric systems like the high-β stellarator and the bumpy torus, and non-circular systems like the belt pinch. The subject of this paper is limited to axisymmetric systems with a circular cross-section of the torus. Since this in general does not imply circularity of the plasma cross-section, also some remarks on systems with weak non-circularity will be made.

Figure 1 shows the zero- and first-order Bessel functions, which represent the final field configuration after a relaxation process in a zero-β slightly resistive plasma, when the "pinch ratio" $\theta = \frac{\mu_o I}{2\pi a B_t}$ is smaller than 1.6, I being the induced current, B_t the initial toroidal field, and a the plasma radius. This configuration, which Taylor[1] derived by minimizing the energy, subject to Woltjer's integral invariant[2] over the total volume and to the invariance of the toroidal flux, is a force-free configuration which is completely determined by the stored volt-seconds and the toroidal flux. Since in such a configuration the current is proportional to the magnetic field ($\vec{j} = \alpha\vec{B}$), it follows from the figure that the configuration can only be sustained if parallel (force-free) currents flow at any position. The complete drawing in Fig. 1 applies to the field configuration of a reversed field pinch, whereas the part at the left approximates that of the screw pinch. Figure 2 shows q as a function of the radius for both configurations. The q-profile of the RFP is a measured profile in HBTX-1[3] at Culham, the one of the screw pinch is a hypothetical q-profile in a high aspect ratio screw pinch with a small vacuum region near the wall. The high-β plasma column itself is in the centre region, where the behaviour of q is uncertain

and largely dependent on the precise initial conditions and on the details of the implosion process. Since the pitch is nearly constant, the screw pinch can - for stability - not rely on shear stabilization. Instead, like in tokamaks, it depends on the toroidal periodicity condition, which implies that q has to be larger than 1. Since $q = rB_t/RB_p$, this leads to high values of the toroidal field and small values of the aspect ratio A = R/b. In SPICA[4], for instance, this value is equal to 3.

In the reversed field pinch q changes rapidly as a function of r, except near the axis. By sign reversal of q, very strong shear can be imposed without ever creating a pitch minimum, even if a vacuum region near the wall is present. The stability is governed by shear and wall stabilization; there is no direct necessity for high toroidal fields or for a small aspect ratio.

The question arises how in practice the field configurations can be produced. Figure 3 gives a simple illustration of the principle of pitch conservation in an imploding plasma shell. The torus has been replaced by a cylinder with length $2\pi R$. If the conductivity in the moving shell is sufficiently high, the fluxes ϕ_t and ϕ_p in toroidal and poloidal direction are conserved[5], so $\phi_t = 2\pi r dB_t = \text{const.}$ and $\phi_p = 2\pi R dB_p = \text{const.}$, which implies that $\phi_t/\phi_p = rB_t/RB_p = q = \text{const.}$ This mechanism offers a possibility for fast programming of q-profiles in inward moving plasmas. In screw pinches it is the usual method[6]; here an approximately constant q-profile is needed which makes the programming extremely simple, as it asks for a constant field ratio at the wall of the discharge chamber during the pinching action of the rising fields. The described mechanism is also the principle mechanism underlying the concept of the flux-conserving tokamak[7] and it can be applied to create a reversed field configuration, although the necessary strong q-variation complicates the programming during the initial phase.

For the reversed field configuration other options exist for its production, of which I mention the well-known self-reversal mechanism, which has been observed in many experiments and of which a number of descriptions is available[8].

In the next section a review is given of the existing and of some older RFP-experiments with the main experimental results. Some proposed experiments will also be discussed shortly. Thereafter, the same will be done for the screw pinches.

The experiments in table I are quite similar: the minor radius varies from 4 to 7.7 cm, the filling pressure from 10 to 100 mtorr and the main mode of operation is fast field programming with rise times of 1 to 10 μs.

TABLE I

	HBTX-1 CULHAM	ETA-BETA PADUA	ETL-TPE-1 TOKYO	STP NAGOYA	ZT1	ZT1-der.	ZT-S
					LOS ALAMOS		
Minor radius (cm)	6.5	5	5	4	5	5	7.7
Major radius (cm)	100	40	40	12	37	37	40
Wall material	quartz	quartz	pyrex	quartz	sectored alumina		
Filling gas (mtorr)	40 D_2	20-80 H_2	30-50 He	20-30 D_2	10 - 100 D_2		
Plasma current (kA)	40-200	30-150	100	50	30-200	40-70	30-140
Production mode	progr.	progr.	progr.	progr.	p r o g r a m m e d		
Remarks	self-reversal applied	self-reversal applied	also screw pinch	primarily high-beta tokamak	$\dot{I}=1.4\times10^{12}$ A/s	$\dot{I}=10^{11}$ A/s	

Because of the fast programming, the walls are exclusively made of insulating material. The machine which differs most from the others is ZT-1, where a very high toroidal electric field ($E_{tor} \sim 1$ kV/cm) has been applied. Although very high ion temperatures were produced in this way, the configuration suffered from skin formation near the wall and too high values of β_p to be stable. In the derated version[9] the temperature dropped substantially and field profiles with more favourable stability characteristics were obtained.

These experiments have shown that completely stable high-β RFP-configurations can be obtained by means of the fast field programming technique. The thus produced profiles are predicted to be stable according to ideal and resistive MHD-theory. Besides, the lifetime of these stable discharges is governed by classical diffusion. Since the temperatures obtained are low (between 10 and 40 eV), and the dimensions are small, the energy confinement time is limited to about 15 μs and the resistivity destroys the configuration in some tens of microseconds. The low temperature is attributed to line radiation from impurities. In ZT-S, for instance, the impurity level was found to be 0.3 to 0.5%, mainly oxygen, which is too high for the ohmic heating to burn through[10]. Improvement is expected from a low impurity level ($\sim$ 0.1%) or from a high initial temperature produced by fast compressional ion heating and/or anomalous resistivity. In HBTX-1 it was shown[11] that the electron temperature scales as I^2 up to 110 eV at 150 kA. However,

like in the other fast programmed reversed field pinches, no stable discharges could be produced above a current level of 40-60 kA.
Spontaneous reversal of the toroidal B- and E-fields has been observed in Perhapsatron[12] and ZETA[13] already long ago. Recently, it was also demonstrated in ETA-BETA[14] and in HBTX-1[15]. In this mode the set-up phase is analogous to the tokamak start-up in the sense that both pass through a turbulent state before reaching a quiescent mode of operation. The way in which the reversal proceeds depends on the pinch ratio θ ($= B_{pwall}/B_{tav}$) and on the compression ratio. At relatively high θ-values ($\theta \sim 3$) and high compression ratio, the reversal is associated with a large m=1 kink instability[16]. At low θ-values ($\theta \gtrsim 1.2$) and low compression ratio the reversal is produced by a series of small m=1 instabilities. If the current or the magnetic Reynolds number is high enough, this reversed field configuration can be sustained by maintaining the plasma current[17], as has also been demonstrated in numerical simulations[18]. The importance of the magnetic Reynolds number ($S = \tau_R/\tau_H$) lies in the fact that the field distribution decays on the resistive time-scale τ_R, whereas the RFP-restoring instabilities act on an MHD time-scale τ_H. At high magnetic Reynolds number, fast regeneration of the RFP can then become possible by small amplitude fluctuations, thus keeping the profile continuously close to a "Taylor state", like it is from the beginning in a programmed screw pinch. Since the exact needed level of fluctuations for sustained reversal and the associated losses are not exactly known, it is important to determine the scaling of the fluctuation level with S in future experiments.

Proposed RFP-experiments

Some experiments in table II have not yet been officially approved of and the design parameters and completion dates may not be final.
The engineering design of HBTX-1A is based on the use of a spare ORMAK shell and core from Oak Ridge. The experiment is intended for filling the gap between today's fast experiments and RFX, which will not be completed before 1982. Since in future experiments the residual level of fluctuations is crucial to the question whether the losses can or cannot be compensated by ohmic heating only, in HBTX-1A the conditions will be studied in which quiescent plasmas are established by means of the self-reversal effect. Therefore, a metal-walled torus, slowly rising magnetic fields, and a high value of S (up to 5×10^4) will be used as well as field-matching techniques. Furthermore, the effects of impurity, minor radius scaling, β- and transport properties will be studied. A time-dependent model, tested with

TABLE II

	HBTX-1A Culham	RFX Culham	ETA-BETA II Padua	ZT-40 Los Alamos
minor radius (cm)	25	60	12	20
major radius (cm)	80	180	50	114
wall material	metal	metal	quartz metal	ceramics metal
plasma current (kA)	300-500	700 (↑2000)*	200	600
τ_{rise} (μs)	100-500	2-10 ms (10-50)	2-100	2.5-30
τ_{decay}	1-5 ms	10-20 ms (50-100)	> 100	$\lesssim$ 100 μs
completion dates	1979	1982-'83 (1985)	1978	1979

* Values between brackets are those for an envisaged second stage of RFX.

ZETA data, was used to predict a temperature of 100-150 eV at I = 450 kA. The Christiansen-Roberts code[18] predicts somewhat higher values.
Whereas in this experiment the emphasis is placed on studying the setting-up phase of the quiescent state, in RFX the main interest is in the sustainment phase, when the configuration decays slowly and the plasma parameters are considerably higher. It is expected that a highly quiescent state can be obtained in this experiment, since the parameter range encompasses that of ZETA. The predicted temperature here is up to 500 eV.
In close cooperation with Culham, a new RFP was designed in Padua (see table II). An interesting feature of this machine is that pinches produced in quartz as well as in metal vessels can be compared. This comparison may help in deciding whether fast programmed pinches, which are heated mainly during the implosion phase, remain a viable alternative to the slow pinches which rely on joule heating. Furthermore, the electric circuitry is designed to make a wide range of rise times possible, thus allowing a gradual transition from the fast production modes to the slow ones compatible with metal walls. In the metal-walled torus, where a rise time of 100 μs is employed, the conditions for spontaneous (or aided) field reversal will be a matter of investigation. The possibility to replace the continuous conducting shell by an array of conductors is being considered for a later stage.
The prime objective of the programmed version of ZT-40 is to increase the confinement time by an order of magnitude over that of ZT-S. From minor

radius scaling ($\tau \propto b^2$), which was demonstrated in ZT-S[19], the confinement time of ZT-40 would become 150-200 μs if the diffusion constant were left unchanged. It is to be expected that this time can be improved by a decrease in resistivity. At an impurity level of 0.1% the temperature should reach values between 100 and 200 eV at a density of $1\text{-}5\times10^{15}$ cm^{-3} and higher temperatures can be reached if stable operation is possible at lower densities. Another objective of ZT-40 is to determine the maximum current density (and the minimum electron density) compatible with stability to micro-perturbations. The machine is primarily designed to operate with an insulating (either quartz or Al_2O_3) wall, the rise time of the fields being in the μs-range. For longer rise times (>> 10 μs) also a metal discharge tube is being considered.

Screw pinches and/or high-beta tokamaks

TABLE III

	SPICA	STP-2	STP-3	ETL-TPE-1	ETL-TPE-2
	Jutphaas	Nagoya		Tokyo	
minor radius (cm)	20	10	15	5	22 × 14
major radius (cm)	60	25	50	40	40
wall material	quartz	quartz alumina	alumina	pyrex	quartz
filling gas (mtorr)	5-20 D_2	< 10		10-150 He,D_2	
plasma current (kA)	400	75		100	600
toroidal field (T)	1.4	1.5	5	2	2.5
$\tau_{\frac{1}{4}}$ (μs)	10	4.5		3	4.7
$\tau_{1/e}$ (μs)	1000	100 (const)	∿ 10^4	150	600
T (eV)	60	50	↑ 1000	30-100	400
remarks		B_v	B_v		elliptical
completion date			1979		1979

This part of the paper is concerned with devices which derive their magnetic field configuration from a fast pinching action due to a simultaneous rise of the current and the toroidal field. Naming them high-beta tokamaks or screw pinches is a matter of taste. When the experimentalist wants to stress

the similarity with the tokamak configuration, he usually chooses the former name. When the force-free current region has approximately a constant q-profile, the name screw pinch is more appropriate, also for historical reasons.

In the experiment ETL-TPE-1[20] the q-profile is changed by varying the time delay between the onsets of the fast rising toroidal current (I_z) and the toroidal magnetic field (B_z). The value of β is varied by means of the toroidal bias field strength. A typical result of the time dependence of the plasma parameters is given in Fig. 4, where the toroidal current has been crowbarred in such a way that it matches the decay of the toroidal field. For given values of I_z and B_z optimum values with respect to stability have been found for the bias field and the time delay between I_z and B_z. In such an optimum the q-profile is nearly flat, $q > 1$, and $\beta_p = 1\text{-}2$. The maximum time of stable plasma confinement is 70 μs. Since the aspect ratio ($A = R/b = 8$) is rather large, it is very hard in this experiment to combine good high-β equilibrium, which requires a high plasma current, with good stability characteristics, for which the value of q has to be greater than 1. At these q-values the large shift of the plasma column immediately after the implosion phase is also responsible for a substantial loss of energy, which can amount up to 50% of the input (implosion) energy. An improvement may be expected for smaller aspect ratios. A new experiment (TPE-2), with aspect ratio 2.9, is being constructed and may produce its first results in 1979. In this machine the plasma position is controlled by pulsed vertical fields and compensating coils will reduce the error fields through the gaps. The cross-section of the tube will be slightly elliptical (ellipticity 1.6).

STP-2 in Nagoya[21] indeed has a low aspect ratio, but also here a violent movement of the plasma to the outer wall is observed after the implosion phase, accompanied by a serious loss of energy. In STP this loss has been reduced by pulsed vertical fields which compensate the outward drift and keep the plasma near the centre of the tube[22]. The result of this improvement is shown in Fig. 5, where the decay of T_e is given for a discharge with and one without a vertical field. A similar difference is observed for the measured pressure distribution over the cross-section. It is found that with the help of this compensating field higher β-values can be confined for longer times.

It is shown in this experiment that the dominant poloidal mode number is 2, which, at these q-values, is the mode number predicted by Freidberg and

Haas[23] for a toroidal high-β tokamak surrounded by a vacuum region. Since it is not the predicted dominant mode for a screw-pinch plasma with a broad, rather homogeneous, current distribution and since this low aspect ratio experiment shows a very large equilibrium shift when no vertical field is applied, it is possible that a constant pitch region does not fully develop. STP-2 has undergone some important changes: e.g., both the toroidal field and the plasma current can be maintained for more than 100 μs without decay and a complete Al_2O_3 torus without joints has been completed. In the meantime a new experiment, STP-3, is being constructed, which is also a low-aspect ratio high-β tokamak with circular cross-section. The projected temperature after fast implosion heating and adiabatic compression is 500-1000 eV. Besides the programmed vertical field, feedback-controlled vertical and horizontal fields will be applied.

After a series of small experiments in Jutphaas[6] the first large bore experiment with small aspect ratio, SPICA[4], showed reasonably good confinement properties already in 1974[24], but the low value of the bias field produced β-values for which the column became unstable after some tens of microseconds. This led to a rapid decay of the toroidal current ($\tau_{1/e} \sim 100$ μs). Since then the value of the bias field has been enlarged and discharge characteristics improved accordingly at $q_{wall} \sim 1.5$. In contrast with the Japanese experiments mentioned above, there appears to be no dramatic temperature drop during or after the outward drift of the column. No measures have been taken to stop this drift and the column settles at an equilibrium position that is in agreement with theory. The measured $\int n_e d\ell$ remains roughly constant up to 150-200 μs and its behaviour suggests that in the equilibrium position the column is vertically elongated. The most interesting observation is that the decay rate of the plasma current during this time has increased to values ($\gtrsim$ 700 μs) which approximate that of the primary circuit (see Fig. 6), while the inductance increases at a very slow rate. This shows that the resistivity of the low-density plasma outside the main column is quite low, that current scrape-off at the walls hardly takes place and that current peaking as predicted by Hoekzema[25] takes place on a long time-scale. A self-amplifying effect of current scrape-off due to an eccentric equilibrium position is negligible if the width of the vacuum region is small[24].

For the SPICA discharge to behave well, the history of q_{wall} is crucial. Where in ETL-TPE-1 the best results were obtained when I_z started somewhat before B_z, in SPICA q_{wall} has to start at $q = \infty$, drop rapidly to $q \approx 1.5$,

and remain constant thereafter. The exact procedure of pre-ionization and pre-heating also appears to be an important initial condition[26]. Finally, measurements in SPICA suggest that the impurity level plays an important role; clean discharges giving more stable plasmas. From theoretical calculations[27] it follows that the highest beta-values may be confined when vertically elongated plasma cross-sections with their centre of gravity towards the major axis are combined with force-free fields. The SPICA configuration may be close to this optimum configuration, the maximum β obtained being 20%. Improvement can be expected if also the discharge tube is chosen non-circular, e.g. D-shaped or racetrack-shaped, with a moderate ellipticity. Such a new torus is currently being considered for SPICA.

Final remarks. The flux-conserving tokamak[28], which is closely related to the screw pinch as it exploits the same principle, and high-β tokamaks which operate at long time-scales (like TOSCA[29]) have not been included in order not to overcrowd this review. Reactor considerations have also been left out.

The experiments on the RFP and the screw pinch are accompanied by an impressive number of publications on numerical simulation of the setting-up phase and the relaxation state. The codes have been reasonably successful in describing experimental results and they have been used to predict the performance of proposed experiments. The results are presented in several papers at this and preceding conferences. Interesting new theoretical results on the resistive interchange mode in the RFP[30] and on MHD-equilibrium and stability of the high-β tokamak[27,31] as well as the most recent experimental results on implosion heating of toroidal θ-pinches[32] are presented at this conference.

This work was performed under the Euratom-FOM association agreement with financial support from ZWO and Euratom.

References

1. Taylor, J.B., Proc. 3rd Topical Conf. on Pulsed High Beta Plasmas, Culham 1975, Suppl. to Plasma Phys. 59 (1977).
2. Woltjer, L., Proc. Nat. Acad. of Sciences, 44, 489 (1958).
3. Verhage, A.J.L., UKAEA Research Group Report CLM-R161 (1976).
4. Bobeldijk, C. et al., Proc. 3rd Int. Symp. on Toroidal Plasma Confinement, Garching, G 5 (1973).

5. Van der Laan, P.C.T., Proc. Coll. Interaction of Electromagnetic Fields with a Plasma, Saclay, Vol. IV, 1095 (1968).
6. Bobeldijk, C. et al., Proc. 3rd Int. Conf. on Plasma Phys. and Contr. Nucl. Fusion Res., Novosibirsk 1, 287 (1968).
7. Clarke, J.F. and Sigmar, D.J., Phys. Rev. Lett. 38, 70 (1977).
8. Dancy, D.J., Poc. 3rd Topical Conf. on Pulsed High Beta Plasmas, Culham, 1975, Suppl. to Plasma Phys. 605 (1977).
9. Baker, D.A. et al., Proc. 5th Int. Conf. on Plasma Phys. and Contr. Nucl. Fusion Res., Tokyo, Vol. III, 35 (1974).
10. Baker, D.A. et al., LA-UR-77-459 (1977).
11. Butt, E.P. et al., Proc. 5th Int. Conf. on Plasma Phys. and Contr. Nucl. Fusion Res., Tokyo, Vol. III, 417 (1974).
12. Conner, J.P., Proc. 2nd U.N. Conf. on Peaceful Uses of Atomic Energy, Genève, 32, 297 (1958).
13. Butt, E.P. et al., Proc. 2nd U.N. Conf. on Peaceful Uses of Atomic Energy, Genève, 32, 42 (1958).
14. Buffa, A. et al., this conference.
15. Butt, E.P. et al., Proc. 3rd Topical Conf. on Pulsed High Beta Plasmas, Culham 1975, Suppl. to Plasma Phys. 419 (1977).
16. Gowers, C.W. et al., 6th Int. Conf. on Plasma Phys. and Contr. Nucl. Fusion Res., Berchtesgaden 1976, Suppl. to Nucl. Fusion 1, 429 (1977).
17. Bunting, C.A. et al., this conference.
18. Christiansen, J.P. and Roberts, K.V., this conference.
19. Baker, D.A. et al., 6th Int. Conf. on Plasma Phys. and Contr. Nucl. Fusion Res., Berchtesgaden 1976, Suppl. to Nucl. Fusion 1, 419 (1977).
20. Ogawa, K. et al., Proc. 5th Int. Conf. on Plasma Phys. and Contr. Nucl. Fusion Res., Tokyo, Vol. III, 445 (1974).
21. Hirano, K. et al., Phys. Rev. Lett. 32, 1104 (1974).
22. Hirano, K. et al., Proc. 6th Int. Conf. on Plasma Phys. and Contr. Nucl. Fusion Res., Berchtesgaden 1976, Suppl. to Nucl. Fusion 1, 503 (1977).
23. Freidberg, J.P. and Haas, F.A., Phys. Fluids 16, 1909 (1973).
24. Bobeldijk, C. et al., Proc. 5th Int. Conf. on Plasma Phys. and Contr. Nucl. Fusion Res., Tokyo, Vol. III, 409 (1974).
25. Hoekzema, J.A., Proc. 3rd Topical Conf. on Pulsed High Beta Plasmas, Culham 1975, Suppl. to Plasma Phys. 541 (1977).
26. Oomens, A.A.M. et al., this conference.
27. D'Ippolito, D.A. et al., this conference.
28. Sigmar, D.J., this conference.

29. Robinson, D.C. and Wootton, A.J., this conference.

30. Robinson, D.C., this conference.

31. Dory, R.A. et al., this conference.

32. Chen, Y.G. et al., this conference.

33. Bobeldijk, C. et al., Proc. 6th Int. Conf. on Plasma Phys. and Contr.Nucl. Fusion Res., Berchtesgaden 1976, Suppl. to Nuclear Fusion 1, 493 (1977).

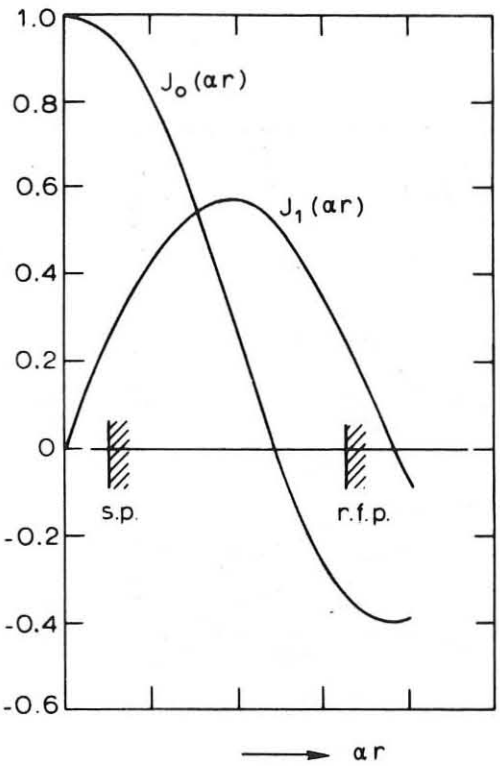

Fig. 1.

Solution of $\vec{j} = \alpha\vec{B}$ in terms of the cylindrical magnetic field components. The left-hand part approximates the field configuration of a constant-pitch screw pinch, the complete picture represents a $\beta = 0$ reversed field pinch.

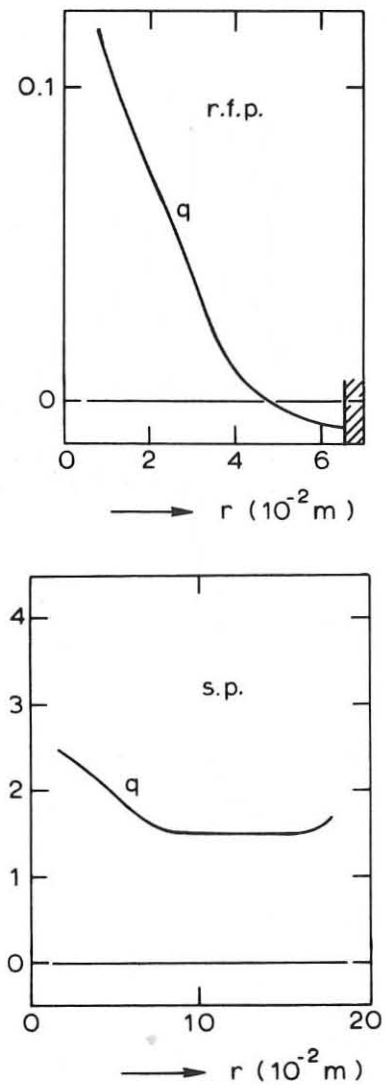

Fig. 2.

q as a function of radius for a) a reversed field pinch (top)
b) a screw pinch (bottom).

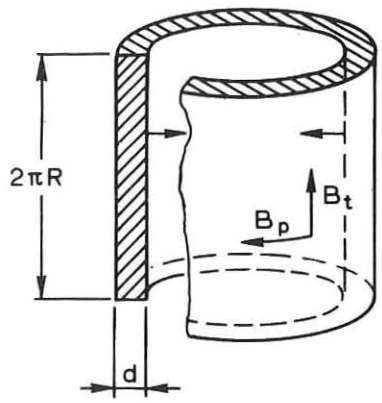

Fig. 3. Flux conservation in a collapsing cylindrical plasma shell. This model illustrates the principle of pitch convection in a screw pinch.

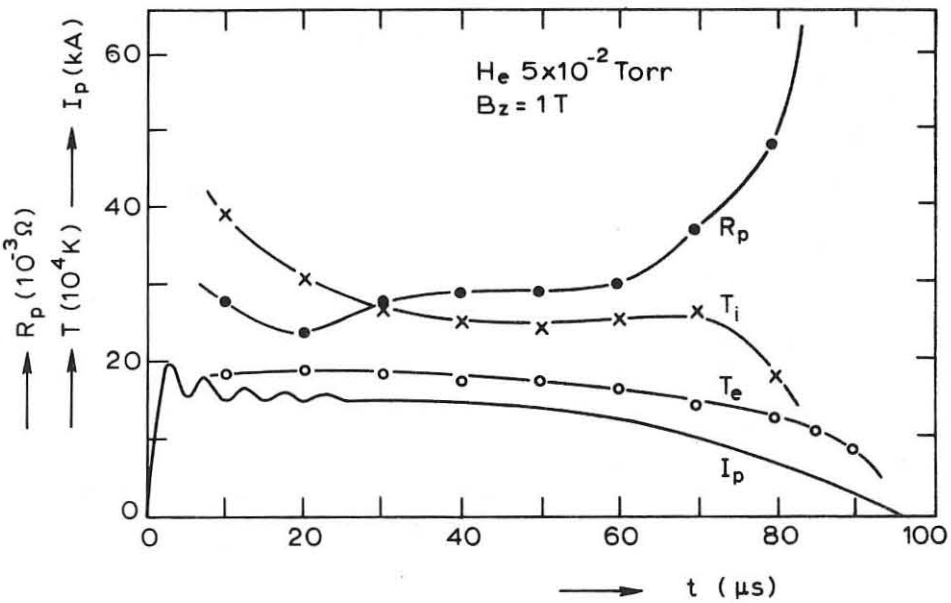

Fig. 4. Time dependence of T_i, T_e, and the plasma resistance, R_p, in a discharge in ETL-TPE-1, when the external toroidal current is crowbarred.

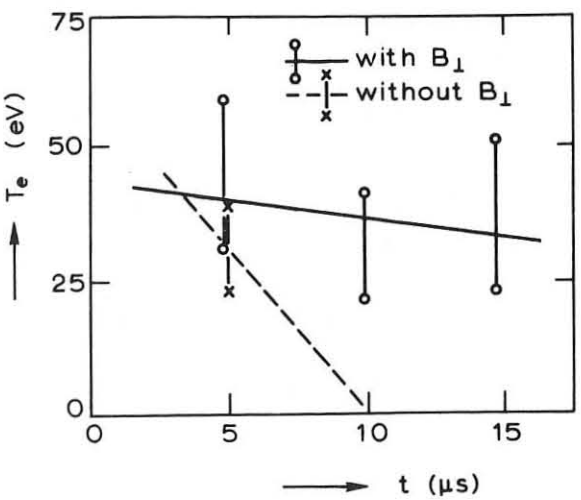

Fig. 5.

Time evolution of the electron temperature at the tube axis with and without pulsed vertical field in STP.

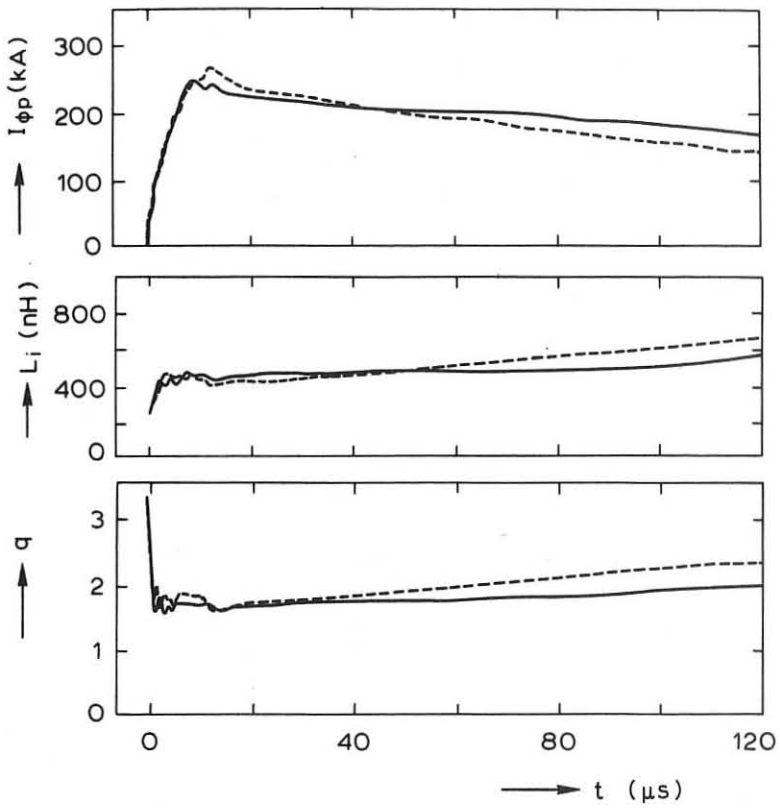

Fig. 6. Decay of plasma current, the inductance L_i, and q in stable (——) and unstable (---) discharge in SPICA (Ref. 33).

NEW RESULTS IN HIGH-BETA STELLARATOR AND BELT-PINCH RESEARCH

E. Fünfer

Max-Planck-Institut für Plasmaphysik, 8046 Garching, Fed.Rep. of Germany,
EURATOM Association

I. Introduction

The production of hot plasmas with stable equilibrium and high ß is the aim of all fusion-orientated plasma experiments. However, high-ß plasmas can, at least for the moment, only be achieved by means of shock compression heating. Therefore the essential criterion of the two experiments to be discussed here, namely the High-Beta Stellarator and the Belt-Pinch, is the high ß value which is achieved experimentally by fast magnetic compression. In contrast, with the tokamak it is not yet possible to achieve beta values which are necessary for a fusion reactor, although the tokamak gains more and more importance. On the other hand, regarding stability, the tokamak is superior to high-ß plasmas produced by fast magnetic compression, at least in so far as the fast MHD modes have not yet been completely overcome in the present high-ß machines.

In view of these facts it seems justified to pursue both concepts with their respective experimental techniques. It is clear that a number of questions which in tokamak experiments cannot be solved today because of too small ß-values, can be answered with little effort in the existing or planned high-ß experiments. On the other hand, problems as for instance transport phenomena and impurities can be investigated better in a tokamak due to the long lifetime of the plasma. High-ß experiments with their still short confinement times yield until now only limited results to this effects.

The High-Beta Stellarator is not axisymmetric and is therefore a true alternative to the tokamak. The third dimension increases the number of possible equilibria and thus the chance to find a particularly favourable one.

In the Belt-Pinch, an enhancement of ß is intended by configurational studies of axisymmetric equilibria. Configurations with elongated cross-sections are expected to confine plasmas with considerably higher ß-values than are achievable in circular cross-section tokamaks.

II. High-Beta Stellarator (HBS and Scyllac)

The Principle

In the following, mainly the High-Beta Stellarator experiments in Garching (HBS) and the Scyllac experiments in Los Alamos are being discussed.

High-beta stellarators /1, 2/ are understood to be configurations with the following properties: toroidal equilibrium with nested magnetic flux surfaces and $\beta \lesssim 1$, but without essential toroidal net current. Such a configuration is completely 3-dimensional. The magnetic axis normally describes a spatial curve, e.g. a toroidally closed helix. The rotational transform ι is finite. The structure of the flux surfaces is M+S-like, i.e. there exists a stronger corrugation on the inner side of the torus than on the outer side.

Todate there is no rigorous proof of the existence of equilibria with finite β, not even within the scope of the ideal MHD theory (except in the special case of plane magnetic axis and $\ell = 0$ /3/). On the other hand, a large number of such 3-dimensional equilibria are conceivable, and it is possible that among them there are some with particularly favourable properties.

Theoretical Basis

A fairly detailed analysis of periodic configurations has so far only been carried out in a surface current model and by investigating only such equilibria which can be described in small parameter expansion around the linear 0-pinch /4 - 10/. This analysis has revealed that for reasons of stability, preference is given to the helical $\ell = 1$ configuration. Additional weak fields with $\ell = 0$ and $\ell = 2$ symmetry produce the M+S structure and thus the toroidal equilibrium and suppress the Pfirsch-Schlüter currents. It seems also that for stability reasons so far only large aspect ratios $A \gtrsim 100$ ($A = R/a$) are useful (R = major torus radius, a = plasma radius).

The m = 1 instability can be avoided by wall stabilization at large A if a small compression ratio r_w/a is used (r_w = wall radius). Theoretically a critical β is then obtained above which the wall stabilization becomes effective. This makes the slow heating up of plasma beginning with low β impossible. The high-β regime must be reached faster than MHD instabilities can grow. So far this can only be done with shock waves. Therefore the HBS is at present also from this point of view linked with shock heating.

But it might be possible to find more favourable equilibria providing greater freedom for the production and heating of plasma.

Another approach to m = 1 stability is the feedback method as tried in the Scyllac experiments, thereby avoiding the low compression ratio which is necessary for wall stabilization /6/.

Based upon the results of sharp boundary calculations, the theoretical investigations and the experiments were focussed on equilibria with mainly $\ell = 1$ symmetry, i.e. with helical magnetic axis. An important step ahead has been made with the calculation of unscaled helical equilibria with arbitrary boundary and diffuse pressure profile /11/. However, the subsequent stability analysis was restricted to circular cross-section and $\varepsilon \ll 1$. ($\varepsilon = ha$, h = helical wave number). Lateron, a stability analysis of these 2-dimensional, helical MHD equilibria was carried out <u>without</u> any scaling /12/. In HBS and Scyllac configurations with a compression ratio of $r_w/a \approx 2$, the m = 2 mode is the dominating one. Fig. 1 shows a comparison of growth rates of the m = 2, $k \approx 0$ mode versus δ_1 (δ_1 = relative amplitude of the helix), calculated in the surface current model, the 2D-code /12/, and a δW-analysis /11/.

(Several attempts to calculate toroidal high-ß equilibria with diffuse pressure profile were at first not very successful /2/ or led to singular solutions /13/.)

A more detailed description of all the theoretical investigations cannot be given here. In general, the analytical results of the surface current model calculations could be largely confirmed so that they are still being successfully applied. In addition, there were indications of improved stability. For example, investigations of slender $\ell = 1$ high-ß equilibria with a small vacuum range outside the plasma showed that a magnetic well exists already at relatively low ß values ($ß \gtrsim 0.23$) and that at ß values of $ß \geqslant 0.75$, stability in the sense of the Mercier criterion is obtained over the entire plasma cross-section except for a very small area around the magnetic axis /14/. If strong, non-circular cross-sections are allowed for, the Mercier criterion and even a sufficient criterion can be fulfilled on the magnetic axis /15/.

Experimental Tests

The theoretical results were tested in linear helical θ-pinches in Garching /16/, in Los Alamos /17/, and in Jülich /18/. Regarding helical equilibrium and m = 1 stability, good agreement was obtained with MHD theory.

Toroidal equilibria were investigated in Garching /20/ and in Los Alamos /21/. The necessity for M+S-like deformation in high-ß plasmas was impressively demonstrated. The ISAR T1-B experiments have shown that extremely large helical plasma distortions can be achieved (radius of helix = 3 - 5 a). Regarding stability, the results hardly differ from those found in the linear experiment. Problems such as initial dynamics, self-induced toroidal currents, damping of helical Alfvén modes etc. cannot be dealt with further in this paper /16 - 21/.

The wall stabilization of the m = 1 mode has not yet been proven in the ISAR T1 and Scyllac experiments because they have too large compression ratios. In the linear experiment "Helix" in Jülich, a surprisingly favourable m = 1 stability was found in contrast to theory /18/, but here, other interpretations are possible.

The feedback stabilization of the m = 1 mode as alternative to wall stabilization has brought first successful results to Scyllac /22/. Helical $\ell = 1$ and bumpy $\ell = 0$ equilibrium fields in a 120° sector are produced by shaped coils. A helical quartz tube is used to facilitate the formation of helical plasma equilibrium. The streak photographs in Fig. 2 (Los Alamos) show the transverse motions of the plasma column in the horizontal and vertical plane without feedback (upper photograph) and with feedback (lower photograph). Without feedback stabilization, the m = 1 instability carries the plasma to the wall in about 15 usec. With feedback stabilization, the plasma confinement is extended to more than 50 μsec (in the central region of the sector). This confinement time is many e-folding times of the m = 1 instability. The plasma confinement is terminated by end effects in the sector and radial diffusion in the 120 eV plasma which reduces the plasma ß.

An $\ell = 1,2$ equilibrium configuration with a large helical plasma distortion (radius of the plasma helix $\approx 3 \cdot a$) is now installed in the Scyllac feedback sector. This configuration avoids bumpy plasma distortion and its troublesome transient effects. First results seem to be very encouraging /22/.

The Finite Ion Larmor Radius and Longtime Effects

The m $\geq$ 2 modes are unstable according to the ideal MHD theory. Between the experiment and the original sharp boundary model /23/, there was at first disagreement concerning the critical value of the ion Larmor radius r_L above which the fast m = 2 modes should disappear. Fig. 3 shows the theoretical situation. The m = 2 growth rate γ (normalized to the ideal MHD growth rate γ_{MHD}) is plotted versus the ratio $\eta = r_L/a$. We define the gyro radius at the transition regime 2 and 3 to be the critical one.

ISAR T1-B is a toroidal HBS with extremely large helical $\ell = 1$ amplitude. The most important data are summarized in Table 1.

Major diameter	271 cm	
Minor average coil diameter	17 cm	
Inner tube diameter	9.2 cm	
Number of helical periods on the torus	16	
Bank energy	0.5 MJ	1.5 MJ
Maximum magnetic field	1.4 T	3.1 T
Rise time	4.7 us	6.4 μs

Table 1: The experiment ISAR T1-B

By varying filling pressure, filling gas (hydrogen, Deuterium) and bank energy, the ion gyro radius r_L and the ion-ion-collision time τ_{ii} were varied over a large range. In Fig. 4, the experimental results are shown in a η versus ($\omega_L \cdot \tau_{ii}$)-plane (ω_L = ion Larmor frequency). Fast m = 2 modes were observed only for $\eta < 0.14$. This critical limit is much more optimistic than originally predicted. Meanwhile improved theoretical results have been achieved /25 - 28/, as shown in Fig. 5. The critical ion gyro radius is shown as function of ß, appropriately normalized for comparison. The best theoretical results lie within the experimental error bars.

The problem of gyro stabilization has thus been solved satisfactorily, at least on the fast MHD scale. With the above results we have investigated the possibility of obtaining simultaneously wall stabilization of the m = 1 mode and gyro stabilization of the m $\geq$ 2 modes for HBS reactor dimensions. At the same time α-particle orbits must

not hit the wall. This seems possible, in particular at aspect ratios of $A \geqslant 200$ which may still be feasible. The long-time behaviour of gyro effects under reactor conditions is still doubtful. There exist at present only rough estimates /29/.

Theoretical Work in Progress

An interesting method allowing a systematic analysis of toroidal configurations without rotational symmetry is still in progress /30/. A power series expansion of the unknown functions in the distance of the magnetic axis up to 3rd order is used to calculate toroidal, 3-dimensional equilibria. The stability behaviour of these configurations is investigated in the vicinity of the magnetic axis by means of necessary and sufficient criteria. The discussion of the stagnation points of the magnetic flux surfaces yields estimated maximum ß-values of MHD-stable equilibria.

Since some years promising efforts are being made in order to find 3D solutions by applying numerical methods. The procedures /31, 32/ are based on a properly defined variation principle for the potential energy of the plasma integrated over the volume. The potential energy is minimized following the steepest descent while at the same time magnetic fluxes and mass are conserved. This way only stable solutions should be obtained.

In another study /33/, MHD equilibria and their stability are investigated by integration of the non-linear, time-dependent MHD equations. Non-ideal MHD effects (resistive effects, shear viscosity etc.) can be implemented straight forward into this code.

All these investigations are still in their initial stage. Yet, there are already some results which are encouraging enough for us to pursue the HBS concept. For instance, the 3D numerical calculations /32/ agree satisfactorily with the experimental results and indicate improved stability at triangular plasma cross-sections /34/. However, it is not yet certain whether this permits to dispense with the wall stabilization and its restriction to small compression ratios, which seem to be necessary at present.

A Next Experiment

The HBS II project /35/ is the next step of the Garching high-beta stellarator group. It is still a shock-heated toroidal stellarator without additional adiabatic heating to provide for low compression ratio in order to wall-stabilize the $m = 1$ long wavelength

modes. Although the dimensions are large, the magnetic field and the energies are rather modest, as can be seen from the following Table 2.

Temperature $T_i = T_e$	= 600 eV
Electron density n_e	= 8×10^{14} cm^{-3}
ß	= 0.8
Torus radius	= 8 m
Minor coil radius	= 10 cm
Minor plasma radius	= 4 cm
Radius of the helical distortion	= 6 cm
Toroidal magnetic field B	= 0.7 T
Rise time	$\leq$ 0.5 µs
Fast bank energy	= 0.5 MJ
Magnetic pulse duration	> 50 µs

Table 2: High-Beta Stellarator HBS II

The main object of HBS II will be to prove wall stabilization of m = 1 modes and to investigate the limits of gyro stabilization on an extended time scale. The experiment is in the coil region still flexible enough to eventually incorporate new theoretical results which may arise from computer equilibrium and stability calculations in the future.

III. Belt-Pinch

The Principle

The Belt-Pinch represents an axisymmetric high-ß equilibrium which stands in a close relation to the tokamak. In present day tokamak experiments, beta is limited to rather low values. In the belt-pinch, however, configurations are investigated which could open the range of higher ß in axisymmetric geometry. In these modifications, very high $ß_{pol}$-values are obtained by strong shock heating and non-circular plasma cross-sections. The possible gain in ß can easily be deduced from the well-known equation for beta in a tokamak which does not take into account restrictions with respect to q due to instabilities.

In the case of a vertically elongated cross-section with minor half axis fixed, an

additional geometry factor has to be taken into account, yielding:

$$\beta = \frac{1}{q_b^2} \cdot \frac{1}{A^2} \cdot \beta_{pol} \cdot \left(\frac{e+1}{2}\right)^2$$

(q_b = inverse rotational transform at plasma boundary; A = aspect ratio;
e = ratio of the half axis b/a)

With the optimistic assumption that the critical q_b-value still is in the range of 3 - 4, already modest elongations should allow medium ß-values of about 10% /36/. A further increase of b/a to 5 or more is sufficient for high-ß equilibria with ß larger than 50% /37/.

Theory

During the recent few years, much theoretical effort has been spent on the question of plasma stability for finite ß and non-circular cross-section. According to these efforts, increased beta values as well as strong non-circularity give rise to different types of ideal MHD modes which usually are stable in the conventional low-ß tokamak.

From local stability criteria it can be shown that for elongated cross-sections, the q-value on axis (q_o) must be increased well above one in order to provide stability against localized modes. Some improvement, however, can be expected if triangular deformations are applied /38, 39/. Other internal modes seem to have stability conditions similar to those of the localized modes /40, 41/, as is shown by recently developed, large MHD spectral codes. At finite ß, however, the unstable forces due to the plasma pressure gradient becomes essential and ballooning-type distortions set a severe limitation for ß /42, 43, 44/. In contrast to the internal modes just mentioned, external modes grow on a much faster time scale and can destroy the confinement within a few microseconds. For the standard tokamak (circular cross-section, large spect ratio and $\beta_{pol} \leq 1$), a $q_b \geq 3$ and a ratio of $q_b/q_o \leq 3$, which means a centrally peaked plasma current, are known to stabilize these external kink modes. First results of the new spectral codes indicate that this also holds for elongated cross-sections: the kink branch approaches its marginal point for practically the same favourable q-ratio /42/. For a fixed q_o-value, there follows a strong increase of beta

with b/a according to the above relation for ß. Taking into account the internal modes which cause q_o to rise above one, the gain in ß is reduced, but there still seems to be a considerable advantage compared with circular cross-sections. Further improvement of ß by increasing the $ß_{pol}$-value, however, again leads to the problem of ballooning modes covering also the surface region /42, 43/. Considering all requirements for ideal MHD stability, ß-values above about 5% might be realistic with an optimized plasma shape.

A complete experimental verification of the critical ß-values does not yet exist. A contribution to this important question has been obtained in the different belt-pinch experiments where the stability properties of elongated high-ß equilibria have been investigated at least for the time scale of the fast MHD modes.

A further problem of non-circular cross-section is its sensitivity with respect to axisymmetric displacement modes. Theoretically and experimentally it has been shown that the modes can easily be suppressed by a conducting shell close to the plasma. For long times, a feedback system is necessary /45, 46, 47/.

Shock-Heated Belt-Pinch Experiments

Like the High-Beta Stellarator, also the belt-pinch experiments use the fast shock compression in order to produce a toroidal high-ß plasma. Fig. 6 shows schematically the arrangement of such a belt-pinch experiment. The plasma is compressed mainly by the fast rising toroidal field which is generated by a single turn toroidal coil. The inner part of this coil is helically wound. In combination with the outside vertical coil, this inner helix works as OH-transformer for the fast induction of the toroidal plasma current. The further programming of vertical and shaping coils finally provides the toroidal equilibrium during the discharge. Because of the small distance between the plasma and these coils, plasma loss due to vertical displacement instability can be avoided.

Table 3 summarizes the main physical results obtained in different belt-pinch experiments /48 - 52/. As shown in this table, the experimental range of non-circular cross-sections covers b/a ratios from 3 to 30. The plasma density varies from about 10^{14} to $10^{16}\,cm^{-3}$. A special problem in most of the experiments is the limited temperature of

Experiment	b/a	critical q_b	initial T(eV)	$\langle n_e \rangle (cm^{-3})$	β-decay (μs)	remarks	coil-cross section
TENQ (Jülich)	~4	≤2	~100(Ti) ≤70(Te)	$3 \cdot 10^{14}$	~50	stable operation at $\beta_{pol} \leq 2$	1m
Lausanne BP	~20÷30	?	~50	$7 \cdot 10^{15}$	≥30	confinement limited by displacement	
TORUS I (New York)	10÷15	<3	~10	$\sim 10^{16}$	~10	corresponds to first BPI at Garching	
TERP (Maryland)	~3	1.5÷2.5	~5	$\sim 2 \cdot 10^{14}$	~10	mode analysis by internal probes	
BP IIa (Garching)	6÷12	≤2.8	~100(Ti) ~35(Te)	$\sim 2 \cdot 10^{14}$	~60	β-decay mainly due to radiation losses (influence of internal modes?)	
HV BP (Garching)	~10	?	700(Ti) ~300(Te)	$\sim 5 \cdot 10^{13}$	?	investigation of fast shock compression	

Table 3: Main physical data obtained in different belt-pinch experiments

$T \leq 100$ eV. The reason for this limitation is mainly the large poloidal circumference of the experiments, which in practice allows only a modest electrical field strength that determines the shock energy. Furthermore, the small wall distance necessary to maintain the elongated cross-section and to avoid displacement modes excludes strong adiabatic heating. In experiments with smaller b/a, lower ß-values are required. This is achieved by bias fields which reduce the effectiveness of the shock compression (TENQ). Only in the Garching High-Voltage Belt-Pinch /52/, where relatively small dimensions are combined with extremely high voltage and rather low densities, collision-free plasmas in the keV-range have been produced. The disadvantages of this experiment, however, are the high neutral background and the comparatively large ratio of gyro radius to plasma thickness 2 a.

Experimental results on Equilibrium and Stability

The typical arrangement of the poloidal field coils as sketched in Fig. 6 provide an elongated cross-section with more or less flattened ends (race-track). As an example, Fig. 7 shows two plots of poloidal flux surfaces for different β_{pol}-values in Belt-Pinch IIa.

These pictures have been obtained with the aid of a numerical equilibrium code /53/ which fits several experimental input parameters (pressure and magnetic field profiles and ß values) /51/. During the first phase of high $ß_{pol}$ ($ß_{pol} \approx A$), the race-track geometry is very pronounced. For later stages, the equilibrium has a tendency towards an ellipse with remarkable triangularity. From these calculations it can be deduced that the toroidal current distribution stays roughly homogeneous in the z-direction during a discharge. Compared with a simple ellipse, these plasma forms have strongly elongated flux surfaces also in the central plasma region. As a consequence, a modest ratio of q_b/q_o can be maintained even at high ß and elongated cross-section. At this point it is interesting to note that the proposed "flux conserving tokamak"-concept is based on the idea to preserve initial, modest q_b/q_o-ratios by means of a fast plasma heating towards the high $ß_{pol}$-values /54/. For this reason, in the belt-pinch experiments not only the high $ß_{pol}$-values but also details in pressure and current profiles are quite similar to those of the FCT-equilibria.

Typical radial profiles of p, B_t, B_p, and toroidal current density j_t for a high-ß belt-pinch equilibrium are shown in Fig. 8. - Note the strong shift of the maximum toroidal current density to the outside region due to the high ß-value of the plasma.

Concerning plasma stability at high beta values, all belt-pinch experiments show the same encouraging result: above a critical q_b around typically 3, fast growing MHD modes (except for displacement instabilities in some special cases /49, 51/) can be avoided. Below this obvious stability limit, however, different types of pronounced kink modes have been observed /50, 37/. For instance in the Belt-Pinch II experiment, the occurrence of such modes resulted in an explosive destruction of the high-beta equilibrium within typically 10 - 20 μs.

In the recent experiments in Belt-Pinch IIa, a strong reduction of the impurity level did improve the high-ß confinement time by a factor of 2 to more than 100 μs. Again no macroscopic instabilities are observed. The time behaviour of all measured plasma parameters has been compared with simulations using the Garching high-ß multi-fluid transport code /55/.

For the new, improved parameters, the experimentally observed decay of the plasma energy content seems to be somewhat faster than predicted by the collision dominated model and a certain influence of internal modes on transport cannot be excluded.

Conclusions

Modifications of the simple tokamak configuration in the direction of non-circular cross-section and high β_{pol}-values indicate that the critical β can be enhanced. Extreme conditions in this direction have been realized in the different belt-pinch experiments. As the main result of these experiments, the fast kink modes as the first barrier of high-β confinement, are obviously stabilized by $q_b \gtrsim 3$ with a sufficiently high shear ($q_b/q_o \approx 3$), even at strongly non-circular cross-sections. This allows to investigate the high-β regime and especially transport problems in toroidal geometry for time scales which have not been realized in other high-β configurations so far. For longer time scales, one has to suspect the appearance of internal kink or ballooning modes which are outside the scope of the fast pulsed experiments at present.

Acknowledgements

The author wishes to acknowledge with gratitude many valuable contributions and discussions with the members of the Garching HBS and Belt-Pinch teams, as well as the Los Alamos Scyllac group.

References

/1/ Kaufmann M., 3rd Top.Conf.on Pulsed High-ß Plasmas, Culham 1975, p.5

/2/ Davidson R.C., Freidberg J.P., 3rd Top.Conf.on Pulsed High-ß Plasmas, Culham 1975, p. 13

/3/ Lortz D., ZAMP 21 (1970), 196

/4/ Blank A.A., Grad H.,Weitzner H., Plasma Physics and Contr.Nucl.Fusion Research 1968, IAEA Vienna (1969), Vol. II, p. 607

/5/ Ribe F.L., Report LA - 4098 (1969)

/6/ Ribe F.L., Rosenbluth M.N., Phys.Fluids 13, 2572 (1970)

/7/ Weitzner H., Phys. Fluids 14, 658 (1971)

/8/ Rosenbluth M.N. et al., Phys. Fluids 12, 726 (1969)

/9/ Freidberg J.P., Phys. Fluids 14, 2454 (1971)

/10/ Todoroki J., NUP-A-76-2, - to be published

/11/ Marder B.M., Phys. Fluids 19, 1395 (1976)

/12/ Schneider W., Herrnegger F., Nucl. Fusion 16, 925 (1976)

/13/ Herrnegger F., Nührenberg J., 2nd Top.Conf.on Pulsed High-ß Plasmas, Garching 1972, IPP 1/127, B2

/14/ Herrnegger F., Nührenberg J., Nucl.Fusion 15, 1025 (1975)

/15/ Correa D., IPP 1/149 (1974)

/16/ Fünfer E. et al., IPP 1/130 (1973), and
Fünfer E. et al., Plasma Physics and Contr.Nucl.Fusion Research 1971 IAEA Vienna (1971), Vol. III, p. 189

/17/ Burnett S.C. et al., Plasma Physics and Contr. Nucl.Fusion Research 1971, IAEA Vienna (1971), Vol. III, p. 201

/18/ Bogen P. et al., Plasma Physics and Contr. Nucl.Fusion Research 1976, IAEA Vienna (1977), Vol. I, p. 551

/19/ Fünfer E. et al., Nucl. Fusion 15, 133 (1975)

/20/ Fünfer E. et al., 7th Europ.Conf.on Contr.Fusion and Plasma Physics, Lausanne (1975), Vol. II, p. 151 (see also this conference)

/21/ Cantrell E.L. et al., Plasma Physics and Contr.Nucl.Fusion Research 1974, IAEA Vienna (1975),Vol. III, p. 13 (see also this conference)

/22/ Quinn W.E., Los Alamos, priv. communication (see also this conference)

/23/ Freidberg J.P., Phys. Fluids 15, 1102 (1972)

/24/ Neuhauser J. et al., Nucl.Fusion 17, 3 (1977)

/25/ Turner L., Phys. Fluids 20, 654 (1977)

/26/ Lewis H.R., Turner L., Nucl. Fusion 16, 993 (1976)

/27/ Freidberg J.P. et al., Plasma Physics and Contr. Nucl.Fusion Research 1976, IAEA Vienna (1977), Vol. III, p. 123

/28/ Hermegger F. et al., Plasma Physics and Contr.Nucl.Fusion Research 1976, IAEA Vienna (1977), Vol. II, p. 183

/29/ Tasso H., Plasma Physics and Contr.Nucl.Fusion Research 1976, IAEA Vienna (1977), Vol. III, p. 371

/30/ Lortz D., Nührenberg J., 3rd Int. (Kiev) Conf. on Plasma Theory, Triest (1977) B-1/1-2 (see also this conference)

/31/ Schlüter A., Chodura R., 3rd Top.Conf.on Pulsed High-ß Plasmas, Culham 1975, p. 187

/32/ Betancourt O., Garabedian P., Proc.Nat.Acad. Sciences (USA), 73, (1976) 984

/33/ Barnes D., Brackbill J.U., 3rd Top.Conf.on Pulsed High-ß Plasmas, Culham 1975, p. 111

/34/ Barnes D., Plasma Physics and Contr.Nucl. Fusion Research 1971, IAEA Vienna (1971), Vol. II, p. 203

/35/ Braun W. et al., Plasma Physics and Contr.Nucl.Fusion Research 1974, IAEA Vienna (1975), Vol. III, p. 25

/36/ Clarke J.F., ORNL-Report TM 5429 (1976)

/37/ Gruber O., Wilhelm R., Nucl.Fusion 16, 243 (1976)

/38/ Lortz D., Nührenberg J., Nucl.Fusion 13, 821 (1973)

/39/ Peng Y.-K. et al., ORNL-Report TM 5267 (1976)

/40/ Kerner W., Nucl.Fusion 16, 643 (1976)

/41/ Wesson J.A., Sykes A., Plasma Physics and Contr.Nucl.Fusion Research 1974, IAEA Vienna (1974), Vol. I, p. 449

/42/ Berger D., Thesis University of Lausanne - to be published

/43/ Todd A.M.M. et al., Phys.Rev.Lett., Vol.38,Nr. 15, p. 826 (1977)

/44/ Bateman G., Peng Y.-K., Phys.Rev.Lett., Vol.38,Nr. 15, p. 829 (1977)

/45/ Lackner K., McMahon A.B., Nucl.Fus. 14, 575 (1974)

/46/ Rosen M.D., Phys.Fluids 18, 482 (1975)

/47/ Rebhan E., Salat A., Nucl.Fus. 16, 805 (1976)

/48/ Graffmann E. et al., Plasma Physics and Contr.Nucl.Fusion Research 1976, IAEA Vienna (1977), Vol. I, p. 351

/49/ Hofmann F. et al., ibid., p. 305

/50/ Chu, C.K. et al., ibid.,p. 511

/51/ Gruber O. et al., ibid.,p. 311

/52/ Söldner F., Steuer K.-H., ibid., Vol. III, p. 89

/53/ Becker G., Lackner K., ibid., Vol. II, p. 401

/54/ Dory R.A., Peng Y.-K., ORNL-Report TM-5555

/55/ Becker G., Düchs D.F., Nucl.Fus. 16, 763 (1976)

Figure Captions

Fig. 1: Growth rate γ versus δ_1 of the m = 2, k ≅ 0 mode

Fig. 2: Transverse motions of the plasma column in the horizontal and vertical plane without feedback (top) and with feedback (bottom)

Fig. 3: Theoretical m = 2 growth rate γ for a Vlasov fluid model (normalized to the ideal MHD growth rate γ_{MHD}) plotted versus the ratio of the Larmor radius to the plasma radius, $\eta = r_L/a$

Fig. 4: The experimental results are summarized by representing each set of plasma parameters by η_a and $(\omega_L \cdot \tau_{ii})_a$ at $t \approx 4$ μs. Individual points are drawn for deuterium only. The experimental m = 2 stability boundary is shown, yielding $\eta_{crit} \approx 0.14$

Fig. 5: Critical ion radius r_L as a function of ß (normalized with $\tilde{\gamma} = \frac{\gamma}{\gamma_{MHD}}$ and a)

Fig. 6: Technical arrangement of the Belt-Pinch II experiment

Fig. 7: Poloidal flux surfaces at two times with $ß_{pol} = 4$ (left) and $ß_{pol} = 1.5$ (right)

Fig. 8: Radial profiles of toroidal and poloidal magnetic fields, toroidal current density and plasma pressure at t = 10 μs in Belt-Pinch IIa

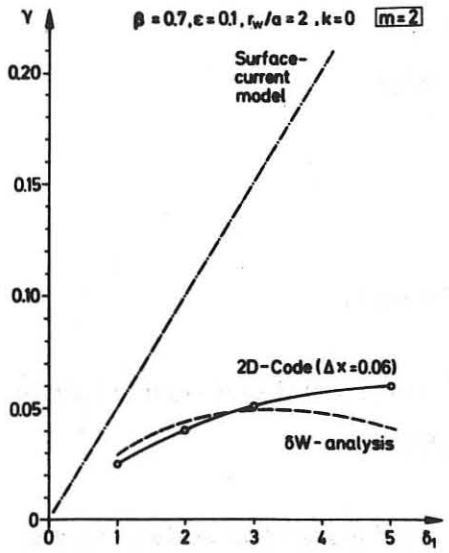

Figure 1

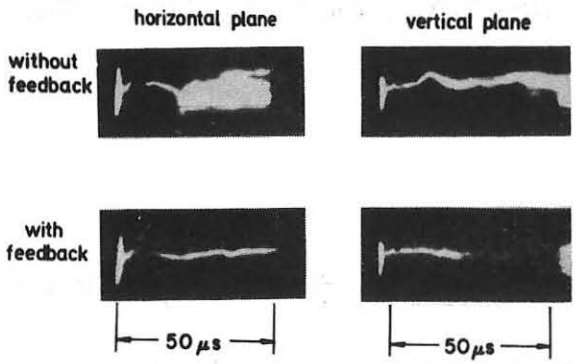

Figure 2

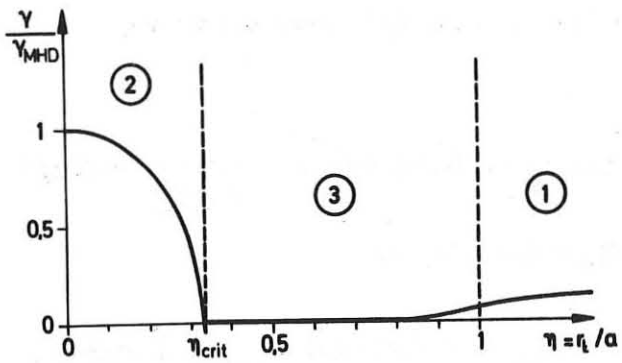

Figure 3

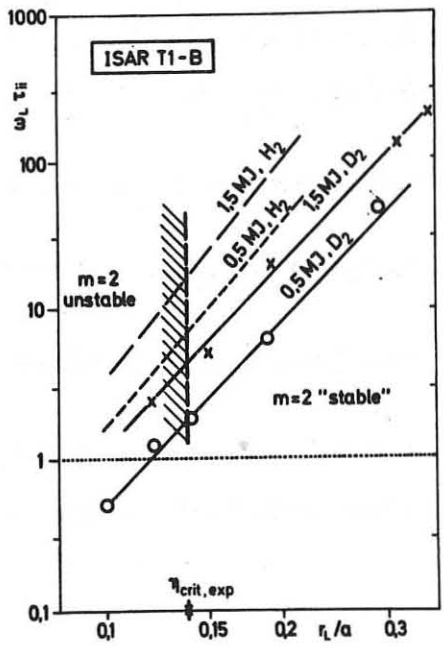

Figure 4

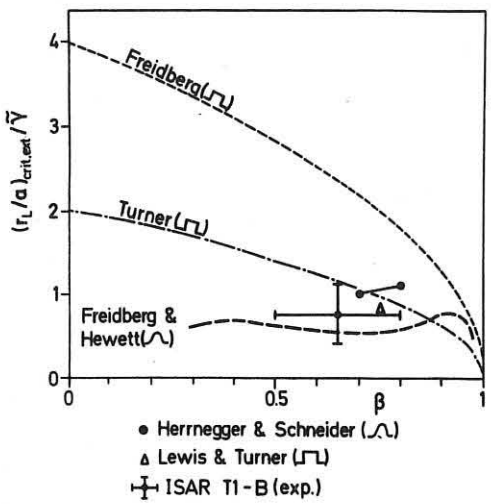

Figure 5

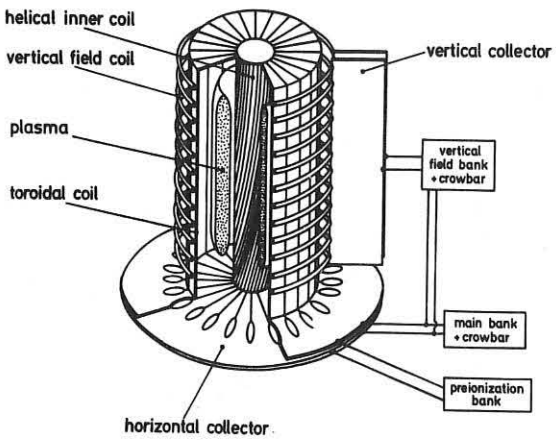

Figure 6

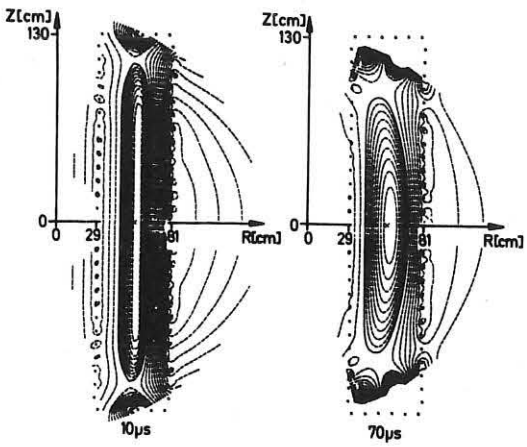

Figure 7

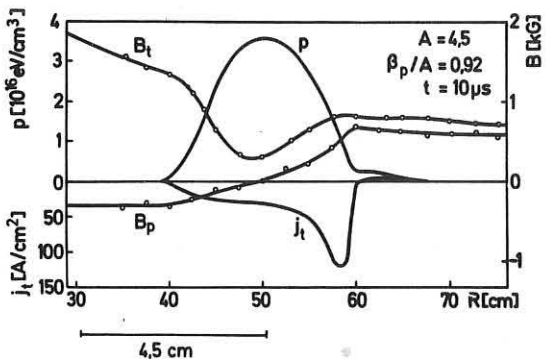

Figure 8

PROGRESS IN LASER-FUSION RESEARCH

O.N. Krokhin

P.N. Lebedev Physical Institute, Moscow, USSR

Giving an introduction to a laser-fusion research carried out now I shall give more attention to the comparison of experimental and theoretical results especially on the possibility of the mathematical simulation of the whole process. The results obtained till now by different study groups are, in general, in a good agreement. This gives us the confidence in correct understanding and intepretation of physics of the laser radiation interaction with matter, the dynamics of the fuel compression and the transport phenomena. There are also some results, however, which need more detailed examination. Moreover, there exists also, in several points, some discrepancy between different experimental results and their theoretical explanation. The aim of the investigations both performed now and planned for future is to make these problems more clear and to determined the ways for the further development.

GENERAL PROGRAM LASER-CTR

- DEVELOPMENT OF HIGH-POWER HIGH-EFFICIENT LASERS
- HIGH-GAIN TARGET PERFORMANCE
- DEVELOPMENT OF REACTOR CONCEPTION INCLUDING FUSION AND FUSION-FISSION APPROACHES
- NEW TECHNOLOGY AND MATERIALS

Fig. 1

The general program of the laser-fusion research includes the items shown in Fig. 1. It is clear that these items are closely connected with each other. The high gain of a target (of the order of several hundreds) would simplify the problem of the development of new lasers as we do not need the high effeciency of lasers in this case (it can be of the order of one percent only). Also the approach of fusion-fission reactor design would reduce some of the difficulties of both laser and target programme. In addition, among the very important problems the development of new laser technology especially of optical elements with high reliability is worth mentioning.

LASER RADIATION-PLASMA INTERACTION

FLUX DENSITY ON TARGET		DOMINANT PHYSICAL PROCESSES OF INTERACTION		
NEODYMIUM	CO_2	ABSORPTION	ENERGY TRANSPORT	THERMODYNAMIC CONDITION
10^{13}-10^{14}	10^{12}	REVERSE BREMS-STRAHLUNG PARAMETRIC RESONANT	CLASSICAL ELECTRON HEAT CONDUCTION	NEARLY THERMODYNAMIC EQUILIBRIUM
10^{15}-10^{16}	10^{12}	RESONANT PARAMETRIC	FLUX LIMITED ELECTRON HEAT CONDUCTIVITY INHIBITION OF CONDUCTIVITY	HOT ELECTRONS ($\sim$ %) HOT IONS ($\sim$1 %)

Fig. 2

The physical phenomena of laser radiation interaction with a plasma is schematically presented in Fig.2. Various mechanisms of the absorption are dominant for different power densities of the interacting beam. The experiments show that the absorbed part of the total flux remains on the level of approximately 50% through the whole region of the power variation. Perhaps, at a high intensity of radiation, there exists some similarity in the absorption of the neodymium and CO_2 radiation due to sharpening of the plasma density profile by the ponderomotoric forces. The occurence of hot electrons in the interaction region could result in an initial preheating of fuel preventing its subsequent high compression. Also the inhibition of the electron heat conduction leads to the decrease of the momentum transferred into a target.

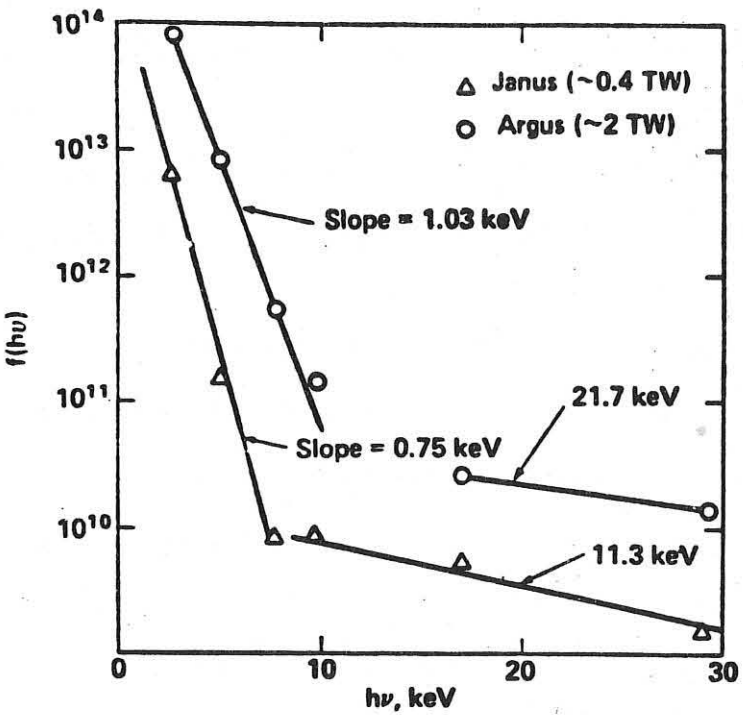

Fig. 3 H.G. Ahlstrom, Proc. US-Japan Seminar on Laser Interaction with Matter. Osaka Univ. 1977.

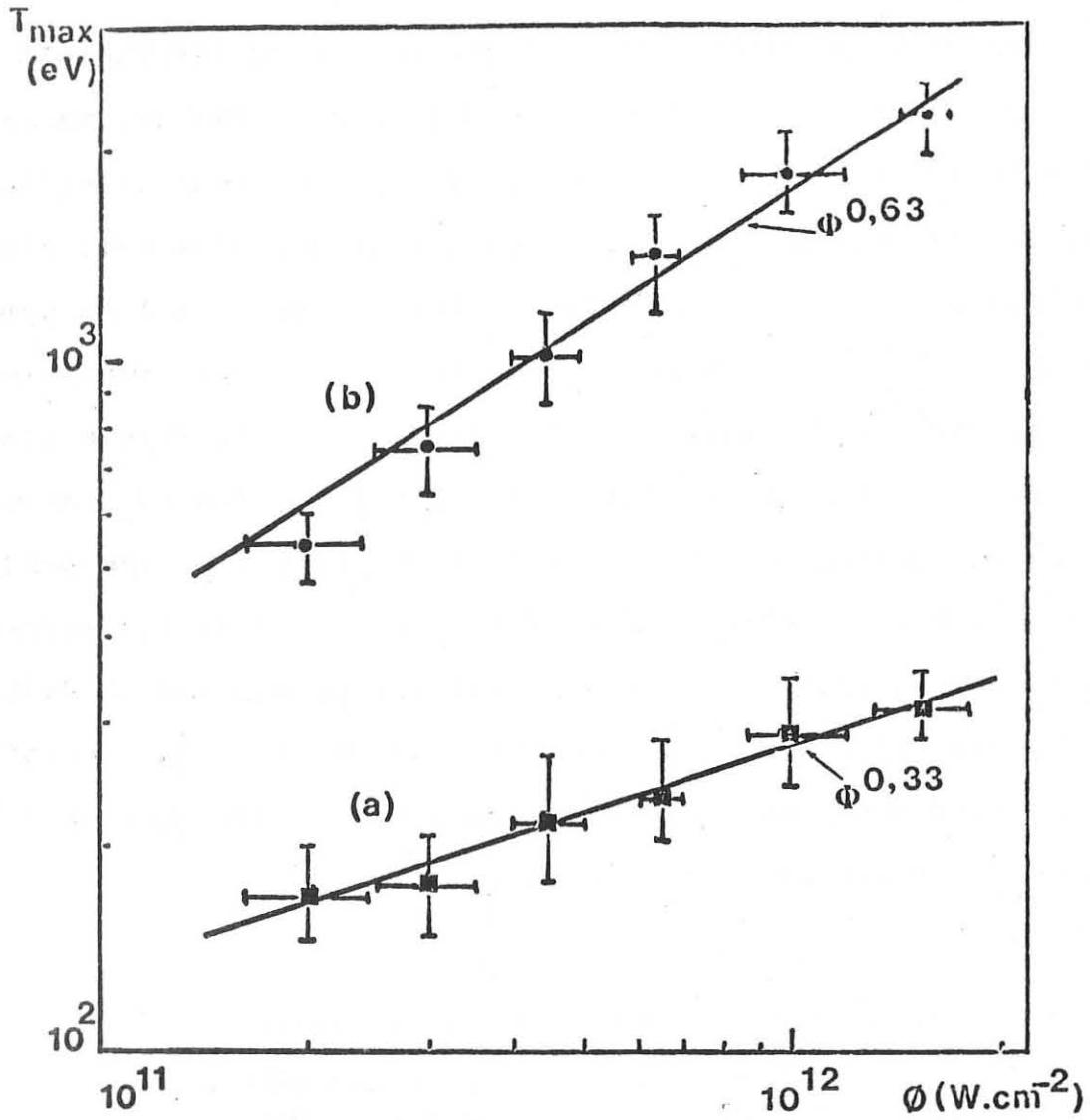

Fig. 4 E. Fabre et al., "Plasma Physics and Controlled Nuclear Fusion Research", vol. II, 1976 (IAEA, Vienna 1977)

In the Fig. 3 the presence of two groups of electrons in the interacting corona is illustrated. The main part corresponds to thermal electrons with temperature of the order of 1 keV typically, but the "tail" of electron distribution has a "temperature" of the order of few tens of keV. In the Fig. 4 the flux dependence of both these temperatures is shown for the case of the target illumination by CO_2 laser radiation. The target compression driven by the pressure arising at the ablation front can be affected by Rayleigh-Taylor instabilities

resulting in degradation of the spherical symmetry of the compression. The unstable region corresponds to the layer of the target material near the ablation front in which the signs of the pressure and density gradients are opposite (Fig.5).

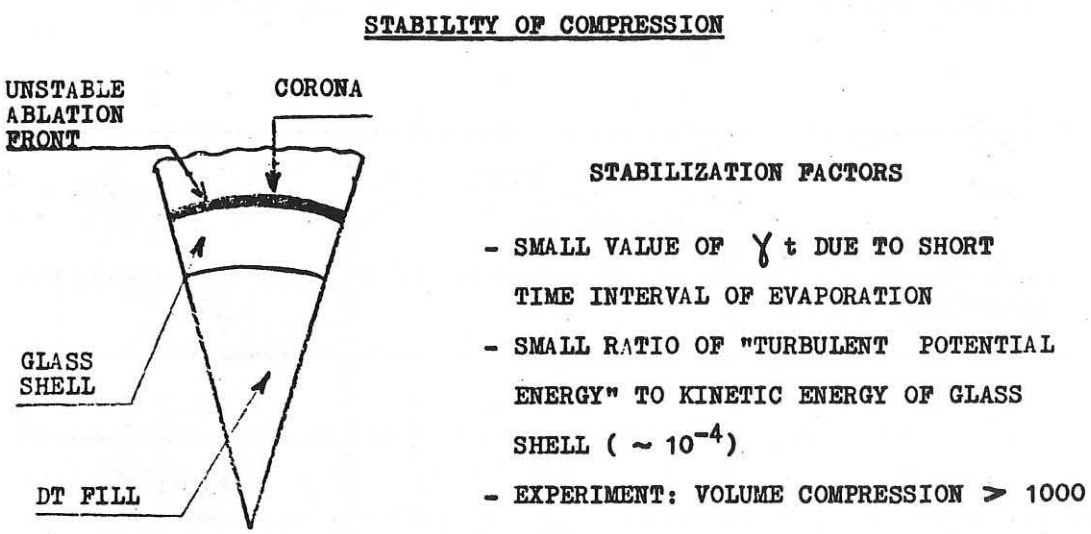

Fig. 5

Nevertheless, the one-dimensional analysis of the ablation process shows that the thickness of this layer is very small. This leads to some stabilisation of the material flow due to the very short time within which the layer is affected by the Rayleigh-Taylor instability. Another important circumstance is connected with the relatively small value of energy associated with turbulent motion of the plasma. The ratio of this energy to the kinetic energy of the accelerated layer is of the order of 10^{-4} only. It corresponds to the velocity ratio of some 10^{-2}. This is quite a small value which cannot lead to a large asymmetry of the compression even for very thin glass shells (aspect ratio $\sim$ 50).

P.N.LEBEDEV INSTITUTE "KALMAR" EXPERIMENT

TARGET PERFORMANCE : DIAMETER 140 μm

WALL THICKNESS 2.2 μm

DD FILL 5.4 mg/cc

LASER PULSE: 2.5 ns, 0.04 TW

	LEBEDEV INST. EXPERIMENT	CODE " LUCH "
ABSORBED ENERGY	20	30
ρ max	6 ÷ 8	9.7
ρR	10^{-2}	5.4×10^{-3}
T_i		0.67
T_e	1	0.67
FUSION EVENTS	$(3 \div 6) \times 10^6$	4.4×10^6
COMPRESSION VELOCITY	$(5 \div 10) \times 10^6$	8.6×10^6
COMPRESSION TIME	1.4×10^9	1.33×10^{-9}

Fig. 6

It is very important to discuss the problem of numerical simulation of processes of the laser-target interaction and of the compression of fuel. The numerical modelling is based on the gasdynamical and energy transport equations accounting for the dominant physical processes and their characteristics. These processes are: the mechanism of absorption which determines the value of the absorption

coefficient, electron heat conductivity, radiation losses and transport, transport of the hot electrons. The usual method of the computer simulation consists of fitting the introduced parameters to achieve good agreement with experimental data. This procedure implies, however, a certain degree of freedom and may lead to some discrepancy between computed and experimental data under highly different experimental conditions, e.g. at significantly higher or lower power densities and so on. The Fig.6 shows the experimental data obtained on 9-beam installation "Kalmar" at Lebedev Physical Institute. This data are compared with calculated ones by means of code "Luch" developed at the Institute of Applied Mathematics by A.Samarsky group and at Lebedev Physical Institute by N.Basov group. It was assumed that the main part of the radiation absorption is determined by parametric instabilities, which is consistent with direct measurements, and that the electron heat conduction is classical one. Similar results and similar conclusions were obtained by Limeil group and were presented on "IV Workshop on Laser Interaction and Related Plasma Phenomena" in November 1976.

The Fig.7 (according to Univ. of Calif. Report UCRL--79736 by W.C. Mead) presents the Argus experimental results obtained at the Lawrence Livermore Laboratory and their comparison with the expected from the simulation parameters. One can see a good agreement between the experimental data and the Livermore simulation model achieved by fitting the code parameters to the experimental situation. This model takes into account the presence of the hard electrons, the inhibition of the flux limited electron thermoconductivity and transport of radiation.

LLL "ARGUS" EXPERIMENT

TARGET PERFORMANCE: DIAMETER 105 μm

WALL THICKNESS 0.78 μm

DT FILL 1.7 mg/cc

LASER PULSE: 4.2 ps, 2.5 TW

	LLL EXP.	LLL CALC.	LLL EXP.	CODE "LUCH"*
ABSORBED ENERGY	12	13.5	21.8	21.8
ρ_{max}	0.2	0.16		0.37
ρR	3.10^{-4}	3.10^{-4}		4.10^{-4}
T_i	5	4.6	5.4	18*
T_e				3
FUSION EVENTS	4.10^8	3.6×10^8	$(2 \div 5) \times 10^8$	$2.7 \times 10^{8*}$

* GASDYNAMICAL DESCRIPTION OF FUEL IONS BEHAVIOR IS INCORRECT; FUSION EVENTS ARE CORRECTED ACCORDING TO HENDERSON (PHYS.REV.LET. 33,1142, (1974).

Fig. 7

On the other hand the calculations by code Luch were made by the same way as for the Kalmar experiment. Probably, the large discrepancy in the value of temperature occurs at first from the more strong shock wave given by Luch model. Inadequacy of the gasdynamical description is due to the large free path of the fuel ions. Under the experimental

conditions indicated in Fig.7 the"cut off" energy corresponds to approximately 6 keV. Moreover, the measured ion temperature of some 4-5 keV can be, probably, connected with the escape of the energetic ions.

RECENT LASNEX CALCULATIONS INDICATE THAT THE SOVIET PELLET MODEL IS OPTIMISTIC

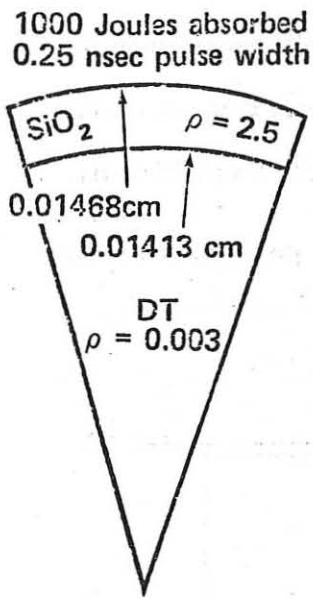

Model	θ_i* (keV)	ρ* (g/cm^3)	ρR* (g/cm^2)	Fusion events
Soviet	10	3.8	1.0×10^{-2}	1.4×10^{13}
3-T [1]	2.6	8.0	8.2×10^{-3}	1.9×10^{11}
2-T + pbins [2]	1.7	3.2	4.5×10^{-3}	2.7×10^{10}
3-T [3] w/o e – i coupling	11.9	2.9	4.2×10^{-3}	1.3×10^{13}
LLL [4]	5.0	0.17	6.5×10^{-4}	6.3×10^{10}

*Fuel averaged values at peak reaction rate

Fig. 8

In the Fig. 8 the results of several computer simulations of pellet compression by 1000 J energy absorbed within 0,25 ns are compared. The Livermore calculations correspond to:

1. three temperature model - for electrons, ions and radiation
2. two temperature model with multigroup transport for radiation
3. three temperature model without electron-ion relaxation
4. multigroup electron and radiation transport and inhibited thermoconductivity.

The last model agrees favorably with the Livermore Argus experiment at the absorbed energy in the range of 10-20 J.

There exists a large difference between our result and the Livermore one, but this only demonstrates the sensitivity of the yield on parameters introduced in a model. The different models have their own optimum target parameters - the diameter and the wall thickness. Target which is shown at the first row in Fig. 8 corresponds to the maximum output in our model which agrees favorably with "Kalmar" experiment.

The sensitivity of the yield on the target parameters is shown in Fig. 9.

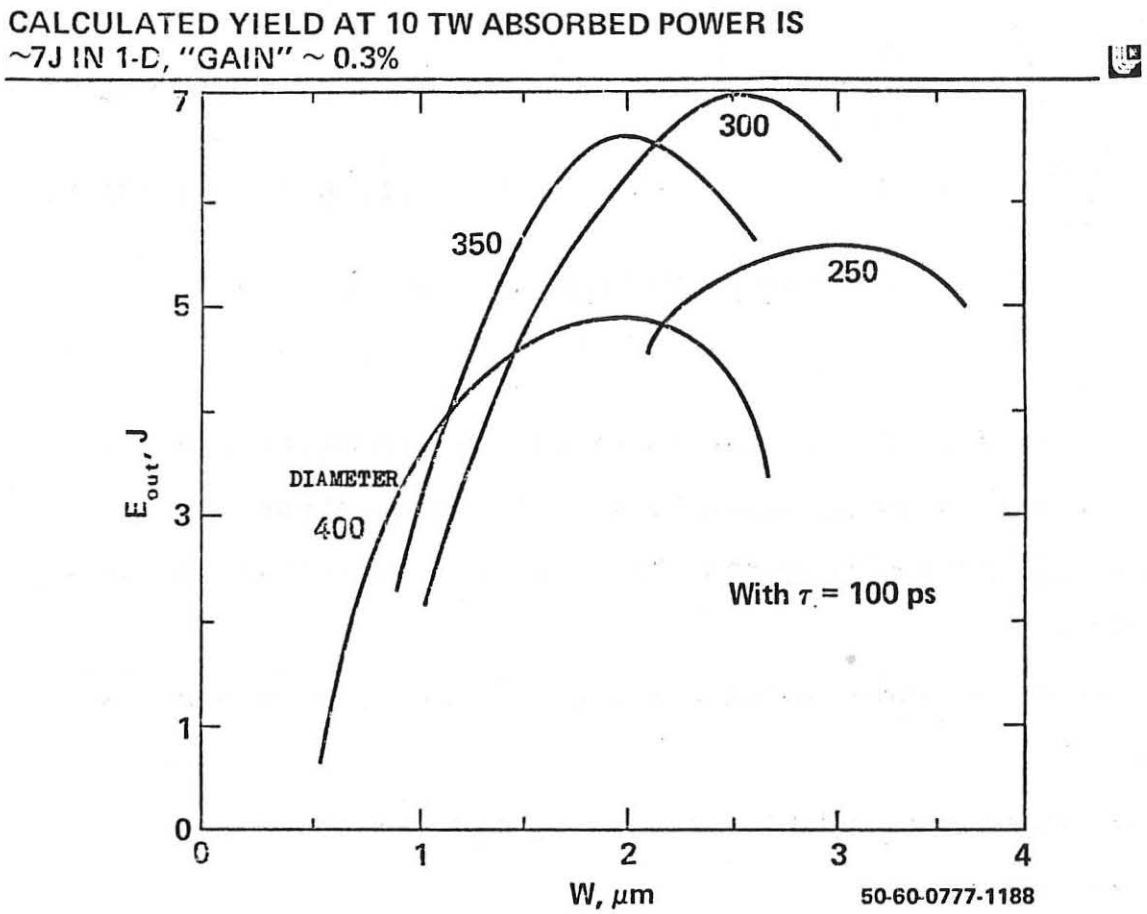

Fig. 9

This Figure gives the dependence of the yield on target diameter and on the thickness of its wall. The curves have

smooth maxima with a width of $\sim$ 1 μm and a sharp fall outside this region. But the difference in the maximum yield is negligible for the diameter change from 250 to 400 μm. Our target is located very far on the right hand side of the Livermore curve corresponding to the wall thickness of 5.5 μm, being thus very far from the optimum region of the Livermore model. The maximum yields predicted by Luch and LLL models, however, differ only by a factor of 4, which is not too much from the point of view of accuracy of such predictions.

The last two Figures are reproduced from the Report of Univ. of California UCRL - 79736 by W.C. Mead et al. with a comment: "Models other than turning off electron-ion coupling might produce similarly high yields and that we do not intend to imply that your calculations were done in that way"- (J.T. Larsen, private communication).

TARGET PERFORMANCE: Diameter 300 μm
Wall thickness 2.6 μm
DT fill 5 mg/cc

LASER PULSE 100 ps

	LLL model	Luch model
Absorbed energy	1000	1000
max	0.35	0.50
R	7×10^{-4}	1.6×10^{-3}
T_i	15	19.1
T_e		4.6
Fusion events	3×10^{12}	7.8×10^{12}

Fig. 10

In the Fig.10 parameters of the target corresponding to the maximum yield from Fig.9 are indicated. The final parameter calculated by means of these two models differ only slightly.

The new laser installations based on the neodymium and CO_2 high power laser will operate in one-two years. After the completation of these facilities we can expect a noticable advance in understanding the physical processes of the laser driven compression, the instability problem as well as better computer simulation models.

I should like to underline the importance of the development of laser technology. The laser which are available till now are mostly scientific instruments and not the technical ones and cannot be considered, therefore, as suitable form the practical fusion. I should not like to exclude also various possibilities of "mixing" of the different approaches within the inertial confinement programme. From this point of view,too, the laser-fusion program seems to be the most advanced one in the investigation of physics towards the realization of pulsed thermonuclear reactions.

SANDIA'S RECENT RESULTS IN PARTICLE BEAM FUSION RESEARCH

Gerold Yonas

Sandia Laboratories

Albuquerque, New Mexico 87115, U.S.A.

The dual goals of the Sandia particle beam fusion program are to determine the feasibility of using pulsed high-voltage accelerators of intense particle beams to achieve ignition of inertially confined thermonuclear fuel and to determine methods for practical application of those results to fusion reactors. Pulsed power accelerators potentially offer a potentially efficient (up to 50 percent) and relatively inexpensive (several tens of dollars per joule) route to an experimental reactor ignition system if the yet to be answered physics questions have a favorable outcome. These physics issues encompass the following: (1) power concentration and dielectric breakdown, (2) beam focusing and transport, (3) beam target interaction, and (4) implosion hydrodynamics. These interdependent elements of the program are being investigated to determine which of the three particle approaches (electrons, light ions, or heavy ions) will provide an optimal route to our goals.

The use of electron beams will require low inductance power concentration methods to deal with the ultra-high currents ($\sim 10^8$ A) thought to be needed at MeV electron energies and either substantial improvements must be made in vacuum insulator flashover strength, or instead multiple, magnetically insulated vacuum transmission lines must be used to deliver power from low stress insulators to the target region.[1,2] Numerical time-dependent 2-D simulations of the electron flow in magnetically cutoff lines predict efficient power transport with energy loss only due to pulse front erosion.

Experiments have already confirmed those predictions and studies are continuing on the use of rectangular transmission lines which would permit further power concentration.

If such multiple lines are terminated in a single or double diode configuration, the resulting low impedance load will experience substantial energy losses due to enhanced ion current generation in the self-pinched electron flow.[3] Two-dimensional particle flow simulations indicate that a dual diode arrangement, such that the ions reflex between two anodes through a common hollow cathode, will suppress the net ion current and still permit efficient electron focusing.[4] Reduction in the ion current can also be achieved by utilizing higher impedance diodes and this step would be facilitated by raising the electron accelerating voltage. Pellet design calculations which employ higher electron voltages by shaping of the power and voltage pulse have not been successful in reducing the power requirements. This appears to be a result of the bremsstrahlung preheat of the pusher. Nevertheless, higher voltages may be usable if the electron stopping distance can be substantially shortened in low-Z ablators as a result of the beam self-magnetic field penetration into the deposition region with subsequent modification of the electron stopping distance.[5] Monte Carlo simulations of this effect predict measurable changes in beam-target coupling for current densities > 1 MA/cm^2 and $I > I_{Alfvén}$.[6] Deposition experiments with focused beams interacting with thin foils are being carried out using soft X-ray and optical diagnostics. In our experiments on Hydra, the currents and current densities have not as yet reached high enough values to expect enhanced deposition. We have observed enhancement with targets which protrude

from the anode thus perturbing the electron flow and causing beam stagnation.[7] Magnetic enhancement of deposition in thin foil targets has been reported by the Kurchatov electron beam group[8] apparently using a diode which achieves higher current densities and operating in a turbulent plasma pinch rather than a beam mode.[9]

Beam deposition in thin foils and exploding pusher targets are being studied with two opposing beams irradiating a common spherical target using the Proto I generator operating at the 1 TW level. Current densities of $\sim 10^7$ A/cm^2 have been measured with thick targets and although symmetry of irradiation with thin targets has been found to be within a few percent, the maximum ablator temperatures appear to be less than 10 eV. The measured temperatures are too low to produce measurable neutron yields. Numerical simulations indicate that relatively thick targets are needed for efficient energy absorption and it is believed that higher power levels than available on Proto I will be needed to produce measurable neutron yields from simple targets.

Successful neutron production experiments have been performed[10] using the 0.25 TW beam from the Rehyd generator and employing a more complex target concept. An exploding pusher consisting of a thin spherical plastic shell 3 mm in diameter and containing a 25 to 50 μ diameter CD_2 filament was imploded symmetrically with a velocity of 4 cm/μsec by a single beam.[11] Approximately 10^6 neutrons with an energy of 2.5 ± 0.2 MeV have been detected using neutron time-of-flight techniques. With a simple target, this beam power would be insufficient to produce measurable neutrons but here magnetic reduction of thermal conduction allows one to reach higher final fuel temperatures with a lower compression ratio.[12] Fuel preheat and magnetic insulation are achieved

using a 5 to 10 kA, 1 μsec prepulse which is collected by a thin foil attached to the target. This prepulse current pre-explodes the wire thus creating the necessary initial conditions. Null experiments support the contention that magnetic thermoinsulation is essential for success of these targets and these results open up promise for substantial reduction in pellet ignitor requirements. This target approach should permit the use of longer power pulses (~100 ns) than possible using more conventional target designs.[13] Thus far, 1-D calculations indicate that breakeven power levels are reduced by about a factor of four and allowable pulse durations are increased by almost an order of magnitude.

Another approach to utilize higher impedance diodes and thus reduce inductance restrictions on minimum power pulse widths is to subdivide the beam current into multiple beams which are then individually transported and combined at the target. In contrast to the Kurchatov cusp transport approach,[14] we have proposed to propagate separate focused beams in plasma discharge channels. Such channels have been formed in air at 1 atm using a fine wire to define the path of a 50 kA discharge. With the focused beam injected into the low-density, high-conductivity 1-cm-diameter channel formed after a delay of ~10 μsec, efficient and stable propagation over 1 m has been observed.[15] Experiments on beam combination with multiple channels and theoretical modeling of beam transport and combination are underway. Use of laser guided discharges in a background gas[16] may provide a means of achieving the standoff necessary for high gain reactor applications.

In view of the advantages of ion beam deposition,[17] an alternate approach is to utilize the self-pinched low-impedance diodes discussed above as ion sources with ballistic focusing of the resultant space charge neutralized beam.[18,19]

Externally applied magnetic fields can be used for electron current suppression in relatively high impedance diodes thus permitting controlled beam collimation, ion source production, and beam extraction.[20] Such techniques are being developed for us at diode power levels approaching 1 TW on Hermes and Proto I.[21] Magnetic insulation for electron current suppression may also be useful in space charge neutralized high current, multistage linear accelerators.[22] The prospects of this application are under study for producing high quality beams which can be propagated over substantial distances to a target. Such a pulsed power driven high current linear accelerator would have negligible power flow problems and would readily lend itself to repetitively pulsed applications.

Scaling of intense particle accelerators to higher power levels is continuing with primary emphasis on Proto II which has been tested at the 6 TW level with a 20 ns pulse. The accelerator is also being operated in 50 and 80 ns modes in order to determine component characteristics over a wide range of parameters. Another test facility (MITE), has also been completed to evaluate a single module of the 36 module electron beam fusion accelerator which is planned for completion in 1980. If the initial steps now planned prove successful, then an ignition experiment using an upgrade of EBFA would be carried out in the 1985 time frame to set the stage for a later experimental power reactor. Economic analyses have shown that high efficiency and low cost I.C.F. ignition systems would be able to compete with other postulated long-term energy sources with pellet gains < 10 in hybrids and ~ 100 for pure fusion reactors.[23]

REFERENCES:

1. E. I. Baranchikov, et al., Zh. Tekh. Fiz., 46, 1069 (1976).
2. K. D. Bergeron, J. Appl. Phys., 48, 3065 (1977).
3. J. W. Poukey, et al.; also, Shyke A. Goldstein, et al., both from First Int'l. Topical Conf. on Electron Beam and Technology, Albuquerque, New Mexico (1975).
4. J. P. Quintenz and J. W. Poukey, J. Appl. Phys., 48, 2287 (1977).
5. G. Yonas, et al., Nucl. Fusion, 14, 731 (1974).
6. M. M. Widner, et al., Phys. Rev. Lett., 38, 548 (1977).
7. M. J. Clauser, et al., Phys. Rev. Lett., 38, 398 (1977).
8. S. L. Bogolyubskii, et al., JETP Lett., 24, 178 (1976).
9. L. I. Rudakov, Kurchatov Institute, private communication.
10. J. T. Chang, M. M. Widner, A. V. Farnsworth, R. J. Leeper, T. S. Prevender, L. Baker, J. Olsen, to be presented at the 2nd Int'l. Topical Conf. on High Power Electron and Ion Beam, Cornell Univ., Ithaca, New York.
11. J. T. Chang, et al., Phys. Rev. Lett., 34, 1266 (1975).
12. The use of magnetic thermal insulation in inertially confined targets has been discussed in the following: F. Winterberg, Phys. of High Energy Density, Academic Press, 376 (1971); M. V. Babykin, et al., Nucl. Fusion Suppl., 75 (1972); D. J. Meeker, et al., Bull. Am. Phys. Soc., 20, 1352 (1975).
13. M. A. Sweeney and M. J. Clauser, Appl. Phys. Lett., 29, 231 (1976).
14. E. I. Baranchikov, et al., IAEA-CN-35/F7B, 185 (1977).
15. P. A. Miller, et al., Phys. Rev. Lett., 39, 92 (1977).

16. J. R. Greig, R. E. Pechacek, A. W. DeSilva and D. W. Koopman, "A Study of Aerosol Initiated CO_2 Laser-Produced Air Sparks," Naval Research Laboratory, unpublished.

17. M. J. Clauser, Phys. Rev. Lett., 35, 848 (1975).

18. J. W. Poukey, et al., Phys. Rev, Lett., 35, 1806 (1975).

19. G. Cooperstein, et al., IEEE Int'l. Conf. on Plasma Science, Austin, Texas (1976).

20. S. Humphries, invited paper, American Physical Society Meeting, Atlanta, Georgia (November 5-11, 1977).

21. G. W. Kuswa, et al. (ibid. Ref. 10).

22. S. Humphries, to be published J. Appl. Phys.

23. S. Varnado, "Prospect of Generating Power with Particle Beam Driven ICF," to be presented at Alternative Energy Sources Symposium, Miami Beach, Florida (December 1977).

GENERATION AND APPLICATIONS OF HIGH POWER ION BEAMS TO FUSION RESEARCH*

R. N. Sudan
Laboratory of Plasma Studies, Cornell University
Ithaca, NY 14853 USA

I. INTRODUCTION

At the 1973 European plasma Physics conference in Moscow, towards the end of my paper[1] on electron beam/plasma interaction I ventured the hope that "by suitable modifications of E-beam technology, it might prove feasible to create ion beams in the 10^5 A range". Soon after, this possibility was demonstrated at Cornell[2] by the successful generation of a 0.5 kA, 100 keV proton beam. Since then, extensive work at Cornell, NRL, and Sandia has pushed the parameters to well beyond the prediction so that intense ion beams of over a 100 kA are routinely available. Indeed, the main limitations on ion beam parameters are those imposed by present day pulsed power machines. Ion beams of 6 MeV has recently been generated on the Hermes machine in Sandia,[3] 200 kA beams at $\lesssim$ 1 MeV have been reported from NRL,[4(a)] and $\sim$ 100 kA beams at $\sim$ 300 keV have been routinely obtained on the Neptune machine at Cornell.[5]

II. ION DIODE TECHNOLOGY

The principal difficulties to be overcome in producing ion beams from a diode energized by a high power voltage pulse as compared to an electron diode are twofold: (1) the creation of an ion-emitting dense plasma $n_i \gtrsim 10^{16}\,cm^{-3}$ on the anode surface within a time interval of say, 10^{-8} sec. from the initial of the voltage pulse, (2) the suppression of the electron current which is larger than the ion current by a factor of $(m_i/Z_i m_e)^{1/2}$ in a simple planar diode is necessary for reasonable device efficiency.

The solution to the first difficulty was obtained by employing insulating anode surface instead of the normal conducting surface.[2] On the application of a voltage pulse the electric field within the diode has a tangential component to the anode surface. This component can initiate local electrical breakdown. The anode surface material is generally a hydrogenous plastic e.g. mylar and a dense hydrogen surface plasma is formed very rapidly within a few nanoseconds. The actual details of this process is not well understood but in practice it works very well. Figure 1 shows details of a configuration that has been successfully employed. This arrangement is one in which the mylar sheet is backed by a conductor and an array of copper pins, machined flush, pierce the mylar to provide local breakdown centers. More than a

hundred shots can be fired with this anode before any deterioration sets in. Electron current suppression can be handled in two ways: (a) electron reflexing and (b) magnetic insulation.

Reflex Triode[2]

In this device the cathode and anode are made in the form of meshes transparent to charged-particle flow. Electrons emerging from the anode create a virtual cathode on the far side and are reflected by the resulting space charge. The anode is made of a mesh of insulating nylon wires or a thin mylar sheet. The anode plasma formed by the surface flashover emits ions which are accelerated in both directions and emerge as two ion beams from either end. A magnetic field coaxial with the applied electric field prevents the electrons from wandering off at the edges. The theoretical understanding of the performance depends critically on whether the anode is a mesh[2] or a thin sheet.[6,7] A reduction in the electron power by a factor of 10-20 can be achieved for a transparent mesh anode. Ion currents well above the Child-Langmuir limit are observed when the anode is a thin sheet of plastic. This point is discussed at length in Refs. 6 and 7.

Magnetic Insulation

A magnetic field perpendicular to the diode electric field exceeding the critical field B^* required to turn the electrons within the gap would be effective in cutting down the electron current.[8] However, it is desirable that the $\underline{E} \times \underline{B}$ electron Hall current should have a closed circuit[9] to prevent charge build-up as in the cylindrical geometry shown in Fig. 2. This principle of magnetic insulation has proved very useful and cylindrical magnetic diodes[10,11,5] with the anode design of Fig. 1 have been successfully operated in the voltage range 100 kV to 10 MV. Child-Langmuir current densities are easily achieved and for $B >> B^*$ it could approach the ideal efficiency. The diode current is adjusted by varying the ion emission surface. Beams are extracted through cathodes provided with slots, and such diodes survive several hundred shots.

If a closed circuit is not provided for the electron Hall current as in the parallel plate diode[12] shown in Fig. 3 then an interesting phenomena occurs when $B > B^*$. At this value of the field the electrons are prevented from crossing the gap and the Hall current begins to flow orthogonal to $\underline{E}$ and $\underline{B}$. RF emission is observed[12] at just at this field (Fig. 3). The probable cause of this emission is the build-up of space charge at the ends leading to RF emission by some "diocotron-like" mechanism. This emission has the effect of

allowing the electrons to cross the gap thus shorting the build-up of charge. In equilibrium the total current is the sum of the ion current I_i and the Hall electron current, $I = I_i + I_H$, where $I_H = I_{CL}(d/L)(B^*/B)$ for $B > B^*$, I_{CL} is the electron Child-Langmuir current, d is the gap and L is the diode length. The planar diode perveance $P = I/V^{3/2}$ is therefore higher than for a cylindrical diode of the same area.

In situations where the self-magnetic field of the diode current becomes comparable to the external field the analysis gets quite complicated. In the complete absence of an external field pinching of the electron flow takes place at high currents. If the anode is ion emitting by virtue of the energy deposited by the pinch the ratio of the ion current to electron current has been shown to be: $I_i/I_e = (m_e/m_i)^{1/2}(R/d)(B/B^*)$ where R is the cathode radius.[13a,b] But as an ion source the pinch suffers from potentially higher divergence, electrode damage and somewhat less controllable discharge. It is possible that self-fields, which are unavoidable, could be used to advantage in different geometry.[14]

III. ION BEAM EXTRACTION AND PROPAGATION

Propagation in Vacuum

Early experiments[2b] in which an ion beam from a reflex triode was allowed to propagate in a drift tube at a pressure of $\lesssim 10^{-4}$ Torr with no magnetic field, showed dramatically that the ion beam emerged completely neutralized from the cathode. The drop in beam energy density measured calorimetrically as a function of distance was explained in terms of the geometrical beam divergence. Without neutralization the beam would be unable to propagate more than a few mm. It is in this property that intense ion beams differ notably from relativistic electron beams which require a gas or plasma environment for neutralization and propagation. The source of these electrons has not yet been resolved in detail but presumably they could originate from the region of the virtual cathode. These beams were also magnetically neutralized indicating that the mean drift velocity of the neutralizing electrons is approximately the same as that of the ions.

Propagation Across a Magnetic Field

Several experiments have been performed to investigate the propagation of ion beams across a uniform magnetic field using magnetically insulated diodes as a source. For the configuration shown in Fig. 2 the measured ion current density as a function of radius[11] is shown in Fig. 2 (inset). This shows that the

ion beams follow approximately single particle trajectories; in other words space charge neutralization along the magnetic lines of force has occurred. In this particular experiment a small fraction of the ion beam was allowed to impinge on a plastic surface thus providing a synchronized source of electrons. In the second experiment[12] shown in Fig. 3a the ion beam emitted from a planar diode spiralled down the magnetic field for a few turns. This is evident from Fig. 4, where the response from several ion collectors spaced down the axis is plotted as a function of axial distance. Note that ion are rotating close to their gyro-period. Magnetic probe measurements on the axis show diamagnetic fields of 140 G maximum indicating a circulating current of $\sim$ 110 A/cm, which indicates that magnetic neutralization does not occur, in contrast, to field-free propagation. This result is not surprising since for complete magnetic neutralization a radial electric field $E_r = Bv_i/c$ would be required. If the radial thickness of the beam is approximately an ion Larmor radius thaen the potential ϕ is given by $e_i\phi \simeq m_i v_i^2$;;here v_i is the ion azimuthal velocity. Potentials of this magnitude cannot be set up without breakdown occurring and neutralization therefore takes place by electron currents along the lines of force.

IV. ION BEAM FOCUSING

Geometrical Focusing

One can take advantage of the propagation features of intense ion beams to geometrically focus these beams. An experiment using large area cylindrical magnetically insulated ion diode was (see Fig. 5) performed to confirm this possibility.[5] The cathode was constructed of aluminum rings 0.64 cm thick and spaced 0.80 cm apart. Since the magnetic field is pulsed, the cathode rings prevent the flux from penetrating into the interior region. This arrangement provides magnetic insulation in the A-K gap but allows the ions to propagate inwards in a field-free region, as shown in Fig. 2a. Ion collector probes and damage on target plates give evidence of beam convergence. However, since the ions suffer a small deflection in the A-K gap they do not all reach the axis but miss it by an amount $\Delta \alpha dB$ where d is the A-K gap distance and B is the insulating field. This is verified by the fact that the damage pattern on both sides of either plate are offset from each other by Δ. Ion current densities up to 90 A/cm^2 are observed over an area of 1070 cm^2. The total ion current $\lesssim 10^5$ A with an efficiency estimated at 45% to 70%. Damage to targets appear to indicate a 10:1 radial focusing and over 500 A/cm^2

has been observed using biased charge collectors at the focal region. By examining each of the beamlets emerging from spaces between the cathode rings we estimate a radial and axial divergence of no more than 3° and 5° respectively.

The region interior to cathode is next filled with a steady bias magnetic field opposite in direction to the pulsed field used for gap insulation. By adjusting this bias field $B_{int} \simeq -B\ d/R$ where R is the cathode radius the ion trajectories can be brought together to meet at the line focus (see Fig. 6).

Magnetic Focusing

The use of magnetic lenses for focusing low current unneutralized charge particle beams is well known in high energy accelerators. A priori it is not obvious that such lenses could influence charge neutralized intense ion beams which appear physically more closely related to a highly directed plasmoid. However, in view of the experimental evidence supporting the concept of single particle trajectories for such beams, an experiment (see Fig. 7) to test the focusing of an ion beam by a simple dipole lens is in progress. The "field-inclusion" diode used as ion beam source for this particular experiment is unique in that the insulating magnetic field is almost entirely enclosed within the A-K gap allowing the beam to emerge into a field-free region.[15] This feature is very useful when ions are required to be injected into a field-free region. The cathode is shaped like a θ-pinch coil which is energized from a capacitor bank to produce the insulating field. The anode is within the coil and the pulsed field is contained in the region between the cathode and anode.

Preliminary results are shown in Fig. 7. The current density at a particular z-location is plotted against the amp-turns in the dipole lens. There is clear indication of focusing. Particle simulation of ion trajectories in the dipole field also shows such beam focusing.

V. APPLICATIONS TO FUSION RESEARCH

Many of the potential uses to which intense ion beams can be put in fusion research have been anticipated in discussions of relativistic electron beam applications. However, there may be significant advantages in many cases to replacing electron beams with ion beams, e.g. for heating plasmas in a long solenoid reactor.[16] Let me discuss two of these applications.

Pellet Fusion

Calculations[17a,b] of the energy deposition of 1-10 MeV proton beams in

gold foils have shown that the power levels required for breakeven with protons are as low as 60 TW, an order of magnitude less than that required with electron beams. This option has provided a serious impetus for ion beam research. A reactor chamber is likely to be 10-15 m in radius to contain the products of thermonuclear burn and the question of beam transport and focusing over this important for success may favor protons or even heavier ion.[18] Now the strong focusing achieved in electron diodes is a result of strong self-magnetic fields produced by beams with $\nu >> \gamma$; $\nu \equiv Nr_e$ is the Budker parameter, N is the number of electrons per cm and r_e is the calssical electron radius, γ is the usual relativistic factor. However, this very facility for self-focusing makes transport difficult because the self magnetic fields can give rise also to unwanted instabilities, like the "pinch" and "kink" modes. Increasing the particle mass reduces ν/γ in proportion, so that a proton beam of the same power is less unstable than an electron beam. Moreover, such beams do not require an ambient gas or plasma for electrostatic neutralization and are also magnetically neutral when propagating in vacuum. Since the equilibrium self-fields are small, focusing of such beams can only be accomplished either by appropriate geometrically shaping of emission surfaces or by external magnetic fields as discussed in Sect. IV. A conceptual design[11] for a spherical, magnetically insulated, 10 MV, 12.6 MA diode can achieve 63 TW on a target 1.5 mm dia., with the anode Child-Langmuir current density at 5 kA/cm^2 for an emission area of 2625 cm^2. But in order to focus the beam on the target it is necessary for the beam divergence not to exceed 0.5° and for the radius of the sphere to be within 25 cm. Because of this small radius of curvature of the emitting surface such a device cannot serve as the basis for a reactor design. Thus geometrical focusing cannot lead all the way to a reactor. However, if magnetic focusing of these beams is practical, and preliminary indications from a small scale experiment appear to justify some optimism, then intense proton beams could be viable as the "ignitor" for pellets but further improvements in identifying and reducing the sources of beam divergence are necessary.

Field Reversed Ion Rings

A field reversed configuration obtained by injection of ion beams into a magnetic mirror similar to the Astron like geometry produced by relativistic electron beams[19] is another important application for this technology. There are two possible scenarios for a reactor based on this concept. In the first, know as the "Field Reversed Mirror",[20] the closed-line region produced by the

circulating ion current reduces mirror end losses and the system Q is enhanced from the marginal figure just in excess to unity, to about $3 \sim 5$. This arrangement requires a steady sequence of pulses of ions with energy between one and a few hundred keV. One possible mode of injection is to convert the pulsed ion beam into a neutral beam by passage through a charge-exchange grid. This approach is being pursued by Prono[21] at Livermore.

The alternative approach is to form an ion ring by the resistive trapping of an injected 10-20 MeV ion beam. The ring is adiabatically compressed by an external field to increase its energy to a few hundred MeV.[22,23] After compression the D-T plasma confined within the closed line region is heated by the fast ions and allowed to burn. At the end of the burn phase the ion energy is recovered by adiabatic expansion. There can be more than one ring in the burn region simultaneously to improve the reactor economy.

At Cornell the experimental effort is devoted to the injection and trapping of ion rings. A small experiment[12] which demonstrates the injection and propagation phases has been discussed in Sect. III Fig. 3. The field reversal on axis δB is given by $\zeta = \delta B/B = N_i r_i/R$ where N_i is the number of fast ions in the ring, r_i, and R are the ion classical radius, ring major radius respectively. For $R \sim 10$ cm and $\zeta \lesssim 2$, $N_i = I\tau/e_i \simeq 10^{17}$ is required. For a pulse time $\tau \simeq 10^{-7}$ sec we need an injection current $I \gtrsim 10^5$ A. If pulse duration of a microsecond is feasible in diodes, the margin for success is greatly improved. In any case, the injection system must be designed for high trapping efficiency. Fig. 8 shows a "field exclusion" ring-shaped, magnetically insulated diode[24] whose anode emission surface is made to coincide with a flux surface by adjusting the ampere-turns contained within the anode. All the ions emitted from this surface have the same canonical angular momentum and therefore form a tight rotating bunch with minimum axial and radial spread after passing through the cusp shaped field. Preliminayy experiments have shown that the diamagnetic signal from a magnetic probe on axis are in agreement with the estimates of the circulating ion current. Experiments on the resistive trapping of this ring are in progress. Numerical studies on two dimensional (r,z) particle codes show that the efficiency of resistive trapping improves with the number of injected ions to about 90% at $N \simeq 10^{17}$ for a particular design of the resistors and magnetic field profile.[25]

Finally, I would like to say that intense ion beam technology and physics is still in its infancy and much further work is needed to establish the

nature and extend of its role in fusion research.

ACKNOWLEDGEMENTS

This paper is essentially a review of the experimental work performed at Cornell by P. Dreike, C. Eichenberger, M. Greenspan, S. Humphries, J. Maenchen and L. Wiley; and I am indebted to them for many discussions.

*Work supported by the U.S. Energy Research and Development Administration and the Office of Naval Research.

REFERENCES

1. R. N. Sudan, "Application of Intense Relativistic Electron Beams to Controlled Thermonuclear Fusion", Proc. VI Europ. Conf. on Cont. Fus. and Plasma Phys., Moscow, July 1973, Vol. II, p. 184.

2. (a) S. Humphries, J. J. Lee and R. N. Sudan, Appl. Phys. Lett. 25, 20 (1974); (b) J. Appl. Phys. 46, 187 (1975).

3. S. Humphries, private communication.

4. (a) C. A. Kapatenakos et al., Proc. II Symp. Coll. Methods of Accel., Dubna, 1976, Vol. II, p. 286; (b) C. A. Kapatenakos, J. Golden, F. C. Young, Nucl. Fusion 16, 151 (1976); (c) J. Golden and C. A. Kapatenakos, Appl. Phys. Lett. 28, 3 (1976).

5. M. Greenspan, S. Humphries, J. Maenchen and R. N. Sudan, Phys. Rev. Lett. 39, 24 (1977).

6. D. S. Prono, J. M. Creedon, I. Smith and N. Bergstrom, J. Appl. Phys. 46, 3310 (1975).

7. T. Antonsen and E. Ott, Phys. Fluids 19, 52 (1976).

8. F. Winterberg, Phys. Rev. 174, 212 (1968).

9. (a) R. N. Sudan and R. V. Lovelace, Phys. Rev. Lett. 31, 1174 (1973); (b) G. Bekefi and T. J. Orzechowski, Phys. Rev. Lett. 37, 379 (1976); Phys. Fluids 19, 43 (1976).

10. P. Dreike, C. Eichenberger, S. Humphries and R. N. Sudan, J. Appl. Phys. 47, 85 (1976).

11. S. Humphries, R. N. Sudan and L. Wiley, J. Appl. Phys. 47, 2382 (1976).

12. C. Eichenberger, S. Humphries and R. N. Sudan, J. Appl. Phys. 48, 2738 (1977).

13. (a) J. W. Poukey, Appl. Phys. Lett. 26, 145 (1975); (b) S. Goldstein and R. Lee, Phys. Rev. Lett. 35, 1079 (1975).

14. S. Humphries, Plasma Phys. 19, 399 (1977).

15. L. Wiley, J. Maenchen, R. N. Sudan and S. Humphries, to be presented at 19th Annual APS Plasma Phys. Conf., Atlanta, Nov. 1977.

16. (a) E. Ott and R. N. Sudan, Appl. Phys. Lett. 29, 5 (1976); (b) D. D. Ryutov, private communication.

17. (a) M. Clauser, Phys. Rev. Lett. 35, 848 (1975); (b) J. Shearer, Lawrence Livermore Laboratory Report No. UCRL-76519, (1975).

18. "ERDA Summer Study of Heavy Ions for Inertial Fusion", Lawrence Berkeley Laboratory, July 1976.

19. M. L. Andrews, H. Davitian, H. H. Fleischmann, B. Kusse, R. E. Kribel and J. A. Nation, Phys. Rev. Lett. 27, 1428 (1971).

20. W. C. Condit et al., Lawrence Livermore Laboratory Report No. UCRL-52170 (1976).

21. D. S. Prono, private communication.

22. R. N. Sudan and E. Ott, Phys. Rev. Lett. 33, 355 (1974).

23. H. H. Fleischmann and T. Kammash, Nucl. Fus. 15, 1143 (1975).

24. P. Dreike and R. N. Sudan, to be presented at the 19th Annual APS Plasma Physics Conf., Atlanta, Nov. 1977.

25. A. Mankovsky, R. N. Sudan and J. Denavit, to be presented at the 19th Annual APS Plasma Physics Conf., Atlanta, Nov. 1977.

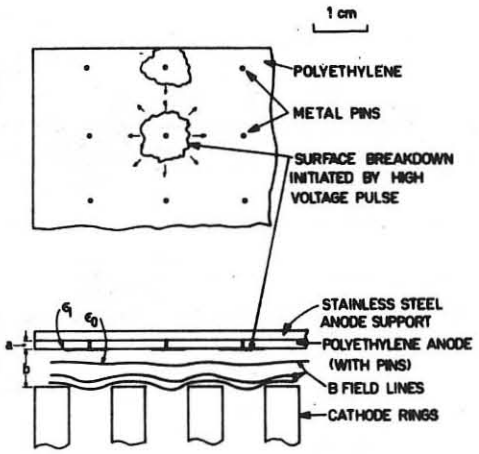

Figure 1

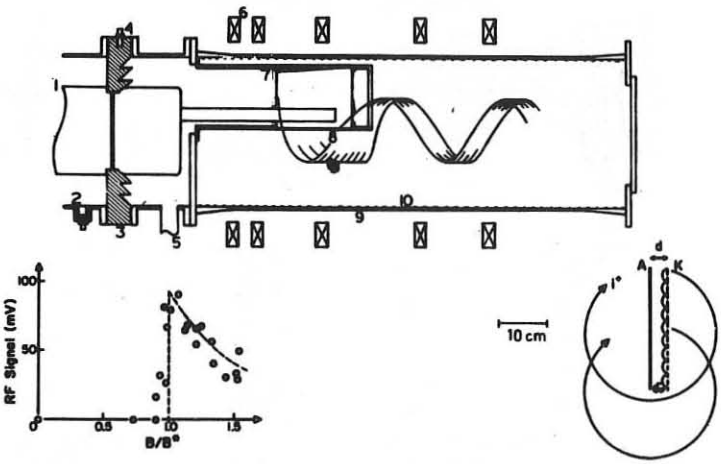

Figure 3

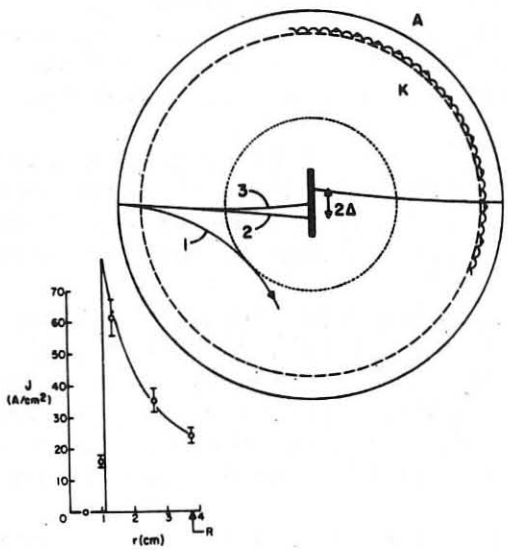

Figure 2

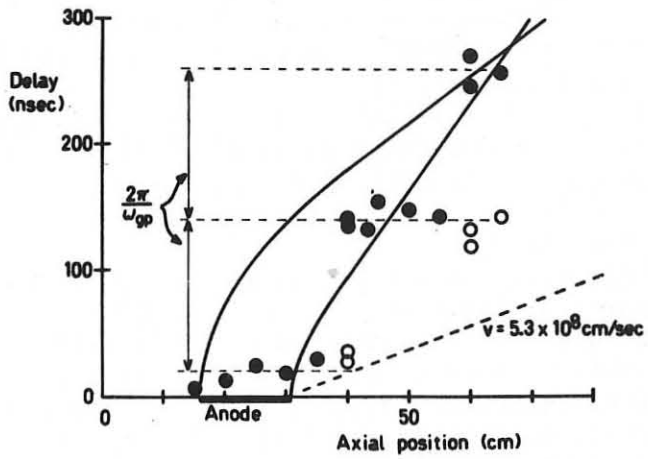

Figure 4

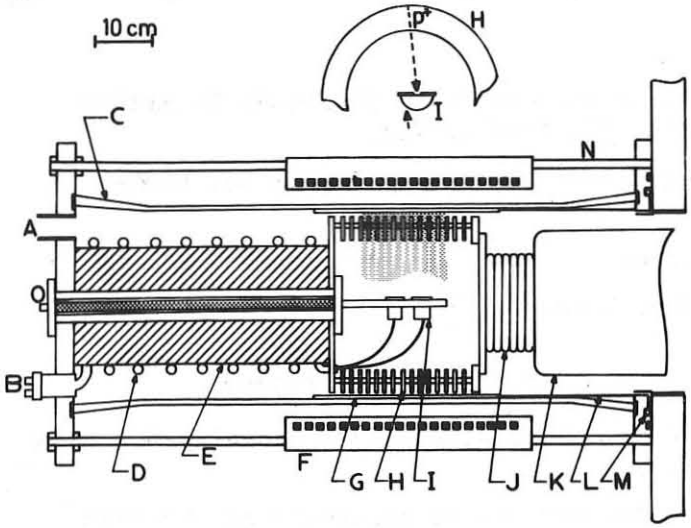

Figure 5

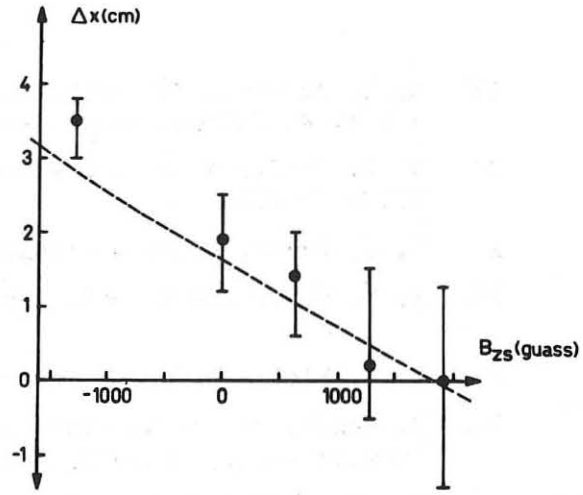

Figure 6

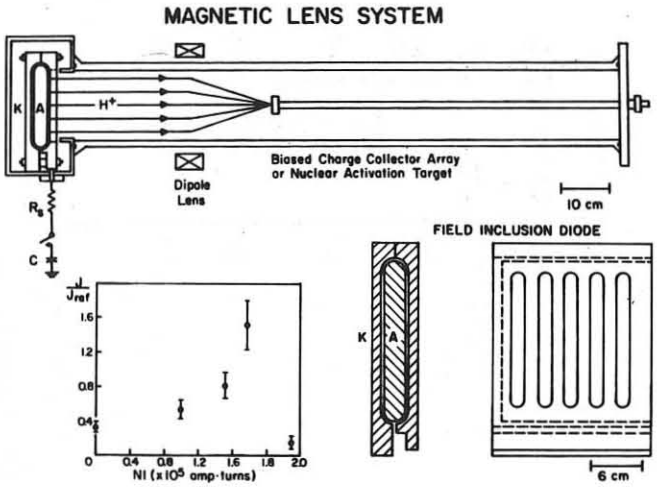

Figure 7

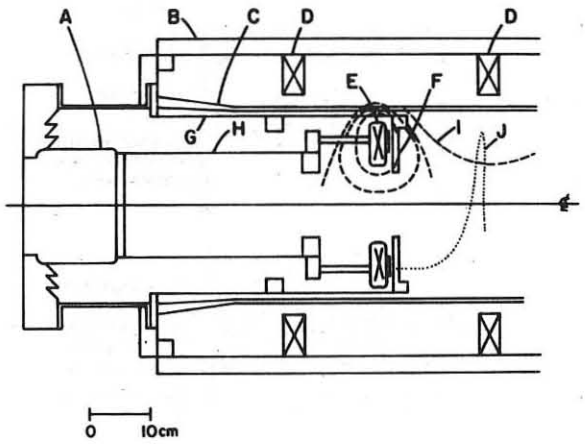

Figure 8

Figure 1. Details of plasma anode for magnetically insulated diode.

Figure 2. Schematic of cylindrical magnetically insulated diode showing electron trajectories and ion trajectories for (1) $B_{int.} = B$, (2) $B_{int.} = 0$ and (3) $B_{int.} = -B\ d/R$. Inset shows observed ion-current density vs. radius for case (1): (Ref. 11).

Figure 3. Parallel-plate magnetically insulated diode for ion injection across field. Inset shows measured RF signal against insulating magnetic field (Ref. 12).

Figure 4. Trajectory of spiralling ion beam injected from diode of Fig. 3 as recorded by magnetic probes plotted as a z-t diagram; $2\pi/\omega gp$ is the cyclotron time (Ref. 12).

Figure 5. Layout of cylindrical geometrical focusing experiment; A, pumping port; B, diagnostic isolator output; C, glass vacuum vessel, 30 cm i.d.; D, diagnostic isolation inductor; E, Delrin support rod; F, 20-turn, 20-kG magnetic coil; G, anode, H, cathode assembly; I, ion-current-density probes; J, bellows for electrical connection; K, high-voltage terminal from the Neptune C generator; L, return conductors; M, Rogowski loop-current monitor; N, support rods; O, resistive diode-voltage monitor (Ref. 5).

Figure 6. Plot of the position Δx of the most intense damage on a plate located on the axis (see Fig. 2) as a function of bias field B_{zs}; dotted line is estimated position.

Figure 7. Layout of magnetic focusing experiment using "field-inclusion" diode. Inset shows plot of relative ion current density at target as function of ampere-turns in dipole lens.

Figure 8. Layout of ion ring injection experiment using annular ring anode: A, Omnipulse Output; B, Experiment Frame; C, Glass Vacuum Vessel; D, External Coils; E, Anode Coil; F, Extraction Cathode; G, Cathode Stalk; H, Anode Stalk; I, Field Lines; J, Proton Orbit Projection.

PRESENT STATUS OF TWO R.F. HEATING SCHEMES : I.C.R.H AND L.H.R.H.

T. CONSOLI

ASSOCIATION EURATOM-CEA
Département de Physique du Plasma et de la Fusion Contrôlée
Service IGn - Centre d'Etudes Nucléaires
85 X - 38041 GRENOBLE CEDEX

ABSTRACT : Among the large number of wave-plasma interaction, Ion-Cyclotron Resonant Heating (I.C.R.H.) and Lower Hybrid Resonant Heating (L.H.R.H.), are two promising additional R.F. heating schemes for toroidal hot plasma. They both offer the advantage of using power generators which requires a moderate development for next generation machines. It seems important to try to state in the limits of this paper the present experimental situation of these two R.F. heating methods as it results from the vast litterature published from the last European Conference (Lausanne September 1975).

L.H.R. COUPLING STRUCTURES AND WAVE LAUNCHING.

The L.H.R. frequency for plasma densities in the range of few 10^{13} to 5.10^{14} and toroidal magnetic B_T between 10 to 100 kG is in the $0,5 < f < 3$ GHz bandwidth (Fig. 1). In this frequency range one can use in preference to loops waveguide launching, which presents obvious technological advantages in the thermonuclear context.

The Grill is a simple and elegant solution (Fig. 2) for launching L.H.R. waves in a toroidal machine which satisfies the accessibility condition. It is provided by an array of 2,4, or more guides /1/, /2/ mounted with their small side parallel to the toroidal magnetic field ; and each guide is excited in the fundamental TE_{01} mode. The phasing between the single elements of the Grill is adjustable, so as to excite in the toroidal vessel a retarded wave. By means of suitable size and phase choice, the average value of $N_{//}$ can be varied in order to heat either the electrons or the ions.

The coupling efficiency of the Grill /2/ depends upon the distance x_p between the edges of the Grill and the plasma, and upon the density gradient $L_n = (n)_{res} \cdot (\frac{dn}{dx})^{-1}_{at\ x = x_p}$. The coupling requires $x_p < (\lambda_{vacuum})_{RF}$.

Other less simple and internal structures in the liner have also been proposed for the excitation of slow waves /3/, /4/.

An excellent experimental verification of BRAMBILLA's Grill theory has been obtained on the Princeton's linear device H_1 with 2 and 4 guide arrays /5/ Fig. 3. The behaviour of the coupling system was, as predicted by the theory, determined by the plasma parameters near the antenna.

An apparent disagreement between BRAMBILLA's theory and the experiment was noted when a four guide Grill was used on A.T.C. for the E.L.D heating. Later this disagreement was explained by an error in the calibration of the phase of each guide of the Grill /6/. Once the real values of the phases 0, 0, π π and 0 π π 0 established, theory and experiment agree again.

Coupling by one loop (Tokamak TM_3 and LIWEREX linear machine) or two phased loops (WEGA) or 22 ring slow wave structures (F.T.I) have been used with success. On WEGA when the two loops are well matched, a transmission of 95% of the input power is obtained. The phasing of the loops is important according to the density where they are immersed.

LOWER HYBRID WAVE PROPAGATION, RESONANCE CONE.

The L.H.W. propagation and the resonance cone has been observed by many authors /7/, /8/. A clear experimental demonstration was made by P. BELLAN and M. PORKOLAB /9/ in the Princeton L_3 plasma column. The dispersion relation and wave packet propagation was verified. The wave packets were experimentally localized in space. They propagate as predicted by the theory along two resonance cones which make a small angle with respect to the confining magnetic field. The waves were damped by E.L.D. and as result the main body of electrons was heated and high energy electron tail was observed.

L.H. WAVE HEATING.

Ion heating of a linear or toroidal plasma using L.H.R. mode has been studied at Garching (LIWEREX) at Kurchatov (TM_3) /10/, at M.I.T. (ALCATOR), at the IOFFE Institute (F.T.I.) at Princeton (A.T.C.) /11/ and at Grenoble (WEGA) /12/. The F.T.I. experiment (see 3) aimed at the study of the

production of fast ion tail during L.H.R.. A flux of fast neutral of high energy (~ 1 keV) was observed during the H.F. pulse. This flux increases sharply when L.H.R. conditions are met. This leads the authors to the conclusion that the fast ion production occurs mainly in the L.H.R. region, and takes about 15% of the input power. This conclusion is in contradiction with what has been observed on the WEGA and A.T.C. Tokamaks. The application of the H.F. pulse did not change the current, the loop voltage and the equilibrium of the discharge. A small increase (10 % - 25 %) of the density and of the electron temperature T_e in the central part of the discharge was noticed. The A.T.C. and WEGA which are very similar were conducted with improved experimental conditions. A better understanding of L.H.R.H. was thus possible. The double loop on WEGA and the double guide Grill on A.T.C. in opposite phases are very appropriate coupling structure. Almost complete transmission (> 95%) has been obtained with matching. Natural matching was excellent (70 % - 80 %) and in agreement with theoretical predictions.

The heated component (electron or ion) depends strongly upon the $N_{//}$ energy spectra excited by the slow wave coupling structure. For low average $N_{//}$ ion heating should prevail according to linear or parametric instability theory, while for $N_{//} \gtrsim 5$ electron Landau damping should prevail. The former conditions prevail in LIWEREX, TM_3 (Fig. 4a), F.T.I., ALCATOR, A.T.C. (Fig. 4b), WEGA (Fig. 4c). The fate of the transmitted energy is still not completely understood. On the one hand as it appears from the A.T.C. and WEGA results, the charge exchange analysis (Fig. 4b and 4c) and DOPPLER broadening on impurity lines as O^{VII} (Fig. 5a-b) /11/, /12/ show that the ions of the bulk are heated ; on the other hand an energetic tail in the ion energy distribution is observed in the charge exchange curves. The fast ions have after the R.F. pulse a life time shorter than 100 μs (Fig. 4c), which means that they are produced in the outer layer of the plasma and badly confined since they are lost after so short a time. As a verification, the WEGA group has shown that fast neutral flux is progressively reduced when a collecting plate is pushed deeply in the tenuous plasma (Fig. 6) /12/.

The location of O^{VII} ions is known by the radial electron temperature profile $T_e(r)$. This temperature is determined by THOMSON scattering, radiometry and soft X-ray methods. The highly ionized oxygen ions are very deep inside the plasma, at few cm from the axis of the discharge. Experiments

with and without R.F. heating prove without any ambiguity that bulk plasma heating occurs.

During the R.F. pulse on the WEGA device, it has been observed that the electron temperature remains quite constant, while the electron density and the loop voltage increase. For a constant applied R.F. power the density increase is proportional to the pulse length.

However the increase of T_i cannot be attributed to the improved efficiency of ohmic heating, due to gas or impurity influx produced by the R.F. /12/. An equivalent increase of density has been simulated with light neutral gas (D_2) puffing. It has produced a variation of T_i less than 30% of that produced by the R.F. power, and with a different time history. The bulk heating is then reliable ; what still remains undetermined experimentally is the sharing of the transmitted power among the wall, the low density plasma, the ion tail and in the bulk ions.

The observed heating has been simulated with the Fontenay's code. The results of the gas puffing experiments were nicely reproduced by assuming a reasonably enhanced neutral in flux from the wall. On the other hand to reproduce the results of the R.F. experiment it was necessary to suppose an energy source in the ion energy balance of about 50 kW localized at $r/a \lesssim 0{,}5$ (for larger radii the energy confinement time was too low for a built up of T_i to be observed) in agreement with the experimental measurement through O^{VII} DOPPLER broadening.

CONCLUSIONS ON L.H.R.H.

The coupling of a waveguide array to a plasma is effective. Reflection coefficient of 95% can be obtained, when the Grill is well matched. Heating of ions and electrons of the plasma bulk has been shown by correlated charge exchange analysis and O^{VII} line DOPPLER broadening. Tails in the ion or electron energy distributions have been observed. They are correlated with parametric instabilities in the R.F. noise spectra. These instabilities are a general but not necessarily dominant process in L.H.R.H., it might be possible to avoid them in the future. No deleterious effects on the M.H.D. equilibria have been observed.

The distribution of the transmitted R.F. energy between the wall, the tenuous plasma and the bulk is not yet known. However it has been possible to double the ion temperature of the bulk plasma in a Tokamak. The recent results on WEGA suggest that 30% of the launched power could be transferred to the bulk ions.

ION CYCLOTRON WAVE LAUNCHING AND COUPLING.

I.C.R.H. has also been the object of an intense theoretical and experimental research during these last two years /13/-/15/. In the I.C. waves frequency range, coupling can be facilitated by the existence of cavity eigenmode in the plasma loaded toroidal chamber.

These modes were first observed in 1971 by V.L. VDOVIN et al. /16/ and by N.V. IVANOV et al. /17/ and analyzed theoretically in a series of publications /13/ to /21/.

The existence of toroidal modes is beneficial in that it enhances the plasma loading of the launching structure and allows efficient heating of the plasma. In medium size devices the eigenmodes are well separated. Mode selection requires an appropriate antenna design and needs mode tracking /22/. The situation is not so good for fusion reactor /26/. In large devices, the toroidal cavity becomes highly oversized so that the modes are so dense that their selection might be impossible. It seems then difficult to extrapolate present experiments on fast waves "mode physics" to fusion device.

The coupling of R.F. energy to the fast toroidal eigenmodes is obtained generally by loops. It has also been proposed to use special wave guides /23/, /24/ (ridge wave guides and loaded wave guides) in large torus ($2a > 3m$) and at high magnetic field ($B > 50$ kGs). For loaded guides, as an example, with titanium dioxyde, the dielectric has to be protected by Faraday shield. In both cases, loop and guide, the antennas must be matched to the toroidal loaded cavity by external circuits.

I.C.R.H. IN TOROIDAL DEVICE.

V.L. VDOVIN et al. /25/ have shown on the Tokamak TM_1, wave generation and heating of ions at $\omega_{RF} = n\omega_{ci}$, $n = 1,2$ in a Deuterium plasma. The

wave launching system consisted of two asymmetrically placed coupling coils insulated with a quartz jacket, and placed along the plasma column. For a correct phasing the efficiency $P_{wave}/P_{emitter}$ of this launching system is up to 80-90% and only 40-50% in the case of one symmetrical loop. The modes generated in the plasma were identified and their attenuation along plasma measured by R.F. probes.

Charge exchange analysis shows an increase of the perpendicular ion temperature of 100 eV for an R.F. power comparable to the ohmic heating (~ 60 kW). The perpendicular energy distribution has a tail corresponding to an ion population of 430 eV (Fig. 7) as in the case of L.H.R.H.

The efficiency of magnetosonic waves heating at $2\omega_{ci}$ was about 30-40% and a little less at ω_{ci}. The lifetime of the bulk ion was 200-300μs and that of the fast ions of the tail much less.

In connection with the energetic ions of the tail, strong neutral influx is observed, which has as a consequence to increase the rate of energy exchange between ions and electrons. A very important result of this experiment was the presence of a small percentage of protons in the chamber (of the order of 1%) which strongly decreases the quality factor of the modes from the theoretical expected value. The two ion hybrid resonance appear to be at the origin of the observed anomalous damping.

The situation is different in large Tokamaks, where the role of hydrogen will be negligible, the ratio $(\frac{\text{Area}}{\text{Vol}}) \sim \frac{1}{R}$ being reduced. It is hoped that in high discharge current and high magnetic field the energetic ions of the tail will be better confined, and this will prevent the bombardment of the walls. J. ADAM et al. /26/ have investigated I.C.W. generation and damping between ω_{ci} and $2\,\omega_{ci}$ at low R.F. power on the T.F.R. Tokamak in addition to the two ion hybrid mechanisms previously observed by V.L.VDOVIN. High Q modes where found at $\omega_{RF} = 2(\omega_{ci})_H$ in an hydrogen plasma, but not at $\omega_{RF} = 2\,(\omega_{ci})_D$ in a deuterium plasma. This effect can be attributed to the existence of a resonant layer where the fast wave is converted into a slow mode, if $\omega_{RF} < (\omega_{ci})_H$. In addition J. ADAM et al. have shown the feasibility of mode tracking resonance conditions. A selected mode has been maintained by this method during 5 ms, in a time varying density plasma.

I.C.R.H. ON THE S.T. AND A.T.C. TOKAMAKS.

In these Tokamaks the coupling structures are single or multiple (2 or more) phased, electrostatically shielded, fractional (length of the loop $\lesssim$ cross section perimeter) loops. In both Tokamaks the majority of the diagnostics used in L.H.R.H were in operation.

In both machines, it was possible to determine the perpendicular and parallel components of the ion temperature by both charge exchange and spectroscopic measurements. The second charge exchange neutral detector looking tangentially was located on the opposite side of R.F. coils. It is then reasonable to assume that the entire plasma was at the temperature indicated by this detector.

The main results at $\omega_{RF} = 2\ \omega_{ci}$ reported in /27/ can be summarized as follows. Using two half turn coils separated by half a wave length, it has been possible to reach a wave generation efficiency (at 25 MHz) up to 90% and a plasma loading in good agreement with theory. The experiment shows that the I.C.W. is strongly damped. For fast wave excitation the R.F. probes along the torus reveal the propagation of the wave many times around the machine and consequently the predicted m = - 1, n = 4, $\rightarrow$ 8 toroidal eigenmodes are observed. The measurement of loading resistance versus time exhibits periodic splitted peaks which were explained theoretically as the effect of the poloidal magnetic field. When 70 kW, 5-10 ms R.F. pulses were applied at $2\ \omega_{ci}$ to a ($n = 6 \times 10^{12} cm^{-3}$) D_2 plasma, perpendicular and parallel charge exchange neutral analysis showed the considerable ion heating ($\sim$ 100 eV), 20 % efficiency and the formation of an energetic anisotropic ion tail (Fig.8). Comparing $T_{\perp i}$ and $T_{i//}$, it appears that $T_{i//}$ increases more slowly (Fig. 9) than $T_{\perp i}$ and decreases approximatively with the same slope. DOPPLER broadening measurement gave similar results. No variation of T_e and loop voltage was observed. Unfortunately, an important influx of neutral particles is associated with the R.F. pulse and probably with the fast ion tail. This influx produces constriction of the current channel which evolves into MHD instability. The injected R.F. energy in S.T. was thus limited to about 1 KJ.

Another consequence of the impurity influx is the increase of the electron-ion equipartition rate and thus of the ohmic heating of the ions. The density variation during the R.F. pulse has been simulated with neon gas puffing during 10 ms. As a result it appears that the observed ion heating must be partially attributed to impurity influx.

On A.T.C. the perpendicular and tangential ion energies were determined by three different methods /28/ :

a) charge exchange neutral particle analyzer (with three channels perpendicularly and only one channel in the direction of the toroidal magnetic field).

b) Spectroscopic measurement of T_i by O^{VII}, C^{V} and C^{IV} DOPPLER broadening.

c) Neutron counting after R.F. heating followed by magnetic compression.

Here again these measurements indicated a body heating with (ΔT_i) up to 200 eV for an applied R.F. power of 145 kW during 10 ms with an important tail in the distribution function of the ions. This tail may again consist of protons present in small quantities in deuterium plasma.

There is some evidence that body ions are heated, because $(\Delta T_i)_\perp$ and $(\Delta T_i)_{//}$ obtained by charge exchange and DOPPLER broadening are comparable, and also because the temperatures reached by adiabatic compression are in agreement with the predicted increase due to compression for an initial temperature resulting from the R.F. heating. Finally the positions of O^{VII} and C^{V} lines which were determined by optical measurement of T_i and $T_e(r)$, give an information on the heated regions.

The heated plasma relaxes after the R.F. pulse in few milliseconds. This relaxation time is consistent with the calculated ion energy replacement time (Fig. 10). Although the test of neon gas puffing has not been made on A.T.C. to simulate, an improved electron-ion energy exchange triggered by impurity influx, the authors of Ref./28/think that the measured heating is mostly attribuable to the R.F. pulse. On the other hand no significant deterioration of the energy confinement by R.F. pulse was observed.

The most recent experiment on I.C.R.H. on a Tokamak has been made on T_4 by Buzankin et al. (Proc. of VIth I.A.E.A Conference Berchtesgaden, 6-13 October 1976, Vol. III p.61), in a deuterium plasma containing a known small percentage of hydrogen. This experiment has demonstrated the preferential heating of protons, with the formation of a tail only on the proton population when I.C. resonance was excited.

No bulk heating and tail were observed out of resonance and far from the antenna. Near the antenna, due to near field effect, local heating occurs.

The same experiment has also shown the existence of an upper limit in the injected power. Above 50 kW disruptive instabilities were triggered as on ST, by impurity influx due probably to the wall bombardment.

In summary the threshold for these instabilities was, 50 kW on T_4, 100 kW on ST, more than 140 kW on A.T.C.. This threshold seems to depend on the geometrical and physical parameters.

IN CONCLUSION.

- ST. and A.T.C. experiments have clearly demonstrated body heating.
- TM_1 and T_4 devices have shown the role, in the R.F. energy absorption, of a small percentage of H, when I.C.R. is excited. This effect will be exploited in the case of a two component (D,T) plasma.
- The formation of a tail only in the proton energy distribution rises the question on the nature of the ions in tails observed in all I.C.R.H. experiments.
- Disruptive instabilities triggered in S.T., A.T.C., T_4 were likely due to the impurity influx and not to the R.F pulse. This influx can be attributed to wall bombardment, or to an uncontrolled displacement of the discharge, or to another presently unknown cause.
- In large devices the density of toroidal eigenmodes in the frequency domain imposes mode selection and needs mode tracking.
- The selection of the desirable mode might be unresolvable if the frequency domain becomes near continuous.
- It seems impossible to extrapolate present experiments on fast wave mode physics to fusion device.

Experiments planned on large machines as T.F.R. 600, PLT, JET, will provide the appropriate correct conditions for the required next steps. Systematic research with improved diagnostics are needed to reach the reliability required for the thermonuclear reactor.

If the present effort is maintained the evolution in the next ten years of these R.F. heating methods compared to neutral beam heating, might be as on the diagram represented on Fig. 11.

ACKNOWLEDGEMENTS.

I should like to express my appreciation to Drs. M. BRAMBILLA P. LALLIA and J. ADAM for helpful discussions.

REFERENCES.

/1/ - P. LALLIA, Proc. of the II Topical Conf. on R.F. Plasma Heating, Lubbock (Texas) June 20-22 (1974) and Proc. of the Varenna Symposium, September 4-17 (1974).

/2/ - M. BRAMBILLA, Review of the Grill Theory, Workshop on L.H.R.H., M.I.T. 10-12 March 1977.

/3/ - I.P. GLADKOVSKY et al., paper presented at this Conference.

/4/ - Y.F. BARANOV, III^{d} Int. Meeting on Toroidal Plasma Heating, Grenoble 28 June - 2 July 1976.

/5/ - S. BERNABEI et al., P.P.P.L. 1288, September 1976.

/6/ - W. HOOKE, Private communication.

/7/ - R.K. FISHER, R.W. GOULD, Phys. Fluids, 14, 857, 1971 ; R.J. BRIGGS, R.R. PARKER, Phys. Rev. Lett. 29, 852, 1972.

/8/ - R.R. WEYNANTS, III^{d} Int. Meeting on Toroidal Plasma Heating, Grenoble 28 June - 2 July 1976.

/9/ - P. BELLAN and M. PORKOLAB, Matt 1090, November 1974, and Matt 1196, January 1976.

/10/ - V.V. ALIKAEV et al., Zh. Tech. Fiz., 45 March 1975.

/11/ - S. BERNABEI et al., Proc. of the III^{d} Symp. on Plasma Heating, Varenna 6-17 September 1976.

/12/ - J.G. WEGROWE et al., paper presented at this Conference.
P. BLANC et al., Proc. of the III^{d} Int. Meet. Grenoble 28 June - 2 July 1976.
P. LALLIA, Proc. of the III^{d} Symp. on Plasma Heating, Varenna 6-17 September 1976.
G. PACHER et al., Bull. of Meet. of A.P.S. San Francisco, November 1976.
G.F. TONON et al., III^{d} Int. Conf. on Waves and Instabilities in Plasmas, Palaiseau, June 27 - 1st July 1977.

/13/ - J. ADAM, A. SAMAIN, Report EUR-CEA-FC 709.

/14/ - R.R. WEYNANTS, Phys. Rev. Letters, 33, 78 (1974).

/15/ - J.P.M. SCHMITT, Observation on resonant heating at $n\Omega_{ci}$ to be published in Phys. Rev. Letters, February 1977.

/16/ - V.L. VDOVIN et al., Sov. Phys. JETP Letters, 14, 149 (1971).

/17/ - N.V. IVANOV et al., Sov. Phys. JETP Letters, 14, 138 (1971).

/18/ - F.W. PERKINS, Symp. on Plasma Heating and Injection, Varenna (1972), Proc. of the III^{d} Int. Meeting, Grenoble 1976, Vol. II, p. 373.

/19/ - J. ADAM, J. JACQUINOT, Report EUR-CEA-FC 886, April 1977.

/20/ - W.M. HOOKE et al., PPPL, 19 Avril 1976.

/21/ - T.H. STIX, PPPL, Matt 1113, 1975.

/22/ - J.C. HOSEA and F.J. PAOLONI, Bull. Am. Phys. Soc. 20, 1243 (1975).

/23/ - F.J. PAOLONI, Matt 1173, December 1975.

/24/ - E.P.R.I. Research Project, ER-28, September 1976.

/25/ - V.L. VDOVIN et al., Third Int. Meeting on Plasma Heating, Vol. II, Grenoble 1976.

/26/ - J. ADAM, Equipe T.F.R., Proc. of the VIth I.A.E.A. Conf. Berchtesgaden 6-13 October 1976, Vol. III, p. 39.
J. ADAM et al., Proc. of the VIth I.A.E.A. Conf. Tokyo 11-15 November 1974, Vol. 1, p. 65.

/27/ - J.C. HOSEA, Proc. of the Symposium on Plasma Heating, Varenna, September 1976, p. 55.

/28/ - H. TAKAHASHI, Matt 1140, October 1975 ;
H. TAKAHASHI et al., PPPL 1332, March 1977.

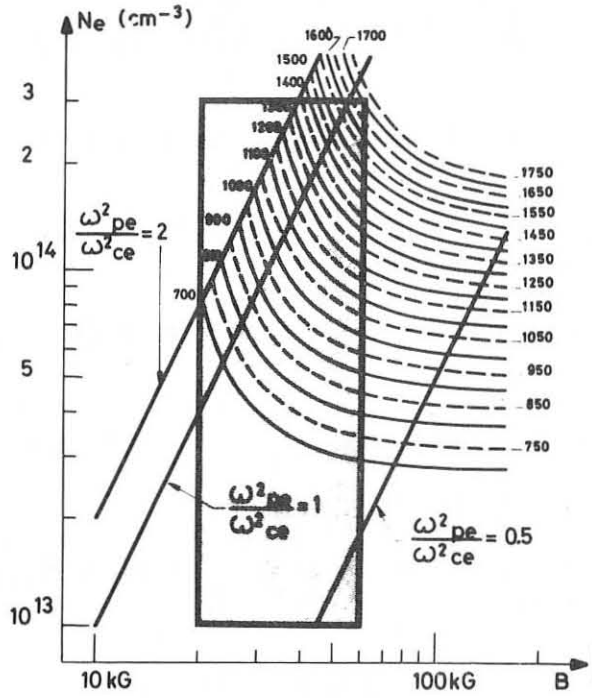

Fig.1 - LHR frequencies as a function of B_T, n_e

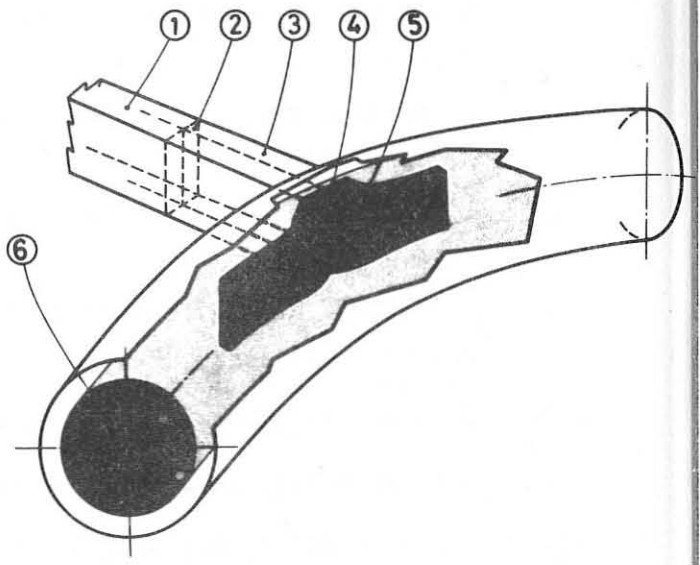

Fig.2 - The two guide GRILL for L.H.W. Launching
1-The splitted guide, 2-Vacuum window, 3-Connecting movable section. Crossing zone of the two L.H.R. cones, 5-Axially propagating waves, 6-The plasma core.

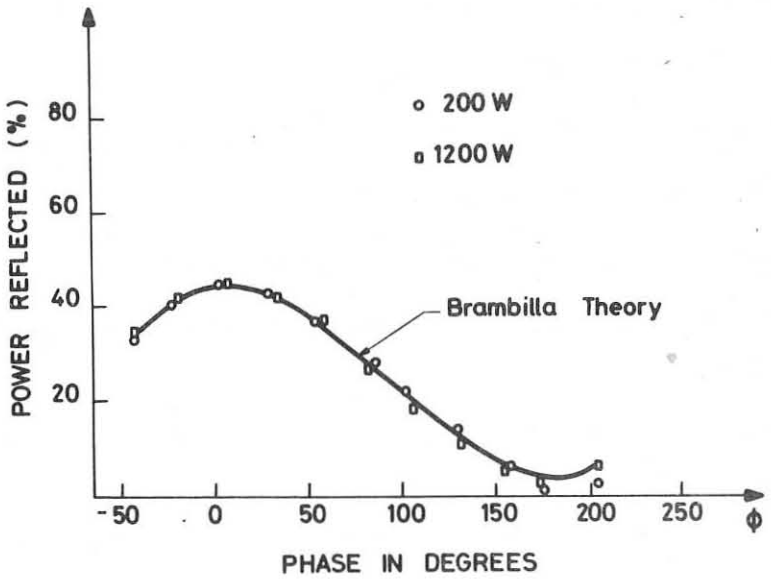

Fig.3 - Reflected power as a function of the phasing between the two guide (Princeton's H_1 experiment) from ref. /5/.

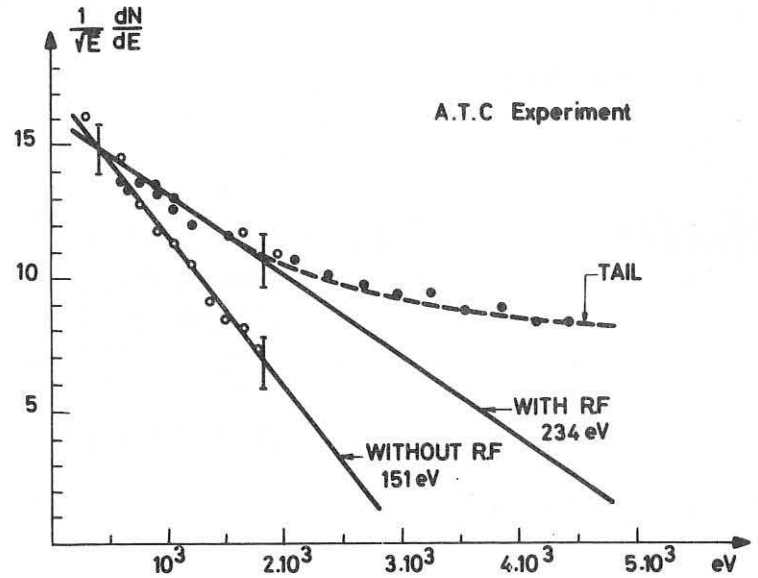

Fig.4a - Ion energy distribution on A.T.C. (measured by charge exchange) from Ref. /11/.

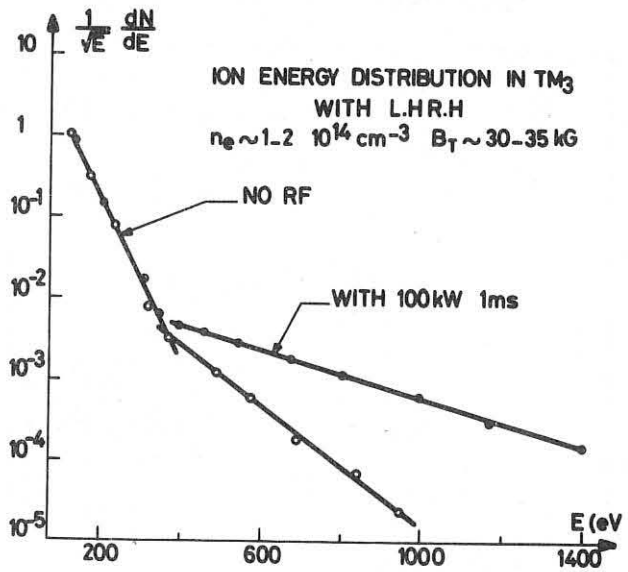

Fig.4b - Ion energy distribution on TM_3 (measured by charge exchange) from Ref. /10/.

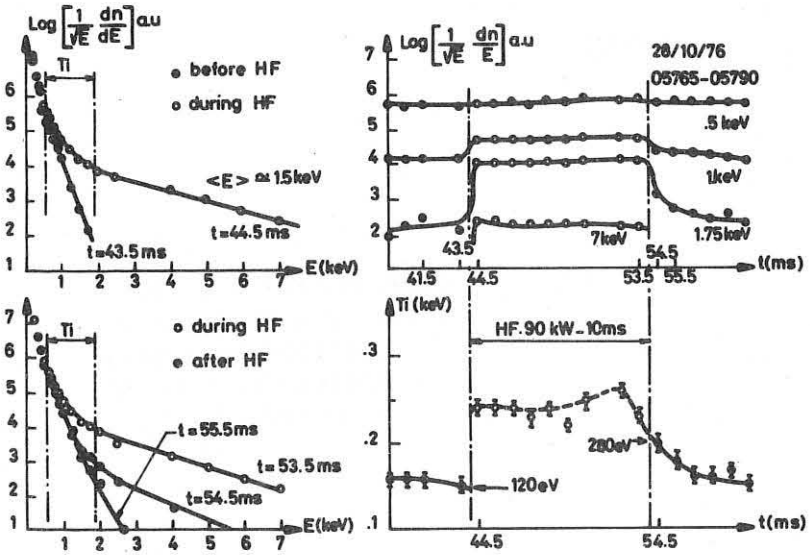

Fig.4c - Detailed analysis of the ion energy distribution of the bulk and the tail on WEGA. from Ref. /12/.

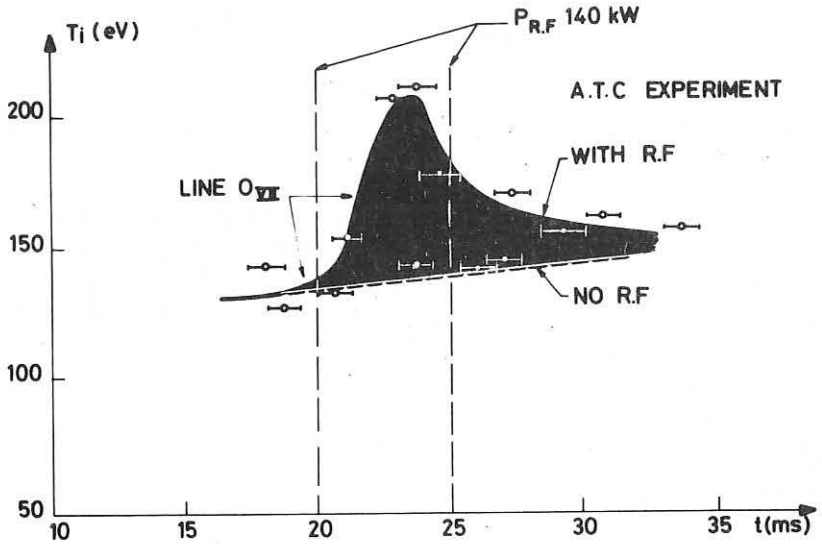

Fig.5a - T_i determination by Doppler broadening of O_{VII} line on A.T.C. (from ref /11/)

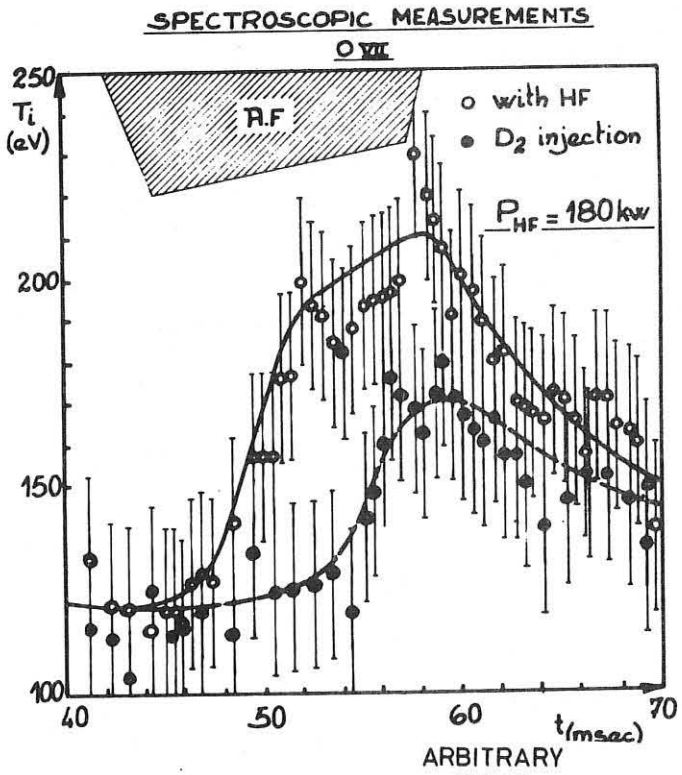

Fig.5b - Same measurements on WEGA. (from Ref /12/) upper curve with R.F. injection, lower curve with D_2 injection.

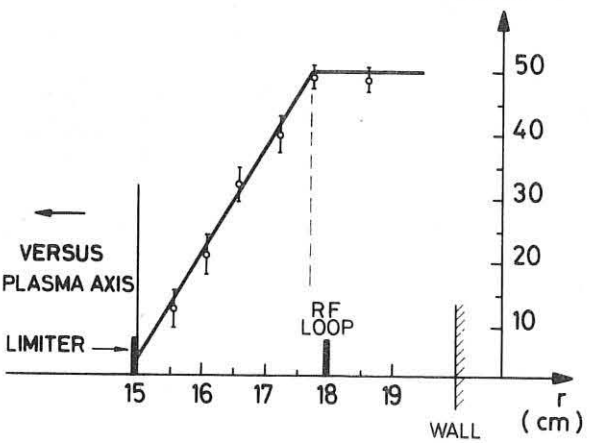

Fig.6 - Fast neutral flux at 3 keV as a function of the position of a movable collecting electrode (from Ref. /12/).

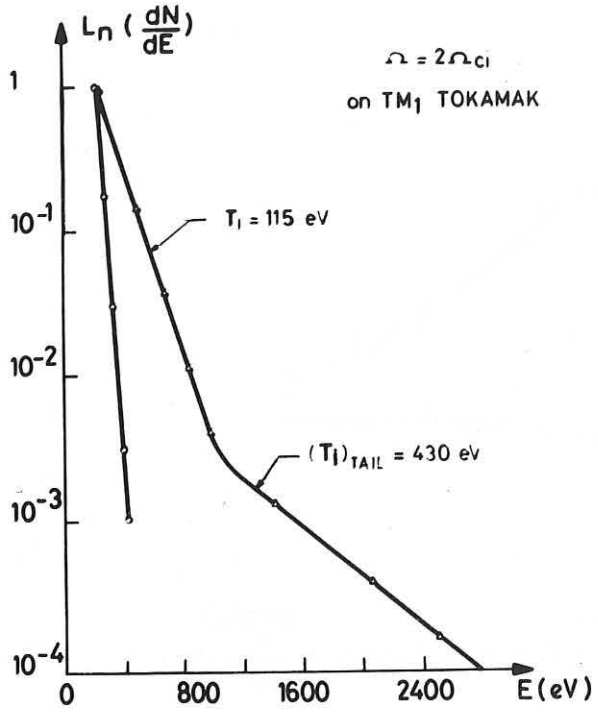

Fig.7 - Ion energy distribution by charge exchange on TM_1 (from Ref. /25/).

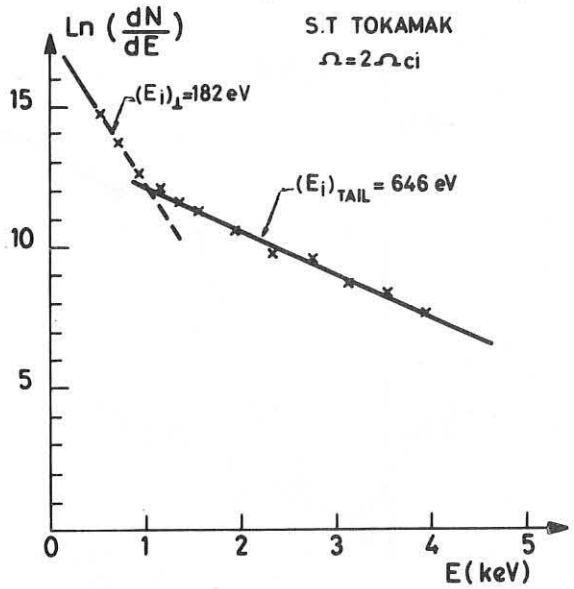

Fig.8 - Ion energy distribution by charge exchange on S.T. (from Ref. /26/).

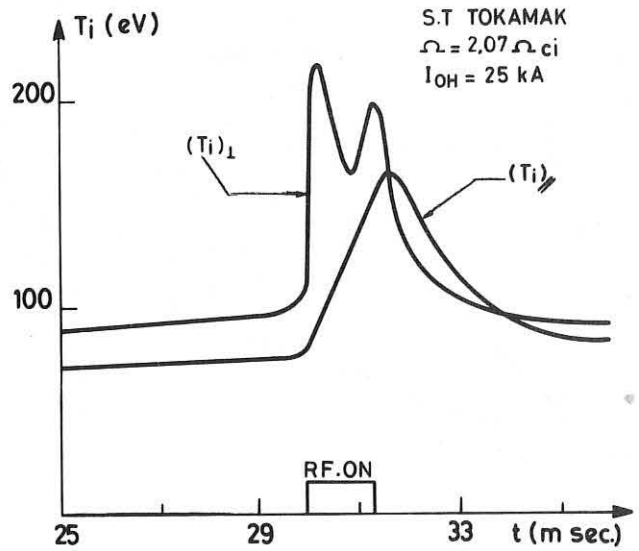

Ref.9 - $(T_i)_{\perp}$ and $(T_i)_{//}$ by charge exchange measurements on S.T. (from Ref. /26/).

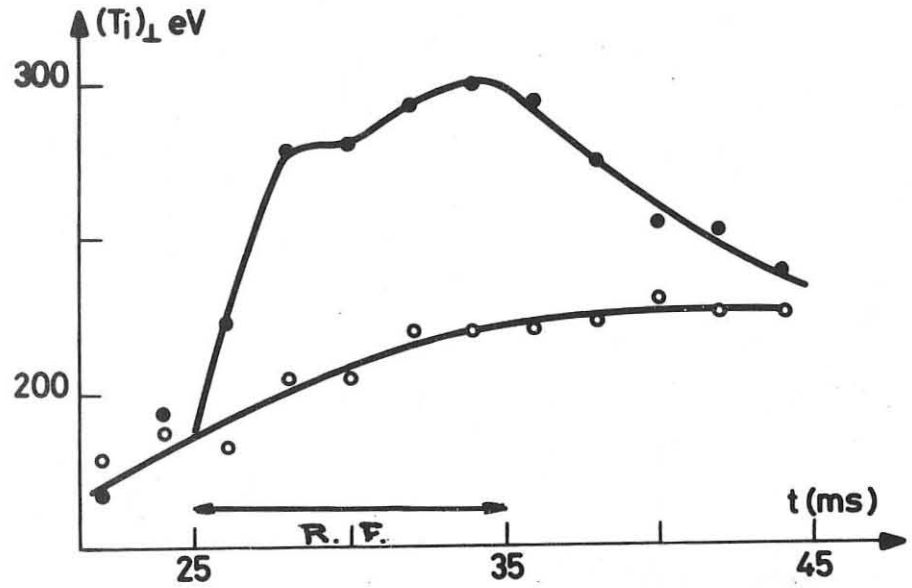

Fig. 10 - $(T_i)_\perp$ on A.T.C. measured by charge exchange (upper curve with R.F., lower curve with no R.F.). (from Ref. /28/).

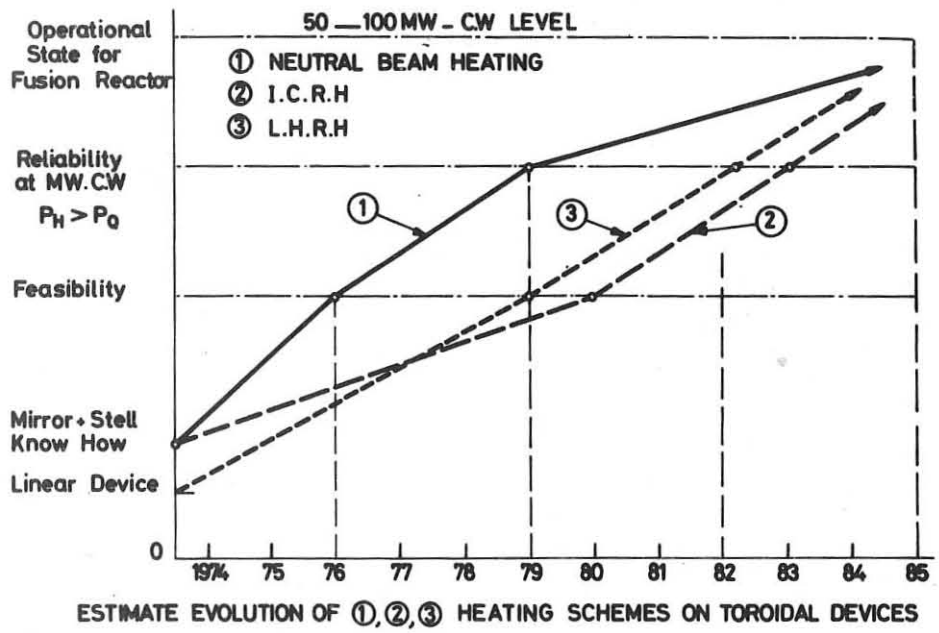

Fig. 11 - Estimate evolution of ① ② ③ heating schemes on toroidal devices.

FUSION REACTOR PROBLEMS

R Carruthers

Culham Laboratory, Abingdon, Oxon OX14 3DB
(Euratom/UKAEA Fusion Association)

"Can we have fusion power?"; "can we build a fusion reactor? - this is the type of question which is increasingly being asked.

There is only one honest answer - "We don't know and it will take a lot of time and effort to find out." To answer the question as quickly and economically as possible requires a carefully thought out programme. It is not just a matter of getting the physics "right" and the engineering "right," putting the two together and expecting to have a fusion reactor. The physics and engineering must at all times be concerned with mutually consistent solutions.

In my lecture at the 6th Conference in Moscow four years ago,[1] I called these the problems of the interface region. Since then, plasma physics has made encouraging progress and there is every hope of achieving the basic reactor plasma parameters quite soon. Engineering studies of fusion reactor concepts have examined some generic technological problems in greater depth. Progress towards wholly consistent solutions still leaves much to be desired.

Today I will examine these problems of self-consistency and show that before trying to answer the question "Can we build a fusion reactor?" it is necessary to have a much more plausible answer to the question "What is a fusion reactor?"

1. Fusion Reactor Studies

First let us look at the state of conceptual studies of fusion reactors. Many thick volumes have emerged, some dealing with full scale reactors[2], others with experimental power reactors. They embody a variety of ingenious models as the basis of optimisation studies and conclude with seemingly precise estimates of cost in $/kW.

This is a dangerous trend. If something can be costed so precisely, why will it take so many decades of R and D and so much expenditure before it can be built? Cost estimates are a valuable discipline to ensure that we are not pursuing ideas which are orders of magnitude removed from reality, but the results

must give proper emphasis to cautionary qualifications. Important items in the reactor system are often treated superficially because they cannot be adequately defined whilst others are very sensitive to the chosen plasma model. These uncertainties can affect the cost estimates by large factors but this is rarely made apparent in the studies.

On the positive side, we can say that these studies have given a better understanding of many generic technological problems - breeding blankets and shields, radiation damage, heat transfer and methods of magnet design. We also have some insight into reactor concepts which incorporate ideas for meeting the operational requirements for construction and maintenance.

To make progress we have to remember that the value of systems studies is not only to provide a progressively greater insight into the technological problems of the different confinement systems, but also to make comparative assessments of the likelihood of the realisation of each different system. This requires that the effort devoted to investigating and developing the engineering concepts of the different confinement systems is sufficient to bring them all to a similar standard and that the models studied must be equally plausible and wholly consistent right through from the plasma to all the engineering sub-systems. For this to come about, the engineering design studies must have an increasing influence upon the plasma physics programme - the concept of "scientific feasibility" as a purely plasma physics objective is unrealistic.

2. Fusion Reactor Plasma Parameters

We need to understand how to set up the plasma required in a fusion reactor which is not the same as a full understanding of all the physical phenomena which might arise in such a plasma - after all, man used the observed fact of chemical combustion a long time before the development of combustion theory!

Relevance to reactor requirements must be the basis of future experiments. There must be flexibility because all reactor requirements and relevent experiments are not yet easily or accurately defineable. The necessary understanding and clarification will only come from a greater interaction between plasma physics and technology. The present weakness of this interaction is exemplified by the widely held view that the objective of plasma physics studies is to define the parameters for a fusion reactor. The plasma parameters for a fusion reactor have been fairly closely defined for many years, and the real plasma physics objective must be to

find the means of achieving and maintaining these specifiable paramaters.

These parameters can be derived from simple models and it is important to remember that these basic requirements remain unchanged even though complex models may be required for optimisation studies and difficult technological problems must be resolved to meet them.

To clarify these basic requirements, let us regard a fusion reactor as a collection of "black-boxes. (Figure 1). There are six principal boxes. Most of the studies concentrate on only two of these boxes - the confinement system and the energy conversion unit, with an underlying assumption that the other four peripherals will not seriously modify the results. There is no justification for this assumption - the peripherals could be expensive and their interaction back on the confinement system could modify the assumed model to a considerable extent.

The Confinement System

Let us first examine the confinement system, since it is the engineering constraints on this unit which define the basic plasma parameters. The key constraint here is the power loading of the first wall. The essentials of the argument are that the costs of engineering hardware, per unit area of first wall, are determined by the blanket thickness and this is a function of the scale length for neutron capture and shielding of the magnetic field system. Hence the cost per unit area is a function of engineering design and for any given design, minimum cost is obtained from a plasma which gives the highest possible power per unit area.

We can put limits on the range of wall loadings likely to lead to an acceptable reactor. The upper limit is due to a simple engineering constraint, Heat is deposited directly in the first wall by radiation, energetic particles, neutrons and backscattered gammas. Removal of this heat leads to a temperature gradient across the wall and consequent mechanical stress. Homeyer[3] first treated this problem in 1965 using the "onion-skin" model. Subsequent studies based upon a cellular structure, no charged particle power and only hydrogen bremsstrahlung suggests an upper limit to wall loading of about 10 MW m^{-2}. Reactor studies at lower power loadings were undertaken because of the concern at the high rate of radiation damage and these all indicate that at 1 MW m^{-2} the reactor costs would be unacceptably high. (Rember 10 to 1 in wall loading is essentially 1 to 10 in capital costs, a large factor).

Making the assumption of quasi-steady-state operation, relatively flat plasma profiles and a plasma which fills the containment tube, it is possible to draw a simple relationship between wall loading, plasma radius and energy confinement time. This I show for a self-heated reactor, i.e. $n\tau_E \gtrsim 2 \times 10^{14} cm^{-3} sec$, temperature $\sim$ 15keV (Figure 2).

By assuming an aspect ratio of 3, lines can be added showing the constraint due to the unit size of the reactor. If we take the region bounded by 1GW and 5GW (thermal), and 5 and 10 MW m^{-2} we see that several parameters are closely defined:-

τ_E	1 - 2 s
Density	1 - 2 x $10^{14} cm^{-2}$
Plasma radius	1.5 - 3 m

This diagram changes only slightly over the temperature range 10-40keV. The peakiness of the plasma profiles has much more effect - the size increasing and the required energy confinement time going down.

We can add on the right hand side a scale of the product of βB^2 - which for the reactor region must be 1.5 - 3 $(Tesla)^2$. This addition helps to show the difficulty of making a low power reactor which would be of real technological value. This technological value comes from working at wall loadings close to the reactor conditions for realistic studies of radiation damage, heat transfer, cyclic stressing etc. Changing the reactor output from 5 GW(th) down to, say, 100 MW(th) requires βB^2 to be raised a factor of about 3. Any large reactor should be designed to operate at the lowest field consistent with β limitations (say 5T and β = 10%) - because higher fields mean higher costs, therefore at the same β limit the smaller reactor will require the development of a high field technology not required by the large unit. This is not impossible to consider - but it needs close examination before one can be sure that it would be a cost-effective exercise.

We have established the range of plasma parameters needed in our reactor, so we can turn to some of the other boxes and see what is needed to establish and maintain these parameters.

Control

I shall discuss control next rather than the more obvious question of start-up,

because I believe that control is the key problem. Different assumed solutions have a considerable effect upon the other three sub-systems.

A quasi-steady-state burn has been assumed in most reactor studies and this implies a certain particle confinement time. However, if this time is too long and only a few particles come out, then the exhaust problem is simple and the question of refuelling does not arise. We can assign an upper limit to the particle confinement time by the extent to which we will permit the plasma to be diluted by helium and hence reduce the reactivity. For a fixed total density, a 10% concentration of helium would reduce the reactivity by about 40%. At a temperature of $\sim$ 15keV this would arise in about 8 energy confinement times, i.e. 8-16 seconds. Particle confinement times can be shorter than this but it must be remembered that the fuel throughput is inversely proportional to τ_p and this directly affects the cost of the exhaust system, fuel clean up, preparation and re-injection.

To maintain a steady burn temperature the energy confinement time must be controlled at the required 1-2 seconds. If too short, the plasma will not self-heat and if too long, then the temperature will rise.

All recent reactor studies sidestep this control problem by assuming a Trapped Ion Mode loss process. Taking the highest estimate leads, conveniently, to just the right values for a large reactor. This illustrates a disturbing inconsistency - if the reactor assumption is correct, then ignition, breakeven, etc. cannot be achieved on a smaller scale and many current programme plans are suspect. However, trapped ion mode losses have yet to be identified and I understand that the current view of plasma physicists is that even should they arise then the loss rate will be only 1/10th to 1/100th of that assumed in the reactor studies. Future reactor studies must therefore deal more realistically with this control problem.

Let us examine some possible approaches and their consequences. Taking the usual $n\tau$ - kT plot - which may be regarded as $(n\tau)_{heating}$ (Figure 3). For stable operation at a given temperature, we must have an energy loss process with a temperature dependency such that:

$$\frac{d(n\tau)_{heating}}{dT} - \frac{d(n\tau)_{losses}}{dY} > 0$$

Trapped ion mode loss scaling is attractive because the negative temperature coefficient is consistent with stability in the 10-20keV range. All other postulated loss processes have a positive coefficient: for example, with enhanced

radiation losses and a $T^{\frac{1}{2}}$ dependency, the ion temperature cannot be controlled to below 40keV. Control by radiation from pulsed injection of impurities in a type of bang-bang servo has been proposed. It can be shown that this is only conceivable if the impurities can be extracted at a much faster rate than the D-T fuel. To justify reactor studies based upon 10-20keV plasmas, we need a predictable and controllable method of either enhancing energy transport or selectively removing α-particles when they have only given up the fraction of their energy needed to heat the incoming fuel. In the absence of plausible ways of doing this, reactor studies should, for consistency, assume radiation cooling and a high ion temperature. This still leaves the question of achieving a high enough particle loss rate without which burn times must be limited to 10's of seconds due to drop in reactivity.

Such a self-consistent mode for a tokamak was studied at Oak Ridge[4] and the result was economically unattractive.

The apparent attractions of a quasi-steady-state tokamak cannot be taken seriously until there is some attempt to show how the related plasma control requirements may be satisfied. We need to consider the effect these requirements will have on the confinement system, the cost of the additional hardware and any increased power losses.

Exhaust

We can now examine the exhaust problems and it will become apparent why I first dealt with control. What are the exhaust requirements? If we take the "inconsistent" plasma model, then we have the condition assumed in reactor studies - all - or at least nearly all - of the unburnt fuel + the α-particles and the α-particle energy can be channelled by a magnetic divertor into a collector region. This again is very convenient because it minimises the direct power input to the first wall. However, if we have to use radiation cooling or any other process for temperature control which is based on energy transport direct to the first wall, then the power input to the first wall surfaces is increased substantially - by a factor of 3-4. The rating limit of 10 MW m^{-2} was determined by this direct input and heat transfer constraints, and for any increase in this direct input the limit must be reduced by the same factor leading to an increase in the capital cost - though not quite proportionately.

Unless we can obtain a high enough particle loss rate, there will be no input

for the divertor which would not be needed, except perhaps to perform a screening function, and we would be constrained to a short, fill-burn-pumpout mode.

If we assume that future research will show us how to achieve the required enhancement of energy and particle losses into a magnetic divertor, then another plasma constraint can be derived. The flow into the divertor will be relatively collisionless for energy to be removed efficiently at a well defined collector. The plasma boundary temperature is then determined by the ratio of particle to energy confinement times - or fractional burn up[5]. This illustrates another conflict of requirements. Good particle confinement to minimise refuelling leads to a high boundary temperature ($\sim$ 15-20keV). Introducing collisional effects to reduce this will lead to the charged particle energy being deposited over a larger area with problems of recovering it efficiently.

Refuelling

If the exhaust process is ill defined, then it is obviously not possible to define the refuelling requirements. This will be zero for the short burn mode. Long containment of D-T with selective removal of α-particles would together be consistent with refuelling by neutral beams of a few hundred keV, whilst with the usually assumed TIM losses, it is necessary to contemplate the high velocity injection of pelletised D-T fuel.

Start-up

Finally, we come to the remaining box, "start-up." Present reactor studies minimise this problem by assuming that start-up can be a relatively leisurely process. This is acceptable if the burn time can indeed be made several hundred seconds and the short energy confinement time of $\sim$ 1 sec turned on when the burn has been initiated, but the start-up model which is consistent with the other sub-systems, itself depends upon the solution of the Control problem.

If quasi-steady-state operation is not possible, then the short burn mode calls for a much more rapid start-up and the additional heating power will certainly be much higher - more like 1GW than 100 MW - and adds to the doubtful viability of such a mode of operation.

Circulating Power

All the components of my simple reactor model contribute to the level of circulating energy - that is the amount of energy produced by the reactor which is used to keep the reactor operating and is not therefore available for sale.

It is well known that this is a severe problem in a mirror-type reactor which has an inherently low plasma Q_p ($Q_p = \frac{\text{Fusion power out}}{\text{Power input to plasma}}$) and it has been assumed that it should be a negligible problem in a toroidal self-heated reactor with a plasma Q of infinity. This is not a correct assumption as was pointed out in a sadly neglected report published by Jülich[6] with contributions from Garching and Culham. Perhaps this was because the results were in engineering terms of overall thermal efficiency and not the familiar Q of physics papers. All reactor studies reach their $/kW costing by assuming a certain thermal efficiency - usually taking a value appropriate to the best thermal cycles envisaged for fission reactors. The Jülich report takes into account the larger heat losses due to the system needed to collect heat from the very extended low density source presented by a fusion reactor, together with likely losses in the various sub-systems and shows that it will be difficult to achieve a net conversion efficiency of more than about 70% that of a fission or fossil fuelled heat source. Any $/kW cost estimates, however doubtful they may be for other reasons, are at least 30% low because of over-estimating conversion efficiency.

Expressed in terms of Q the Jülich report shows that, optimistically, a tokamak might have a net Q = 30 though, pessimistically, or perhaps more realistically, the net Q might be lower than 10! The significance of Q is often misunderstood so I have produced a simple diagram (Figure 4) relating a cost factor to Q_{eff}. Q_{eff} is smaller than the plasma Q_p and is the ratio of the nuclear output to the electrical power consumed at the power station and not therefore available for sale. In this way we obtain a generalised expression in terms of the unit cost of the fusion reactor (X/kW(thermal)), the unit cost of the "conventional" plant (Y/kW(electrical)), and the efficiency of the convertor, η_c.

$$\text{Power Station Cost} = \left[\frac{\eta_c}{\eta_c - 1/Q_{eff}}\right]\left[X + \frac{Y}{\eta_c}\right] \text{ per kW(e)}$$

$\left[\frac{\eta_c}{\eta_c - 1/Q_{eff}}\right]$ is the cost factor and is plotted for $\eta_c = 0.4$.

For reference, a relatively poor "conventional" power station with 10%

recirculating power corresponds to Q_{eff} = 25 and a cost factor of 1.1. Hence, a hypothetical fusion reactor with a Q_{eff} of 10 and the same unit cost (X/kW(th)) as for more conventional equipment would result in a power station costing 23% more and having double the waste heat of the conventional power station.

At this stage the curve should only be used as a general guide. Systems which have difficulty in achieving $Q_{eff} > 5$ are likely to be unacceptably expensive and produce excessive waste heat whilst systems with $Q_{eff} > 15$ may be considered to have promise.

The curve is not applicable to mirror machines in which it is assumed that recirculating power can be handled by efficient and hopefully cheap direct convertors. This brings the Knee in the Q/cost down to a lower Q.

The Ultimate User

I hope that by now I have shown the considerable interaction between the sub-systems of a fusion reactor and how necessary it is to develop an understanding of the control of plasmas - a subject I have called Plasma Engineering. This understanding is essential for our reactor studies to ensure that these studies can provide a sound basis for the correct relative assessment of the reactor potential of different confinement systems.

I must not conclude without mentioning the third party to reactor studies who has so far been somewhat neglected. He is the eventual operator of the power plant. Just as much as plasma physics parameters must be compatible with the constraints of engineering feasibility, so must both plasma physics and engineering meet the requirements of the utility operator (who we hope will purchase our fusion reactors). Utilities in the U.S.A. have already begun to express their views on present tokamak reactor studies. It would be naïve to assume that the energy situation will become so bad that fusion would be welcome, regardless of capital cost, efficiency, reliability and ease of operation. A prototype or commercial fusion reactor must compete with the alternative energy sources.

Having, with great ingenuity, shown how fusion reactors might be built, it is also necessary to consider the plasma parameters required and to see what simplifications can be introduced into the engineering design to approach the reliability and ease of operation, on which the utilities will rightly insist.

We must now face these operator requirements and any constraints imposed upon the engineering design of a fusion reactor. The fusion reactor designer must fully understand and quantify these constraints and the practical requirements of the utility operator so that they are incorporated in the conceptual design studies and allow the consequent, tighter constraints on the plasma parameters to be established.

Conclusions

In this lecture, I have tried to draw attention to important problems which have not been highlighted in published reactor studies. They are mainly plasma/engineering interface problems and show that now plasma physics research has come within striking distance of reactor parameters, it can no longer set its own objectives, The future programme must interact more closely with engineering studies and concentrate upon research which is relevant to reactor plasmas - in particular there must be a vigorous attack on the control problem because the form of the solution has such a major effect on the design of a fusion reactor.

It would take another lecture to consider possible solutions but I have summarised the position in Figure 5 which shows four possible control options and their consequences for the other sub-systems. The third option is the basis of most engineering design studies of tokamaks - yet it is the one having the largest number of uncertainties. Studies of other systems such as mirrors and the reverse field pinch are usually more self-consistent.

Many of the problems arise from the control of a plasma which has ignited and become self-sustaining, i.e. the plasma Q is infinity. Since a plasma Q of, say, 40 would be acceptable, is ignition a necessary or even a desirable objective? If the confinement of D and T is long - tens of seconds - and the α-particles could be preferentially removed at high energy we would have a solution consistent with beam refuelling and the beams might even be consistent with the requirements of plasma profile control and current sustainment for continuous operation.

References

1. Carruthers R. "Engineering Problems in CTR." Sixth European Conference on Controlled Fusion and Plasma Physics, Moscow (1973).
2. For example:- "UWMAK III." Nuclear Engineering Department, University of Wisconsin. UWFDM-150 .
3. Homeyer W G. "Thermal and Chemical Aspects of the Thermonuclear Blanket Problem." Massachusetts Institute of Technology, Research Laboratory of Electronics, Technical Report No. 453 (1965).
4. Etzweiler J F, Clarke J F. "Effects of Fuel Injection on a Cyclic β-limited Radiation Dominated Fusion Reactor." Oak Ridge National Laboratory, ORNL-TM-4083 (1973).
5. Harrison M F A, Harbour P J. Private communication.
6. Darvas J et al. "Energy Balance and Efficiency of Power Stations with a Pulsed Tokamak Reactor." KFA Jülich, Report No. Jul-1304 (1976).
7. De Bellis R J. Utility Requirements for Fusion Power. Electric Power Research Institute, EPRI ER-452-SR (1977).

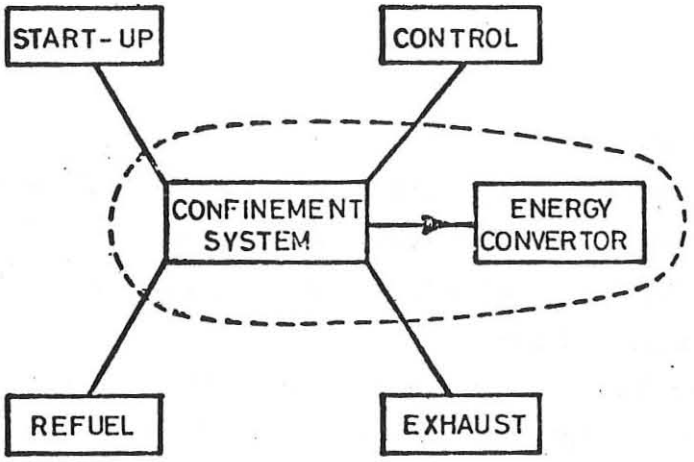

Fig. 1 Basic sub-systems of a fusion reactor

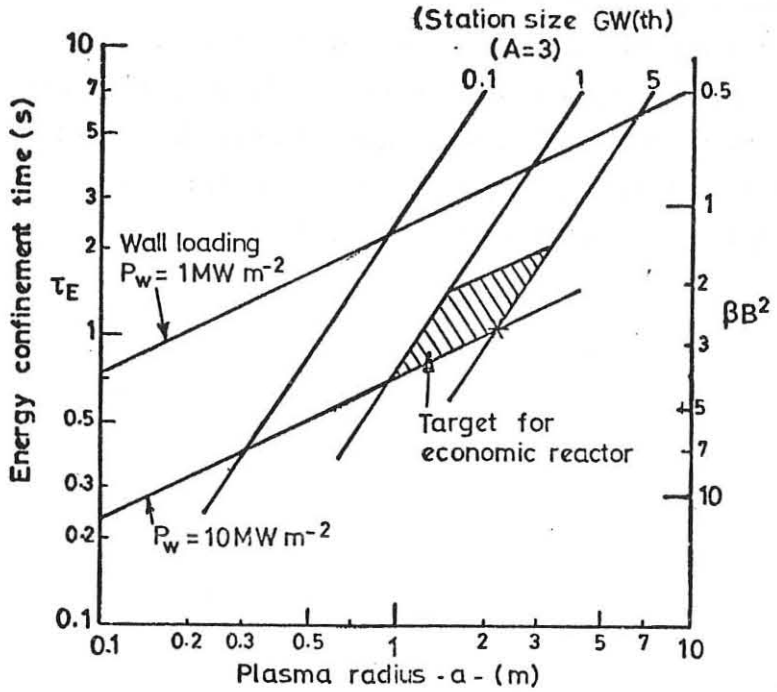

Fig. 2 Plasma parameters for a fusion reactor determined by wall loading and reactor size.

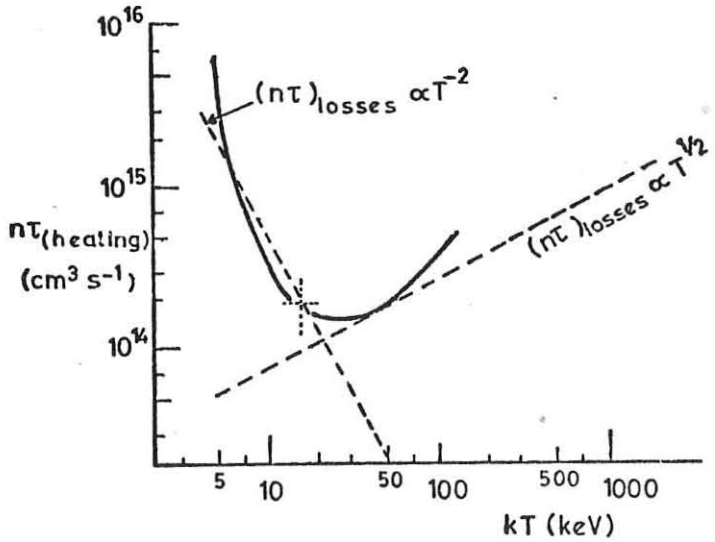

Fig. 3 Control requirements for a stable burning temperature

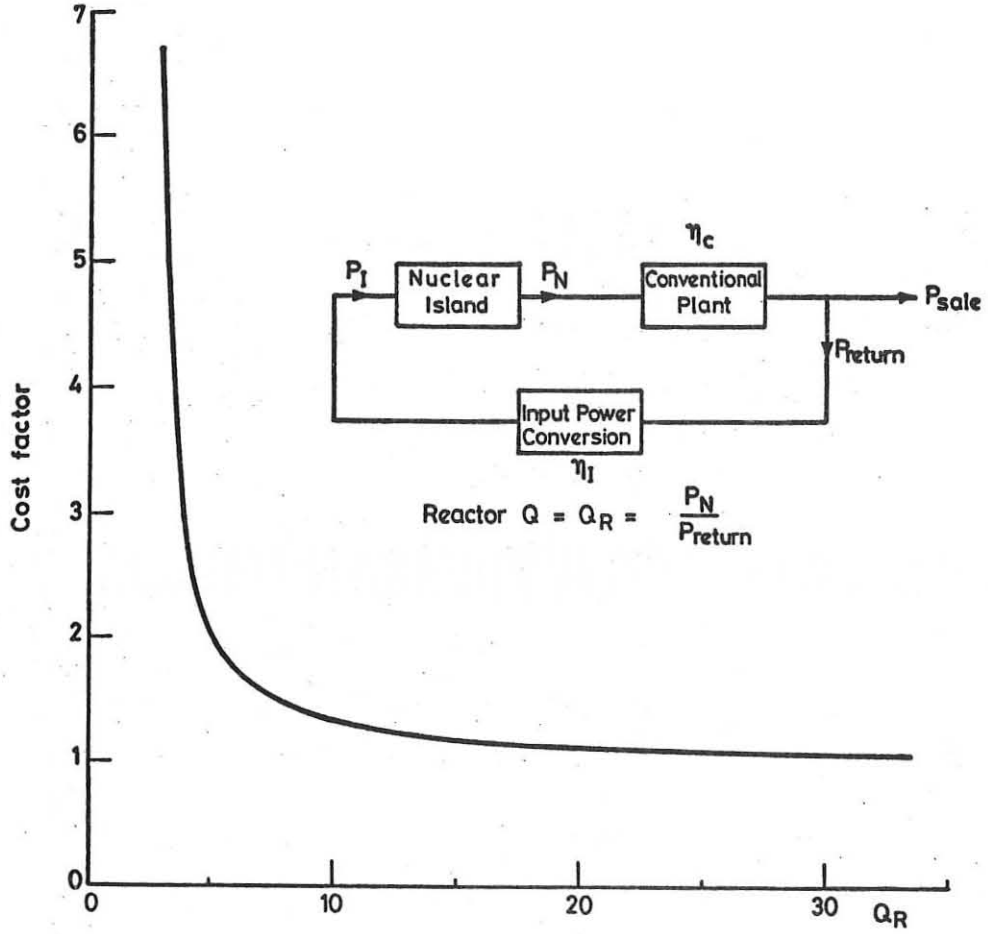

Fig. 4 Fusion power station cost as a function of the reactor Q

FIGURE 5. SOME CONTROL OPTIONS AND THEIR IMPLICATIONS

CONTROL OPTION	REACTOR CYCLE	EXHAUST	REFUELLING	START UP	COMMENT
NO LOSS CONTROL τ_E > 1 sec τ_p >> 1 sec	T → HIGH SHORT BURN (β LIMITED)	PUMP-OUT AT END OF CYCLE	NONE	SHORT-TIME → HIGH POWER	SELF-CONSISTENT HIGH DIRECT WALL LOADING EXPENSIVE
RADIATION LOSS ENHANCEMENT τ_E ~ 1 sec τ_p >> 1 sec	T → 40 keV SHORT BURN (PLASMA DILUTION)	PUMP-OUT AT END OF CYCLE	NONE	SHORT-TIME → HIGH POWER	SELF-CONSISTENT HIGH DIRECT WALL LOADING EXPENSIVE
ENHANCED ENERGY AND PARTICLE TRANSPORT τ_E ~ 1 sec τ_p ~ 10 sec	QUASI-STEADY-STATE BURN (SELF-HEATING)	DIVERTOR WITH EFFICIENT ENERGY RECOVERY	LARGE PELLETS	MODEST POWER IF τ_E CAN BE INCREASED DURING START-UP	A) NO SELF-CONSISTENT MODEL (YET) B) MANY UNSOLVED PROBLEMS PREFERRED BASIS OF TOKAMAK REACTOR STUDIES LEAST EXPENSIVE IF OPTIMISTIC ANSWERS TO A) AND B) ASSUMED
SELECTIVE REMOVAL OF ENERGETIC α's τ_E ~ 1 sec τ_p > 10 sec	QUASI-STEADY-STATE BURN (BEAM HEATED)	DIVERTOR FOR PARTICLE REMOVAL	BEAMS	POWER AMPLIFIER - USES REFUELLING BEAMS	NO IGNITION ∴ NO TEMPERATURE INSTABILITY - BUT CAN THE α's BE REMOVED FAST ENOUGH?

SUPPLEMENTARY PAPERS

13

STATIONARY AXISYMMETRIC STATES WITH DIFFUSION AND HEATING OF TOKOMAK CONFIGURATIONS

(Supplementary papers)

C. MERCIER

ASSOCIATION EURATOM-CEA SUR LA FUSION
Département de Physique du Plasma et de la Fusion Contrôlée
Centre d'Etudes Nucléaires
Boite Postale n° 6. 92260 FONTENAY-AUX-ROSES (FRANCE)

The equilibrium equations of a plasma with Ohmic and other supplementary heating have been given in the contributed paper eqs (2) - (7). They contain the heat transport coefficient. It was shown that for a realistic coefficient (β =-1, N = 6) and Ohmic heating alone the plasma $-\overline{\beta}$ does not exceed a few per cent.

Further numerical calculations have been made using a supplementary heating caracterized by a given radial distribution of the heat source. The intensity of the supplementary heating is expressed in terms of the ratio m = (suppl. heating)/(Ohmic heating).

Two cases have been treated
a) constant radial distribution
b) radial distribution increasing from the center towards the boundary of plasma.

In case a) we obtain :
for D-shaped plasma cross-section : $\overline{\beta}_{max}$ = 14 % with m = 60
for kidney-shaped plasma cross section : $\overline{\beta}_{max}$ = 18% with m = 75

In case b) we obtain
for D-shaped plasma cross section : $\overline{\beta}_{max}$ = 22 % with m = 86
for Kidney-shaped plasma cross section $\overline{\beta}_{max}$ = 25 % with m = 100

A systematic research of the optimum $\overline{\beta}_{max}$ has not been carried out.

We have found that the $\overline{\beta}$ increase linearly with m, the slope being practically the same for all cases treated. The maximum possible value of $\overline{\beta}$ is given by the limit of equilibrium (appearance of a second magnetic axis). In conclusion we may say that the adequate choice of the radial distribution of the supplementary heating is essential for obtaining high plasma $-\overline{\beta}$. It appears also that the kidney shape leads to the best $\overline{\beta}$ balues.

The investigation of the stability of the obtained equilibrium configurations has not yet been done.

25

ELECTROSTATIC POTENTIAL IN THE DIVERTOR SCRAPE-OFF LAYER

U. DAYBELGE and M. A. Mamedow†
Institut für Theoretische Physik, Ruhr-Universität Bochum,
4630 Bochum, F. R. Germany

†University of Baku, Azerb. Soviet Socialist Republic

Abstract: In a tokamak plasma bounded by a simplified poloidal divertor geometry the electrostatic potential variation is determined. Results are plotted as a function of both position and the temperature ratio of electrons and ions.

In this supplement we present some of our results found by the method described earlier. If we consider only the transiting particles, the precise description of the loss and existence regions can be summarized as follows: First consider the case $\sigma = 1$.

(a) $t < 0$. We define $A \equiv (h^2-1)E - (h-1)\mu - h^2\eta\phi - \varepsilon^2 t^2$.

1) If $A < 0$, then there is no loss.

2) If $A > 0$, then the loss region is the exterior of parabola

$$(h-1)^2\mu^2 + 2\mu\left\{-(h-1)\left[(h^2-1)E - h^2\eta\phi - \varepsilon^2 t^2\right] + 2\varepsilon^2 t^2\right\} + \left[(h^2-1)E - h^2\eta\phi - \varepsilon^2 t^2\right]^2 - 4\varepsilon^2 t^2 E = 0 \qquad (1)$$

(b) $t > 0$, then either 1) all ions are lost for $E-\mu-\varepsilon t < 0$, or

2) if $E-\mu-\varepsilon t > 0$, then i) in the region where $A > 0$ all ions are lost, or ii) if $A < 0$, then the loss region is the interior of the skew parabola given in (1).

Now, we consider the case $\sigma = -1$: Supposing first

(a) $t < 0$, then 1) if $A > 0$, then all ions are lost.

2) If however, $A < 0$, then the loss region is the exterior of the skew parabola (1).

(b) $t > 0$, then 1) if $A < 0$, then all ions are lost, or

2) if $A > 0$, then the loss region is the interior of the parabola given by Eq.(1). Additional constraints are $\mu \geq 0$, $E - \frac{\mu}{h} - \eta\phi \geq 0$ and $E - \mu \geq 0$, where the last inequality expresses the assumption that all orbits are transiting and consequently, the potential between the edges of the divertor plates is constant and zero. If we admit, however, the trapped particles into the analysis, we can prove that for sufficiently high E and μ, some particles will reach the plate after having passed below the plate and changing the direction of motion at a turning point. As a result, the potential at the tip of the plates will be continuous.

Results found without trapped particles are given in Figures.1-2.

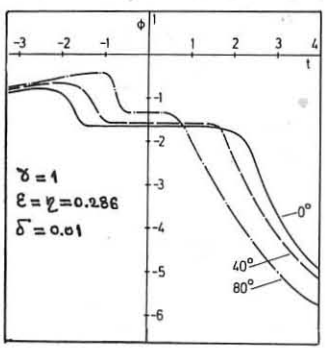

Fig.1. Potential plotted as a function of normalized radius and poloidal angle

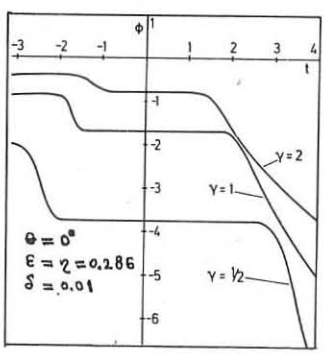

Fig.2. Potential plotted as a function of normalized radius and the temperature ratio: $\gamma = \eta\frac{T_i}{T_e}$.

REDUCTION OF POWER LOSS DUE TO HEAVY IMPURITIES IN DIVA

DIVA GROUP, presented by S. Yamamoto

The toroidal magnetic field is increased to 20 kG, and the movable shell and copper rods have been dismantled. No titanium is flushed in the present experiments. Plasma-wall interaction can now be studied over a wider range of plasma parameters which extend to P_{ohm} = 180 kW, I_p = 45 kA, T_{eo} = 800 eV, $n_{eo} = 0.8\times10^{14}$ cm^{-3} and τ_E = 3 msec. Ion temperature T_{io} agrees with the Artsimovich scaling law, up to 300 eV. In order to study the divertor effects, plasma parameters are investigated with and without the divertor under the conditions in which a_p, n_e, I_p and B_T are appreciably the same. Figure 1 shows the radial profiles of T_e, T_i and n_e, the powers emitted by the plasma along different chords due to the sum of radiations and charge-exchange neutrals P_{py}, oxygen OV and pseudo-continuum. With the divertor, the heat flux to the divertor is 85 kW, i.e. 60% of ohmic dissipations. The particle flux to the divertor is 38% of the total. The divertor reduces the loop voltage by a factor of 2, radiation loss due to oxygen and heavy impurities by a factor of 3, and increases the energy-confinement time from 1.1 msec to 2.9 msec. The divertor effects on the energy-confinement time and the particle-confinement time are studied under various discharge conditions. The energy-confinement time compared with the Alcator scaling law* is shown in Fig. 2-(a), in which open and closed circles denote the cases with and without the divertor, respectively. The divertor increases the energy-confinement time by a factor of 2.5 over the wide range of plasma parameters. A scaling law for the average particle-confinement time is obtained and shown in Fig. 2-(b). These experimental results show that the divertor reduces plasma-wall interaction. Consequently, impurities decrease and the energy-confinement time increases.

* Alcator group, Proc. the Berchtesgarden Conf. IAEA-CN-35/A5 (1976)

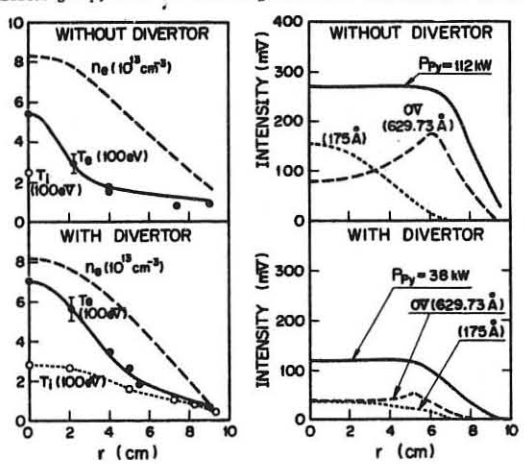

Fig. 1 Plasma parameters with and without the divertor at B_T = 20 kG and I_p = 40 kA.

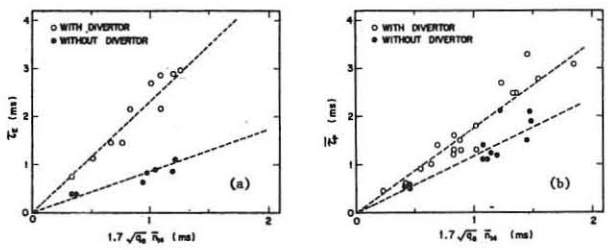

Fig. 2 Energy-confinement time τ_E and average particle-confinement time $\bar{\tau}_p$ for I_p = (14 - 45)kA, q_a = 3.1 - 6.0 and $\bar{n}_{14} \equiv \bar{n}_e/(10^{14}\text{cm}^{-3})$ = 0.1 - 0.4

EXPERIMENTS ON NEODYMIUM LASER PULSE INTERACTION WITH SLAB TARGETS IN THE PICOSECOND REGIME (PART II)

J.A. Zimmermann, J.E. Balmer, T.P. Donaldson, P. Wägli
Institute of Applied Physics, University of Berne, CH-3012-Berne

Abstract: Measurements of electron temperature and ion expansion characteristics were made of plasma generated by short neodymium laser pulses focused onto perspex targets at oblique incidence. Two groups of fast ions were seen, one of which only occurred at p-polarisation.

Further experiments were made with the laser-system described in Vol. 1, to compare absorption at oblique and normal incidence. Laser intensities of 2×10^{13} watts cm^{-2} were focused obliquely onto perspex targets, at an angle θ between the laser k vector and the target normal. In Fig. 1[1] the electron temperature, T_e, measured as a function of θ for p-polarisation, peaks at $\theta = 15^\circ \pm 5^\circ$. A resonance absorption peak at this angle implies a density scale length $L = 3\ \mu m$ ($\sin\theta = 0.7(k_oL)^{-1/3}$), in good agreement with the value calculated from the measured temperature and reflectivity[2] (cf. Vol. 1). Figure 2 shows the thermal ion expansion energy, ε_T, and T_e, to vary as $\cos^2\phi$ (ϕ is the angle between laser E-vector and incidence plane); this functional dependence indicates the presence of resonance absorption. Figure 3 shows the ion current for s- and p-polarisations where distinct thermal and fast peaks can be seen on both traces. The thermal peak for p-polarisation is more energetic due to increased energy absorption (cf. Fig. 2). The fast peak for p-polarisation[3], composed of several ion species, corresponds to an electrostatic acceleration potential V_p = 12 kv, while the fast peak for s-polarisation corresponds to V_s = 1.6 kv. V_s is equal to the ponderomotive potential calculated from the electron quiver energy in the plasma reflection region[4], while V_p is equal to the sum of the ponderomotive potential and the escape potential from the resonance region. It is concluded from these results that resonance absorption is an important heating process at oblique incidence and that there are two distinct sources of fast ions.

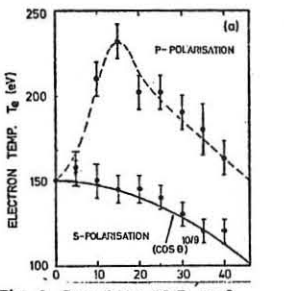

Fig. 1 Dependence of T_e on θ

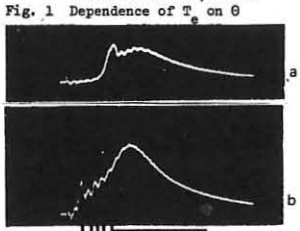

M/Z = 1 2 4 6 8 V=12KV

Fig. 3 Time history of ion current. (a) s-polarisation (b) p-polarisation

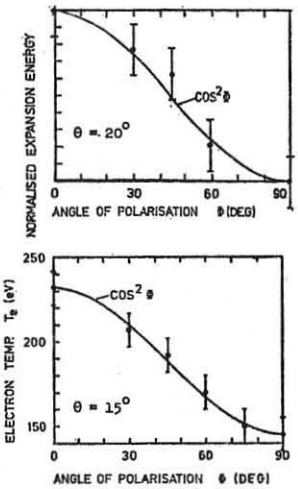

Fig. 2 Dependence of T_e and ε_T on ϕ

(1) J.E. Balmer and T.P. Donaldson; submitted to Phys. Rev. Lett. (1977)
(2) J.E. Balmer, T.P. Donaldson and J.A. Zimmermann; to be published (1977)
(3) P. Wägli and T.P. Donaldson; submitted to Phys. Rev. Lett. (1977)
(4) V.L. Ginzburg, Propagation of Electromagnetic Waves in Plasmas P 365 (Pergamon New York, 1964)

76

Toroidal Confinement with Reduced Energy Losses in Belt-Pinch IIa

G.Becker, O. Gruber, H. Krause, F. Mast, R. Wilhelm
Max-Planck-Institut für Plasmaphysik, 8046 Garching, Fed.Rep.Germany
EURATOM Association

Detailed equilibrium calculations for Belt-Pinch IIa resulted in a sequence of ideal MHD solutions from which two plots of the flux surface structure and corresponding plasma parameters are shown in Fig. 5. In the course of the discharge the initially racetrack-shaped cross-section (10 μs) becomes more elliptical and triangular (70 μs), and the toroidal current density within the plasma remains approximately z-independent ($j_t \approx c_{op} r + c_{oF} \frac{1}{r}$ with only weak ψ-contributions, where c_{op} and c_{oF} are constants related to plasma pressure and toroidal flux function).

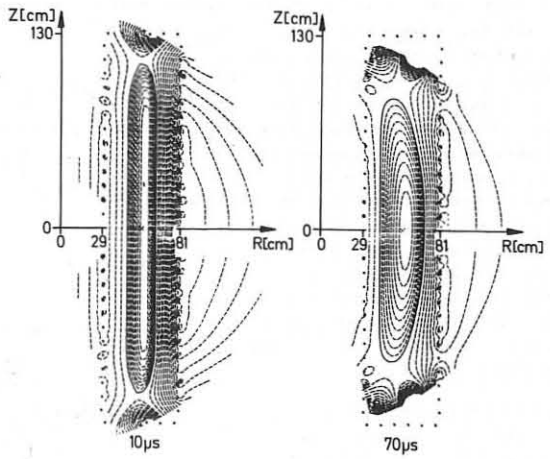

Fig. 5: Equilibrium solutions for t = 10 μs ($\langle\beta\rangle$ = 0.6, $\langle\beta_p\rangle$ = 4.0, q_b = 4.4, q_o = 1.8) and for t = 70 μs ($\langle\beta\rangle$=0.2, $\langle\beta_p\rangle$ =1.5, q_b = 5.2, q_o = 2.0)

Extensive simulation experiments with the Garching high-beta transport code, which use all available experimental data and profiles, have been carried out. Within experimental errors complete agreement is obtained between the experimental particle and magnetic field transport and predictions from the classical multi-fluid transport model. Measured plasma line densities and density profiles including two side maxima are explained by the code with a neutral particle background, which is consistent with the initial parameters of the discharge. Moreover, it has been shown that the gas influx from the vessel walls must be rather small and unimportant. Another main result is that there exists a faster energy loss in the experiments ($\tau_E \approx 60$ μs) than is predicted numerically (τ_E = 180 μs). The enhanced energy loss and the measured electron temperature on the magnetic axis (see Fig. 4) can be simulated by an impurity content of 2.5% oxygen, whereas 1% (oxygen plus carbon) have been measured. The slow rise of T_e (see Fig. 4) is caused by the fact that initially only part of the total ion energy exists in thermal form due to compressional oscillations, so that the heating of the electrons is delayed. Possible explanations for the observed larger energy losses are e.g. unidentified impurities and transient contacts of outer plasma regions with the vessel walls. At present an anomalous energy transport due to microinstabilities or MHD modes cannot be excluded, while particle and field transport has been shown to be classical.

81

CHARACTERISTICS OF SPONTANEOUSLY GENERATED RFP IN ETA-BETA

A. Buffa, S. Costa, R. De Angelis, G.F. Nalesso, S. Ortolani and G. Malesani
Centro di Studio sui Gas Ionizzati
del Consiglio Nazionale delle Ricerche e dell'Università di Padova
(Associazione Euratom - CNR)- Padova (Italy)

New measurements with the 10 - μseconds current risetime arrangment, varying the filling pressure from 5 to 80 mtorr, have been done to study the behaviour of the energy input and losses [1]. Due to the unstable behaviour of the discharges, local measurements of temperature and density were not reliable.

The average electron temperature has been deduced from the current decay time, assuming a Spitzer resistivity; a decrease from about 6 to 3 eV is found varying the pressure from 80 to 50 mTorr.

These values are supported by measurements of the relative intensity of O II and O III lines, which give an average electron temperature of about 4 eV.

Assuming a density corresponding to the filling pressure the average β_θ decreases from ~0.2 at 80 mTorr to ~0.03 at 5 mtorr and in all the cases the plasma energy is much smaller than the magnetic field energy.

In figure 1 the quantity $(W_{input} - W_{field})/W_{input}$ (where the energies (W) are time averaged in the plateau region of the primary current) which is approximately W_{losses}/W_{input} is plotted as function of the filling pressure. Impurity radiation losses could account for the observed behaviour only if the impurity content was increased by more than a factor ten from the 80 to the 5 mtorr case and even if, as pointed out previously, no quantitative accurate impurity measurement were possible this seems higly unlikely to occur.

The losses associated with the magnetic field fluctuations during the setting-up have been estimated, using a semiempiric expression [2]. Due to the low current and temperature, they can account only for a fraction of the observed losses. An estimate of the ratio v_D/v_s shows a variation from 0.5 to 5 decreasing the filling pressure, so that an enhanced anomalous resistivity due to microinstability which can arise in the low pressure conditions can qualitatively explain the energy losses behaviour. A further indication of the anomalously high resistance at low pressure is given by the ratio between the volt seconds produced and the azimuthal flux inside the vacuum vessel as shown in figure 2.

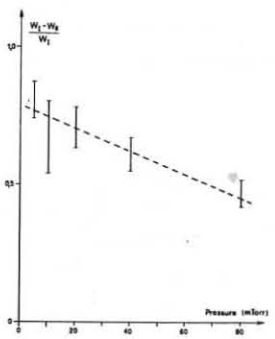

fig. 1

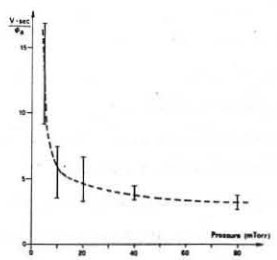

fig. 2

1 Buffa, A. et al., 3rd Int.Meet. Heating Toroidal Plasmas, Grenoble (1976) v.2, p.359.
2 Robinson, D.C., 3rd Top. Conf. on Pulsed High Beta Plasmas, Culham (1975) B1.7.

STUDY OF MAGNETIC SHAPING IN A SHELL-LESS HYBRID TOKAMAK WITH OCTOPOLE

T. Okuda, Y. Tanaka*, K. Sakurai, K. Nakamura, M. Hata and T. Kuzushima

Department of Electronics, Nagoya University, Nagoya 464 JAPAN

The observed radial profile of the impurity line intensity is explained by a model based on the neoclassical transport. The MHD stability properties are improved by the shaping field. A square cross section with high rectangularity is more stable against vertical displacement than elliptical one.

(d) Impurity Transport

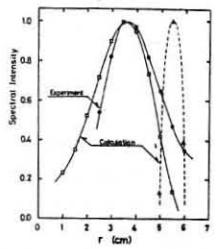

Fig.5. Spectral intensity profiles for C III 4647 A at t=0.5 msec. The symbols ●, □ and Δ denote the measured, the calculated with and without impurity transport, respectively. The amount of the influx is assumed to be 4×10^{20} $m^{-2}s^{-1}$ (at 1 eV). The electron density distribution is given by $n_e=6\times10^{19}[1-(r/a)^6]$.

The observed radial profile of the spectral intensity of carbon impurity line is compared with that predicted by a numerical simulation. The code is based on the rate equation, in which the terms of diffusion and influx of the impurity are included. The Pfirsch-Schlüter diffusion coefficient is used. In Fig.5, the observed and calculated radial profiles of C III line intensity are shown. Consistency between them is satisfactory.

(e) MHD Instabilities

Hybrid tokamak has a distinctive feature that the safety factor at the plasma boundary is increased by the shaping field. Therefore the onset of MHD instabilities arising from resonant helical perturbations at plasma surface will be suppressed.

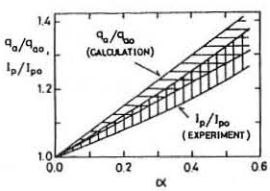

Fig.6. Plots of q_a/q_{ao} and I_p/I_{po} versus $\alpha=I_M/I_p$. q_a: the safety factor at the plasma boundary, I_M: the octopole current, I_p: the plasma current. The subcript 0 denotes the value for $\alpha=0$.

The plasma current at which the m=3 mode change into the m=4 mode is observed as a function of the shaping field. Such critical value of the plasma current I_p is increased by increasing the shaping field. Fig.6 shows that this result is understood on the basis of the safety factor at the plasma boundary.

(f) Elongation and Rectangularity

The positional stability against vertical dispalcement is analyzed for vertically elongated square plasma by using the same procedure as Lackner and MacMahon [6]. In Fig.7, the rectangularity d and the elongation ratio ε are schematically shown. The computed maximum elongation ratio for d=0, 0.1 and 0.2 are 1.3, 1.7 and 3.3, respectively.

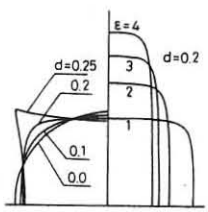

Fig.7. Elongation and rectangularity

Thus, elongated square cross section is more favorable than elliptical one from the point of view of positional stability.

* Present address : Japan Atomic Energy Research Institute.

(6) K. Lackner and A. B. MacMahon, Nuclear Fusion 14 (1974) 575.

ON SAWTOOTH OSCILLATIONS AND MHD-MODES IN THE W VII-A STELLARATOR

W VII-A Team, presented by A. Weller

Max-Planck-Institut für Plasmaphysik, EURATOM Ass.

D-8046 Garching, Federal Republic of Germany

Abstract: In our supplement to Vol. I, No 127 we present some results of sawteeth and modes in the W VII-A Stellarator, vs. peak density n_{eo} and external rotational transform ι_o. H_α-filtered light signals obtained side-on in the W VII-A limiter plane are correlated with sawteeth and modes.

Parameter Study: In W VII-A sawtooth oscillations and modes appear to be mainly depending on the peak density n_{eo} and the external rotational transform ι_o. For low values of ι_o = 0.027 and 0.055 Fig. 1 shows (from top to bottom) the relative amplitudes of sawteeth (⩘), m=2 modes (∿), and so-called predisruptions (γ), resp., vs. n_{eo}. Above $n_{eo}\approx 4\cdot10^{13}cm^{-3}$ the m=2 activity increases further and the sawteeth are reduced. Predisruptions are observed as internal disruptions occuring at the q=2 surface which initiate an internal disruption at the q=1 surface. They are believed to be important for the major current disruption which is present in tokamaks at low q values and high density. Close to the tokamak density limit, they cause (soft) current disruptions at ι_o = 0.027.

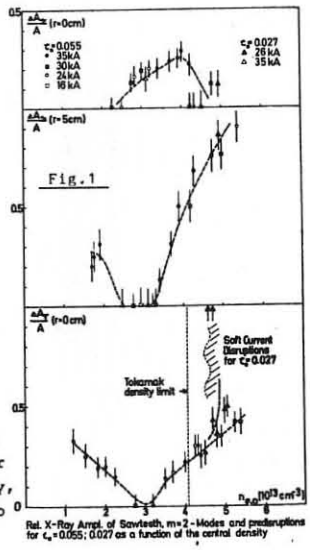

For ι_o = 0.23 the mode activity (mainly m=3, n=2) is small, presumably because of a stabilizing effect of the helical field. A roughly linear increase of $\Delta A_\gamma/A$ is seen with density, current disruptions are not seen up to $n_{eo}=8\cdot10^{13}cm^{-3}$.

At an average ι_o= 0.11, Fig. 2 shows radial profiles of the relative sawtooth and MHD amplitudes, along with the ranges of the m=1 and m=2 modes; n=1 for both. They couple at the radial outside.

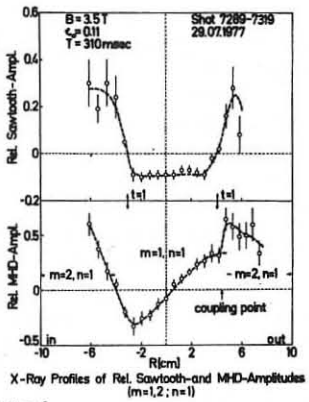

Fig.2

For large ι_o energy losses for electrons due to sawteeth are important; for $\iota_o<0.1$ the m=2 modes are large and cause additional transport.

Light signals obtained side-on in the W VII-A limiter plane have been seen to correlate with the sawteeth and the modes. This is also the case if a H_α-filter (half width 170 Å) is inserted in front of the camera lens. An example is given in Fig. 3 for ι_o= 0.23, $n_{eo}=6\cdot10^{13}cm^{-3}$, detector positions shown in the left of the figure. The light modulation is a few percent. The waveforms are complicated, but clearly correlate with the sawteeth.

Fig.3

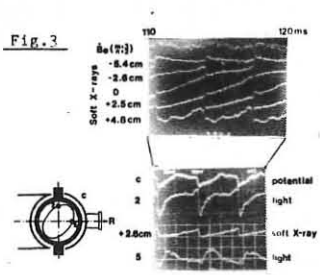

148

FINITE FREQUENCY DENSITY MODIFICATIONS BY LOWER-HYBRID CONES+

P.K. Shukla*, M.Y. Yu*, and K.H. Spatschek**
*Institut für Theoretische Physik, Ruhr-Universität Bochum, 4630 Bochum, F.R. Germany
**Fachbereich Physik, Univ. Essen, 4300 Essen, F.R. Germany

If nonlinear effects associated with the cold plasma lower-hybrid waves near the outer edge of the plasma column are unimportant, the cold plasma wave will reach the lower-hybrid resonanance layer. Large amplitude hot plasma waves will then appear due to linear mode conversion. We study in this supplement the nonlinear behavior of the mode-converted lower hybrid waves with respect to parametric instabilities.

A mode converted lower-hybrid wave $(\omega_o, \underset{\sim}{k}_o)$ can couple with finite frequency density perturbations $(\omega, \underset{\sim}{k})$ to produce a daughter wave $(\omega_1, \underset{\sim}{k}_1)$ near the conversion layer. The equations governing this three-wave process $(\omega_o=\omega_1+\omega, \underset{\sim}{k}_o = \underset{\sim}{k}_1 + \underset{\sim}{k})$ can readily be obtained by standard methods. Thus for the pump wave we have

$$A_o(\phi_o)_{xxxx}+\varepsilon_{1o}(\phi_o)_{xx}+(\varepsilon_{1o}-1)(\nu\phi_{ox})_x + A_o(\nu\phi_{oxx})_{xx}+\varepsilon_{\parallel o}(\phi_o)_{zz} = -(4\pi e/\omega_o)\,\nabla\cdot(n_{es}\underset{\sim}{u}_1), \qquad (1)$$

where $\underset{\sim}{u}_j = -(c/B_o)(\nabla_\perp\phi_j\times\hat{z})$, $\nabla_\perp=\hat{x}\partial/\partial x+\hat{y}\,\partial/\partial y$, $j=0,1$, $\underset{\sim}{B}_o=B_o\hat{z}$, $A_1\approx A_o = 3(\omega_{pi}v_1)^2/2\omega_o^4 + 3(\omega_{pe}v_e)^2/8\Omega_e^4$, $\varepsilon_{\perp 1}\approx\varepsilon_{1o} = 1+\omega_{pe}^2/\Omega_e^2 - \omega_{pi}^2/\omega_o^2$, and $\varepsilon_{\parallel 1}\approx\varepsilon_{\parallel o} = -\omega_{pe}^2/\omega_o^2$. The other notations are standard. Replacing the subscripts 0 by 1, and $\underset{\sim}{u}_1\to\underset{\sim}{u}_o$, $n_{es}\to n_{es}^*$, we obtain the evolution equation for the daughter wave.

The terms involving $\nu=\varepsilon_{1o}(\varepsilon_{1o}-1)|\phi_j|^2/16\pi n_o\kappa TA_o$ arise due to the self-interaction nonlinearity. On the other hand, the terms containing $\underset{\sim}{u}_j$ appear because of the important $\underset{\sim}{E}\times\underset{\sim}{B}_o$ drift. In fact, $n_{es} = ic\alpha_2\mu\phi_o\phi_1^*/4\pi eB_o\omega_o$, where $\mu = k^2P$, $P = \chi_e(1+\chi_1)/(1+\chi_e+\chi_1)$, $\alpha_2 = (\underset{\sim}{k}_1\times\underset{\sim}{k}_o)\cdot\hat{z}$, and $\chi_\alpha(\omega,\underset{\sim}{k})$ is the linear dielectric susceptibility. Defining $\phi_\pm=\delta\phi_{o,1}/(16\pi n_o\kappa T)^{1/2}$, $\delta = (\varepsilon_{1o}/A_o)^{1/2}$, $\eta=\alpha x$, $\xi = (\alpha/\beta)z$, $\alpha=(\varepsilon_{1o}-1)\,\delta/2\varepsilon_{1o}$, $\beta=-\varepsilon_{\parallel o}/2\varepsilon_{1o}\,\delta$, $C = 32\pi^2ec^2\alpha_2^2n_o\kappa T\mathcal{J}\mu/B_o^2\omega_o^2\alpha^5A_o\delta$, and using the usual WKB approximation, we find from (1) a coupled set of nonlinear Schrödinger equations

$$i(\phi_+)_\eta + (\phi_+)_{\xi\xi} + |\phi_+|^2\phi_+ + C|\phi_-|^2\phi_+ = 0, \qquad (2)$$

$$i(\phi_-)_\eta + (\phi_-)_{\xi\xi} + |\phi_-|^2\phi_- + C|\phi_+|^2\phi_- = 0. \qquad (3)$$

Following Manakov [1], Eqs. (2) and (3) can be shown to admit localized solutions. For typical T-20 parameters, the r.f. threshold power for overlapping filaments to occur is roughly 0.6 MW, whereas presently the power being attained is about 0.3 MW. Therefore at the latter power level wave breaking would not occur at the resonance layer, and consequently absorption of the wave energy inside the plasma can be expected.

+ Supported by SFB "Plasmaphysik BOchum/Jülich".

[1] S.V. Manakov, Sov.Phys. JETP 38, 248 (1974)

168

PRELIMINARY CONSIDERATIONS REGARDING THE EFFECT OF α-PARTICLES ON A REFUELLING PELLET

C.T. Chang
Association Euratom-Risø National Laboratory

Slowing down of a 3 MeV α-particle in the ablated cloud surrounding the pellet: The further slowing down of a 3 MeV α-particle in the ablated cloud around the pellet clearly depends on the plasma parameters, $(T_e)_l$ and $(n_e)_l$ of the cloud. Although the exact values of these parameters depend on the interaction mechanism of the 3 MeV α-particle with the D-T pellet, an estimation of its range in the cloud, however, can be made based on some reasonable guess of these parameters.

As the electron temperature $(T_e)_l$ is not likely to exceed 100 eV, it can be shown that the stopping power formula of the 3 MeV α-particle reduces to the conventional one for a cold medium, i.e.

$$\frac{dE}{dx} \simeq -16\pi\left(\frac{m_p}{m_e}\right)^2\frac{n_e}{E}\,\ell n\,(rE^2),$$

where $r = \frac{1}{64\pi e^6}\left(\frac{m_e}{m_p}\right)^2\left(\frac{kT_e}{n_e}\right)$

or $r = 0.1925\times10^{36}\left(\frac{kT_e}{n_e}\right)_l$

$[(kT_e)_l$ in ev, $(n_e)_l$ in $cm^{-3}]$

correspondingly, one may write the range as,

$$R = 2\,\frac{e^2}{(kT_e)_1}\left(\frac{m_p}{m_e}\right)\,Ei^*\,[\ell n(rE_o^2)]$$

By taking E_o = 3 MeV, and assigning some reasonable values of $(T_e)_1$ and $(n_e)_1$ to be expected for the ablated cold plasma, the expected range, R, is shown in the following table

n_e, cm^{-3}	kT_e = 1 ev	kT_e = 5 ev	kT_e = 10 ev
10^{22}	0.0386 cm	0.0305 cm	0.0280 cm
10^{21}	0.2799	0.2349	0.2197
10^{20}	2.197	1.910	1.808
10^{19}	18.08	16.09	15.36
10^{18}	153.6	139.0	133.5

As the electron number density $(n_e)_1$ of the ablated cloud most probably will not exceed 10^{19}, the above result indicates that the cold plasma blanket surrounding the pellet will not be an effective medium for the further slowing down of the α-particles.

POST-DEADLINE PAPERS

172

PARAMETRIC INSTABILITIES IN CURRENT CARRYING PLASMAS

S.S.Pešić

Atomic Physics Laboratory, Boris Kidrič Institute-Vinča,
P.O.Box 522, 11001 Beograd, Yugoslavia.

The effects of the particle drift motion upon the development of low-frequency parametric instabilities in magnetized plasma are studied.

The parametric interaction of intense electromagnetic fields with magnetized plasmas has attracted recently a great deal of attention as an efficient means to transfer the electromagnetic energy into plasmas [1,2]. The object of the present paper was to examine the effects of the particle drift motion upon the development of low-frequency parametric instabilities in magnetically confined plasma.

The dispersion equation governing the parametric coupling (in its linear stage) of a low-frequency electrostatic wave at $(\omega,\vec{k})$ and two high-frequency sidebands at $(\omega\pm\omega_0,\vec{k})$ propagating in two-component hot homogeneous magnetized plasma in which the electrons have an average velocity u with respect to the plasma ions reads,

$$\varepsilon(\omega_\ell) + a_b^2\chi_i(\omega_\ell)\varepsilon_e(\omega_\ell)\{\varepsilon(\omega_\ell-\omega_0)^{-1}+\varepsilon(\omega_\ell+\omega_0)^{-1}\}/4 = 0, \qquad (1)$$

where $\omega_\ell=\omega+i\gamma,\gamma$ is the growth rate of oscillations, $\varepsilon(\omega_\ell+m\omega_0) = 1+\chi_e(\omega_\ell-\vec{ku}+m\omega_0,\vec{k})+\chi_i(\omega_\ell+m\omega_0,\vec{k})$ is the linear permittivity. For a Maxwellian equilibrium distribution function the linear susceptibility for the α-th species of particles is given by,

$$\chi_\alpha(\omega',k) = \frac{2\omega_{p\alpha}^2}{k^2v_{t\alpha}^2}\,\frac{1 + z_{0\alpha}\Psi(\lambda_\alpha,z_{n\alpha})}{1 + i\nu_\alpha\Psi(\lambda_\alpha,z_{n\alpha})/k_{//}v_{t\alpha}}, \qquad (2)$$

where $\Psi(\lambda_\alpha,z_{n\alpha})=\sum_{n=-\infty}^{\infty} I_n(\lambda_\alpha)e^{-\lambda_\alpha}\,Z(z_{n\alpha}),\lambda_\alpha=k_\perp^2v_{t\alpha}^2/2\omega_{b\alpha}^2,z_{n\alpha}=(\omega'-n\omega_{b\alpha})/k_{//}v_{t\alpha},\omega_{p\alpha}$ and $\omega_{b\alpha}$ are the plasma and cyclotron frequencies $v_{t\alpha}$ is the thermal velocity, ν_α is the collision frequency, $I_n(\lambda)$ is the modified Bessel function of the first kind and $Z(z)$ is the plasma dispersion function. Here the collisional effects are accounted for by using the Krook model of the kinetic equation. For a RF electric field of the form $E = E_0\sin\omega_0 t$ the coupling coefficient a_b is given by $a_b^2=(\vec{kr}_{EB})^2 = (ekE/m_e\omega_0^2)^2 f(\theta,\xi,\phi)$, where

$$f(\theta,\xi,\phi) = \left\{\cos\theta\cos\xi + \sin\theta\sin\xi\cos\phi\,\frac{\omega_0^2(\omega_0^2+\omega_{be}\omega_{bi})}{(\omega_0^2-\omega_{be}^2)(\omega_0^2-\omega_{bi}^2)}\right\}^2 + \left\{\sin\theta\sin\xi\sin\phi\,\frac{\omega_0^3\omega_{be}}{(\omega_{be}^2-\omega_0^2)(\omega_{bi}^2-\omega_0^2)}\right\}^2 \qquad (3)$$

$\theta=\sphericalangle\,\vec{k},\vec{B}_0$, $\xi=\sphericalangle\,\vec{E},\vec{B}_0$ and ϕ is the anle between the planes $(\vec{k},\vec{B}_0)$ and $(\vec{E}_0,\vec{B}_0)$. In deriving equation (1) it is assumed that the wavelength of the excited waves is short in comparison with the scale length of the pump field variation and consequently, the spatial variation of the pump field and the confining magnetic field $\vec{B}_0$ is neglected (dipole approximation). Furthermore, it is assumed that the electric field strength is sufficiently weak ($a_b<1$) to consider only the lowest-order coupling (m=1) to the sideband modes.

In the present analysis we shall be primarily interested in resonant and nonresonant decay processes of a RF pump wave of frequency ω_0 near and above the lower hybrid (LH) frequency. This frequency regime is of particular interest from the point of view of RF heating of fusion plasmas. For $\omega_0<\sqrt{2}\omega_{LH}$ the following decay processes of the pump wave are possible: resonant decay into low-frequency ion sound wave ($\omega^2<<\omega_{bi}^2$), backward ion cyclotron wave ($z_{0e}=(\omega-\vec{ku})/v_{te}k_{//}<1$) and ion Bernstein wave ($z_{0e}>1$) and nonresonant decay into ion quasi-modes and purely growing modes. In addition to the foregoing decay processes the forward ion cyclotron wave can be resonantly excited when $\omega_0>\sqrt{2}\omega_{LH}$. We recall that the high-frequency ion sound wave which is defined by $T_i<<T_e$ converts into an ion cyclotron wave in presence of finite ion Larmor radius effects. The low-frequency ion sound wave is heavily damped by ion collisions. We expect the ion quasi-modes and the ion cyclotron wave to be the most unstable in high-temperature plasmas [3].

We have solved numerically the complete dispersion equation (1) to obtain growth rates and coupling coefficients for the considered low-frequency instabilities. The parameters chosen are relevant to the LH heating of toroidal deuterium plasma and in particular, to the low-density plasma region of toroidal discharges ($f_o=8\times10^8$Hz, $B_o=2.2$T, $T_e=100$eV, $T_i=10$-100eV). In the following discussion we shall concentrate mainly on analysing the effects of the particle drift motion upon the nonresonant decay into fluid-like and kinetic quasi-modes. The particle drift motion has a negligible effect upon the growth rate and frequency of the decay waves for $u<v_{te}$ and $\zeta=\omega/k_{//}v_{te}>1$. However, at fixed $k_{//}$ value the coupling coefficient a_b decreases as u/v_{te} approaches ζ. The further increase of u leads to the excitation of ordinary current instabilities (for $\vec{ku}=\sigma(\omega_o)$). To demonstrate the role of the particle drift motion in Fig.1. we have represented the variation of a_b as a function of u/v_{te} for various γ/ω_{bi} values. The considered decay waves propagate in dense plasma ($n\simeq2\times10^{13}$cm^{-3}) at an angle $\theta=\arccos(\sqrt{m_e/m_i})$ to the magnetic field. Therefrom $\omega_o\lesssim\sqrt{2}\,\omega_{LH}$. When $k_{//}$ is kept fixed a_b is increasing for increasing the growth rate or the wave frequency. The variation of a_b with the angle of propagation θ for $u=v_{te}$ is shown in Fig.3. The density of wave propagation decreases (from $n\simeq2\times10^{13}$cm^{-3} to $n\simeq10^{10}$cm^{-3} in the represented θ range) while a_b increases for decreasing the angle θ. When $T_e >> T_i$ similar variation of a_b with θ is observed (Fig.4.). We note that at large angle of propagation the decay into short wavelength waves is characterized by relatively low thresholds. The general conclusion to be drawn from the presented results is that at $\zeta\lesssim u/v_{te}$ the particle drift motion has a profound effect on low-frequency parametric instabilities.

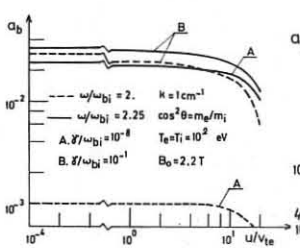

Fig.1. Coupling coefficient a_b versus u/v_{te}.

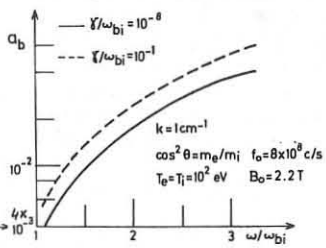

Fig.2. Coupling coefficient a_b versus ω/ω_{bi}.

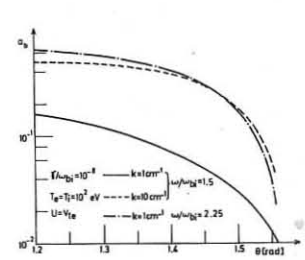

Fig.3. Coupling coefficient a_b versus the angle of propagation θ.

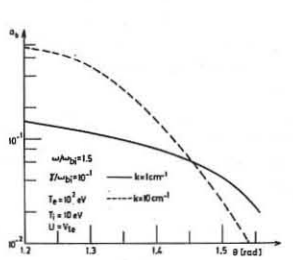

Fig.4. Coupling coefficient a_b versus the angle of propagation θ.

REFERENCES

1. Aliev Yu.M., Silin V.P. and Watson C., Zh. Fksp. Teor. Fiz. 50 (1966) 943 (Sov. Phys. JETP 28 (1966) 626).
2. Porkolab M., Nucl. Fusion 12 (1972) 329.
3. Berger R.L. and Perkins F.W., Phys. Fluids 19 (1976) 406.

RECENT RESULTS ON ION HEATING BY T.T.M.P. ON PETULA

R. BARDET, M. BERNARD, G. BRIFFOD, M. CLEMENT, A. GAUTHIER, M. GREGOIRE, P. GRELOT, M. HESSE, F. PARLANGE, D. PINET, E. PORROT, G. REY, B. TAQUET, J. WEISSE

ASSOCIATION EURATOM-CEA
Département de Physique du Plasma et de la Fusion Contrôlée
Service IGn - Centre d'Etudes Nucléaires
85 X - 38041 GRENOBLE CEDEX

ABSTRACT : Transit Time Magnetic Pumping has been applied on the Petula Tokamak without pumpout and any undesirable effects. A 20-30% subsequent ion temperature increase wase observed according to theory.

INTRODUCTION : Additionnal heating by compressional Transit Time Magnetic Pumping can be applied on the Petula experiment by modulating the toroidal magnetic field at a radio-frequency. For this purpose six R.F. coils, equally spaced around the torus, are connected to a 100-200 Khz generator, the phase of each coil being such as to produce a standing wave with three wavelength along the toroidal direction. This configuration is equivalent to two oppositely travelling waves the phase velocity of which is in the range of the ion thermal velocity. The R.F. coils are located outside the alumina vacuum chamber /1/ in order to avoid effects such as breakdown or impurity release.

HEATING RESULTS : In the experiments reported here a 10ms, 150Khz, 16-17 KV R.F. pulse is applied to the coils which produce a 1.4-1.5% modulation of the toroidal magnetic field.

The characteristics of the plasma into which this RF power was injected /2/ as well as the ion temperature increase due to TTMP heating are summarized in table 1.

Table 1

H_2, I_p = 55-60 kA, B_T = 1.6 Tesla, R = 72 cm, a = 14.5 cm				
T_{eo} (eV)	$\bar{n}_e(10^{13}cm^{-3})$	T_{io} (no RF)	T_{io} (with RF)	B_TRF-modulation b %
600	2.2	210	260	1.5
870	2.5	240	280	1.4
902	3.0	280	330	1.4
* from charge exchange neutrals				

Fig. 1 and 2 show the ion temperature increase deduced from fas neutrals analysis and Doppler broadening effect on O_{VII} line. Both these diagnostics measure the perpendicular temperature thus showing that the energy which is given in the parallel direction by TTMP heating is distributed. The fast neutrals energy distribution shown in fig.3 is true Maxwellian from .6 to 2.3 KeV with no non-thermal tail observed up to 5 KeV. These considerations enable to conclude that there is effective thermalization of the absorbed energy.

From the other hand, when the RF pulse is applied, the plasma current, loop voltage, H_β, C_{IV}, O_{VI} and O_{VII} line intensities do not exhibit any perturbation or significant change. The time evolution of electron density, the measurement of which is perturbed during RF, is similar to that typical of a reference shot without R.F. Therefore it can be pointed out that neither pumpout /3/ nor impurity release and ionization took place during heating.

These experimental situations could be simulated by a one dimension, time independant numerical code /4/ which solves the energy balance equation for the ions. This code takes into account impurities, charge exchange, particle diffusion, neo-classical heat conduction and absorbed R.F. power as given by theory for the so-called linear and non linear regimes /5/ :

$$P_L \sim n_i T_i^{3/2} b^2 C \qquad P_{NL} \sim n_i^2 T_i^{-1/2} b^{1/2} Q \qquad P_{TTMP} = \frac{PL}{1 + P_L/P_{NL}}$$

where b is the RF modulation ratio of the toroidal magnetic field and C,Q depends on T_e/T_i and V_{Ph}/V_{Ti}, the ratio of the wave velocity to the ion thermal velocity.

A typical case is represented in table 2 where P_{EI} is the power given to the ions by electron collisions and τ_i, τ_E the ion energy and total energy confinement times. The ( ) values refer to the experimental datas.

Table 2

	T_{eo}	$\bar{n}_e$	Z_{eff}	T_{io}	P_{EI}(KW)	P_{TTMP}(KW)	τ_i(ms)	τ_E (ms)
No R-F	620 (610)	2.2 (2.3)	2.3 (2.9)	207 (208)	29		5.4	5.1 (4.8)
With R-F	620	2.2	2.3	268 (258)	20	18	5.2	4.7

The e-folding time of the ion temperature after R.F. is turned off is in this case significant of the ion energy confinement time. The 4.5ms experimental value is in agreement with the computed τ_i. The calculated characteristic heating time is about 10 ms justifying the fact that during R.F. T_i increases without saturation effect. (fig.1). The total amount of R.F. power absorbed by the ions is roughly 60% of the power coming from electrons at the beginning of TTMP heating.

To conclude, these experiments have shown that the ion temperature increase is consistent with theory and that no pumpout or undesirable side effects were observed. The modulation ratio needed to to heat bigger machines should not exceed the value experienced on Petula so that TTMP can be considered as a heating method which would not affect the confinement properties of Tokamaks.

REFERENCES :

/1/ GROUPE PETULA, Revue de Physique Appliquée, 12, 955 (1977).
/2/ R.BARDET et al., 8th Eur.Conf.on Contr.Fus.and Plasma Phys., Prague (1977).
/3/ W. MILLAR, CLM-R 144 (1975)
H.D. PACHER, C.MAHN, G.CATTANEI, Bull.Am.Phys.Soc.18, 1353 (1973).
/4/ M. BERNARD, EUR-CEA-FC 891 (1977)
/5/ E. CANOBBIO, Nuclear Fusion, 12, 561 (1972).

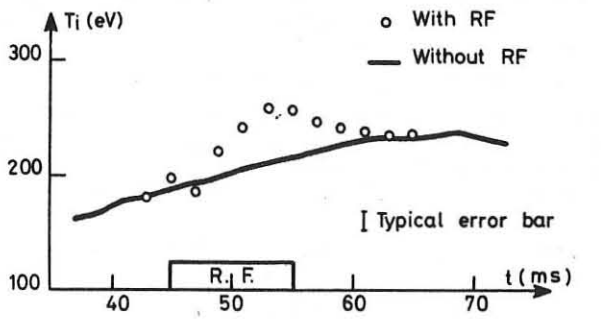

Fig. 1

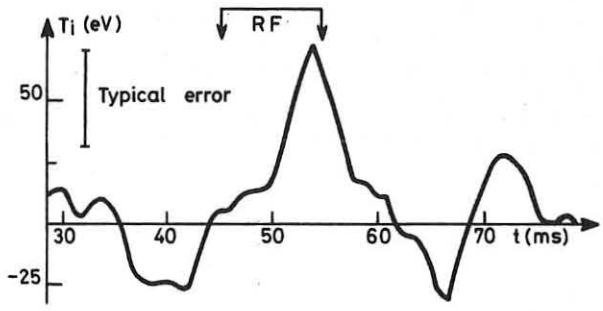

Fig. 2

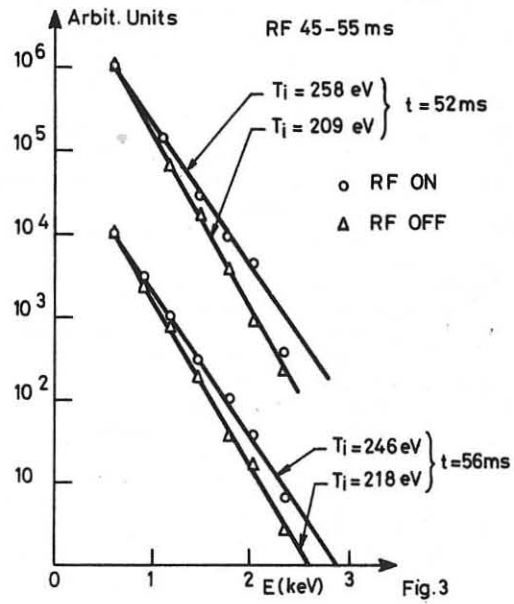

Fig. 3

TURBULENT DIFFUSION CAUSED BY A THERMONUCLEAR ALFVEN INSTABILITY

V.S.Belikov, Ya.I.Kolesnichenko
Nuclear Research Institute
of Ukrainian SSR Academy of Sciences,
Kiev, Union of Soviet Socialist Republics

Abstract: The general expressions for the turbulent particle fluxes, taking into consideration the process of the induced wave scattering by particles are obtained. Provided the thermonuclear Alfven instability is excited these expressions are applied for the investigation of the turbulent diffusion.

As it is known, in a high-temperature plasma the thermonuclear instabilities arising from the thermodynamically non-equilibrium distribution function of the thermonuclear reaction products (α-particles) can be excited. The growth rates (γ) of such instabilities are considerably small as compared with the excited waves frequencies (ω). Therefore one can expect that the weak-turbulent state leading to the anomalous transport processes will be established in a plasma.

Let us assume that the turbulent diffusion arise from the short-wave Alfven instability [1] :

$$\omega = \kappa_\parallel v_A \,, \quad \gamma \simeq \frac{n_\alpha}{n_e}\omega_{B\alpha} \,, \quad \kappa_\perp \rho_\alpha \sim 1 \,, \quad \omega \gg \omega_* \qquad (1)$$

where $\vec{k}$ is the wave vector, V_A is the Alfven velocity, ω_* is the drift frequency; n_j, ω_{Bj} and ρ_j are the density, the cyclotron frequency and the gyro-radius of the particles of species j respectively.

The instability under consideration is weakly sensitive to the magnetic field configuration [2] and has sufficiently small threshold density (n_α^{cr}), so it is one of the most probable instabilities in the thermonuclear reactor.

We shall consider the anomalous particle diffusion in the established turbulent state. In this case the turbulent particle flux across the magnetic field (Γ_j) is given by the following expression [3]:

$$\Gamma_j = \frac{2c}{e_j B}\sum_\nu \int \frac{d\vec{\kappa}}{(2\pi)^3}\kappa_x\left(\gamma_{\vec{\kappa}j} + \gamma'_{\vec{\kappa}j}\right)N^\nu_{\vec{\kappa}} \,. \qquad (2)$$

Here the plasma inhomogeneity and the magnetic field are directed along the OY axis and OZ axis respectively, $N^\nu_{\vec{\kappa}}$ is the number of ν-plasmons; $\gamma_{\vec{\kappa}j}$ and $\gamma'_{\vec{\kappa}j}$ are the growth rates caused by induced emission and scattering of waves by particles, i.e. associated with resonances

$$\omega_\kappa - \ell\omega_B - \kappa_\parallel v_\parallel = 0 \,,$$
$$\omega_{\vec{\kappa}} - \omega_{\vec{\kappa}'} - \ell\omega_B - (\kappa_\parallel - \kappa'_\parallel)v_\parallel = 0 \,, \quad \ell = 0, \pm 1, \ldots \qquad (3)$$

Taking into consideration of the induced wave scattering plays the important role for finding of the ion turbulent flux because of the ions don't interact with the waves in linear on $N^\nu_{\vec{k}}$ approximation.

Note that the terms caused by non-resonant wave-particle interaction are absent in equation (2). As Timofeev shown [4] such terms are negligibly small in the case of the stationary turbulence.

To determine the values entering eq.(2) one should solve the kinetic wave equation together with the quasi-linear equation for the distribution function.

If $\Delta t > \tau_{\alpha e}$ (Δt is the time after the instability arised, $\tau_{\alpha e}$ is the time of α-particles slowing-down by electrons) there is a possibility for the establishment of the quasi-steady state in which the α-particle flux is determined by the resonant α-particle balance equation:

$$\frac{v_0 - v_1}{v_0}\int \frac{n_e}{\tau_f}\,dV = \int \Gamma_\alpha^{st}\,dS \qquad (4)$$

where V and S are the plasma volume and surface; $\tau_f = 4/n\langle\sigma v\rangle$ $\langle\sigma v\rangle$ characterizes the thermonuclear reaction rate; $v_1 = \omega_{B\alpha}/k_{max}$ is the smallest longitudinal velocity of the resonant α-particle, $v_0 = (\varepsilon_0/2m_\alpha)^{1/2}$, $\varepsilon_0 = 3.5$ MeV is the energy of the α-particles produced (see Fig.1). Eq.(4) takes into account that provided $\Delta t > \tau_{\alpha e}$ the particles with longitudinal velocities within the interval (v_1, v_0) enter the resonance region and hence escape from a plasma. The electron and ion fluxes are connected with Γ_α^{st} by the relations:

$$\Gamma_i = -2\left(1 + |\gamma_{el}/\gamma_\alpha\sqrt{\beta}|\right)^{-1}\Gamma_\alpha^{st} \,, \quad \Gamma_e = 2\left(1 + \gamma_\alpha\sqrt{\beta}/|\gamma_{el}|\right)^{-1}\Gamma_\alpha^{st} \qquad (5)$$

where $\beta = 8\pi n_e(T_e + T_i)/B^2$.

One can see that the stationary state (4) takes place in case $\Gamma_\alpha(t=0) > \Gamma_\alpha^{st}$. This condition gives the restriction for the radius of plasma column:

$$a < (\omega_{B\alpha}\tau_f)^{1/4}\rho_i$$

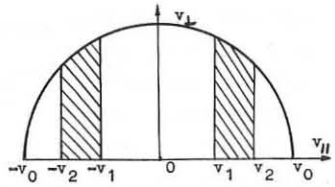

Fig.1. Region of α-particle production (semi-circle $v_\perp = (v_0^2 - v_\parallel^2)^{1/2}$) and resonance regions ($v_1 < |v_\parallel| < v_2$)

When the above inequality is satisfied the time of resonant α-particle confinement within the plasma is short compared with the time of their thermalisation. In the opposite case $\Gamma_\alpha(t=0) < \Gamma_\alpha^{st}$ and the instability under consideration during the time of the order $\tau_{\alpha e}$ is stabilized by Coulomb collisions.

In conclusion let us discuss the problem of energy spectrum of α-particles escaping from a plasma due to the turbulent diffusion [5]. Provided $\omega \gg \omega_*$, the variation of the particle energy is caused by rearrangement of level curves in the velocity space. For Alfven waves such levels are circles centred at $v_\parallel = \pm v_A$, $v_\perp = 0$. So, both particle slowing-down and acceleration occurs during the quasi-linear relaxation. As a result, there establishes an energy distribution, different from zero in the interval $\varepsilon_{min} \leq \varepsilon_\alpha \leq \varepsilon_{max}$ where $\varepsilon_{min} = m_\alpha v_1^2/2$, $\varepsilon_{max} = \varepsilon_0 + m_\alpha v_A(v_2 - v_1)$. As the quasi-linear relaxation is essential for the instability under consideration, the accelerated particles are an appreciable part of the escaping from the plasma ones.

REFERENCES

1. Belikov, V.S., Kolesnichenko, Ya.I., Oraevskij, V.N., Zh. Ehksp. Teor. Fiz. 55 (1968) 2210.
2. Belikov, V.S., Kolesnichenko, Ya.I., Mikhajlovskij, A.B., Yavorskij, V.A., Fizika Plazmy 3 (1977) 263.
3. Belikov, V.S., Kolesnichenko, Ya.I., Nucl. Research Institute, Kiev. Report KIYaI-77-2 (1977).
4. Timofeev, A.V., Fizika Plazmy 2 (1976) 419.
5. Belikov, V.S., Kolesnichenko, Ya.I., Yavorskij, V.A., Nucl. Fusion 16 (1976) 783.

INSTABILITY DUE TO TRAPPED IONS IN A MAGNETIC MIRROR

K.Saeki, S.Iizuka, N.Sato, and Y.Hatta
Department of Electronic Engineering, Tohoku University
Sendai, 980, Japan

Abstract A new type of drift instability is excited by controlling the amount of trapped ions in a mirror machine. The instability rotates in the direction of ion diamagnetic drift.

Trapped-particle instabilities are of current interest in conjunction with plasma confinement in nuclear-fusion devices. A number of theoretical investigations of low-frequency instabilities[1] ($\omega \ll \omega_{ci}$) due to magnetically-trapped particles have been intensively carried on from this point of view. Only a few experiments[2] on these instabilities, however, have been done because it is difficult to control the amount of trapped particles in a collisionless plasma under a mirror configuration of magnetic field. In this report, we inject ions by mounting an ion emitter[3] in the center of a mirror machine. A part of these ions are trapped in the mirror.

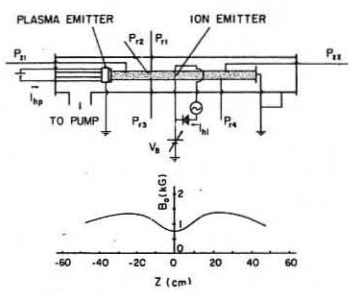

Fig. 1. Experimental setup

Experimental setup is shown in Fig. 1. The magnetic field strength is in the range of 1-2kG at the mirror points with mirror ratio R_m=1-1.7. The distance between the mirror points is 50cm. There are two groups of ions: untrapped ions and trapped ions. Most of the untrapped ions are emitted from a plasma emitter[4] [the mixture of barium-oxcide (BaO) and alminosilicate ($K_2O \cdot Al_2O_3 \cdot 2SiO_2$) coated on a 5-cm-diam nickel plate] which is placed outside the mirror and emits a potassium plasma of temperature 0.15eV and density $10^7 cm^{-3}$. The trapped ions are emitted from the ion emitter which cosists of a Ni-Cr grid coated with so-called "water glass" (potassium-silicate $K_2O \cdot SiO_2$). The mesh-size (1cm) of the grid is larger than the Debye length and is comparable to the ion Larmor diameter. This emitter is heated directly by feeding half-wave rectified current of 50Hz through it. All measurements are done within another half-cycle of no heating. Background pressure is 5×10^{-6}Torr. Plasma parameters and their fluctuations are measured by needle probes and an emissive probe.

The plasma density profile along the axis z depends on the heating current I_{hi} of the ion emitter as shown in Fig. 2. Here, its bias voltage is set equal to or somewhat higher than the space potential. At I_{hi}=0, the plasma density n_o has almost the same shape as the magnetic field strength. As I_{hi} is increased, n_o increases gradually at z=0 because of the ion trapping. Although the ion emitter produces also untrapped ions, but it can be said from this figure that the density of the trapped particles is comparable or larger than that of the untrapped particles.

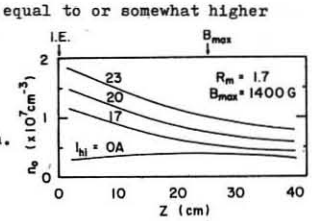

Fig. 2. Axial profile of plasma density

When the trapped ions are injected, we can observe a low-frequency (0.5 to 3kHz) instability of large-amplitude ($\tilde{n}/n_o \sim$ 5 to 50%, $\tilde{n}$: fluctuating density). The dependence of the instability on R_m is shown in Fig. 3, where the magnetic field strength B_{max} at the mirror points is kept at 1.5kG. However, the phenomena do not depend on its strength if R_m is fixed. Figure 4 shows the radial profiles of the plasma density n_o, the space potential ϕ (determined by the emissive probe), and the fluctuating potential $\tilde{\phi}$. It is found that $\tilde{\phi}$ is located in the region around the maximum density gradient, where the radial slope of ϕ is small enough to neglect the doppler shift frequency due to E×B drift compared with the observed frequency. The azimuthal phase measurements indicate that the instability rotates with the mode m=1 in the direction of ion diamagnetic drift. The phase between the fluctuations $\tilde{n}$ and $\tilde{\phi}$ is almost the same.

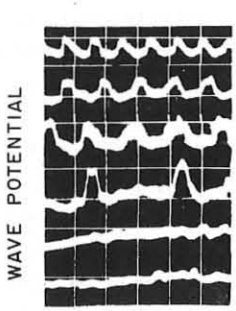

Fig. 3. Dependence of the instability on mirror ratio

The observed instability is very sensitive to the mirror ratio and the amount of trapped ions. It cannot be explained by the flute instability or the normal drift instability.

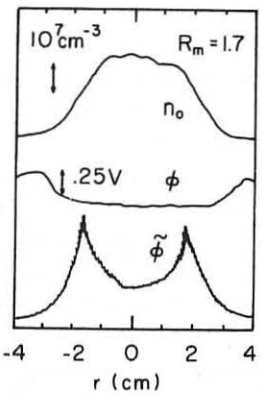

Fig. 4. Radial Profiles of plasma density, space potential and fluctuating potential

References

1 B.B.Kadomtsev and O.P.Pogutse, Zh. Eksp. Teor. Fiz. 51, 1734 (1966) [Sov. Phys. JETP 24, 1172 (1967)]: Nuclear Fusion 11, 67 (1971); B.Coppi et al., Phys. Rev. Lett. 21, 1055 (1968); C.S. Liu and D.K.Bhadra, Phys. Rev. Lett. 25, 1706 (1970); B.Coppi, Phys. Rev. Lett. 29, 1076 (1972).

2 P.Deschamps et al., Phys. Rev. Lett. 31, 1457 (1973); C.A. Primmerman et al., Phys. Rev. Lett. 33, 957 (1974).

3 Y.Hatta et al., J. Inst. Electr. Eng. Japan 85-12, 2041 (1965); N.Satc et al., Appl. Phys. Lett. 24, 300 (1974).

4 K.Saeki, S.Iizuka, N.Sato and Y. Hatta, to be published.

176

ELECTRON BEAM FUSION TARGET EXPERIMENTS

M. J. Clauser, S. A. Goldstein, R. J. Leeper, C. W. Mendel, L. P. Mix, J. N. Olsen, F. C. Perry, and A. J. Toepfer

Sandia Laboratories
Albuquerque, New Mexico 87115 U. S. A.

The interaction of intense relativistic electron beams with fusion targets has been studied using a variety of diagnostic techniques. Enhanced electron beam deposition in thin shell targets was observed on the Hydra accelerator. Results of first target experiments on Proto I are presented.

An important aspect of the particle beam fusion program at Sandia Laboratories is the investigation of the physics of imploding systems. Electron beam driven implosion experiments have been performed in both cylindrical and spherical geometries. From observations of neutron yield from spherical fusion targets and correlation of these measurements with the simultaneous determination of pellet temperature, symmetry of irradiation and other macroscopic pellet parameters, considerable insight into the dynamics of the implosion can be inferred. This information is complemented, by information gained by studying implosions in cylindrical geometry which permit questions relating to pusher integrity and stability to be more carefully investigated. In this paper, recent experiments dealing with the implosion dynamics of fusion targets in both geometries are described and areas of future investigation outlined.

Spherical Target Experiments Preliminary target experiments involving the irradiation and compression of DT gas in a spherical target have been performed on both the Hydra (1.1 MV, 350 kA, 30 kJ) and Proto I (two beams, each with 1.8 MV, 230 kA, 10 kJ) accelerators. Exploding pusher targets were chosen for the initial experiments since their lower mass would permit higher specific energy deposition.

The first Hydra target experiments used 0.8 mm diam, 10 μm wall Ni targets mounted on a stalk in the center of a graphite anode with a 12.7 cm diam tapered hollow cathode. X-ray pinhole photography, optical holography and time-of-flight (TOF) neutron detectors were employed as diagnostics. The x-ray pinhole photography indicated that the peak current densities were less than 1 MA/cm^2 on all the shots, with the current density in the region of the target typically a factor of 2-4 below the peak. Optical holography indicated energy deposition corresponding to 5-8 TW/gm or roughly an order of magnitude above that expected from paraxial electron flow at the measured current densities; however, the enhancement is in good agreement with a PIC code calculation of beam flow in a high γ/γ diode.[1] The TOF neutron detectors indicated $< 10^6$ compressional neutrons. To provide better coupling to the long pulse of the Hydra accelerator, 3 mm diam exploding pusher and ablatively driven targets have been designed and target experiments are beginning. Increases in the Hydra current density of factors of 2-4 have also been obtained and the outlook is good for the generation of compresional neutrons.

The Proto I targets were 1.5 mm diam gold spheres filled with DT gas having a mass of 30 to 60 mg. The pellets were mounted in the center of a thin aluminum anode which was positioned on the midplane between 2.5 cm diam tapered hollow cathodes. The main diagnostics included x-ray pinhole photography, optical wavelength emission measurements and TOF neutron detectors. For these experiments, total energy to each cathode was 5-7 kJ. The pinhole photographs indicated asymmetric target irradiation and radiation measurements implied pellet temperatures of a few electron volts. No compressional neutrons were observed. A possible cause of asymmetric target irradiation is believed to be due to poor grounding of the target. Recent diode work on Proto I has resulted in an increase of 50-100% in the total energy which can be delivered to each cathode and improved means of providing irradiation are being developed.

Cylindrical Implosions Considerable attention has been focused on the stability and integrity of the pusher in inertial confinement pellets. Mass ejection from shocked surfaces,[2] shock-driven instabilities[3] and Rayleigh-Taylor instabilities[4] have been all considered as possible limitations to achieving significant thermonuclear yields. Although the Rayleigh-Taylor instability is believed to dominate the pusher stability near the time of peak compression, no clear picture of the nonlinear development has been obtained. A single mode analysis[5] indicates the pusher will disassemble by injecting mass into the fuel volume; however, if one assumes a spectrum of waves is generated,[6] mode coupling might contribute to a turbulent spectrum causing the instability to saturate at a much reduced level. To look at this instability problem, effects of irradiation symmetry, and the possible ejection of material from shock surfaces, implosion experiments were performed in cylindrical geometry to permit axial optical and x-ray diagnostics.

Preliminary measurements of this type show the effects of irradiation uniformity on the implosion. Figure 1 shows holographic interferograms made of cylinders imploded by electron deposition on the Hydra accelerator. The exposures in both cases were made at $\sim$ 28 ns intervals using a PTM ruby laser having a 4 ns FWHM. Figure 1a shows the implosion of a thin plastic cylinder which is uniformly (to about 14%) irradiated. In this case, the implosion proceeds to an almost circular shell near the axis of the cylinder. Figure 1b shows for comparison a thick (compared to a CSDA range) cylinder, which was irradiated with a front to back asymmetry of $\geq$ 10 to 1. A shock wave propagates through the shell and drives the implosion. Although one might have expected the implosion to form a pancake shaped core, the converging plasma is observed to form a jet with peak-fringe velocities of 1.5 - 2 cm/μsec, in contrast to the body of the plasma which is moving at $\sim$ 20% of this velocity. Thus, the final state for the fuel in a corresponding spherical implosion is a toroidal shaped plasma at relatively low density and temperature — one which would not be expected to produce thermonuclear neutrons.

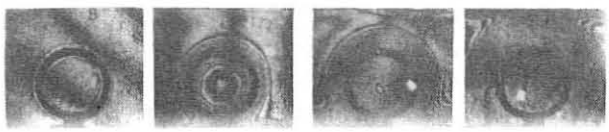

(a) Exploding Pusher (Uniform)

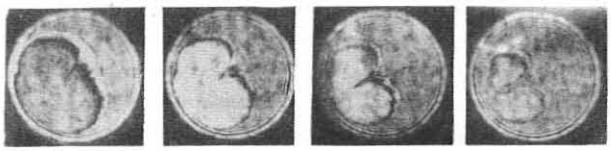

(b) Ablatively Driven (Non-uniform)

FIGURE 1. Cylindrical Implosions

References

1. M. J. Clauser, L. P. Mix, J. W. Poukey, J. P. Quintenz, and A. J. Toepfer, Phys. Rev. Lett. 38, 398 (1977).
2. J. R. Asay, L. P. Mix, and F. C. Perry, Appl. Phys. Lett. 29, 284 (1976).
3. Ye. Ye. Meshkov, Izvestiya, Akad. Nauk SSSR, Mekhanika Zhidkosti i Gaza, Sept. - Oct. 1969, p. 151.
4. G. I. Taylor, Proc. Roy. Soc. A201, 192 (1950).
5. J. R. Freeman, M. J. Clauser, S. L. Thompson, Nucl. Fusion, to be pub.
6. E. S. Fradkin, Tr. Inst. Fiz. Akad. Nauk SSSR, im. P. N. Lebedeva 29, 250 (1965).

The Dynamics of Mirror-Confined D-T Plasma*

T. Kammash and D. L. Galbraith
University of Michigan
Ann Arbor, Michigan, U. S. A.

Abstract: A time-dependent point model utilizing the particle and energy balance equations is used to study the dynamics of a mirror-confined D-T plasma. A modified binary collision theory to represent the interaction among the various species and an appropriately constructed loss cone distributions are used to generate the plasma parameters of interest. The results are then compared with the more accurate and extensive Fokker-Planck calculations and it is shown that they compare very favorably. Because of potential applications to mirrors with partially closed field lines, the effects of beta, injection angle, and the ambipolar potential on confinement and power production are examined in detail.

In an effort to enhance the Q (ratio of fusion to injection powers) value for mirror-confined plasmas several ideas have recently been advanced among which the concept of field reversed geometry appears to be attracting special attention. In this paper an effort is made to assess the effect of partial closing of the field lines with the implicit assumption that such a geometry would contribute to higher betas (ratio of plasma to magnetic pressures) and a reduction in the ambipolar potential. The particle and energy balance equations for all the species of a D-T plasma are used assuming no spatial dependences and utilizing a modified binary collision theory[1] to represent the interaction among the various species. For the electron confinement we use the results of Pastukhov[2] while for the ions we follow a procedure described by Carlson[3] but modified to incorporate loss cone distributions. In order to make use of the Maxwellian fusion reaction rate $\langle \sigma v \rangle$ we employ the procedure described by Kuo Petravic, Petravic and Watson[4] for expanding a function in a series of Maxwellians and calculate the appropriate averages for the loss cone distributions. For brevity the detailed mathematical developments and equations are omitted and only the results are presented.

A computer code is used to solve the equations in question and several important plasma parameters are calculated. It is shown that the above simplified, semi-analytic theory produces almost identical equilibrium results to those obtained by the elaborate, expensive and purely numerical Fokker-Planck calculations as shown in Table I.

Table I

Plasma Mirror Ratio = 10.0
Ion Injection Energy = 100 kev

Quantity	D-T-e Plasma Present Results	D-T-e Plasma Ref(5)	D-T-e-α Plasma Present Results	D-T-e-α Plasma Ref(5)
Density (Cm^{-5})				
Deuterons	1.320×10^{13}	1.32×10^{13}	1.410×10^{13}	1.41×10^{13}
Tritons	1.320×10^{13}	1.32×10^{13}	1.410×10^{13}	1.41×10^{13}
Alphas	----------	---------	7.44×10^{10}	3.00×10^{11}
Electrons	2.64×10^{13}	2.64×10^{13}	2.835×10^{13}	2.90×10^{13}
Ave Escape Energy (kev)				
Deuterons	47.05	45.4	54.52	51.8
Tritons	47.05	50.0	54.52	57.4
Alphas	-----	----	68.89	277.7
Electrons	52.43	55.2	66.00	68.2
Plasma Potential (kev)	43.03	45.5	53.83	57.0

The major discrepency appears in the alpha particle results and this stems from our assumption that the slowing down ("supra-thermal") alphas constitute a negligible addition to the "thermal" alpha population. Some of the interesting results are shown in the accompanying figures where figure (1) shows the dependence of the confinement parameter ($N\tau$); the figure of merit, Q; and the ambipolar potential on the injection angle. It is seen that the Q value is not drastically affected as the injection angle is reduced from 90° to about 70°. Figure (2) reveals that no dramatic changes will occur in Q and ($N\tau$) until very large values of beta are attained at which point the classical confinement commonly used may become questionable. Figure (3) shows also that no significant gain is achieved in Q and ($N\tau$) as a result of drastically reducing the ambipolar potential. It must be kept in mind that the last result bears no implication concerning the reversed potential of the "Tandem Mirror" concept.

*Work supported in part by U. S. ERDA and in part by EPRI

1. T. Kammash and D. L. Galbraith, Nuclear Fusion 13, 133 (1973)
2. V. P. Pastukhov, Nuclear Fusion 14, 3 (1975)
3. G. A. Carlson, Lawrence Livermore Lab. Report UCRL-51434 (1973)
4. G. L. Kuo Petravic, M. Petravic, C. J. H. Watson, BNES Culham, 144 (1969)
5. A. H. Futch et al., Plasma Physics, 14, 211 (1972)

FIGURE 1

$(NT)_\circ$, Q, and $e\Phi$ vs θ_{IN}

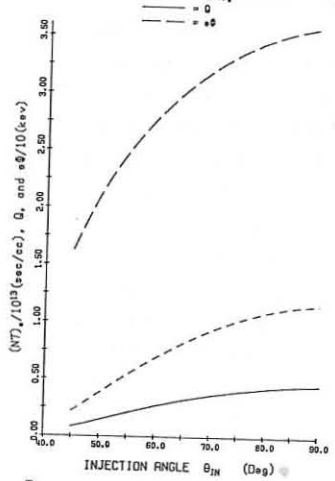

FIGURE 2

Q and $(NT)_\circ$ vs β

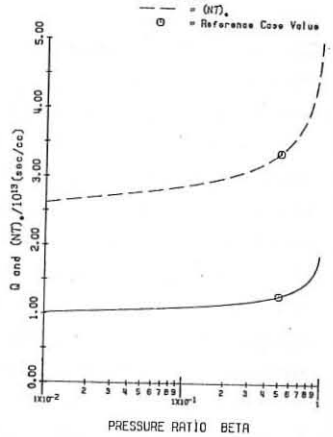

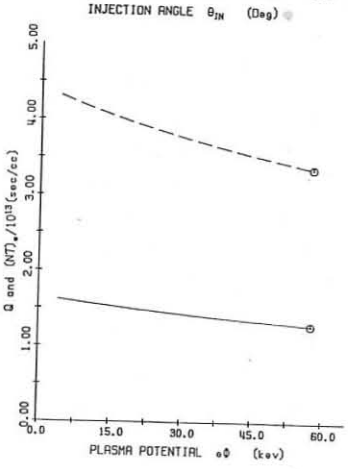

FIGURE 3

Q and $(NT)_\circ$ vs $e\Phi$

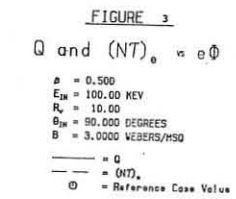

178

MEASUREMENT OF CURRENT DENSITY DISTRIBUTION IN A MEGAJOULE PLASMA FOCUS DEVICE

C. Gourlan, H. Kroegler, Ch. Maisonnier, T. Oppenländer+, J.P. Rager

Associazione EURATOM-CNEN sulla Fusione, Centro di Frascati, C.P. 65 - 00044 Frascati, Rome, Italy.

Abstract: Magnetic field measurements in a large plasma focus show that part of the current flows along the insulator. In optimized devices, this current derivation alone accounts for the observed neutron yield. In non-optimized devices, other (unclear) mechanisms reduce further the neutron yield.

1. Introduction: Among the various electrode geometries realized for the Frascati 1 MJ plasma focus set-up in order to obtain the best possible neutron yield, two of them emerged as the best performers so far. They are: (1) a large diameter (370 mm) small length (350 mm) system, optimized at 250 kJ (20 kV), yielding regularly more than 10^{11} neutrons per shot at this energy level, and, (2), a small diameter (160 mm) long length (560 mm) system, optimized at 500 kJ (28 kV) and yielding $5 \cdot 10^{11}$ neutrons per shot. These results lay a factor of 4 below the notorious scaling laws[1] and a factor of 2 below the best results obtained on other large energy facilities[2],[3]. It is shown in the following that the limitations in neutron yield in these optimized devices are due essentially to a continuous current derivation along the insulator. On the other hand, it is clear that in most others situations (in particular when the voltage applied to the two set-up under discussion is increased), the neutron yield is further limited by other phenomena.

2. Magnetic field distribution in a coaxial gun optimized at low energy level: Small magnetic probes have been used to get an accurate mapping (r,z) of the magnetic field in the large diameter, short length coaxial plasma gun (Fig. 1a) operating at the low energy level (250 kJ, U_o = 20 kV, p_o = 1,5 Torr D_2) for which it is optimized. The validity of the probe measurements has been ascertained carefully, in particular by checking that the cathode return current deduced from the $B_\theta(r)$ profile by radial integration from r = + ∞ is equal to the anode current obtained from B_θ measured near the anode. It is observed that the general performances of the gun, as well as the details of the magnetic field distribution and correlated current density distribution, show out similarities and discrepancies depending on the insulator material (Pyrex, alumina 99,7% purity).

A) For both kinds of insulators, the optimized neutron yields are nearly identical, and the mapping of the magnetic field shows the existence of a current derivation in the immediate vicinity of the insulator (Fig. 2,3). This current increases monotonically with time up to maximum compression (Fig. 4). It amounts to about 650 kA out of the 1.45 MA total current at pinch time. The remaining 800 kA flowing in the pinch justify very well the neutron yield of the facility, considering the scaling of the neutron yield as a function of the pinch current (For instance the very performant Frascati MIRAPI experiment yielded 10^{11} neutrons per shot at 100 kJ for a total pinch current of 900 kA). The coaxial cavity behind the main current sheath is filled with a background plasma, as evidenced by the differences in the shape of the dB/dt signals as a function of z at a given radius. Up to the time of maximum current this plasma carries no appreciable net current.

B) With a pyrex insulator, the magnetic field distribution is characterized by the following features:
- B_θ is independent of z, up to the time of maximum current (e.g. j_r = 0 everywhere);
- $B_\theta(r) \sim r^{-1}$ in the inner half of the channel;
- the current sheath along the insulator is less than 3 mm thick up to the time of the maximum current, and tends to thicken during the implosion phase.

C) With an alumina insulator, the characteristic features are:
- a magnetic field distribution identical to that found with pyrex in the region above the insulator;
- in front of the insulator, the $B_\theta(r)$ distribution corresponds to that created by the superposition of a distribution identical to the pyrex one, plus a demagnetizing current loop (Fig. 1b) of total thickness 2-3 cm. This feature persists steadily during all the run-down phase. The associated z-current, deduced from the $B_\theta(r)$ profile, is in agreement with the r-current deduced from the $B_\theta(z)$ profile and amounts to ≈ 300 kA.

3. Discussion: From these measurements, it is possible to evaluate the actual value of the gun inductance L; if J_{sheath} designs the intensity of the return cathode current and U the voltage drop across the insulator, then $L = \frac{\int U \cdot dt}{J_{sheath}}$ (neglecting sheath resistance). At the time at which the current sheath reaches the end of the gun (easily identifiable on the scope traces), this inductance agrees well with that determined geometrically (≈ 17 nH). Assuming that the same applies in the case of the small diameter head referred to in the introduction (for which probe measurements turned out to be practically impossible), from the geometrical inductance we can infer the value of J_{sheath} at the previously defined time. It results that the current derivated along the insulator has a minimum value of 0,5 MA. Assuming, as observed on the large diameter head, that this insulator current does not decrease during the implosion phase, we find a maximum possible pinch current of ≈ 1,5 MA which would once more agree well with the observed neutron yield, assuming an I^4 scaling. However, it is to be stressed that this simple mechanism of current derivation does not account for the neutron yield limitation in many other situations. In particular, the impossibility to establish a shot to shot correlation between neutron yield and pinch current demonstrates the importance of other physical phenomena.

References and footnote

+ On leave from Stuttgart University

1) L. MICHEL, K.M. SCHÖNBACH, M. FISCHER: Appl. Phys. Lett. 24, 57 (1974).

2) K.D. WARE, A.M. WILLIAMS, R.W. CLARK: Bull. Am. Soc. 18, 1364 (1973).

3) A. BERNARD et al.: Proceedings of the 7th European Conference on Controlled Fusion and Plasma Physics, Lausanne 1975, 60 (1975) Vol. I

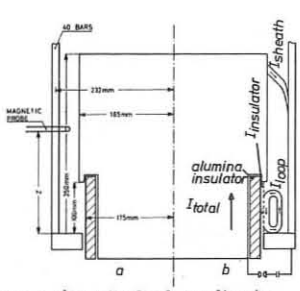

Fig.1.a)sketch of a large diameter small length plasma focus.
b)current loop in front of the alumina insulator.

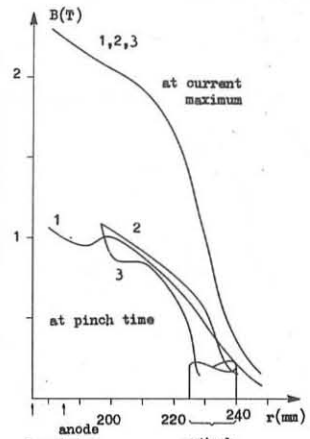

Fig.2. Magnetic field distribution (pyrex insulator).Probe positions (1) z=75, (2) z=150, (3) z=300 mm

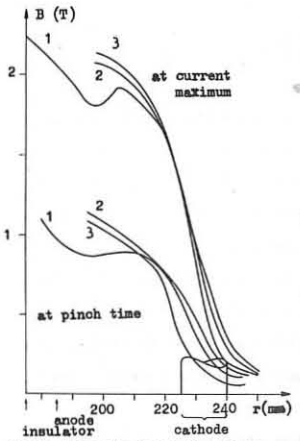

Fig.3. Magnetic field distribution (alumina insulator).Probe positions (1) z=75, (2) z=150, (3) z = 300 mm

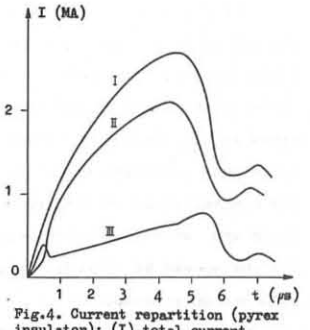

Fig.4. Current repartition (pyrex insulator): (I) total current, (II) cathode return current, (III) surface current along the insulator.

ENERGY EXCHANGE BETWEEN COHERENT RADIATION AND FAST ELECTRON BEAM

L.Kučera,J.Kortán

Institute of Radio Engineering and Electronics,Czechoslovak Academy of Sciences,Lumumbova 1,180 88 Prague 8,CSSR

Abstract:The computer analysis of the stimulated energy exchange between planar wave and about 10MeV electron beam has shown the possibility of beam acceleration by coherent radiation of milimeter wavelength.The amplification of the passing wave has been found also possible.

1.Introduction

Early studies of the stimulated photon-electron scattering have suggested the amplification [1] or frequency conversion [2] of coherent light in the direct relativistic electron beam.

The paper shows some results of computer study of the energy exchange with the dominating forward scattered mode without frequency shift.This mode exhibits gain with increasing electron velocity and its stimulation is not limited by the dispersion in electron velocity.Selective scattering is achieved in beams having energy of an order MeV or higher energy.The mechanism of energy transfer can be explained by the effect of phase shifts between the passing wave and the beam modulation.The beam energy loss and coherent power gain calculation needs the detail analysis of system dynamics.

2.Results of computer analysis

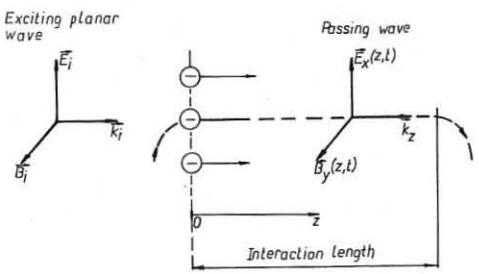

Fig.1 The model of field-beam interaction

The model shown in Fig.1. has been described by a set of partial differential equations,which were for the steady-state transformed into a set of fifteen ordinary nonlinear differential equations.The boundary conditions were determined at the incident interaction boundary z=0.We calculated stationary component,amplitude and phase of electron velocity and concentration,of the transverse electric and magnetic field and of the induced longitudinal electric field.Finally,the spread of electron velocity and the coherent power gain was determined.

For the computer calculation were taken following beam and excitation parameters:

incident beam energy	W(0)=2 upto 10MeV,
incident electron concentration	$N(0)=10^{18}$ upto $10^{20}m^{-3}$,
electric field amplitude of exciting planar wave	$E_o(0)=10^{7}$ upto $10^{10}Vm^{-1}$,
angular frequency	$\omega=10^{12}$ upto $10^{14}s^{-1}$.

In above range of parameters both the beam acceleration

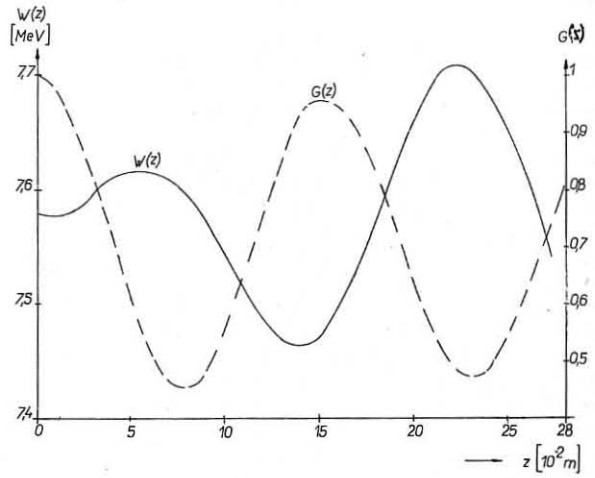

Fig.2 Dependence of the beam energy,W,and of the coherent power gain,G,on the distance from interaction boundary: W(0)=7,575 MeV,$N(0)=10^{20}m^{-3}$,$E_o(0)=10^{9}Vm^{-1}$, $\omega=10^{12}s^{-1}$

and radiation amplification was observed.Fig.2 shows the example of beam acceleration,from Fig.3 the amplification of passing wave is evident.

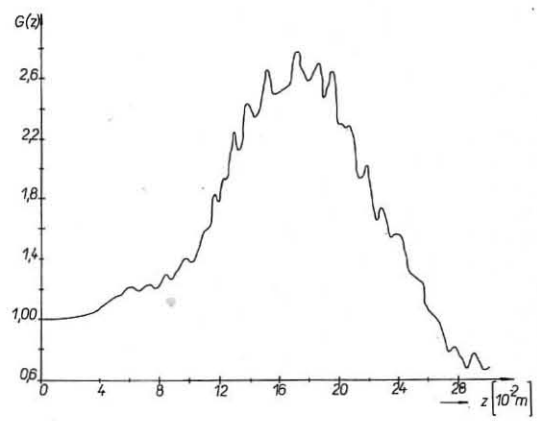

Fig.3 Coherent power gain for W(0)=10 MeV,$N(0)=10^{20}m^{-3}$, $E_o(0)=10^{9}Vm^{-1}$, $\omega=10^{13}s^{-1}$

[1] L.Kučera,J.Kortán,Proc.of WELC,1977,Moscow

[2] R.H.Pantell,G.Soncini,H.E.Puthoff,IEEE J.Quantum Electron. vol.4,pp.905-907

180

LOCALIZATION OF A HIGH-POWER MICROWAVE ABSORPTION IN THE CYLINDRICAL PLASMA COLUMN AT $\omega_{LH} \ll \omega \lesssim \omega_{ce}$

J. Musil, F. Žáček

Institute of Plasma Physics, Czechoslovak Academy of Sciences, Nademlýnská 600, 180 69 Prague 9, Czechoslovakia

Abstract: This paper describes experiments which make possible to determine the place of the absorption of elmag waves in cold (T_e= 5-10 eV) not fully ionized plasma column at $\omega_{ce}/\omega = 1$ and $\omega_{ce}/\omega > 1$

Basic assumption of a successful utilization of elmag waves absorption for the additional heating of a hot magnetoactive plasma is that the energy of elmag waves was absorbed in the whole volume of plasma. Unfortunately many experiments, see e.g. [1], show that elmag waves do not penetrate into the whole volume of plasma because their energy is strongly absorbed already on a surface of the plasma column. Since such surface absorption cannot be used for additional plasma heating to temperatures necessary for ignition of the controlled fusion it is very important to study the localization of elmag waves energy absorption in the cylindrical plasma column.

Experiment: In our experiment elmag waves (f=2.35GHz, $P_{inc} \lesssim$ 4kW) were fed into the straight glass discharge tube (ϕ_{int}= 72 mm) by means of a helical slow-down structure (pitch of the helix s =10 mm) placed outside the discharge tube. At $\omega_{ce}/\omega = 1$ the plasma was generated by the electron cyclotron absorption of the incident power (f = 2.35 GHz). At $\omega_{ce}/\omega > 1$ the preionization was used. In this case the microwave power (f=2.35 GHz) was absorbed in a primary plasma generated by the second helical structure working in C band. The mean electron plasma density was measured by means of an 8mm microwave interferometer. The movable probe which enabled to measure radial distributions of saturated ion current, floating plasma potential and axial component E_z of the electric field of an incident wave was placed inside the discharge tube. Experiments were carried out in an almost uniform magnetic field $\Delta B_o/B_o = \pm 0.05$. The device operated in a pulsed mode with repetition frequency 50 Hz. The working gas was argon.

The main result of our experiment is given in Fig. 1. This figure shows distributions of saturated ion current in the argon plasma (p=0.7 Pa) at $\omega_{ce}/\omega = 1$ (Fig. 1a) and $\omega_{ce}/\omega = 2.2$ (Fig. 1b); the parameter of curves is the mean electron density. From Fig.1 it can be clearly seen that

1) for both magnetic fields radial distributions of the density have a minimum on axis and two expressive maxima on the periphery;

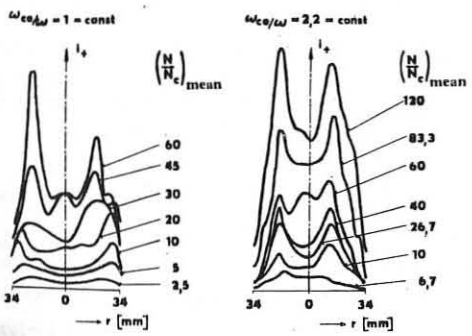

Fig. 1a

Fig. 1b

2) the ratio of density in maximum and minimum varies in dependence on the mean electron density; the maximum ratio is for both magnetic fields approximately the same and equals $(N_{max}/N_{min})_{max} \simeq 2$

3) there are certain densities $(N/N_c)_{mean}$ = 45 at $\omega_{ce}/\omega = 1$ and $(N/N_c)_{mean}$ = 60 at $\omega_{ce}/\omega = 2.2$ when on the axis of the discharge tube the third maximum occurs and the radial distribution is almost homogeneous; this fact is probably connected with a geometrical resonance of the plasma column;

4) for $(N/N_c)_{mean} \lesssim 5$ the ratio N_{max}/N_{min} decreases.

These experiments clearly shows that both in the regime of electron cyclotron resonance $\omega_{ce}/\omega = 1$ and at $\omega_{ce}/\omega > 1$ the energy of elmag waves fed into a plasma density of which $N/N_c > 1$ is absorbed predominantly on a periphery of the plasma cylinder.

Very important information about the place of an absorption offers also Fig. 2. This figure shows the radial distribution of E_z component of the wave entering the plasma, the floating potential $U_f(r)$ and the saturated ion current $i_+(r)$. It can be seen that incident wave is strongly attenuated just at the periphery of the plasma cylinder and it penetrates to the distance cca 1-2 cm from the plasma edge only. This strong damping of the wave is accompanied by the formation of negative spikes in the distribution $U_f(r)$ and by an intense increase of the plasma density with expressive maxima on the plasma periphery. Negative spikes, indicating places of the generation of fast electrons, occur in a region which is responsible for the strong absorption of the incident wave. From the linear theory [2] and experimental results[3] follows that this region lies in the vicinity of the plasma frequency. Therefore it is quite understandable that if the maximum plasma density increases above $(N/N_c)_{max} = 1$ the place of absorption will shift from the axis of the plasma column to its periphery. Such shift can be clearly seen in Fig. 3 where distributions of $U_f(r)$ for three different densities are given.

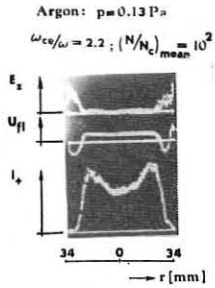

Fig. 2

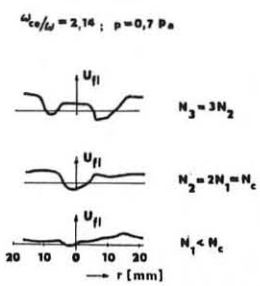

Fig. 3

Conclusion: Experimentally was shown that at $\omega_{ce} = \omega$ and $\omega_{LH} \ll \omega \lesssim \omega_{ce}$ the absorption of elmag waves in the cold partially ionized plasma density of which $(N/N_c)_{mean} > 1$ takes place first of all on the periphery of the plasma cylinder. Such situation is for an additional plasma heating obviously inconvenient. The efficient heating of the plasma column requires to shift the region of absorption from the periphery to the axis. It can be achieved only in the case when the maximum plasma density will be $(N/N_c)_{max} \lesssim 1$ for the electron cyclotron absorption and $(N/N_c)_{max} \simeq 1$ for the absorption at $\omega_{LH} \ll \omega \lesssim \omega_{ce}$. Only in this case an efficient heating of the whole volume of the plasma can be expected.

The authors wish to thank L. Bárdoš for helping with the experiments.

[1] M. Porkolab et al.: Plasma Physics 17 (1975), 405

[2] V.L. Ginzburg: Propag. of elmag waves in Pl., Moscow 1964

[3] V. Kopecký, J. Musil, F. Žáček: Phys.Lett. 50A (1974), 309

DYNAMICAL STABILIZATION OF THETA AND COMBINED PINCHES BY A LONGITUDINAL HF CURRENT

G.G. Zukakishvili, I.F. Kvartskhava, E.K. Tikhanov
Sukhumi Institute of Physics and Technology of the State Committee on Utilization of Atomic Energy, Sukhumi, USSR

It has been shown in Paper /1/ that in a combined pinch for the longitudinal current exceeding Kruskal-Shafranov limit, there arises a MHD instability with m=1 mode and λ =2L wavelength. In Paper /2/, the preliminary results on stabilization of this instability by a longitudinal HF current were reported. Those results indicated that the HF current does not completely penetrate into the region of a dense plasma column, but partially flows through a rarified wall-side plasma. The present report gives the results of investigations of the theta-pinch longitudinal magnetic field influence on the HF current radial distribution. The realizability of the dynamical stabilization of a "rotatory" instability in a theta-pinch with an inverse trapped magnetic field is indicated.

The experiments were carried out in a device described in /1,2/. The diameter of a quartz discharge chamber is 6,5cm. In a coil with the length L=21cm, the field H_z=65kOe has been generated. The longitudinal current in a zeta-pinch is I_z=5-50kA. Zeta and theta pinches were turned on simultaneously in a plasma preheated up to 3eV and had equal periods T=19 μsec. Plasma parameters have been determined basically by the theta-pinch since $H_z^2 \gg H_\theta^2$, and at the initial deuterium pressure $P_o=8.10^{-2}$torr, the parameters were: $n_e=10^{17}cm^{-3}$, T_e=100 eV and T_i=400 eV.

The HF current peak-to-peak value I_z was 25kA, its frequency being $w_s=(3,8-4,7).10^6 sec^{-1}$. In order to measure the longitudinal current distribution along the discharge chamber radius, magnetic probes and two Rogowsky coils have been used. One of the coils measured the total current I_n while another one measured the wall-side current I_{cm}. The wall-side current measuring coil was introduced into the chamber by a quartz tubing with the diameter of 0,3cm, to the depth of 1,5cm. After the fast compression phase the belt was located outside the plasma column.

Fig. 1 represents the traces of the wall-side and total HF currents for two various instants of HF contour switching with respect to the onset of theta pinch (the total HF current traces are synchronized with the current in the theta-pinch coil). It is obvious that at the end of the first halfcycle of the HF contour, the breakdown occurs in a wall-side region. Afterwards, the HF current distribution over the radius depends on the magnetic field amplitude (H_z) and its derivative ($\dot{H}_z$). On switching the HF circuit during the first quarter of H_z field period (i.e., when $\dot{H}_z > 0$), after the breakdown, the HF current in the wall-side region is absent till H_z maximum and appears again when H_z diminishes. With the HF circuit turned on at H_z maximum or its fall, the current flows in the wall-side region all the time, while the wall-side to total current ratio increases with the time (Fig.1b). Thus, at $\dot{H}_z > 0$, the HF current displaces towards the axis into the plasma column region, while at $\dot{H}_z < 0$, it displaces towards the chamber wall. When the peak-to-peak value of H_z is increased up to 65 kOe the pattern does not undergo any changes (Fig.2), but the HF current value in the wall-side region reduces in accordance with the results from /3,4/.

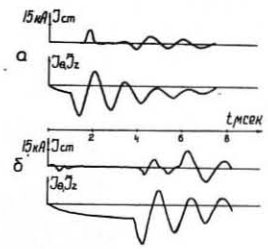

Fig. 1. Theta-pinch with a longitudinal HF current. H = 35 kOe

In a combined pinch, the quasistationary current flows in the dense plasma column region while the HF current undergoes radial oscillations (Fig.3). During those halfcycles when the direction of the HF and quasistationary currents coincide, the current displaces towards the axis, while during opposing halfcycles they displace towards the discharge chamber wall. As a result, a singular effect of rectifying is observed during the longitudinal field growth stage ($\dot{H}_z > 0$), (see Fig.3a). In the pinch region a pulsing current flows (with the peak-to-peak value exceeding Kruskal-Shafranov limit) which leads to the plasma column destabilization.

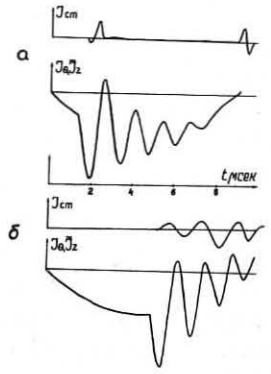

Fig. 2. Theta pinch with the longitudinal HF current. H = 65 kOe.

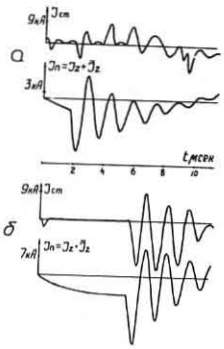

Fig. 3. Combined pinch with the longitudinal HF current. H=35 kOe, I_z = 7 kAmp.

The experimental data analysis shows that the shell of a rarified wall-side gas where the HF current flows has an anomalous high resistance and undergoes radial oscillations due to the action of the electrodynamical force:

$$F_r = \frac{2\pi}{c}\int_0^{\Delta}\left[j_\theta H_z + \tilde{J}_z\left(\tilde{H}_\theta + H_\theta\right)\right] r\,dr$$

where Δ and H_θ are the shell thickness and the quasistationary longitudinal current field, respectively. The induction current (j_θ) arises as a result of $\dot{H}_z \neq 0$. Since the plasma conductance is low, $j_\theta \sim \dot{H}_z$ and $\frac{1}{c} j_\theta \dot{H}_z$ force at $\dot{H}_z > 0$ is directed towards the axis, while at $\dot{H}_z < 0$ it is directed towards the chamber. It is easy to observe that the HF current displacements coincide with the direction of $\frac{1}{c} j_\theta H_z$ force. These relatively slow displacements of the shell are superposed by high-frequency radial oscillations caused by the action of $\frac{1}{c}\tilde{J}_z\left(\tilde{H}_\theta + H_\theta\right)$ force.

Thus, the HF current flows mainly along the shell of a rarified wall-side plasma which undergoes radial oscillations due to the HF current peak-to-peak value, the longitudinal magnetic field and its derivative.

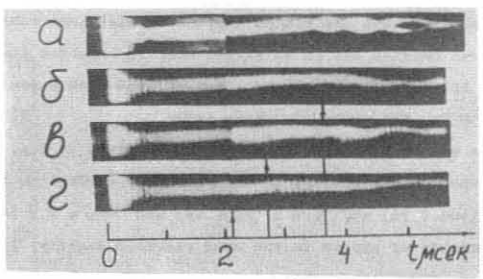

Fig. 4. Theta-pinch with an inverse trapped magnetic field. The instants of the HF current switching are indicated by arrows.

Fig. 4a shows the rotatory instability in the theta-pinch with an inverse field. The HF current turned on stabilizes the rotational instability, the effect of stabilization being better for the HF circuit turned on immediately after the theta-pinch discharge ignition (see Figs.4b,c,d). It is rather difficult to give decisive definitions of the stabilization mechanism at present.

REFERENCES

/1/ I.F. Kvartskhawa et al. Physics and Controlled nuclear fusion research. Vienna. I v. 1", 1971.

/2/ G.G. Zukakischwili et al. Proc. 6 Europ. Conf. on Contr. Fusion and Plasma. Moscow, I, 281, 1973.

/3/ O. Gruber, "Zeitschrift für Physik" B. 251, h. 4, 333, 1972.

/4/ H. Zwicker "Atom. kern energie", v.19, No. 3, 186, 1972.

182

HEATING OF FOILS BY REB

M.V.Babikin, K.A.Bajgarin, A.V.Bartov, S.L.Bogoluybskij, V.V.Vasilevskij, V.I.Liksonov, V.I.Migiritskij, L.I.Rudakov, V.P.Smirnov

I.V.Kurchatov Institute of Atomic Energy, Moscow, USSR

The heating of thin anode foils when Z >>1 by the focused electron beams allows to produce the compression and the heating of dense plasma /1/. The anode plasma temperature of 30-80 eV has been reached first at "Triton" by rising the energy transfer to the material of a target through a high current beam /2/. At the injection of electrons into plasma produced by the explosion of an anode foil the magnetic field of beam penetrates approximately to the skin-layer depth $\delta = \frac{c\sqrt{t}}{\sqrt{4\pi\sigma}}$. This results in radial magnetic drift of the beam electrons with a velocity $V_r = \frac{\gamma mc^3}{2eH^2}\cdot\frac{\partial H}{\partial z} \simeq c\cdot\frac{I_A}{4I}\cdot\frac{r}{\delta}$ (r - beam radius, $I_A = 17\beta\gamma$ (KA)), in the increase in electron density $n = \frac{I}{2\pi r e \delta V_r} = \frac{2I}{I_A}\cdot\frac{I}{\pi r^2 ec}$ and the absorbed energy by a factor of $2I/I_A$ in comparison with the calculations done for the binary collisions. The thickness of a heated zone depends on the depth of the magnetic field penetration. These estimations are confirmed by an exact solution for the beam penetration in the range of $z << r$. At "Triton" the measured energy input per atom of gold reaches 3keV /2/. Both experiment and calculations show that a considerable portion of energy can be transferred from the anode foil to a freely permeable shell via the heatconductivity. The velocity of polyethylene plasma strongly depends on the initial thickness of the polyethylene foil /1/ (some 8.10^6 oms^{-1} for the thickness of 10 μm). The yield of fusion neutrons up to 3.10^6 was registered on the compression and heating of deuterium plasma by a spherical polyethylene shell with a radius of 2mm in a conical cavity extrused in lead. The time of flight measurements of the energy of neutrons give 2,4± 0,25 MeV at a base equal to 2,2mm /1/. In the design of a target the pressure of plasma is limited by the expansion of the cavity walls which is essential only in the final stage of heating as $p \sim r^{-5}$ on adiabatic compression. The compression ratio of 10^3 was evaluated from the residual deformation of the cavity walls. The influence of their density on the heating is proved by the decrease in neutron yield by an order of magnitude using the conical cavity extrused in paraffin. A loss of energy dependent on the thermal conductivity of electrons exceeds the power produced by the shrinking shell at the end of compression at the expected parameters of plasma (T ≈1keV, n≈10^{22} om^{-3}, r-0,2mm) and it prevents the heating of plasma in the process of compression. Argon is added to deuterium to reduce the losses and to satisfy the following ratio $\sum n_\alpha Z_\alpha^2 r \simeq 10^{21} T^{3/2}$ corresponding to the minimum heat conductivity and bremsstrahlung losses from plasma. The maximum of neutron yield versus argon concentration (Fig.1) agrees with this evaluation. By an increase in thermal capacity and in the radiation losses the fall in neutron yield can be explained both at higher argon concentrations and at higher initial density of the compressed gas (Fig.2). The yield of neutrons does not exceed 10% of the optimum yield if the polyethylene shell 100μm thick is used as well as without any polyethylene. Thus, the compression and the heating of plasma by a polyethylene shell is demonstrated.

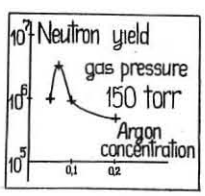

Fig. 1

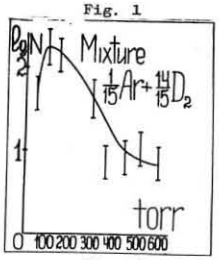

Fig. 2

At Angara-I the cathodes with a sharp annular lug with a diameter of 8mm and a conical cavity 7mm deep at the centre of the lug have been used. At the voltage 1 MV and at the current 330 kA the diameter of the focused beam is equal to 1-2mm the current density - 10-30MAcm^{-2}, power flux density - 10^{13}Wcm^{-2}, the energy release in a diode is equal to 17kJ /3/. The current depends on a shape of the edge and does not depend on a distance between the planes. No change was observed after increasing the distance (at the cathode diameter of 16cm) from 1 to 3cm. The value of current equal to 330kA at the diameter of the channel equal to 2mm cannot be explained by the vacuum current, it depends on the turbulent resistance of the plasma channel. At the magnetic confinement of a pinch formed by a gas of relativistic electrons the development of turbulency has no obstacles as a result of mixing of all the osoillations on a small scale and the velocity of current propagation shouldn't considerably exceed c_s-velocity of ion sound ($I \approx 10^6\sqrt{\gamma}/\alpha$ (A)). When $\alpha = \frac{V_p}{c_s} \simeq 3$ the values of the current are in good agreement with the experiment. The deceleration efficiency of the high-current beam in thin foils has been evaluated at the irradiation of a target made of two hemispheres with different thickness with a diameter of 4mm fashened to different sides of an orifice in the anode. The front foil has been 5 to 45μm thick, the rear foil - 25μm thick. The image of the foils has been registered by X-rays in two pinhole cameras under the angle of 90° to the axis of the beam. The photometric images have shown that when the front foil is 5μm thick its brightness is comparable with the brightness of the rear foil (Fig.3). The golden foil steam divergence dependent on the thickness of foil under the focused beam has been measured (Fig.4). The numerical correlation shows that the temperature of 80eV has been reached in the foil of gold. The velocity of the polyethylene foil 15μm thick placed behind the foil of gold has reached 1-1,5.10^7 oms^{-1} (Fig. 5).

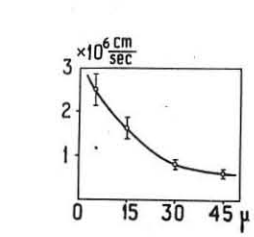

Fig. 4

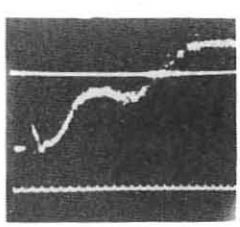

Fig. 5

An expulsion depends on X-rays, the first rise of the curve corresponds to the arrival of the polyethylene steam, the second smooth rise of the curve corresponds to the arrival of the steam of gold (the flight distance - 6cm, time markers - 0,2μs). The specific power 10^{13}Wcm^{-2} and the velocities of divergence mentioned allow to study the processes in the range of plasma temperatures and densities, corresponding to the fusion target of final size.

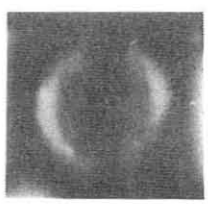

Fig. 3

REFERENCES

/1/ S.L.Bogolyubskij et al., Pis'ma v ZhETP, 24, 206, 1976.

/2/ S.L.Bogolyubskij et al., Pis'ma v ZhETP, 24, 202, 1976.

/3/ M.V.Babikin et al., MACATE International Conference, Dubna, 1976.

EIGHTH EUROPEAN CONFERENCE ON CONTROLLED FUSION AND PLASMA PHYSICS

Prague, Czechoslovakia 19 - 23 September 1977

LIST OF PARTICIPANTS

ADAM J.
CEA, Fontenay, France

ANDERSEN V.
RISO, Roskilde, Denmark

ANDERSON D.T.
Univ. of Wisconsin, Madison, USA

ARSENIN A.A.
IAE Kurchatov, Moscow, USSR

ASHBY D.E.T.F.
UKAEA, Culham, UK

BABICKÝ V.
Inst. Plasma Phys., Prague, Czechoslovakia

BADALEC J.
Inst. Plasma Phys., Prague, Czechoslovakia

BAMIERE C.
SGDN, Paris, France

BARBIAN E.P.
FOM, Rijnhuizen, Netherlands

BÁRDOŠ L.
Inst. Plasma Phys., Prague, Czechoslovakia

BARHUDAROV E.M.
Phys. Inst., Tbilisi, USSR

BARRERO A.
Esc. Techn. Superior, Madrid, Spain

BAUMGAERTEL K.
Zentralinst. f. Elektronenphysik, Berlin, GDR

BECKER G.
IPP, Garching, FRG

BEKEFI G.
MIT, Cambridge, USA

BELIKOV V.S.
Inst. Nucl. Res., Kiev, USSR

BELL M.G.
Austr. National Univ., Canberra, Australia

BERNARD A.
CEA, Limeil, France

BERNARD M.G.
CEN, Grenoble, France

BHATNAGAR V.P.
Ecole Royale Milit., Brussels, Belgium

BISKAMP D.
IPP, Garching, FRG

BLANKEN R.A.
US ERDA, Washington, USA

BLOKH M.A.
Lebedev Inst., Moscow, USSR

BOBELDIJK C.
FOM, Rijnhuizen, Netherlands

BOBROVSKIJ G.A.
IAE Kurchatov, Moscow, USSR

BOCHAROV V.K.
Phys. Techn. Inst., Kharkov, USSR

BOGEN P.
IPP, Jülich, FRG

BOGOMOLOV G.D.
Inst. Phys. Problems, Moscow, USSR

BOHÁČEK V.
Inst. Plasma Phys. Prague, Czechoslovakia

BRAAMS C.M.
FOM, Rijnhuizen, Netherlands

BRAMBILLA M.
CEN, Grenoble, France

BRUHNS H.
Univ. Heidelberg, Heidelberg, FRG

BRUNELLI B.
CNEN, Frascati, Italy

BURTSEV V.A.
Efremov Inst., Leningrad, USSR

CANOBBIO E.
CEN, Grenoble, France

CAP F.
Univ. of Innsbruck, Innsbruck, Austria

CARRUTHERS R.
UKAEA, Culham, UK

CHANG C.T.
RISO, Roskilde, Denmark

CHATELIER M.
CEA, Fontenay, France

CHENEVIER P.
France

CHODURA R.
IPP, Garching, FRG

CHU T.K.
PPPL, Princeton, USA

CHYRCZAKOWSKI S.
Inst. Nucl. Res., Otwock-Swierk, Poland

COENSGEN F.H.
LLL, Livermore, USA

CONRADS H.
IPP, Jülich, FRG

CONSOLI T.
CEN, Grenoble, France

DANILKIN I.S.
Lebedev Inst., Moscow, USSR

ĎATLOV J.
Inst. Plasma Phys., Prague, Czechoslovakia

DAYBELGE U.
Ruhr-Univ. Bochum, Bochum, FRG

DE HAAN P.H.
FOM, Kruislaan, Amsterdam, Netherlands

DE MICHELIS C.
CEA, Fontenay, France

DELCROIX J.L.
Univ. Paris, Orsay, France

DIKIJ A.G.
Phys. Techn. Inst., Kharkov, USSR

DIPPEL K.H.
IPP, Jülich, FRG

DOKOPOULOS P.
Joint Europ. Torus, Abingdon, UK

DRAKE J.R.
Royal Inst. Techn., Stockholm, Sweden

DRŠKA L.
Czech. Techn. Univ., Prague, Czechoslovakia

DUECHS D.F.
IPP, Garching, FRG

DYMOKE-BRADSHAW A.K.L.
Imperial College, London, UK

EGGERT H.
GRS, Köln, FRG

ELSAESSER K.
Ruhr-Univ. Bochum, Bochum, FRG

ENGELMANN F.
FOM, Rijnhuizen, Netherlands

ENRIQUES L.
CNEN, Frascati, Italy

FENEBERG W.
IPP, Garching, FRG

FIELDING S.J.
UKAEA, Culham, UK

FRIEMAN E.A.
PPPL, Princeton, USA

FUENFER E.
IPP, Garching, FRG

FUKUDA M.
IPP, Nagoya, Japan

FUMELLI M.
CEA, Fontenay, France

GATTI G.
CNEN, Frascati, Italy

GEKKER I.R.
Lebedev Inst., Moscow, USSR

GIBSON A.
Joint Europ. Torus, Abingdon, UK

GIERKE G. von
IPP, Garching, FRG

GIRARD J.-P.
CEA, Fontenay, France

GIUPPONI P.
CNEN, Frascati, Italy

GOEDBLOED J.P.
FOM. Rijnhuizen, Netherlands

GOELER S. von
PPPL, Princeton, USA

GOLANT V.E.
Ioffe Inst., Leningrad, USSR

GOTTLIEB M.B.
PPPL, Princeton, USA

GOURDON C.
CEA, Fontenay, France

GOURLAN C.
CNEN, Frascati, Italy

GRAY D.R.
Blackett Lab., London, UK

GREEN B.J.
JET, Culham, UK

GREENE J.
PPPL, Princeton, USA

GRIEGER G.
IPP, Garching, FRG

GROMOV A.I.
Lebedev Inst., Moscow, USSR

GUSTAFSSON H.
Defense Res. Inst. Fack, Stockholm, Sweden

HAGIWARA S.
TBU, Ibaraki-ken, Japan

HAMAL K.
Czech. Techn. Univ., Prague, Czechoslovakia

HAMBERGER S.M.
UKAEA, Culham, UK

HARMS K.D.
Essen Univ., Essen, FRG

HEMZAL K.
Freie Welt, Berlin, GDR

HENKES W.
IKVZ, Karlsruhe, FRG

HICKOK R.L., Jr.
Rens. Pol. Inst., New York, USA

HINES K.C.
Melb. Univ., Melbourne, Australia

HINTZE W.
ZIE, Berlin, GDR

HIOKI Y.
Daido Inst. Tech., Nagoya, Japan

HOEKZEMA J.A.
FOM, Rijnhuizen, Netherlands

HOETHKER K.
IPP, Jülich, FRG

HUGILL J.
UKAEA, Culham, UK

ICHTCHENKO G.
CEN, Grenoble, France

IGNACZ P.
Centr. Inst. Phys., Budapest, Hungary

INOUE N.
Univ. of Tokyo, Tokyo, Japan

JABLOKOV B.N.
Lebedev Inst., Moscow, USSR

JAENICKE R.
IPP, Garching, FRG

JAKUBKA K.
Inst. Plasma Phys., Prague, Czechoslovakia

JARKA J.
UTRIN, Prague, Czechoslovakia

JENSEN T.H.
Gen. Atomic Comp., San Diego, USA

JOUYS J.C.
CEA, Talant, France

JUNGWIRTH K.
Inst. Plasma Phys., Prague, Czechoslovakia

JUNKER J.
IPP, Garching, FRG

JURGENS B.
FOM, Kruislaan, Amsterdam, Netherlands

KALFSBEEK H.W.
FOM, Rijnhuizen, Netherlands

KAPIČKA V.
Dept. Phys. Electr, UJEP, Brno, Czechoslovakia

KAPOUN K.
Tech. Univ. of Mining, Ostrava, Czechoslovakia

KARDON B.
Centr. Inst. Phys., Budapest, Hungary

KARGER F.
IPP, Garching, FRG

KARLSON E.T.
Dept. Theor. Electr., Uppsala, Sweden

KASPERCZUK A.
Inst. Plasma Phys., Warszawa, Poland

KAUFMANN M.
IPP, Garching, FRG

KEILHACKER M.
IPP, Garching, FRG

KERNER W.
IPP, Garching, FRG

KICK M.
IPP, Garching, FRG

KIROV A.G.
Phys. Techn. Inst., Sukhumi, USSR

KLÍMA R.
Inst. Plasma Phys., Prague, Czechoslovakia

KLUEBER O.
IPP, Garching, FRG

KNOEPFEL H.
CNEN, Frascati, Italy

KOECHLIN F.
CEA, Fontenay, France

KOERBEL Š.
Inst. Plasma Phys., Prague, Czechoslovakia

KOFOED-HANSEN O.
RISO, Roskilde, Denmark

KOLÁČEK K.
Inst. Plasma Phys., Prague, Czechoslovakia

KONSTANTINOV S.G.
Nucl. Inst. Phys., Novosibirsk, USSR

KOPECKÝ V.
Inst. Plasma Phys., Prague, Czechoslovakia

KORNHERR M.
IPP, Garching, FRG

KORESHEVA E.R.
Lebedev Inst., Moscow, USSR

KOVÁČ I.
Inst. Plasma Phys., Prague, Czechoslovakia

KOZIARKIEWICZ W.
Inst. Plasma Phys., Warszawa, Poland

KRACÍK J.
Czech. Techn. Univ., Prague, Czechoslovakia

KOZYREV A.N.
IOFFE Inst., Leningrad, USSR

KRAUSE H.
IPP, Garching, FRG

KREBS K.H.
ZIE, Berlin, GDR

KRLÍN L.
Inst. Plasma Phys., Prague, Czechoslovakia

KROKHIN O.N.
Lebedev Inst., Moscow, USSR

KRYŠKA L.
Inst. Plasma Phys., Prague, Czechoslovakia

KUČERA L.
Inst. Radioelectr., Prague, Czechoslovakia

KUCINSKI J.
Inst. Nucl. Res., Otwock-Swierk, Poland

KUNC J.
Warsz. Techn. Univ., Warszawa, Poland

KUZNETSOV Yu. A.
Inst. High Temp., Moscow, USSR

KYNCL J.
Nucl. Res. Inst., Prague-Řež, Czechoslovakia

LACINA J.
Inst. Plasma Phys., Prague, Czechoslovakia

LACKNER K.
IPP, Garching, FRG

LAING E.W.
Glasgow Univ., Glasgow, Scotland, UK

LARRIMORE J.A.
IAEA, Vienna, Austria

LEES D.J.
UKAEA, Culham, UK

LEHNERT B.
Royal Inst. Techn., Stockholm, Sweden

LEWIS H.R.
Univ. of California, Los Alamos, USA

LIBERMAN M.A.
Inst. Phys. Problems, Moscow, USSR

LIKSONOV V.I.
IAE Kurchatov, Moscow, USSR

LOK J.
FOM, Rijnhuizen, Netherlands

LORTZ D.
IPP, Garching, FRG

LUGANSKIJ L.B.
Inst. Phys. Problems, Moscow, USSR

LYON J.F.
Oak Ridge Lab., Oak Ridge, USA

MAISONNIER CH.
CNEN, Frascati, Italy

MALFLIET W.
Antwerp Univ., Wilrijk, Belgium

MANUSHIN V.T.
Inst. High Temp., Moscow, USSR

MASCHKE E.K.
CEA, Fontenay, France

MATSUOKA K.
Inst. Plasma Phys., Nagoya, Japan

MATUSIAK A.
Inst. Nucl. Res., Otwock-Swierk, Poland

MCCORMICK K.
IPP, Garching, FRG

MCCRACKEN G.M.
UKAEA, Culham, UK

MERCIER C.
CEA, Fontenay, France

MIKHAILOV Yu.A.
Lebedev Inst., Moscow, USSR

MIX L.P.
Sandia Lab., Albuquerque, USA

MIYAMOTO K.
Inst. Plasma Phys., Nagoya, Japan

MIYAMOTO T.
Nihon Univ., Tokyo, Japan

MOSES K.D.
ERDA, Washington, USA

MOTOJIMA O.
Kyoto Univ., Gokasho, Japan

MUSHER S.L.
Inst. Automat. Electr., Novosibirsk, USSR

MUSIL J.
Inst. Plasma Phys., Prague, Czechoslovakia

NANOBASHVILI S.I.
Inst. Phys., Tbilisi, USSR

NEDOSPASOV A.V.
Inst. High Temp., Moscow, USSR

NEUHAUSER J.
IPP, Garching, FRG

NICOLAI A.
IPP, Jülich, FRG

NODWELL R.
Univ. Brit. Columbia, West Vancouver, Canada

OHKAWA T.
Gen. Atomic Comp., San Diego, USA

OHLSSON D.E.
Royal Inst. Techn., Stockholm, Sweden

OKUDA T.
Dept. Electr. Nagoya Univ., Nagoya, Japan

OOMENS A.A.M.
FOM, Rijnhuizen, Netherlands

ORNSTEIN L.T.M.
FOM, Rijnhuizen, Netherlands

ORTOLANI S.
CSGI, Padova, Italy

OTT W.
IPP, Garching, FRG

PALUMBO D.
Comm. Europ. Commun., Brussels, Belgium

PANARELLA E.
National Res. Council, Ottawa, Canada

PARIS G.
Central Res. Inst., Budapest, Hungary

PAUL J.W.M.
UKAEA, Culham, UK

PEIRY J.-M.
CRPP, Lausanne, Switzerland

PEREGUD B.P.
Ioffe Inst., Leningrad, USSR

PETERSON L.F.
Austr. National Univ., Canberra, Australia

PETROV V.G.
Inst. High Temp., Moscow, USSR

PETRŽÍLKA V.A.
Inst. Plasma Phys., Prague, Czechoslovakia

PFIRSCH D.
IPP, Garching, FRG

PIFFL V.
Inst. Plasma Phys., Prague, Czechoslovakia

PIKULÍK L.
Inst. Plasma Phys., Prague, Czechoslovakia

POPEL O.S.
Inst. High Temp., Moscow, USSR

POPOV A.M.
Moscow State Univ., Moscow, USSR

POZZOLI R.
CNR, Milano, Italy

PREINHAELTER J.
Inst. Plasma Phys., Prague, Czechoslovakia

PRINZLER H.
ZIE, Berlin, GDR

PROSS G.
Univ. Stuttgart, Stuttgart, FRG

RABINOVICH M.S.
Lebedev Inst., Moscow, USSR

RAEDER J.
IPP, Garching, FRG

RAGER J.P.
CNEN, Frascati, Italy

RAU F.
IPP, Garching, FRG

REID J.
Glasgow Univ., Glasgow, Scotland, UK

REM J.
FOM, Rijnhuizen, Netherlands

RENNER H.
IPP, Garching, FRG

RIEDMUELLER W.
IPP, Garching, FRG

ŘÍPA M.
Inst. Plasma Phys., Prague, Czechoslovakia

RIVIERE A.C.
UKAEA, Culham, UK

ROBERTS K.V.
UKAEA, Culham, UK

ROBINSON D.C.
UKAEA, Culham, UK

ROSLYAKOV G.V.
Nucl. Inst. Phys., Novosibirsk, USSR

RUSANOV V.D.
IAE Kurchatov, Moscow, USSR

RUTGERS W.R.
FOM, Rijnhuizen, Netherlands

RYBNÍČEK J.
Inst. Plasma Phys., Prague, Czechoslovakia

SADOWSKI M.
Inst. Nucl. Res., Otwock-Swierk, Poland

SAEKI K.
Tohoku Univ., Sendai, Japan

SHKVARUNEC A.G.
Lebedev Inst., Moscow, USSR

SALAT A.
IPP, Garching, FRG

SAMUELLI M.
CNEN, Frascati, Italy

SAND F.
EURATOM, Brussels, Belgium

SCHAMEL H.
Ruhr-Univ. Bochum, Bochum, FRG

SCHEP T.J.
FOM, Rijnhuizen, Netherlands

SCHLUETER A.
IPP, Garching, FRG

SCHLUETER J.
IPP, Jülich, FRG

SCHMITTER K.H.
IPP, Garching, FRG

SCHROETTER J.
Inst. Plasma Phys., Prague, Czechoslovakia

SCHUELLER F.C.
FOM, Rijnhuizen, Netherlands

SEDLÁČEK Z.
Inst. Plasma Phys., Prague, Czechoslovakia

SESTERO A.
CNEN, Frascati, Italy

SHAFRANOV V.D.
IAE Kurchatov, Moscow, USSR

SHOHET J.L.
Univ. Wisconsin, Wisconsin, USA

SHPIGEL I.S.
Lebedev Inst., Moscow, USSR

SHUKLA P.K.
Ruhr-Univ. Bochum, Bochum, FRG

ŠÍCHA M.
Charles Univ., Prague, Czechoslovakia

SIGMAR D.J.
Oak Ridge Lab., Oak Ridge, USA

SLAMA L.
CERCEM, Le Bourget, France

SMIRNOV
USSR

ŠOBRA K.
Czech. Techn. Univ., Prague, Czechoslovakia

SOELDNER F.
IPP, Garching, FRG

SOERLEI Z.
Centr. Inst. Phys., Budapest, Hungary

SORIE
Centr. Inst. Phys., Budapest, Hungary

SOROKIN A.F.
Nucl. Inst. Phys., Novosibirsk, USSR

SPIES G.O.
IPP, Garching, FRG

SPIGLER R.
CSGI, Padova, Italy

STAEBLER A.
IPP, Garching, FRG

STEFAN V.
Boris Kidric Inst., Beograd, Yugoslavia

STOECKEL J.
Inst. Plasma Phys., Prague, Czechoslovakia

ŠTOLL I.
Czech. Techn. Univ., Prague, Czechoslovakia

STOTT P.E.
UKAEA, Culham, UK

STREIBL B.
IPP, Garching, FRG

SUDAN R.N.
Cornell Univ., New York, USA

SUGISAKI K.
Electrotechn. Lab., Tokyo, Japan

ŠUNKA P.
Inst. Plasma Phys., Prague, Czechoslovakia

SUPRUNENKO V.A.
Phys. Techn. Inst., Kharkov, USSR

SWEETMAN D.R.
UKAEA, Culham, UK

SYKES A.
UKAEA, Culham,UK

TAYLOR J.B.
UKAEA, Culham, UK

TENNFORS E.
Royal Inst. Techn., Stockholm, Sweden

TOEPFER A.J.
Sandia Lab., Albuquerque, USA

TOI K.
Nagoya Univ., Nagoya, Japan

TOLOK V.T.
Phys. Techn. Inst., Kharkov, USSR

TROYON F.
Ecole Polytechn. Fed., Lausanne, Switzerland

TUTTER M.
IPP, Garching, FRG

UEHARA K.
JAERI, Ibaraki-ken, Japan

ULLSCHMIED J.
Inst. Plasma Phys., Prague, Czechoslovakia

UO K.
PPL Kyoto Univ., Uji, Japan

VAN DER MEER A.
FOM, Rijnhuizen, Netherlands

VAN HEESCH E.J.M.
FOM, Rijnhuizen, Netherlands

VAN INGEN A.M.
FOM, Rijnhuizen, Netherlands

VÁŇA J.
Inst. Plasma Phys., Prague, Czechoslovakia

VEKSTEIN G.E.
Inst. Nucl. Phys., Novosibirsk,USSR

VJACHESLAVOV L.N.
Inst. Nucl. Phys., Novosibirsk, USSR

VOLOSEVICH P.P.
Inst. Appl. Mathematics, Moscow, USSR

VRBA P.
Inst. Plasma Phys., Prague, Czechoslovakia

VRBOVÁ M.
Czech. Techn. Univ., Prague, Czechoslovakia

WAEGLI P.
Inst. Appl. Phys., Univ. Berne, Switzerland

WAGNER F.
IPP, Garching, FRG

WALKER A.C.
UKAEA, Culham, UK

WATARI T.
Nagoya Univ., Nagoya, Japan

WATKINS H.L.
UKAEA, Culham, UK

WEENINK M.P.H.
Techn. Univ. Eindhoven, Eindhoven, Netherlands

WEGROWE J.G.
IPP, Garching, FRG

WEISSE J.
CEN, Grenoble, France

WELDON D.M.
Los Alamos Lab., Los Alamos, USA

WELLER A.
IPP, Garching, FRG

WIENECKE R.
IPP, Garching, FRG

WILNER B.
Royal Inst. Techn., Stockholm, Sweden

WOBIG H.
IPP, Garching, FRG

WOOTTON A.J.
UKAEA, Culham, UK

YAMAMOTO S.
JAERI, Ibaraki-ken, Japan

YONAS G.
Sandia Lab., Albuquerque, USA

ŽÁČEK F.
Inst. Plasma Phys., Prague, Czechoslovakia

ŽIŽKA E.
Inst. Plasma Phys., Prague, Czechoslovakia

T I S K : Č V T S - D Ů M T E C H N I K Y P R A H A